Norwegian University of Life Sciences
Faculty of Chemistry, Biotechnology, and Food Science

Philosophiae Doctor (PhD)
Thesis 2022:31

Understanding and optimizing the role of lytic polysaccharide monooxygenases in enzymatic conversion of lignocellulosic biomass

Forståelse og optimalisering av rollen til lytisk polysakkarid monooksygenaser i enzymatisk nedbrytning av lignocellulosisk biomasse

Heidi Østby

Understanding and optimizing the role of lytic polysaccharide monooxygenases in enzymatic conversion of lignocellulosic biomass

Forståelse og optimalisering av rollen til lytisk polysakkarid monooksygenaser i enzymatisk nedbrytning av lignocellulosisk biomasse

Philosophiae Doctor (PhD) Thesis

Heidi Østby

Norwegian University of Life Sciences

Faculty of Chemistry, Biotechnology, and Food Science

Ås, 2022

Thesis number: 2022:31
ISSN: 1894-6402
ISBN: 978-82-575-1903-2

Table of contents

*: Certain sections of this chapter have been published in a review article by the author (Østby et al., 2020).

Acknowledgements

The work presented in this thesis was carried out at the Protein Engineering and Proteomics (PEP) group at the Faculty for Chemistry, Biotechnology, and Food Science (KBM) at the Norwegian University of Life Sciences (NMBU) in Ås, Norway, from 2018 to 2022. The work was funded by the Norwegian Research Council (NFR) as part of the Enzymes4Fuels project (project number 268002).

First and foremost, I extend my sincere gratitude to my main supervisor, **Vincent Eijsink**. Thank you for giving me the opportunity to complete my PhD in the PEP group, and for your kindness, understanding, and patience when experiments, projects, and manuscripts needed many rounds of rethinking and restructuring. I greatly admire and appreciate your ability to see the big picture through dozens of slides of results. Thank you for believing in me and for instilling in me the confidence and steadfastness needed to finish a PhD degree.

My sincere gratitude also goes to my co-supervisors, **Svein Horn** and **Tina Tuveng**. Svein, thank you for always offering an alternative perspective or insight into results that seemed too complex to understand. I have learned a great deal from your extensive experience – thank you for always being willing to share it with me. Thank you, Tina, for all the hours spent discussing results and planning experiments. Thank you for your never-ending patience, humor, optimism, and kindness. Somehow you always knew to check in with me when I needed it the most.

Special thanks to **Anikó Várnai, Magnus Arntzen, Zarah Forsberg, Olav Hegnar, Dejan Petrović,** and **Piotr Chylenski**, who taught me most of the practical and analytical skills I have acquired throughout my PhD. I cannot thank you enough for never hesitating to share your time and experience. Finalizing this work truly would not have been possible without your patience, kindness, and exceptional knowledge.

I also extend my gratitude to **colleagues at JBEI, NTNU, and Chalmers University** for fruitful collaborations and many interesting scientific discussions.

Thank you to **all members of the PEP, Bioref, and Bioorg groups** for creating such a friendly and dynamic working environment over the past few years. There has always been someone to turn to whenever I have had questions, or just needed someone to share a coffee and frustrations over failed experiments with. My special thanks go to **Line Hansen, Thales Costa, Anton Stepnov, Eirik Kommedal,** and **Anne Cathrine Bunæs**. I am enormously grateful to have been surrounded by such a supportive group of people who truly want the best for one another.

Thank you to my family – my parents **Anne** and **Knut**, my sisters **Marie** and **Hanna**, and my new niece **Lucia** – who have continuously supported me, encouraged me, and cheered me on in every way imaginable since before I can remember. You have always managed to renew my courage and strength even in the most difficult times.

Finally, thank you from the bottom of my heart to my partner **Eddie** and our dog **Mari**. Coming home to you after a long day of sampling has always lifted my spirits. Thank you both for taking such good care of me throughout the past four years. There is no one I would rather move forward into this new chapter of my life with than the two of you.

Heidi Østby
Ås, May 2022

Summary

Lignocellulosic biomass holds great potential for production of biofuels and other chemicals traditionally produced from fossil fuels. However, its significant recalcitrance presents a substantial challenge in industrial biorefining, where chemical and/or physical pretreatment methods and enzymatic saccharification are used to convert the polysaccharides within the lignocellulosic structure to fermentable sugars. One way of overcoming this innate recalcitrance is by developing strategies for improved enzymatic conversion, via process optimization or by exploring new enzyme activities.

The discovery of lytic polysaccharide monooxygenases (LPMOs) and their role in plant biomass degradation, and, more recently, the ability of these enzymes to catalyze a fast and specific peroxygenase reaction, has altered our understanding of the mechanisms of lignocellulose depolymerization, and revealed new avenues for potential improvement of this process. However, achieving such improvement requires in-depth understanding of how LPMOs function, including their substrate specificities, their catalytic mechanism, and the conditions under which they perform best, both alone and during synergistic action with hydrolytic enzymes. In addition, for process improvement and general understanding of LPMO activity, we must be able to analytically interpret and quantify the complex product mixtures generated by LPMOs. The work presented in this thesis has addressed several of these topics both from a fundamental and an applied perspective.

Paper I of this thesis describes the implementation of a recently developed chromatographic platform for high-performance anion exchange chromatography with pulsed amperometric detection (HPAEC-PAD) using dual electrolytic eluent generation in analytical methods for separation and quantification of LPMO-generated carbohydrate products. In this platform, the eluents are based on potassium methanesulfonate and potassium hydroxide. We established methods for simultaneous detection of native, C1-, and C4-oxidized cello-oligosaccharides, as well as separate methods for analysis of gluconic and glucuronic acid. The developed methods showed increased sensitivity and precision in

detection and quantification of LPMO products compared to traditional HPAEC-PAD using manually prepared eluents based on sodium hydroxide and sodium acetate.

In the study described in **Paper II**, we evaluated the use of a relatively simple, LPMO-rich fungal enzyme cocktail produced by *Thermoascus aurantiacus* in saccharification of pretreated lignocellulosic biomass, and showed that this cocktail performs nearly as well in saccharification of lignin-poor sulfite-pulped spruce at 60°C as the commercial cellulase preparation Cellic CTec2 at 50°C. These results underpin the potential of the *T. aurantiacus* fungus as a producer of enzymes for use in industrial biorefining processes, where maintaining higher temperatures during saccharification can be advantageous. Furthermore, addition of H_2O_2-producing glucose oxidase to saccharification reactions with Cellic CTec2 showed that *in situ* H_2O_2 production can drive LPMO activity in saccharification of lignin-poor substrates. The results obtained in this study were substrate-dependent: when using a lignin-rich substrate, the *T. aurantiacus* cocktail was less advantageous, and addition of glucose oxidase was detrimental to the saccharification efficiency of Cellic CTec2. These results highlight the importance of adapting process conditions to individual lignocellulosic feedstocks and enzyme preparations.

Paper III and **Paper IV** of this thesis describe the functional characterization of AA9 LPMOs. In **Paper III**, we demonstrate the C4-oxidizing activity of *Sc*LPMO9A from *Schizophyllum commune* on a range of hemicellulosic substrates and soluble cello-oligomeric substrates, including cellotetraose and cellohexaose (with apparent preferential -3 - +3 binding), and its strong peroxygenase activity when acting on soluble and insoluble amorphous substrates. In contrast to the traditionally-perceived role of LPMOs in depolymerization of crystalline substrates, *Sc*LPMO9A appeared to have little-to-no activity on crystalline cellulose. Although further investigation of these observations is needed, including determination of potential active site residues that may contribute to the observed substrate preferences, these results are intriguing and may aid in providing insight into hitherto unknown biological roles of LPMOs. The research presented in **Paper IV** uncovered the glucuronoxylanolytic activity of two LPMOs from *Neurospora crassa*. By quantification of cellulose- and xylan-derived oxidized products, this study demonstrated

that preferential cleavage of xylan or cellulose in a mixture of these two polysaccharides can vary substantially between xylan-active LPMOs, suggesting that these LPMOs may have evolved to target different co-polymeric structures within plant biomass. Phylogenetic analysis and structural modeling also enabled the identification of additional putatively xylan-active LPMOs.

The results reported in this thesis add to our understanding of LPMO action and how best to leverage this action for current and future academic and industrial applications.

Sammendrag

Lignocellulose innehar et stort potensial for produksjon av biobrensel og andre kjemikalier som tradisjonelt produseres fra fossile kilder. Men dens komplekse sammensetning gir betydelige utfordringer i industriell bioraffinering, hvor kjemiske og/eller fysiske forbehandlingsmetoder og enzymatisk nedbrytning brukes for å omdanne polysakkaridene i lignocellulosen til fermenterbare sukkere. En måte å løse denne kompleksiteten på er å utvikle strategier for forbedret enzymatisk omdanning, via prosessoptimalisering eller ved å utforske nye enzymaktiviteter.

Oppdagelsen av lytisk polysakkarid monooksygenaser (LPMOer) og deres rolle i nedbrytning av plantebiomasse, og, nylig, evnen disse enzymene har til å katalysere en hurtig og spesifikk peroksygenasereaksjon, har endret vår forståelse av mekanismene for nedbrytning av lignocellulose, og åpnet opp for nye mulige forbedringer av denne prosessen. Dog, det å få til slike forbedringer krever mer kunnskap om hvordan LPMOer fungerer, inkludert deres substratspesifisiteter, den katalytiske mekanismen og om hvilke forhold de presterer best under, både alene og i synergi sammen med hydrolytiske enzymer. I tillegg, for å kunne forbedre prosessen og generelt forstå LPMO-aktiviteten, må vi kunne analysere og kvantifisere de komplekse produktblandingene som LPMOer gir. Arbeidet presentert i denne avhandlingen adresserer flere av disse temaene, både fra et fundamentalt og et anvendt perspektiv.

Artikkel I beskriver implementeringen av en nylig utviklet kromatografisk plattform for høypresisjons-ionebytterkromatografi med pulserende amperometrisk deteksjon (HPAEC-PAD) ved bruk av dobbel elektrolytisk eluentgenerering i analytiske metoder for separasjon og kvantifisering av karbohydratprodukter produsert av LPMOer. I denne plattformen er eluentene basert på kaliummetansulfonat og kaliumhydroksid. Vi etablerte metoder for samtidig deteksjon av native, C1- og C4-oksiderte cello-oligosakkarider, samt separate metoder for analyse av glukonsyre og glukuronsyre. Metodene som ble utviklet her viste økt sensitivitet og presisjon ved deteksjon og kvantifisering av LPMO-produkter

sammenlignet med tradisjonell HPAEC-PAD, hvor eluentene lages manuelt og er basert på natriumhydroksid og natriumacetat.

I studien beskrevet i **Artikkel II**, evaluerte vi bruken av en relativt enkel, LPMO-rik enzymblanding produsert av soppen *Thermoascus aurantiacus* i sakkarifiseringen av forbehandlet lignocellulose, og viste at denne blandingen presterer nesten like godt i sakkarifisering av ligninfattig sulfitt-prosessert gran ved 60°C som det kommersielle cellulasepreparatet Cellic CTec2 ved 50°C. Disse resultatene understreker potensialet til *T. aurantiacus* som produsent av enzymer for bruk i industrielle bioraffineringsprosesser hvor det å opprettholde høye temperaturer kan være fordelaktig. Tilsetting av H_2O_2-produserende glukoseoksidase til sakkarifiseringsreaksjonene med Cellic CTec2 viste i tillegg at *in situ* H_2O_2 produksjon kan drive LPMO-aktiviteten ved sakkarifisering av ligninfattige substrater. Resultatene oppnådd i denne studien var substratavhengige: ved bruk av et ligninrikt substrat var enzymblandingen fra *T. aurantiacus* mindre fordelaktig, og tilsetting av glukoseoksidase var uheldig for sakkarifiseringseffektiviteten til Cellic CTec2. Disse resultatene fremhever viktigheten av å tilpasse prosessbetingelsene til individuelle lignocellulosesubstrater og enzympreparater.

Artikkel III og **IV** beskriver den funksjonelle karakteriseringen av AA9 LPMOer. I **Artikkel III** demonstrerte vi C4-oksideringsaktiviteten til *Sc*LPMO9A fra *Schizophyllum commune* på en rekke hemicelluloser og løselige cello-oligomer-substrater, inkludert cellotetraose og celloheksaose (med tilsynelatende -3 – +3 binding), og enzymets sterke peroksygenaseaktivitet på løselige og uløselige amorfe substrater. I motsetning til den tradisjonelt antatte rollen til LPMOer i depolymeriseringen av krystallinske substrater, ser *Sc*LPMO9A ut til å ha liten til ingen aktivitet på krystallisk cellulose. Selv om videre undersøkelser av disse observasjonene er nødvendig, inkludert bestemmelse av mulige aminosyrer i det aktive setet som kan bidra til de observerte substratpreferansene, er disse resultatene interessante og kan gi innsikt i LPMOers hittil ukjente biologiske roller. Forskningen presentert i **Artikkel IV** avdekket aktivitet på glukuronoxylan for to LPMOer fra *Neurospora crassa*. Ved kvantifisering av oksiderte produkter fra cellulose og xylan, demonstrerte denne studien at foretrukket kløyving av xylan eller cellulose i en blanding

av disse to polysakkaridene kan variere betydelig mellom xylan-aktive LPMOer, noe som antyder at disse LPMOene kan ha utviklet seg til å virke på ulike co-polymeriske strukturer i plantebiomasse. Fylogenetisk analyse og modellering av strukturer gjorde det også mulig å identifisere andre mulige xylan-aktive LPMOer.

Resultatene rapportert i denne avhandlingen gir utvidet kunnskap om vår forståelse av LPMO-aktivitet og hvordan best bruke dette i nåværende og fremtidige akademiske og industrielle anvendelser.

Abbreviations

AA	Auxiliary activity
AscA	Ascorbic acid
BG	β-glucosidase
CAZyme	Carbohydrate-active enzyme
CBH	Cellobiohydrolase
CDH	Cellobiose dehydrogenase
DP	Degree of polymerization
EG	Endoglucanase
GA	Gallic acid
GH	Glycoside hydrolase
Glc4gemGlc	4-Hydroxy-β-D-xylo-hexopyranosyl-(1,4)-β-D-glucopyranosyl (C4-oxidized cellobiose)
GOx	Glucose oxidase
HPAEC	High-performance anion exchange chromatography
LOD	Limit of detection
LOQ	Limit of quantification
LPMO	Lytic polysaccharide monooxygenase
MALDI-TOF MS	Matrix-assisted laser desorption ionization time of flight mass spectrometry
Nc	*Neurospora crassa*
PAD	Pulsed amperometric detection
PASC	Phosphoric-acid swollen cellulose
PUL	Polysaccharide utilization locus
ROS	Reactive oxygen species
Sc	*Schizophyllum commune*
SEB	Steam-exploded birch
SPS	Sulfite-pulped spruce
Ta	*Thermoascus aurantiacus*
Tr	*Trichoderma reesei*

List of papers

Paper I
Chromatographic analysis of oxidized cello-oligomers generated by lytic polysaccharide monooxygenases using dual electrolytic eluent generation.
Østby, H., Jameson, J.-K., Costa, T., Eijsink, V. G. H., & Arntzen, M. Ø. (2022). *Journal of Chromatography A*, 1662: 462691.

Paper II
Substrate-dependent cellulose saccharification efficiency and LPMO activity of Cellic CTec2 and a thermostable enzyme cocktail from *Thermoascus aurantiacus*, and the impact of H_2O_2-producing glucose oxidase.
Østby, H., Várnai, A., Gabriel, R., Chylenski, P., Horn, S. J., Singer, S. W., & Eijsink, V. G. H.
Manuscript submitted for publication.

Paper III
Functional characterization of a lytic polysaccharide monooxygenase from *Schizophyllum commune* that degrades non-crystalline substrates and displays strong peroxygenase activity.
Østby, H., Christensen, I. A., Hennum, K., Várnai, A., Courtade, G., Hegnar, O. A., Aachmann, F. L., & Eijsink, V. G. H.
Manuscript.

Paper IV
Quantifying oxidation of cellulose-associated glucuronoxylan by two lytic polysaccharide monooxygenases from *Neurospora crassa*.
Hegnar, O. A., Østby, H., Petrović, D. M., Olsson, L., Várnai, A., & Eijsink, V. G. H. (2021). *Applied and Environmental Microbiology*, 87(24): e0165221.

Other publications by the author:

Enzymatic processing of lignocellulosic biomass: principles, recent advances and perspectives.
Østby, H., Hansen, L. D., Horn, S. J., Eijsink, V. G. H., & Várnai, A. (2020). *Journal of Industrial Microbiology and Biotechnology*, 47(9-10): 623–657.

Comparison of six lytic polysaccharide monooxygenases from *Thermothielavioides terrestris* shows that functional variation underlies the multiplicity of LPMO genes in filamentous fungi.
Tõlgo, M., Hegnar, O. A., Østby, H., Várnai, A., Vilaplana, F., Eijsink, V. G. H., & Olsson, L. (2022). *Applied and Environmental Microbiology*, 88(6): e0009622.

Discovery and characterization of a thermostable two-domain GH6 endoglucanase from a compost metagenome.
Jensen, M. S., Fredriksen, L., MacKenzie, A. K., Pope, P. B., Leiros, I., Chylenski, P., Williamson, A. K., Christopeit, T., Østby, H., Vaaje-Kolstad, G., & Eijsink, V. G. H. (2018). *PLOS ONE*, 13(5): e0197862.

1 Introduction

1.1 Moving towards a bio-based economy

1.1.1 The limitations of a fossil-fuel based economy

Global warming and climate change are increasing at an alarming rate, primarily due to human activities. According to the latest predictions, the average global temperature will have risen by up to 2°C above pre-industrial levels by the end of the 21st century unless drastic mitigative actions are taken, and the devastating consequences of climate change on our planet are already prevalent in the form of heatwaves, droughts, increases in intensity and frequency of climate and weather extremes, and loss of ecosystems. A central cause of climate change is the release of CO_2 resulting from combustion of fossil fuels such as coal, crude oil, and natural gas, energy-rich hydrocarbons of biological origin stored for millions of years in the Earth's crust (Gomez et al., 2008; Stern et al., 2016; Arias et al., 2021; Liu et al., 2021; Meinshausen et al., 2022).

As a consequence of the industrial revolution and the invention of the coal-powered steam engine in the late 18th century, coal rapidly became humankind's most essential energy source. From the middle of the 19th century and through the 20th century, deposits of crude oil and natural gas were discovered in many places around the world, and the burning of these carbon-rich fossil fuels to produce heat and energy, and to power vehicles and machines, became an integral part of our global society and economy (Gomez et al., 2008; Chu and Majumdar, 2012). It was not until the 1970s, after years of growing concern over the possible harmful effects of fossil fuel combustion, that a general scientific consensus regarding these concerns began to emerge. The first Intergovernmental Panel on Climate Change (IPCC) report, published in 1990, declared that global warming was a reality, and that it would continue to increase over the coming decades (Houghton, 1990).

Today, we know that the central problem associated with consuming fossil fuels is the resulting direct and indirect emissions of CO_2, CH_4, and N_2O, so-called anthropogenic greenhouse gases, which trap heat within the atmosphere causing a rise in global temperature. While numerous human activities contribute to the release of greenhouse gases, the production of heat and electricity, industrial processes, and transportation are three of the major contributors to greenhouse gas emissions on a global scale (Stern et al., 2016; Arias et al., 2021; Liu et al., 2021).

1.1.2 Focus on renewables

The detrimental effects of fossil fuel combustion, coupled with their lack of renewability, has incited a shift in policy-making and scientific research over the past few decades, as the world has begun focusing on more sustainable alternatives. Private industries and public institutions alike now devote billions of dollars each year worldwide towards research on renewable energy sources (Trancik, 2014). Strategies for replacing fossil fuels include harvesting solar and wind power to produce heat and electricity, and producing traditionally fossil fuel-based products (such as petroleum or specialized chemicals) from biomass.

Plant biomass represents an interesting candidate for production of sustainable fuels and chemicals. This type of biomass consists of plant matter and can be sourced directly from food crops (e.g. corn or sugarcane), from forestry, or from side streams in the agriculture and forestry sectors. Through the process of biorefining, the various, largely polymeric components of plant cell walls are separated and converted to building blocks for the generation of fuels and chemicals. For example, carbohydrate structures within plant biomass are hydrolyzed using chemical and/or biochemical methods to obtain fermentable sugars. Subsequent fermentation by suitable microbes enables the production of ethanol or specialized chemicals (Gomez et al., 2008; Galbe and Wallberg, 2019).

1.1.2.1 Plant biomass feedstocks

In biorefining of plant biomass, a distinction should be made between first- and second-generation feedstocks. This label distinguishes between biomass that can alternatively be used directly as a food source for human consumption (first-generation, e.g. corn, sugarcane) and inedible feedstocks, such as lignocellulosic biomass (second-generation, e.g. agricultural and forestry residues, woody biomass) (Gomez et al., 2008; Lee and Lavoie, 2013). The ethical ramifications associated with producing fuels and specialty chemicals from first-generation feedstocks due to global food insecurity and hunger have resulted in an increased scientific focus on development of technologies for efficient conversion of second-generation lignocellulosic feedstocks (Odling-Smee, 2007; Gomez et al., 2008; Williams, 2008; FAO, 2021).

Lignocellulosic biomasses can be categorized into hardwoods (angiosperms, e.g. birch, beech), softwoods (gymnosperms, e.g. spruce, pine), grasses (e.g. switchgrass), and agricultural waste (lignocellulosic portions of food crops, e.g. corn stover, rice straw) (Ho et al., 2014; Isikgor and Becer, 2015). Woody biomass (softwood and hardwood) is significantly more recalcitrant to degradation than agricultural waste and grass-based feedstocks, in part due to larger amounts of lignin in the former (Álvarez et al., 2016).

In nature, the polysaccharides in lignocellulose (cellulose and various hemicelluloses) are degraded to metabolizable sugars by fungi and bacteria. Through a variety of mechanisms, including the use of highly specialized enzymes working synergistically, these microorganisms have evolved to overcome the natural recalcitrance of the complex lignocellulosic material (Payne et al., 2015; Bomble et al., 2017). The enzymatic saccharification steps employed in industrial valorization of lignocellulose aim to exploit the innate properties of these microorganisms, while adjusting process parameters to suit the nature of the feedstock and the spectrum of end products to be produced. The understanding and optimization of polysaccharide-degrading enzyme systems are of major importance for the exploitation of non-edible biomass.

1.2 Lignocellulose

As the most abundant raw material on Earth, lignocellulose represents a promising candidate for production of fuels and chemicals from a renewable source. Lignocellulose, found within the cell walls of plants, primarily consists of three main elements: cellulose and various hemicelluloses, both polysaccharides, and lignin, an aromatic polymer (**Figure 1**). In addition to contributing to physical plant characteristics, such as rigidity and strength, it is clear that the lignocellulosic structure within the plant cell wall has evolved to confer resistance to pathogenic attack (Somerville et al., 2004; Underwood, 2012). The precise composition of lignocellulose, i.e. the ratio of cellulose, hemicellulose, and lignin, varies not only within the different layers of the plant cell wall, but also from species to species. As a general estimate, woody biomass contains 20-50% cellulose, 15-35% hemicellulose, and 10-30% lignin (Pauly and Keegstra, 2008; Payne et al., 2015). In addition to these three major components, lignocellulosic biomass also contains minor amounts of alternative compounds, including structural proteins, enzymes, pectin, phenolic compounds, minerals, and ash (Isikgor and Becer, 2015; Zhong et al., 2019).

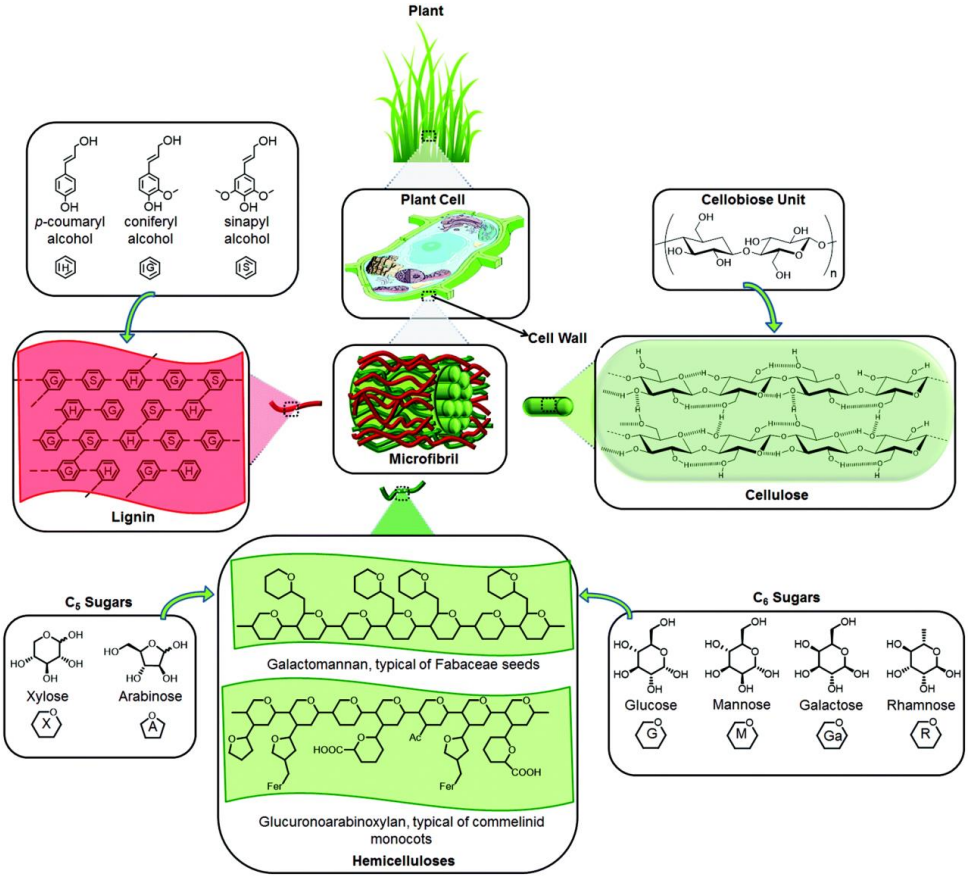

Figure 1. Structural components of lignocellulose. The figure shows individual building blocks of cellulose, hemicelluloses, and lignin, and how the polymers comprised of these building blocks may assemble within a plant cell wall. Densely packed cellulose chains interlinked via hydrogen bonding form microfibrils, which are embedded within a hemicellulose and lignin matrix, as shown in the center of the figure. For the hemicelluloses, potential acetylation and esterification with ferulic acid of glucuronoarabinoxylan are represented by "Ac" and "Fer," respectively. The figure was reproduced from (Isikgor and Becer, 2015).

The plant cell wall contains the majority of the plant's dry weight and is organized into several layers, including the middle lamella, the primary and secondary cell walls, and the warty layer (**Figure 2**). The presence or absence of these layers, as well as the prevalence

of cellulose, hemicellulose, and lignin within each layer, can vary broadly according to the stage of cell growth, type of cell, and plant species (Zeng et al., 2017). During plant cell growth, the primary cell wall is formed first, and consists of cellulose microfibrils embedded in a hemicellulose and pectin matrix. The role of this layer is primarily to provide strength and flexibility during growth. The middle lamella binds to the primary cell walls of adjacent cells, and collectively, these layers are referred to as a compound middle lamella. The compound middle lamella is generally rich in pectin, which assists in cell adhesion (Cosgrove, 2005; Zeng et al., 2017; Melelli et al., 2020). The secondary cell wall, if present, will form at the final stage of cell growth, and is found between the primary cell wall and the plasma membrane. This is a thick, rigid layer which strengthens and supports the cell (Somerville et al., 2004). If present, this layer generally accounts for most of the plant cell mass, and contains the majority of the lignin present in the cell. The secondary cell wall is organized into three sublayers (S_1, S_2, and S_3), deposited sequentially on the inside of the primary wall during the lifetime of the cell. The warty layer, located inside the S_3 layer, is found only in certain tree species, and primarily consists of cross-linked lignin precursors formed during the final stage of cell life (Zeng et al., 2017; Melelli et al., 2020).

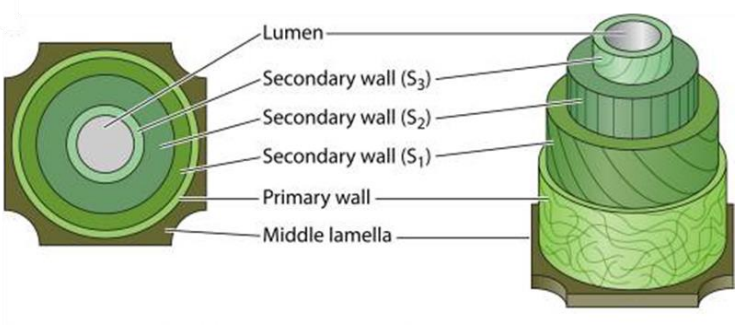

Figure 2. Structure of the plant cell wall. The figure shows the primary layers of the plant cell wall (middle lamella, primary cell wall, and cell secondary wall), as well as the three sublayers of the secondary cell wall (S_1, S_2, and S_3). The figure was adapted from (Rytioja et al., 2014).

1.2.1 Cellulose

Cellulose is primarily found within plant cell walls, but can also be produced by algae, fungi, and some bacterial species (Brown, 2004; Habibi et al., 2010). In bacteria, cellulose is thought to aid in bacterial flocculation and plant attachment. In contrast to plant-derived cellulose, bacterial cellulose tends to have a higher degree of crystallinity, and is not complexed with hemicellulose or lignin (Lupaşcu et al., 2022).

Cellulose is a linear, unbranched homopolymer made up of D-glucose monosaccharides, linked via β-1,4-glycosidic bonds. Each D-glucose molecule is rotated 180° relative to the previous unit, and thus, the disaccharide cellobiose (consisting of two glucose monomers connected via a β-1,4-glycosidic bond) is the continuously repeating unit of cellulose (**Figure 1**) (Klemm et al., 2005; Taylor, 2008; Habibi et al., 2010). The covalent glycosidic bonds that link the monosaccharides together are named according to the carbon atoms involved in bond formation (e.g. 1,4 – C1 on one and C4 on the other). The bonds are given the designation α or β according to the configuration of the anomeric carbon, C1 (Klemm et al., 2005). The β-configuration results in a highly linear polymer chain, which allows for tight packing of these chains in fibrils and even crystalline materials, as in cellulose (Winger et al., 2009).

Cellulose chains have a non-reducing end (the C4-OH carbon of the final D-glucose molecule, normally shown to the left, as in **Figure 1**) and a reducing end (the C1-OH carbon of the hemiacetal group on the other final D-glucose unit, which is in equilibrium with the aldehyde form, normally shown to the right) (Klemm et al., 2005). The degree of polymerization (DP) of cellulose chains varies according to their source, and changes as a result of pretreatment during industrial processing (Baruah et al., 2018). While generally considered insoluble, short cello-oligosaccharides with a DP <8 are soluble (Brown, 2004). The linear nature of cellulose chains enables their packing into dense structures known as microfibrils, estimated to consist of between 18 and 36 cellulose chains that interact through hydrogen-bonding and van der Waals forces (the precise number of chains within a microfibril has been debated) (Somerville, 2006; Fernandes et al., 2011; Newman et al.,

2013; Kubicki et al., 2018). Due to fiber formation, only a limited number of cellulose chains are exposed to the environment and thus accessible to enzymes secreted by cellulose-degrading organisms (Payne et al., 2015). Of note, even the enzymatic degradation of exposed chains is challenging because enzyme action requires that a single chain loosens from its fiber context, which is energetically demanding (Beckham et al., 2011). When complexed with hemicellulose and lignin, the cellulose microfibrils become increasingly shielded, and thus even less susceptible to enzymatic attack. Taken together, the above properties make the cellulose polysaccharide in lignocellulosic biomass highly recalcitrant to enzymatic degradation (Taylor, 2008; Sarkar et al., 2009).

Cellulose in lignocellulosic biomass can be made more accessible through a variety of thermal and chemical treatments that are discussed in section 1.3.1. In research on cellulose-active enzymes, crystalline cellulose is often treated to make it more amorphous, and thus more susceptible to enzymatic hydrolysis. A common example is treating the commercially available model crystalline cellulose Avicel with phosphoric acid to produce phosphoric-acid swollen cellulose (PASC), as described in (Wood, 1988).

Crystalline cellulose naturally occurs primarily as two allomorphs, I_α and I_β (**Figure 3**). I_β is the form found in higher plants, and is the more stable of the two, whereas I_α cellulose is most commonly found in bacteria and algae. While cellulose chains lie parallel to one another in both forms, differences between the two allomorphs are found in the organization of the hydrogen bonding between chains in microfibrils (Brown, 2004; Habibi et al., 2010). In addition, five alternative polymorphs of cellulose have been described (II, III_I, III_{II}, IV_I and IV_{II}), which can be generated from natural cellulose via different forms of pretreatment, including treatment with alkali and liquid ammonia (Somerville, 2006; Habibi et al., 2010). Cellulose II has an antiparallel arrangement of cellulose chains (**Figure 3**) and is considered to be the most thermodynamically stable cellulose polymer. However, naturally occurring cellulose I_β has been shown to be more recalcitrant to enzymatic hydrolysis than cellulose II, presumably due to differences in the hydrophobic interactions between cellulose chains within the microfibril structure (Brown, 2004; Habibi et al., 2010; Wada et al., 2010; Kubicki et al., 2018).

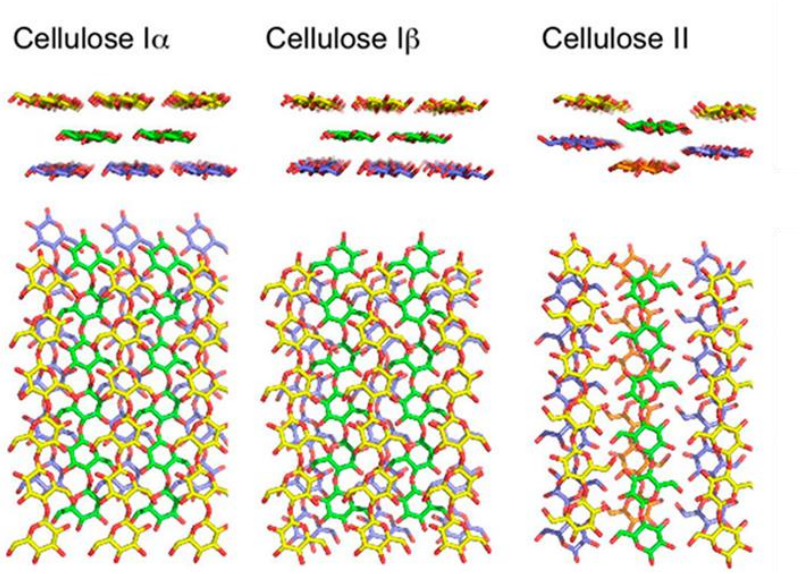

Figure 3. Molecular structures of cellulose. The figure shows molecular structures of the allomorphs of naturally-occurring cellulose I, I_α and I_β, as well as cellulose II, a cellulose polymorph that can be generated from cellulose I. The figure was adapted from (Meier et al., 2018).

1.2.2 Hemicellulose

The term hemicellulose denotes a group of amorphous, heterogeneous polysaccharides encompassing a range of diverse pentoses, hexoses, and uronic acids connected via a β-1,4-linked backbone (mixed-linkage glucan is an exception; see section 1.2.2.4). In contrast to cellulose, hemicellulose backbone sugars can be substituted with additional sugar moieties, or with acetylations, methylations, or esterifications at several positions. This branching contributes to the large structural and physiochemical variability found in this group of polysaccharides (**Figure 4**). Consequently, the sugar composition of hemicellulose-rich lignocellulosic biomass varies significantly depending on the feedstock (Scheller and Ulvskov, 2010). Hemicellulose contents vary widely between different types of plants, as discussed further below.

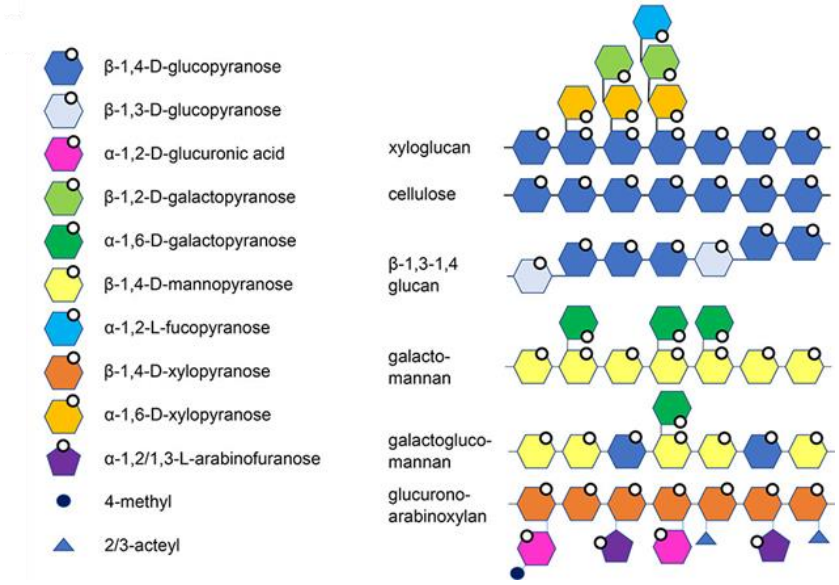

Figure 4. Structural variability of hemicelluloses. The figure shows the range of building blocks found in hemicelluloses and how these can be assembled into different hemicellulose forms. The figure was adapted from (Meier et al., 2018).

The main role of hemicelluloses in the lignocellulosic macrostructure is thought to be strengthening of the plant cell wall through interactions with both cellulose and lignin (Scheller and Ulvskov, 2010). Beyond hydrogen bonding and hydrophobic interactions common between these polymeric compounds, covalent bonds formed between hemicellulose and lignin, forming so-called lignin-carbohydrate complexes, contribute to the overall recalcitrance of lignocellulosic biomass (Raji et al., 2021). Thus, while hemicelluloses as such usually are easier to enzymatically degrade than cellulose, they do contribute to the overall recalcitrance of lignocellulose. In addition, the structural diversity and complexity of hemicellulose itself contributes to recalcitrance due to the large number of enzyme types required to achieve complete depolymerization (Álvarez et al., 2016).

While cellulose saccharification only yields easily fermentable glucose, saccharification of hemicelluloses yields mixtures of various pentoses and hexoses, depending on the plant material. Although many hemicellulosic sugars can be fermented in biorefining to produce fuels and chemicals, not all strains commonly used for fermentation can ferment all hemicellulosic sugars. During lignocellulose processing, many hemicelluloses can be readily extracted using, for example, acid or alkaline pretreatments (Carvalheiro et al., 2008; Galbe and Wallberg, 2019).

Softwoods and hardwoods differ considerably in their hemicellulose content, contributing to a difference in resistance to chemical and enzymatic degradation. As a general rule, hardwoods are less resistant to degradation than softwoods (Álvarez et al., 2016). This is because hemicellulose in hardwood generally consists of xylans (specifically glucuronoxylan, see section 1.2.2.1), which are more readily removed by certain types of chemical pretreatment (e.g. acid hydrolysis) than the glucomannans (specifically galactoglucomannan, see section 1.2.2.3) found in softwoods (Isikgor and Becer, 2015; Nitsos et al., 2018).

1.2.2.1 Xylan

Xylans are the most abundant hemicellulose found in hardwoods and grasses, and consist of a β-1,4-linked backbone of D-xylose units, with various substituents. Xylans are frequently acetylated at the O-2 and/or O-3 positions, thought to contribute to interactions with cellulose and lignin. Xylans can be organized into three general groups, glucuronoxylan, arabinoxylan, and glucuronoarabinoxylan, corresponding to their primary substituents. Glucuronoxylan, the predominant form of xylan in hardwood, normally has α-1,2-linked D-glucuronic acid and 4-O-methyl-D-glucuronic acid substitutions in addition to acetylations (Scheller and Ulvskov, 2010; Grantham et al., 2017; Zhang et al., 2021a). Arabinoxylan is predominantly found in grass and cereal species, while glucuronoarabinoxylan is found both in cereal and grass species and within the secondary cell wall of softwood species. These xylan forms contain α-1,2-linked D-glucuronic acid and/or 4-O-methyl-D-glucuronic acid, and α-1,2- and/or α-1,3-linked L-arabinose

substitutions, as well as acetylations. The arabinoses may also be esterified with ferulic acid at their O-5 positions (Karppi et al., 2020; Raji et al., 2021; Zhang et al., 2021a).

The presence or absence of substitutions along the xylan backbone impacts various physiochemical properties of the polysaccharide, such as solubility and interactions with other polymers in the plant cell wall. In particular, recent studies have shown that xylan substitutions primarily occur on even-numbered xylose units of the backbone. Although xylan adopts a 3-fold screw conformation in solution, when complexed with cellulose, these substitution patterns enable the formation of a flattened 2-fold screw conformation in which its substitutions are located on one side of the backbone (**Figure 5**). This results in an unsubstituted xylan surface which can engage in hydrogen bonding with the cellulose surface (Busse-Wicher et al., 2014; Busse-Wicher et al., 2016b; Simmons et al., 2016; Grantham et al., 2017).

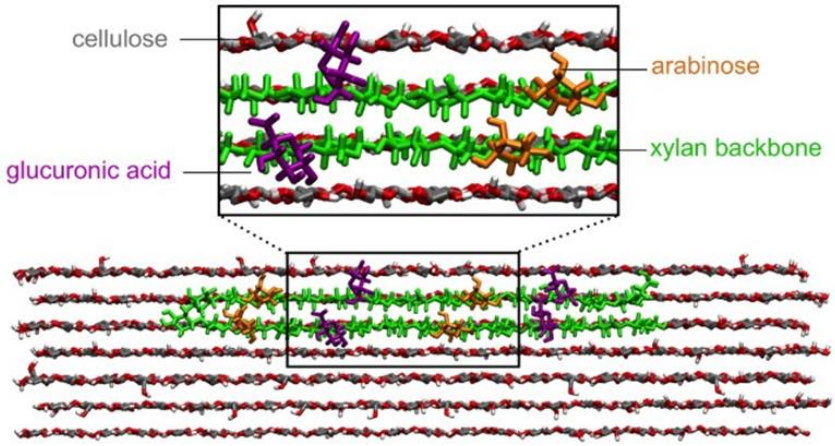

Figure 5. Molecular dynamics simulation of xylan complexed with cellulose. The figure shows two xylan chains in the 2-fold screw conformation, enabling adsorption onto cellulose chains. In this conformation, backbone substitutions are oriented away from the cellulose microfibril. The figure was adapted from (Busse-Wicher et al., 2016b).

Of note, the substitutions of xylan also affect its susceptibility to certain degradative enzymes. For example, it is well known that certain xylanases (e.g. family 10 glycoside hydrolases) are less sensitive to backbone substitutions than others (e.g. family 11 glycoside hydrolases) (Biely et al., 1997).

1.2.2.2 Xyloglucan

Xyloglucans have a β-1,4-linked backbone of D-glucose units, many of which are substituted with D-xyloses at their O-6 sites through α-1,6-linkages. The xylose substituents and the glucose backbone can both be further substituted with D-galactose, L-galactose, L-fucose, and/or L-arabinose at various positions. In total, 24 unique structural motifs of xyloglucan have been identified. The types and locations of xyloglucan substitutions vary greatly with the plant species, cell type, and stage of cell growth. In addition, xyloglucan can be acetylated either directly on the glucosyl backbone or on galactose or arabinose moieties (Pauly and Keegstra, 2016). Xyloglucans have been isolated from all land plants, and are thought to strongly associate with cellulose, forming an extensive network essential to cell wall structural stability during growth (Pauly and Keegstra, 2016; Zhang et al., 2021a). However, recent studies have demonstrated that the model plant *Arabidopsis thaliana* can grow normally in the absence of xyloglucan (Kim et al., 2020), indicating that the true role of this polysaccharide is yet to be fully elucidated (Zhang et al., 2021a).

1.2.2.3 Mannan

Mannans comprise a group of hemicelluloses consisting either of a β-1,4-linked D-mannose backbone (e.g. linear mannan and galactomannan), or a β-1,4-linked backbone of D-mannose and D-glucose (e.g. glucomannan and galactoglucomannan). The unbranched linear chains of linear mannan and glucomannan give these polysaccharides properties similar to cellulose, including their insolubility in water (Voiniciuc, 2022). Galactomannan has a D-mannose backbone, but is substituted with α-1,6-linked D-galactose, making this polysaccharide more viscous and giving it the ability to form gels (Malgas et al., 2015; Hlalukana et al., 2021). Galactoglucomannan has a backbone consisting of β-1,4-linked D-

mannose and D-glucose, but is substituted with α-1,6-linked D-galactose at the O-6 positions of the mannose residues. All mannan forms can carry O-linked acetylations at the C2- and C3-positions of the backbone mannose units (Voiniciuc, 2022). Galactoglucomannan is the most complex form of mannan, and is the primary form of hemicellulose found in softwoods (Zhang et al., 2021a).

1.2.2.4 Mixed-linkage glucan

β-1,3;1,4-glucan, also called mixed-linkage glucan, differs from the hemicellulose types discussed above in that it contains only glucose, is unbranched, and has both β-1,3 and β-1,4 glycosidic linkages in its backbone. In contrast to cellulose, mixed-linkage glucan is flexible and soluble even at very high degrees of polymerization, due to the presence of the β-1,3 linkages that create kinks in the otherwise β-1,4-linked backbone (Fincher, 2009). It is primarily found in grass species where it is thought to serve as a storage carbohydrate (Fry et al., 2008; Scheller and Ulvskov, 2010; Burton and Fincher, 2014).

1.2.3 Lignin

In contrast to cellulose and hemicellulose, the final major component of lignocellulose, lignin, is not a polysaccharide but a polyphenolic polymer made up of monolignols, derivatives of aromatic alcohols (Parthasarathi et al., 2011). The heterogeneous lignin structure is made up of *p*-coumaryl alcohol, coniferyl alcohol, and sinapyl alcohol derivatives, three monolignol units referred to as *p*-hydroxyphenyl (H), guaiacyl (G), and syringyl (S), respectively. These lignin precursors differ in the number of methoxy-groups on their aromatic ring (0, 1, and 2, respectively; **Figure 1**). In addition to the three monolignols, caffeyl alcohol and 5-hydroxyconiferyl alcohol can also be incorporated into the polymeric lignin structure. Monolignols can be acetylated, which further contributes to the large chemical and structural variability in lignin structures. Similarly to in hemicellulose, lignin composition varies considerably between plant species and between different cell types (Zhong et al., 2019). Softwood biomass has a higher lignin content than

hardwood, and contains mostly G-type lignin, whereas hardwood contains both G- and S-lignin (lignin type GS). Less methoxy-groups in G-type lignin (one per monolignol compared to two in S-type lignin) results in increased condensation reactions, explaining why softwood lignin is difficult to remove in pretreatment processes (Nitsos et al., 2018). Grass species contain H-, G-, and S-type lignin, but generally contain more H-lignin than hardwoods and softwoods (Parthasarathi et al., 2011; Zhong and Ye, 2015). Lignin plays a critical role in plant structural stability via stiffening of the stem and roots (Zhong et al., 2019).

Interestingly, lignin is redox-active and can engage in a variety of reactions, especially in the presence of oxygen (Felby et al., 1997; Arantes et al., 2012; Bissaro et al., 2018b). For example, lignin can reduce oxygen to form H_2O_2, and reduce H_2O_2 to H_2O. Lignin also has the ability to act as an electron source for oxidative enzymes requiring a reducing agent such as LPMOs, which are at the core of the research described in this thesis (Cannella et al., 2012; Westereng et al., 2015; Kracher et al., 2016; Brenelli et al., 2018) (section 1.3.4.5).

Lignification of plant cell walls occurs in the final stages of cell growth. Oxidative free radical coupling of the three monolignols results in the formation of lignin polymers, which subsequently may participate in the formation of lignin-carbohydrate complexes (Zeng et al., 2017; Zhong et al., 2019). These close associations with the cell wall polysaccharides significantly contribute to the overall enzymatic recalcitrance of the lignocellulose structure (Gomez et al., 2008; Kellock et al., 2019). The difficulties associated with cost-effective and efficient removal of lignin during pretreatment of lignocellulosic biomass for subsequent enzymatic saccharification play a major role in determining the economic viability of biorefining processes (Zeng et al., 2014; Nitsos et al., 2018). Due to the chemical association of lignin with cellulose and hemicellulose within the plant cell wall, care must be taken to preserve the structural integrity of these polysaccharides during lignin removal (Galbe and Wallberg, 2019; Sethupathy et al., 2022).

Lignin has traditionally been considered a waste stream of biomass processing, and is often burned to produce heat and electricity. Biorefining efforts to valorize lignin have proven

difficult, due in part to its irregular chemical structure and general recalcitrance to depolymerization (Sethupathy et al., 2022). Nevertheless, numerous value-added chemicals and fuels have been identified as potential value-creating lignin-derived products (Parthasarathi et al., 2011; Kellock et al., 2019; Ponnusamy et al., 2019).

1.3 Enzymatic depolymerization of cellulose in lignocellulosic biomass

Conversion of lignocellulosic biomass to a fermentation product such as ethanol ("biofuel") involves five main steps, namely collection and delivery of feedstock to the plant, pretreatment of the feedstock (at the point of collection or on-site), enzymatic saccharification, fermentation, and product formulation (**Figure 6**). In order to make the process viable, all these steps must be considered from an economic point of view, with primary focus on feedstock handling, pretreatment and enzyme efficiency, and enzyme costs (Wingren et al., 2003; Adav et al., 2011). The principles of enzymatic hydrolysis of cellulose are the primary focus of this thesis, with a special emphasis on the role of lytic polysaccharide monooxygenases (LPMOs). Common biomass pretreatment technologies are also briefly discussed.

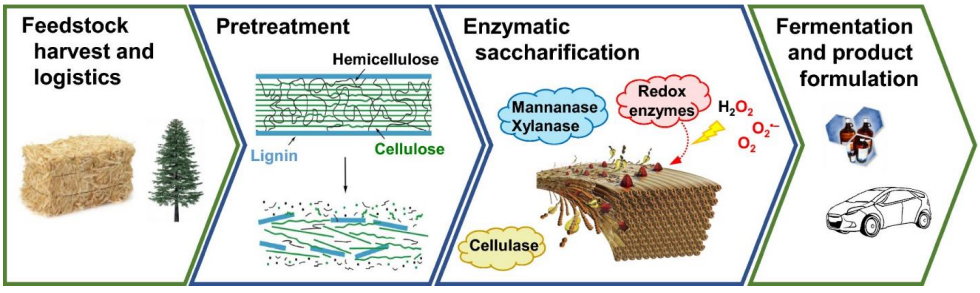

Figure 6. The main steps of the conversion of lignocellulosic biomass to ethanol. Depending on the choice of microorganism in the fermentation step, a range of different fuels and chemicals may be produced. The figure was reproduced from (Østby et al., 2020).

1.3.1 Biomass pretreatment

Multiple pretreatment technologies are available to enhance accessibility of lignocellulosic biomass to enzymes and hence promote cellulose saccharification, as reviewed by (Yang and Wyman, 2008), (Sun et al., 2016) and (Cantero et al., 2019). These methods include wet oxidation (Schmidt and Thomsen, 1998), hydrothermal pretreatment (Petersen et al., 2009), steam explosion (Brownell and Saddler, 1987; Pielhop et al., 2016), dilute acid treatment (Nguyen et al., 2000), ammonia fiber expansion (Balan et al., 2009), sulfite pulping (Wang et al., 2009; Rødsrud et al., 2012), and methods based on the use of ionic liquids and organic solvents (Zhou et al., 2018). Several of these have been used at demonstration or industrial scale in recent years. The choice of pretreatment method depends on the type of feedstock as well as on the spectrum of desired end products (Rødsrud et al., 2012; Duwe et al., 2019).

Hydrothermal pretreatment, ammonia fiber expansion, and ammonium recycle percolation technologies cause cellulose decrystallization, some hydrolysis of hemicellulose, as well as lignin removal (Bals et al., 2010), and are primarily used for grass-type biomass (e.g. corn stover, switch grass). Pretreatment methods such as steam explosion and alkaline and sulfite pulping can also be used for woody biomass (e.g. poplar and spruce). Recent improvements in pretreatment technologies include combined removal of lignin and hemicellulose prior to mechanical refining (Chen et al., 2014; Wu et al., 2019; Kuhn et al., 2020), restructuring native cellulose to the more accessible polymorph cellulose III in a low-moisture extractive ammonia process (da Costa Sousa et al., 2016), and the use of biomass-derived solvents for biomass pretreatment (Luterbacher et al., 2014; Socha et al., 2014; Kim et al., 2019). A key target in the development of pretreatment technologies is to maximize cellulose hydrolyzability, while conserving the value of other biomass components and avoiding formation of compounds that may inhibit downstream fermentation processes (e.g. acetic acid, uronic acid, and formic acid released from the degradation of hemicelluloses) (Jönsson and Martín, 2016).

While some pretreatment technologies aim to increase plant cell wall accessibility via reorganization of plant cell wall polymers without removal of matrix polymers (e.g. ammonia fiber expansion and ammonium recycle percolation), other technologies increase enzymatic accessibility of cellulose via fractionation of the biomass by separating lignin (e.g. alkali and sulfite pulping), hemicellulose (e.g. steam explosion), or both (e.g. ionic liquid or organosolv pretreatment, or sulfite pulping) from cellulose. The impact of each of these technologies on cellulose crystallinity varies.

Although true fractionation of biomass into its main, undamaged constituents would seem beneficial for downstream processing, detailed analysis of several types of pretreated biomass using glycome profiling and immunolabeling of plant cell wall polymers has indicated that no one pretreatment technology can completely separate cellulose from the other cell wall polymers (DeMartini et al., 2011; Pattathil et al., 2015; Zhang et al., 2018; Avci et al., 2019). Indeed, studies on the optimization of enzyme cocktails for biomass saccharification have revealed the need for a wide-spectrum enzyme cocktail, including cellulases and hemicellulases, and have shown that the composition of the optimal enzyme cocktail depends on pretreatment and biomass type (Banerjee et al., 2010; Kallioinen et al., 2014; Chylenski et al., 2017a).

1.3.2 Classification of enzymes involved in microbial biomass degradation

Carbohydrate-active enzymes within the scope of lignocellulose degradation encompass a vast range of cellulolytic and hemicellulolytic enzymes. Collectively, these enzymes (and those active on non-lignocellulosic polysaccharides, such as chitin or starch) are referred to as CAZymes (carbohydrate-active enzymes) and are compiled in the CAZy database (http://www.cazy.org). The CAZy database currently contains five separate enzyme classes and one class of associated modules. The module and enzyme classes are further organized into families based on sequence similarity (Drula et al., 2022). Two of the CAZy enzyme classes (glycoside hydrolases and auxiliary activities) are discussed in detail in sections

1.3.3 and 1.3.4, respectively. The remaining enzyme classes in the CAZy database include glycosyltransferases, which catalyze the formation of glycosidic bonds (Lairson et al., 2008), polysaccharide lyases, which perform non-hydrolytic, "eliminase-type" cleavage of specific glycosidic bonds in uronic-acid-containing polysaccharides (Linhardt et al., 1986), and carbohydrate esterases, which remove ester-linked methyl and acetyl substitutions from polysaccharides (Sista Kameshwar and Qin, 2018). The class of associated modules contains carbohydrate-binding modules (CBMs), non-catalytic domains frequently found attached to CAZymes that help bring the catalytic domain of the enzyme into close proximity with the substrate (Boraston et al., 2004). From an applied perspective, recent studies have shown that the advantage conferred to an enzyme carrying a CBM in terms of improved substrate binding decreases proportionally with increasing substrate concentration to the extent that the presence of a CBM may become unfavorable at high substrate concentrations (Várnai et al., 2013; Pakarinen et al., 2014; Jensen et al., 2018).

While lignocellulolytic activity has been observed in many realms of life, including in bacteria, archaea, algae, oomycetes, fungi, mollusks, insects, and crustaceans (Cragg et al., 2015), the majority of lignocellulose deconstruction is performed by aerobic and anaerobic bacteria, and filamentous fungi (Bomble et al., 2017). These microorganisms have evolved three central mechanisms to degrade lignocellulosic biomass, differing primarily in the way in which the hydrolytic enzymes come into contact with their natural substrate(s).

1.3.2.1 Free enzymes

In a common paradigm for fungal and bacterial lignocellulolytic degradation, so-called free enzymes are secreted into the environment where they can act upon relevant substrates (Bomble et al., 2017). This model of lignocellulose degradation is utilized by aerobic bacteria and fungi, and is well-studied in e.g. the filamentous fungus *Trichoderma reesei* (Bischof et al., 2016) and in the thermophilic soil bacterium *Thermobifida fusca* (Wilson, 2004).

Free enzymes secreted by a single microorganism (which are part of its secretome) are tailored to work together synergistically to degrade different components of lignocellulosic biomass. **Figure 7** shows a comprehensive overview of various types of reactions occurring during the degradation of lignocellulose, and the enzyme types that may be involved. In general terms, when depolymerizing polysaccharides such as cellulose, hydrolytic endo-acting enzymes (endoglucanases) cleave glycosidic bonds within amorphous regions of cellulose chains, creating new chain ends. Exo-acting cellulases (cellobiohydrolases) act on reducing or non-reducing cellulose chain ends, including those generated by endo-acting hydrolases, and depolymerize the cellulose chains processively, releasing short oligomers. Resulting cello-oligosaccharides (primarily cellobiose) are subsequently cleaved by β-glucosidases, generating monomeric sugars that can readily be taken up by microorganisms and used in metabolic processes (Kostylev and Wilson, 2012; Payne et al., 2015).

Importantly, a recently discovered group of oxidative enzymes known as lytic polysaccharide monooxygenases (LPMOs) also plays a role in depolymerization of the cellulose polysaccharide by catalyzing the cleavage of glycosidic bonds at crystalline surfaces of the cellulosic substrate. In doing so, LPMOs contribute synergistically to substrate depolymerization by creating new binding targets for hydrolytic enzymes (Vaaje-Kolstad et al., 2005a; Harris et al., 2010; Vaaje-Kolstad et al., 2010; Horn et al., 2012). Of note, when cellulose is complexed with hemicellulose and lignin, as in lignocellulosic biomass, alternate enzyme types are also required for comprehensive substrate degradation, including hemicellulolytic enzymes active on xylan and mannan (Bhattacharya et al., 2015), and oxidoreductases able to act on lignin, such as laccases and peroxidases (Silva et al., 2021) (**Figure 7**). Hemicellulases and non-LPMO oxidoreductases are discussed in sections 1.3.3.2 and 1.3.4.6, respectively.

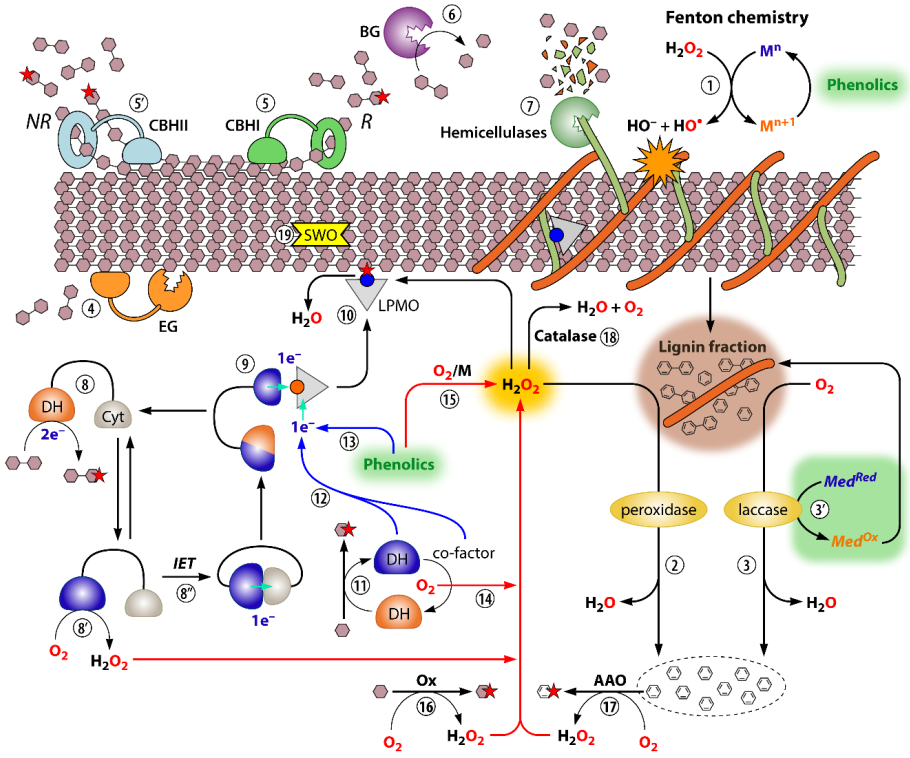

Figure 7. An overview of reactions that may occur during depolymerization of lignocellulose. Steps 1, 2, and 3 illustrate the modification and depolymerization of the lignin fraction. Step 1 shows the generation of hydroxyl radicals by non-enzymatic Fenton chemistry involving transition metals (M), traditionally performed by brown-rot fungi, while steps 2 and 3 show the lignin activity of peroxidases and laccases, respectively. The oxidization of mediators (Med), which can contribute to lignin modification, is also shown for laccases (step 3'). The activities of hydrolytic cellulose-degrading enzymes are shown in steps 4, 5, 5', and 6. Endoglucanase (EG) activity is shown in step 4, where the enzyme cleaves glycosidic bonds within a cellulose chain (endo-acting). Steps 5 and 5' illustrate cellobiohydrolase I (CBHI) and II (CBHII) activity. These are hydrolytic enzymes which respectively degrade cellulose chains from the reducing (R) and non-reducing (NR) ends, releasing oligomers with a low degree of polymerization, primarily cellobiose. These products are cleaved to D-glucose by β-glucosidase (BG), shown in step 6. Note that oxidative LPMO activity within cellulose chains will also result in hydrolytic enzymes releasing short-chain oxidized products, indicated with a red star. Hemicellulolytic hydrolases depolymerize the hemicellulose fraction, shown in step 7. Steps 8, 8', and 8" show the oxidation of cello-oligosaccharides by the dehydrogenase (DH) domain of cellobiose dehydrogenase (CDH), the use of the acquired electrons to generate H_2O_2 from O_2, or the transfer of these electrons to the CDH cytochrome domain (Cyt), respectively.

Step 8" illustrates that reducing power required to catalytically activate LPMOs can be acquired from numerous sources, as also shown in steps 9, 11, 12, and 13. In step 9, the reducing power comes from the cytochrome domain attached to the dehydrogenase, whereas steps 11 and 12 show the acquisition of reducing power from a single-domain dehydrogenase, which can reduce the LPMO through its co-factor. In step 13, reducing power for the LPMO comes from reduced phenolics. Once reduced, and in the presence of a co-substrate (H_2O_2 or O_2), LPMOs can oxidize cellulose within a cellulose chain (step 10). Steps 14-17 illustrate various ways in which H_2O_2 can be generated within the reaction system, including via reactions involving O_2 and single-domain dehydrogenases (step 14) or phenolics (step 15), or via oxidation of carbohydrate-derived compounds by oxidases (step 16), such as glucose oxidase. H_2O_2 can also be generated by the oxidation of lignin-derived products via the action of aryl-alcohol oxidases (AAO) (step 17). Excess H_2O_2 within the system is consumed by catalases (step 18). Finally, expansins/swollenins (SWO) may also contribute to lignocellulose depolymerization by disrupting cellulose (step 19) and hemicellulose structures. Steps 4-7 and step 10 illustrate primary activities relevant to the scope of this thesis, and are discussed in more detail in the main text. The figure was reproduced from (Bissaro et al., 2018b).

1.3.2.2 Cellulosomes

Another depolymerization strategy commonly observed among anaerobic fungi and bacteria acting on lignocellulosic biomass are cellulosomes, complexes consisting of a "molecular scaffold" with carbohydrate-active enzymes displayed on its surface. The scaffold, known as a scaffoldin subunit, may be tethered to the surface of the microorganism, and carries multiple catalytic modules (enzymes) as well as a carbohydrate-binding module. In contrast to the free enzyme strategy, polysaccharide degradation via cellulosomes is normally reliant on the organism being in direct physical contact with its substrate (Alves et al., 2021).

1.3.2.3 Polysaccharide utilization loci

The term polysaccharide utilization loci (PULs) refers to gene clusters within the genomes of anaerobic members of the *Bacteriodetes* phylum that encode enzymes required for depolymerization of complex carbohydrates. Genes within PULs are co-regulated, and the proteins they encode are transported to and organized within the outer membrane and the

plasma (inner) membrane. In this arrangement, enzymes located within the outer membrane can perform initial hydrolysis of the substrate to produce oligomers. These short-chain polysaccharides are then transported into the periplasmic space between membranes where further degradation occurs (Hemsworth et al., 2016; Grondin et al., 2017).

1.3.3 Glycoside hydrolases

It was first postulated in 1950 by Reese *et al.* that cellulose degradation occurs via a two-step process. The first step was suggested to be the conversion of crystalline cellulose to shorter, more accessible chains by a component described as C_1. The second step was described as the conversion of this more accessible cellulose to oligomers and monomers by another component known as C_x (Reese et al., 1950). Over the years, the quest towards the isolation and identification of the C_1 and C_x components in fungal secretomes led to the identification of a core set of fungal cellulose-active glycoside hydrolases (GHs). The primary function of GHs is to perform selective hydrolysis of glycosidic bonds (Davies and Henrissat, 1995). At the time of writing, the CAZy database GH class of enzymes contained 173 families. GH activity has been demonstrated on a wide range of carbohydrates, including amorphous and crystalline cellulose, hemicelluloses, pectin, starch, and chitin. In the sub-sections below, GHs with cellulolytic or hemicellulolytic activity are discussed.

1.3.3.1 Cellulases and cellulase cocktails

Cellulose-active glycoside hydrolases can be classified into endoglucanases (EGs), cellobiohydrolases (CBHs), and β-glucosidases (BGs). As previously mentioned, the respective roles of EGs and CBHs are to cleave cellulose chains within non-crystalline regions, and to cleave off cellobiose or cello-oligomers from reducing or non-reducing cellulose chain ends. BGs depolymerize soluble cello-oligosaccharides liberated by CBHs and EGs (Wood, 1985). BG action is important in cellulose degradation, as cellobiose is an end-product inhibitor of CBHs (Sternberg et al., 1977).

Cellulose-active microorganisms often produce different kinds of GHs from various families. As an example, the model organism *T. reesei* secretes two CBHs (*Tr*Cel7A, a reducing end-specific CBH, and *Tr*Cel6A, a non-reducing end-specific CBH), four EGs (*Tr*Cel7B, *Tr*Cel5A, *Tr*Cel12A, and *Tr*Cel45A), and four BGs (*Tr*Cel3A, *Tr*Cel3B, *Tr*Cel3F, and *Tr*Cel3G) (Martinez et al., 2008; Adav et al., 2012). Two additional enzymes in the *T. reesei* secretome were initially annotated as EGs (*Tr*Cel61A and *Tr*Cel61B), but it is now clear that these enzymes are, in fact, LPMOs, discussed in section 1.3.4.

Since the postulation of the C_1–C_x theory for cellulose depolymerization, the nature of the C_1 factor has been interpreted in many ways. For example, CBHs were originally presumed to act as the C_1 factor (Halliwell and Griffin, 1973). CBHs are exo-acting GHs that have a characteristic tunnel-shaped active site, enabling them to thread the cellulose chain while processively cleaving glycosidic bonds. Processivity is a key attribute of CBHs that makes them especially powerful in depolymerizing the highly compact structure of crystalline cellulose (Teeri et al., 1998; Beckham et al., 2014; Vermaas et al., 2019). On the other hand, processivity leads to stalling of CBHs when their path is blocked by other enzymes or substrate-derived obstacles (Igarashi et al., 2011; Kurasin and Väljamäe, 2011; Cruys-Bagger et al., 2012; Fox et al., 2012; Jalak et al., 2012). It is believed that through their hydrolytic action, EGs may be able to assist "blocked" CBHs, enabling them to continue the processive depolymerization of cellulose chains (Jalak et al., 2012; Hemsworth et al., 2016). Of note, early work on processive chitinases illustrated that the processivity of enzymes such as CBHs is accompanied by these enzymes being "sticky" (i.e. having low off-rates), and that as a consequence, these enzymes are rather slow (Horn et al., 2006). It has been suggested that CBHs can break non-covalent linkages between adjacent chains in crystalline cellulose since they thread single cellulose chains into their active site cleft and, thus, are potentially capable of extracting a longer piece of cellulose chain out of its crystalline context (Ghattyvenkatakrishna et al., 2013; Knott et al., 2014b). Such a function would indeed resemble the "decrystallization" function implied by Reese *et al.* when proposing the C_1-C_x theory. The CBH *Tr*Cel7A is the most abundant enzyme in the *T. reesei* secretome (Gritzali and Brown, 1979), and harbors a long substrate-binding tunnel, enabling strong interactions with a single cellulose chain and contributing to the processive

action of this enzyme (Beckham et al., 2014; Knott et al., 2014a; Knott et al., 2014b). Despite the undoubtedly crucial role of CBHs in cellulose depolymerization, today, LPMOs are generally considered to be the C_1 component proposed by Reese *et al.*

To gain a deeper understanding of the mechanisms behind enzymatic biomass decomposition, individual enzymes have been studied alone and in combination with other enzymes, cellulase cocktails, or fungal secretomes. Synergism (i.e. the concomitant action of two enzymes resulting in a higher yield than the yield obtained from adding individual enzyme contributions) between EGs and CBHs acting on cellulose was demonstrated by Henrissat and colleagues in 1985 (Henrissat et al., 1985), and has been extensively studied (Nidetzky et al., 1994; Väljamäe et al., 1999; Jalak et al., 2012; Olsen et al., 2017). Other types of synergy are also well-documented, such as synergy between cellulases and hemicellulases, and between cellulases and LPMOs.

Most commercial cellulase cocktails used in industrial saccharification of lignocellulosic biomass are fungal-derived because several fungi are efficient degraders of plant biomass and may show high production levels of catalytically efficient cellulases (Payne et al., 2015). In addition, fungi secrete lignocellulose-degrading enzymes into the medium, enabling easy separation from the producing organism (Merino and Cherry, 2007). Many cellulase cocktails are based on the secretome of *T. reesei*. Importantly, secretomes differ between fungal species and even between fungal strains, and vary considerably depending on the carbon source used when growing the fungus (Adav et al., 2011; Poidevin et al., 2014; Bengtsson et al., 2016). This variation must be considered when searching for natural enzymes or secretomes for the conversion of biomass. Importantly, lignocellulosic feedstocks may be pretreated in different manners, and the pretreatment will affect the nature of the optimal enzyme cocktail for subsequent saccharification (as illustrated in Paper II of this thesis). Throughout the years, individual components of enzyme cocktails have been the subject of enzyme improvement (Percival Zhang et al., 2006), either through screening for novel enzymes from alternative organisms (e.g. (Rosgaard et al., 2006; Suda et al., 2014)), or by applying enzyme engineering technologies (e.g. (Day et al., 2004; Scott et al., 2010)). Work done on commercial enzymes is not generally known to the public, and

it is not clear what types of improvements have been made to the cellulases present in modern commercial cellulolytic enzyme cocktails. Typical targets for improvement of individual cellulases may include increased hydrolytic efficiency and/or stability at process conditions, reduced end-product inhibition, and reduced lignin binding.

Notable examples of commercial cellulase cocktails include the *T. reesei*-derived Celluclast 1.5 L (which lacks adequate BG activity, as demonstrated by (Rosgaard et al., 2006)) and Cellic CTec2, both produced by Novozymes, and Accellerase 1500, produced by DuPont. As reviewed in (Bischof et al., 2016), *Trichoderma reesei* was discovered by researchers at the Natick Army Research Laboratories during World War II. Screening of 14,000 molds isolated from rotting cellulose-based army equipment in the Solomon Islands for the ability to degrade crystalline cellulose resulted in the identification of the renowned ancestor of all current commercial *T. reesei* strains, QM6a. Random mutagenesis of the *T. reesei* strain QM6a led to the *T. reesei* strain RUT-C30, which is the prototype hyperproducer of cellulases and is commercially available (Peterson and Nevalainen, 2012; Bischof et al., 2016). Decades of genetic engineering of *T. reesei* has resulted in detailed knowledge of regulators and transcription factors involved in enzyme expression, which has contributed to the generation of novel cellulase hyperproducing mutants. While *T. reesei* has played a vital role in the history of understanding and exploiting natural lignocellulose-degrading enzyme systems, other filamentous fungal species, including *Aspergillus* sp., *Neurospora crassa*, and *Myceliophtora thermophila*, have also been studied in detail (de Vries, 2003; Dunlap et al., 2007; Visser et al., 2011), and may provide useful sources of enzymes, or be developed as expression hosts for production of individual enzymes or cellulase cocktails.

While still based on the original *T. reesei* secretome, modern commercial cellulase cocktails will contain engineered variants of the original cellulases, as well as novel enzymes for which genes have been inserted into the genome, such as LPMOs. Expression of recombinant proteins in filamentous fungi is traditionally based on the use of native expression systems, using innate transcriptional regulators and promoters. Transcriptional regulatory systems have been studied in a variety of filamentous fungi, and it has become clear that these systems are not widely conserved. Hence, knowledge of these systems is

often not transferrable from one host organism to another, which is one of the reasons why the development of new filamentous fungal expression hosts is relatively slow (Fitz et al., 2018; Mojzita et al., 2019). For species such as *T. reesei*, *Aspergillus niger*, and *Aspergillus oryzae*, important regulatory systems are well-explored (Mojzita et al., 2019). In addition, relevant transcriptional regulators have been studied to varying extents for *N. crassa*, *M. thermophila*, and *Thermoascus aurantiacus* (Visser et al., 2011; Craig et al., 2015; Schuerg et al., 2017).

Of note, recent work by Singer and colleagues has demonstrated that *T. aurantiacus* has promising potential to become a thermophilic fungal expression host. *T. aurantiacus* secretes a limited number of plant cell wall-degrading enzymes, and the natural secretome, despite being relatively simple, has high efficiency in biomass hydrolysis. It is worth noting that *T. aurantiacus* secretes a high proportion of the well-studied LPMO *Ta*LPMO9A (previously *Ta*GH61A) (Langston et al., 2011; Quinlan et al., 2011; McClendon et al., 2012; Müller et al., 2015; Schuerg et al., 2017; Petrović et al., 2018), which may very well be one of the central LPMOs in commercial cellulase cocktails, although this is not known. Paper II of this thesis describes a study comparing the efficiency of a *T. aurantiacus* cellulase cocktail with the commercial cellulase preparation Cellic CTec2 in saccharification of sulfite-pulped spruce and steam-exploded birch at high temperature and high substrate loading. Although thermostable enzymes have clear advantages in industrial settings, no thermostable cellulase cocktails are currently available commercially (Patel et al., 2019).

1.3.3.2 Hemicellulases

Depending on the type of biomass and pretreatment technology, in addition to cellulose, pretreated biomass contains varying amounts of linear and branched polysaccharides, including the hemicelluloses xylan, glucomannan, and xyloglucan, as well as pectin, all of which adhere to cellulose fibers (Somerville et al., 2004). The most well-studied hemicellulases are xylan- and glucomannan-specific enzymes, including GHs that cleave the polysaccharide main chain (xylanases and mannanases), as well as debranching GHs that

remove substitutions from the polysaccharide backbone (Malgas et al., 2015; Malgas et al., 2019).

Considering the complexity of hemicelluloses, many different types of hemicellulases can potentially contribute to biomass saccharification. Contributions can be in the form of generating more fermentable sugar through saccharification of the hemicelluloses, and/or by removing hemicelluloses that hamper cellulose depolymerization. As to the role of hemicellulases in promoting cellulose hydrolysis, the latter being the main topic of this thesis, several examples showing a beneficial effect of hemicellulase activity on cellulose saccharification can be found in literature, as reviewed in (Bhattacharya et al., 2015). Synergism of enzymes acting on different plant cell wall components was described already in the late 1990s for cellulases and xylanases acting on birch kraft pulp, and for cellulases, xylanases, and mannanases acting on spruce kraft pulp (Tenkanen et al., 1999). More recently, in a study using commercial enzyme preparations, Hu *et al.* showed that replacement of small amounts of the commercial cellulase preparation Celluclast 1.5 L with the commercial xylanase preparation Multifect Xylanase significantly increased both cellulose and xylan hydrolysis yields for steam-exploded corn stover, due to the synergistic action of cellulases and xylanases (Hu et al., 2011). By replacing approximately 14% of the total enzyme loading with the xylanase blend, cellulose and xylan yields were improved by approximately 14% and 18%, respectively, without requiring an increase in total enzyme loading. Furthermore, using a fiber quality analyzer, which enables detection of changes in fiber properties of residual substrate following hydrolysis, Hu and co-workers demonstrated that the concomitant action of xylanases and cellulases resulted in increased fiber fragmentation as compared to reactions with Celluclast 1.5 L alone. Thus, hydrolysis of xylan improved the accessibility of the cellulose for the cellulases in the commercial preparation.

In another early example, Qing and Wyman demonstrated that addition of Multifect Xylanase and a commercial β-xylosidase preparation to a mix of the commercial cellulase cocktail Spezyme Cellulase and Novozyme 188 β-glucosidase improved glucan and xylan hydrolysis of ammonia fiber expansion-pretreated corn stover by nearly 30% and 25%,

respectively (as compared to yields obtained when using only the cellulase mix) (Qing and Wyman, 2011). The boosting effect of adding xylanases to the cellulase blend was not observed in hydrolysis of Avicel, and was small when using dilute acid-pretreated corn stover. These differences can be explained by the properties of the cellulosic substrate. Avicel consists of pure microcrystalline cellulose and does not contain any hemicellulose fractions. Dilute acid pretreatment, in contrast to ammonia fiber expansion pretreatment, results in low amounts of residual hemicellulosic sugars in the substrate (Yang and Wyman, 2009). It is clear that, as previously discussed, the composition of the lignocellulosic biomass and the choice of pretreatment significantly impact the enzyme cocktail required for its optimized depolymerization. For a particular feedstock, it is therefore essential to identify key plant cell wall components that may hinder access to cellulose and other plant cell wall polysaccharides and to identify the corresponding CAZymes that cleave these, as synergistic action of multiple enzyme types is essential to achieve maximum saccharification.

To cope with the variation of hemicellulose types and contents in a range of industrially-relevant biomasses, several enzyme companies have developed hemicellulolytic preparations, such as the Cellic HTec series produced by Novozymes, or Accellerase XC produced by DuPont. These may be used to supplement base cellulolytic preparations such as those described in section 1.3.3.1.

Of note, some EGs (and certain LPMOs) may also contribute to hemicellulose conversion because they are capable of cleaving the polysaccharide backbones of hemicellulosic polysaccharides, including xyloglucan, xylan, and/or glucomannan. For so-called promiscuous EGs, this has been demonstrated by, for example, Vlasenko and co-authors, who showed xylan activity for multiple family 7 EGs, and by Mikkelson and colleagues, who observed significant mannanase activity for *Tr*Cel5A (Vlasenko et al., 2010; Mikkelson et al., 2013). Examples of LPMOs potentially contributing to hemicellulose depolymerization are discussed in section 1.3.4.2.

1.3.4 Auxiliary activities and lytic polysaccharide monooxygenases

The Auxiliary Activities (AA) class of the CAZy database contains 17 families, and comprises LPMOs and redox-enzymes that act in concert with CAZymes, such as lignin-active enzymes (Levasseur et al., 2013). LPMOs are found in families AA9-11 and AA13-17. Fungal LPMOs are found in families AA9-11, AA13-14, and AA16. Of note, fungal LPMOs of the AA10 type are very rare and, while bacterial AA10s have been intensely studied, none of the putative fungal AA10s have been characterized. As LPMOs (and, in particular, AA9s) are central to the research described in this thesis, the following sections will primarily focus on these LPMOs, discussing the history of their discovery, substrate specificities, structural features, catalytic mechanism, applications in industrial conversion of biomass, oxidative regioselectivity, and methods for detection and analysis of their products. Section 1.3.4.6 will briefly touch upon other oxidoreductases, some of which may be relevant for understanding and optimizing LPMO reactions, such as glucose oxidase.

1.3.4.1 Historical perspective

Following the C_1-C_x hypothesis for cellulose degradation postulated in 1950 (Reese et al., 1950), for decades, cellulose depolymerization was presumed to primarily occur via the action of hydrolytic enzymes. It was not until 1974 that preliminary evidence for the participation of redox enzymes in cellulose degradation came to light. By comparing the hydrolysis of powdered cellulose by a fungal secretome and isolated GHs from the same secretome, Eriksson and co-workers noted a significant increase in cellulose hydrolysis when the complete fungal secretome was used. This led the authors to assume that an alternate enzyme necessary for cellulose hydrolysis was present in the secretome. Furthermore, in the same study, Eriksson and colleagues observed a significant decrease in substrate degradation when cellulose hydrolysis was performed by the same secretome under anaerobic conditions, indicating that the additional enzyme used an oxidative mechanism to depolymerize the substrate. In retrospect, this study provided an early indication of the role of LPMOs in cellulose degradation (Eriksson et al., 1974).

In spite of these early observations, it took many years for the true nature of LPMOs to be uncovered. In the 1990s and early 2000s, several proteins now known to be LPMOs were being discovered and characterized, but were classified either as family 33 carbohydrate-binding modules (CBM33) (at the time referred to as chitin-binding proteins (CBPs), as many were found to bind to chitin) (Schnellmann et al., 1994; Kolbe et al., 1998; Suzuki et al., 1998; Saito et al., 2001) or as hydrolytic endoglucanases with notably low activity (GH61s) (Raguz et al., 1992; Armesilla et al., 1994; Karlsson et al., 2001). In 2005, Vaaje-Kolstad and colleagues obtained the first crystal structure of a CBM33 protein. This protein, CBP21 (also known as *Sm*LPMO10A or *Sm*AA10A), is secreted in large amounts along with hydrolytic chitinases by the gram-negative bacterium *Serratia marcescens* when grown on chitin (Suzuki et al., 1998). Surprisingly, the crystal structure of CBP21 showed that conserved aromatic amino acids, previously assumed to be essential for binding of CBM33 proteins to chitin, were located within the protein core. Additionally, the authors noted that CBP21 had a flat surface with multiple highly conserved, primarily hydrophilic residues (Vaaje-Kolstad et al., 2005b). In the same year, Vaaje-Kolstad and colleagues showed that CBP21 was essential for efficient chitin degradation. In a seminal study, the authors demonstrated that the inclusion of CBP21 in reactions of chitinases acting on insoluble crystalline chitin strongly promoted substrate degradation. It was also shown that mutations of the polar residues of the protein surface did not affect the ability to bind to chitin, but negatively influenced the ability of CBP21 to boost chitinase activity. While CBP21 was still presumed to be non-catalytic, it was clear that this protein significantly contributed to chitin depolymerization in conjunction with hydrolytic chitinases (Vaaje-Kolstad et al., 2005a).

Similar observations made for several GH61 proteins were described by Merino and Cherry in 2007. The authors found that supplementation of Celluclast 1.5 L with various GH61s from the secretome of the cellulolytic fungus *Thermothielavioides terrestris* (syn. *Thielavia terrestris*) in saccharification of acid-pretreated corn stover led to significantly increased cellulose conversion, indicating synergistic effects between the GH61s and the hydrolases in Celluclast 1.5 L. Notably, inclusion of *T. terrestris* GH61s in reactions of Celluclast 1.5 L with pure cellulosic substrates such as Avicel and PASC did not result in enhanced cellulose

degradation, leading the authors to speculate that the ability of GH61s to boost cellulolytic activity is dependent on the presence of non-cellulosic components within the substrate, such as lignin or hemicellulose (Merino and Cherry, 2007). These substrate-dependent differences in the ability of GH61 proteins to increase cellulose depolymerization would later be attributed to the presence of lignin in the acid-pretreated corn stover, much as the authors predicted. The first crystal structure of a GH61 (at the time known as Cel61B from *Hypocrea jecorina*, syn. *T. reesei*) was solved in 2008 by Karkehabadi and colleagues, who observed that Cel61B had highly conserved polar residues on its surface, which lacked the classical substrate-binding cleft and active site residues of EGs and was instead mostly flat. Importantly, the authors noted the resemblance of the GH61 structure with that of CBP21 (Karkehabadi et al., 2008). Today, Cel61B is known as *Tr*LPMO9A.

Another important piece of the puzzle was elucidated by Harris *et al.* in 2010, who showed that the ability of GH61 proteins to enhance cellulose hydrolysis was dependent on the presence of divalent metal ions. By adding GH61 from *T. aurantiacus* or from *T. terrestris* to a *T. reesei* cellulase mixture and assessing cellulose hydrolysis of acid-pretreated corn stover in the presence of various divalent metal ions, Harris and co-workers showed that saccharification was considerably boosted in the presence of several of the tested metal ions. The ions tested were Ca^{2+}, Co^{2+}, Mg^{2+}, Mn^{2+}, and Ni^{2+}, and all were reported to have similar effects. The authors reasoned that two conserved histidine residues were likely involved in metal binding, as point mutations of these resulted in inactive GH61s. Solving the structure of GH61E from *T. terrestris* showed that in addition to having a relatively flat surface, it did not contain the conserved catalytic acid residues necessary for traditional hydrolytic polysaccharide cleavage, further supporting the notion that GH61 proteins were not hydrolytic GHs (Harris et al., 2010).

A breakthrough occurred in 2010, when, in a landmark publication, Vaaje-Kolstad *et al.* showed that CBM33 proteins were in fact enzymes capable of oxidative polysaccharide degradation. Using newly developed chromatographic and mass spectrometry methods enabling oxidized product identification and quantification, Vaaje-Kolstad and colleagues showed that incubation of CBP21 with chitin generated products carrying an oxidized sugar

unit on one end, and, notably, that many of these products were longer oligosaccharides, indicative of an "endo-type" activity. The authors also found that supplementing the reaction with a reductant significantly boosted the reaction efficiency, and, by performing experiments under anaerobic conditions, showed that O_2 was required for CBP21 activity. The authors pointed out that based on the above-mentioned structural and functional similarities, GH61s were also likely to be oxidative enzymes (Vaaje-Kolstad et al., 2010).

These findings were followed by the discoveries of oxidative cleavage of cellulose by another CBM33 enzyme (Forsberg et al., 2011), and by several GH61s (Langston et al., 2011; Phillips et al., 2011; Quinlan et al., 2011; Westereng et al., 2011; Beeson et al., 2012). Notably, the studies by Quinlan *et al.* and Phillips *et al.* uncovered that LPMOs are mono-copper enzymes, and that the copper ion is coordinated by two conserved histidine residues, referred to as the histidine brace (Phillips et al., 2011; Quinlan et al., 2011).

Today, CBM33 and GH61 enzymes are called LPMOs, and have been reclassified as AA families 10 and 9, respectively, in the CAZy database (Levasseur et al., 2013). LPMOs are now generally considered to be the long sought-after C_1 factor postulated by Reese and colleagues (Reese et al., 1950; Vaaje-Kolstad et al., 2010; Horn et al., 2012; Morgenstern et al., 2014). This notion is supported by multiple studies showing that LPMOs from various AA families induce fibrillation of cellulose fibers (Villares et al., 2017; Hu et al., 2018; Valls et al., 2019).

1.3.4.2 Substrate specificity

Within the CAZy database, the AA9 family has the highest number of characterized enzymes (34 at the time of writing). AA9s have been found to display a wide range of substrate specificities, including on cellulose (as discussed in a historical context for GH61s above) and various hemicelluloses such as glucomannan, mixed-linkage glucan, and xyloglucan (Agger et al., 2014; Isaksen et al., 2014; Bennati-Granier et al., 2015; Cannella et al., 2016; Frommhagen et al., 2016; Kojima et al., 2016; Nekiunaite et al., 2016; Fanuel et al., 2017; Ladevèze et al., 2017; Simmons et al., 2017; Jagadeeswaran et al., 2018; Kadowaki et al.,

2018; Petrović et al., 2019; Monclaro et al., 2020; Frandsen et al., 2021) (Paper III of this thesis). Oxidative degradation of cellulose-associated xylan has also been demonstrated, and recent work shows that xylan activity may be quite significant for certain AA9 LPMOs (Frommhagen et al., 2015; Hüttner et al., 2019; Tõlgo et al., 2022) (Paper IV of this thesis). The xylan activity of these LPMOs has been observed only when xylan is complexed with cellulose. As discussed in section 1.2.2.1, a likely reason for the impact of association with cellulose is that insoluble forms of hemicelluloses associated with cellulose adopt different conformations than their soluble forms (Busse-Wicher et al., 2016a).

The AA10 family comprises LPMOs active on cellulose and chitin, and its members are primarily of bacterial origin as mentioned above, although some recent noteworthy exceptions exist, including the first LPMO isolated from a plant species (Yadav et al., 2019). At the time of writing, very few members of the remaining LPMO families had been functionally characterized. Some examples include AA11s active on chitin, including the recently studied *Af*AA11A and *Af*AA11B from *Aspergillus fumigatus* (Rieder et al., 2021a; Støpamo et al., 2021), AA13s active on starch, including *Nc*AA13 from *N. crassa* and *An*AA13 from *Aspergillus nidulans* (Vu et al., 2014b; Lo Leggio et al., 2015), two *Pycnoporus coccineus* (syn. *Trametes coccinea*) AA14s active on xylan (Couturier et al., 2018), and one cellulose-active AA16 from *Aspergillus aculeatus* (Filiatrault-Chastel et al., 2019). The AA15 family contains three characterized LPMOs, one of which is active on cellulose and chitin, and the other two of which are chitin-active. Two of these LPMOs were isolated from *Thermobia domestica*, a detritivorous insect, and the third was isolated from *Aphanomyces astaci*, an oomycete pathogen of crustaceans. Of note, the *T. domestica* LPMOs were the first to be isolated from a higher animal (Sabbadin et al., 2018; Sabbadin et al., 2021a). Finally, the AA17 family contains pectin-active LPMOs isolated from the oomycete plant pathogen *Phytophthora infestans* (Sabbadin et al., 2021b). A recent detailed overview of LPMO families and their substrate specificities appears in (Vandhana et al., 2022).

While the primary role of LPMOs has long been considered to be related to degradation of biomass polysaccharides, recent studies have indicated that these enzymes also have other biological functions, including as purported virulence factors of opportunistic pathogens

(Loose et al., 2014; Paspaliari et al., 2015; Agostoni et al., 2017; Li et al., 2020; Askarian et al., 2021; Sabbadin et al., 2021a; Sabbadin et al., 2021b). Further exploration of alternative LPMO functions is needed, and represents an exciting area of future research.

Further functional characterization of LPMOs will also aid in elucidation of the biological rationale for the multiplicity of LPMOs found in the genomes of fungi (Várnai et al., 2021). In-depth functional characterization of LPMOs in the context of depolymerization of complex biomass has become a reality due to significant efforts and developments in LPMO research over the past decade. Paper III of this thesis describes the functional characterization of *Sc*LPMO9A, an AA9 LPMO from the fungus *Schizophyllum commune*.

1.3.4.2.1 LPMOs active on soluble oligomeric substrates

In addition to the above-mentioned polysaccharide substrates, a number of LPMOs have also been shown to oxidize soluble cello-oligosaccharides (Isaksen et al., 2014; Bennati-Granier et al., 2015; Frandsen et al., 2016; Simmons et al., 2017; Jagadeeswaran et al., 2018; Kadowaki et al., 2018; Frandsen et al., 2021). Oxidative cleavage of soluble cello-oligosaccharides is demonstrated for *Sc*LPMO9A from *S. commune* in Paper III of this thesis.

Of note, activity on soluble chito-oligomers has also been demonstrated for CBP21 and for *Af*AA11B (Bissaro et al., 2018a; Rieder et al., 2021a). While CBP21 showed only very weak activity on chitohexaose, at high substrate concentrations, *Af*AA11B showed strong activity on chito-oligosaccharides with a DP between three and six, and interestingly, low activity on crystalline chitin.

As discussed above, organisms capable of degrading polysaccharide substrates such as complexes of cellulose and hemicellulose found in plant biomass often encode a range of CAZymes, including, for example, β-glucosidases and β-xylosidases. The role of these GHs is to cleave short oligomers generated by the actions of hydrolytic enzymes in collaboration with LPMOs. It is therefore unlikely that lignocellulolytic organisms have evolved specialized LPMOs for cleaving short oligomeric substrates. While the biological purpose of

cleavage of soluble oligosaccharides by LPMOs remains unclear, this ability has been very important in LPMO research because it has enabled structural characterization of LPMO-substrate complexes (Frandsen et al., 2016).

1.3.4.3 Structural features

X-ray crystallography studies have been paramount in establishing a general overview of LPMO structures and topology. While modeling and structural data continue to update our understanding of differences between LPMO families, and in particular, the ways in which structure may relate to function in terms of substrate specificity and oxidative regioselectivity, certain LPMO features are shared amongst all families. LPMOs may occur as single domain proteins or be multi-modular, containing CBMs, GH modules, and/or other modules, connected via linker regions (Mekasha et al., 2016; Mutahir et al., 2018; Tamburrini et al., 2021; Zhang et al., 2021b).

All LPMOs are characterized by the presence of two conserved catalytic histidines involved in coordination of a single copper ion, known as the histidine brace (Quinlan et al., 2011), which forms the solvent-exposed active site on the LPMO surface (**Figure 8**). The redox state of the copper ion, which changes from Cu(II) to Cu(I) during LPMO catalysis (section 1.3.4.4), changes the sphere in which it is coordinated (Vaaje-Kolstad et al., 2017). Of note, studies of divalent metal binding by CBP21 have shown that the histidine brace binds Cu(I) more tightly than Cu(II) (Aachmann et al., 2012). When the copper ion is in its reduced form (Cu(I)), the coordination sphere has a T-shaped geometry. In this three-coordinate copper coordination state, two nitrogen ligands are provided by the imidazole side chain and amino group of the conserved N-terminal histidine. In fungi, this histidine is post-translationally methylated, and this modification may be involved in protecting LPMOs from autocatalytic damage (Petrović et al., 2018). The imidazole group of a second conserved histidine contributes a third nitrogen ligand. Other central amino acids that are conserved in several LPMO families include a glutamine proximal to the active site, which, like its glutamate counterpart in AA10 LPMOs (Vaaje-Kolstad et al., 2005b; Bissaro et al., 2020), is essential for AA9 activity (Harris et al., 2010), and a conserved proximal axial

tyrosine (or phenylalanine) residue. This tyrosine, present in LPMOs from families 9, 11, and 13, is located within the protein core and helps shape the copper site, but is not usually considered to interact directly with the copper. The precise role of this tyrosine residue is debated, but a recent study has indicated that it may assist in protecting the active site from oxidation when the LPMO is not bound to substrate (Paradisi et al., 2019; McEvoy et al., 2021). Of note, most AA10 LPMOs have a phenylalanine in this position.

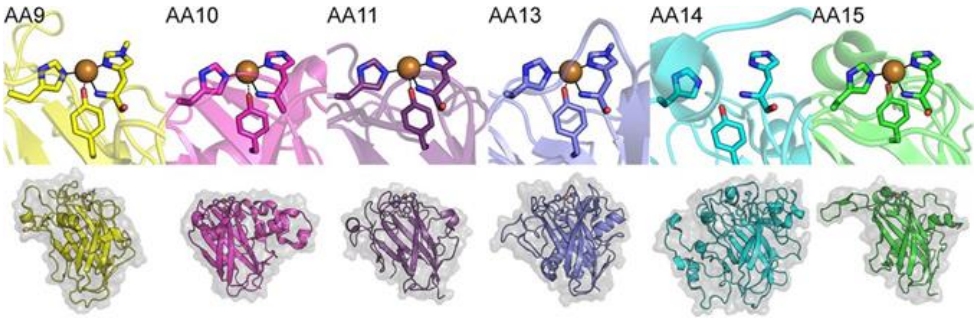

Figure 8. Surface topologies and active sites of representatives of LPMO families AA9-11 and AA13-15. The top row shows the characteristic histidine brace residues and the associated tyrosine (stick representation), replaced by a phenylalanine in most AA10 LPMOs. The copper atom is shown as an orange sphere for all LPMOs except *Pc*AA14, for which the structure was solved without copper (although copper-binding was demonstrated via electron paramagnetic resonance spectroscopy (Couturier et al., 2018)). The shared IgG-like fold and variation in surface topologies can be seen in the bottom row of the figure. Note that although not included in the figure, the structure of one AA17 LPMO from *P. infestans* has been solved (PDB code 6Z5Y) (Sabbadin et al., 2021b). PDB codes of the structures represented in the figure are 5ACH (AA9), 5OPF (AA10), 4MAI (AA11), 4OPB (AA13), 5NO7 (AA14), and 5MSZ (AA15). The figure was reproduced from (Tandrup et al., 2018).

An additional shared feature is the highly conserved LPMO core (**Figure 8**), comprised of an immunoglobulin G (IgG)-like β-sandwich, which consists of two β-sheets containing seven or eight β-strands. The β-strands are connected by loops of varying length and with varying content of short helices, which contribute to defining both the surroundings and plane of the substrate-binding surface of the LPMO. The variable loop regions are the major contributor to structural variety amongst LPMO surfaces and are likely important

determinants of LPMO substrate specificity (Li et al., 2012; Vu et al., 2014a; Beeson et al., 2015; Borisova et al., 2015; Vaaje-Kolstad et al., 2017). Fungal LPMOs generally contain several aromatic amino acids within these loop regions, the side chains of which are part of the substrate-binding surface. On the LPMO surface, these residues are separated by distances corresponding to the distance between monomers in the polysaccharide chains, indicating that they are involved in interactions with the substrate (Li et al., 2012; Wu et al., 2013).

Early crystal structures indicated that LPMOs primarily have an open and flat surface (Vaaje-Kolstad et al., 2005b; Karkehabadi et al., 2008), now known to enable binding to crystalline substrate surfaces (Vaaje-Kolstad et al., 2010; Aachmann et al., 2012; Eibinger et al., 2014). Generally, this rule remains true, as the majority of solved LPMO structures show flat binding surfaces where the active site and the polysaccharide substrate come into contact (Vaaje-Kolstad et al., 2017; Vandhana et al., 2022). However, newer solved structures have uncovered a certain degree of variability in substrate-binding surface topologies amongst different LPMO families, and it is believed that these differences likely correlate with variations in substrate specificity. For example, *Pc*AA14B, the only AA14 LPMO for which the structure is known, contains two distinct loops that create a rippled surface area, which likely contributes to its activity on xylan (Couturier et al., 2018; Tandrup et al., 2018). In addition, the active sites of starch-active AA13 LPMOs share a shallow groove-like shape, likely optimized for binding of the α-1,4-linked helical starch polysaccharide (Lo Leggio et al., 2015).

The first crystal structure of an LPMO complexed with a bound oligosaccharide was solved in 2016 for *Ls*LPMO9A from *Lentinus similis* (Frandsen et al., 2016), and enabled a detailed study of the primarily polar interactions between residues in and near the LPMO active site and the carbohydrate substrate. In the same year, Courtade and colleagues studying *Nc*LPMO9C interacting with soluble substrates by nuclear magnetic resonance (NMR) spectroscopy found that the substrate binding surface of this LPMO involves amino acids located in variable loop regions (Courtade et al., 2016). Accordingly, in a recent study of *Ls*LPMO9A and other AA9 LPMOs, Frandsen *et al.* concluded that two loop regions

containing polar amino acids play an essential role in the ability to oxidatively cleave soluble cellodextrins (Frandsen et al., 2021).

Elucidation of hemicellulose activities of several cellulose-active LPMOs has indicated that certain structural features are shared amongst LPMOs active on similar substrates, including features associated with the ability to cleave substituted hemicelluloses. Recent examples of publications that discuss these issues include (Lenfant et al., 2017; Simmons et al., 2017; Laurent et al., 2019; Monclaro et al., 2020; Sun et al., 2020; Frandsen et al., 2021). The ways in which structural elements can influence LPMO substrate specificity are also addressed in Paper IV of this thesis, which demonstrates xylanolytic activity of two AA9 LPMOs from *N. crassa*.

1.3.4.4 Catalytic mechanism

As soon as it became clear that LPMOs are oxidative enzymes capable of cleaving crystalline polysaccharides (Vaaje-Kolstad et al., 2010), the search for their catalytic mechanism was underway. As discussed above, subsequent studies by Quinlan *et al.* and Phillips *et al.* showed that LPMOs are copper-dependent redox enzymes and that the copper ion is coordinated within the histidine brace of the LPMO active site (Phillips et al., 2011; Quinlan et al., 2011). Based on the original findings by Vaaje-Kolstad and colleagues, LPMOs were classified as monooxygenases, oxidoreductases that utilize molecular oxygen to catalyze the hydroxylation of a substrate. In 2017 however, the monooxygenase paradigm for LPMO catalysis was called into question by Bissaro and colleagues, who instead proposed that LPMOs are peroxygenases that utilize H_2O_2 as their co-substrate during catalysis (Bissaro et al., 2017). Proposed monooxygenase and peroxygenase modes of catalysis are discussed in more detail below.

The reduction of the LPMO copper co-factor from Cu(II) to Cu(I) via an electron donor, referred to as the "priming reduction" in the peroxygenase paradigm (Bissaro et al., 2017; Bissaro et al., 2018b), is crucial for the LPMO reaction. It has been shown that the reducing power needed by LPMOs can be delivered in many ways, including via other redox enzymes,

small molecule reductants, and compounds derived from lignin and plant biomass. The ability of lignin and plant-derived phenolic compounds to provide these reducing equivalents was demonstrated already in early studies of the boosting effect of GH61 proteins (now known as LPMOs) on enzymatic conversion of lignocellulosic substrates (Merino and Cherry, 2007; Harris et al., 2010), and has, after the discovery of LPMO activity, been further demonstrated and detailed in several studies (Hu et al., 2014; Westereng et al., 2015; Kracher et al., 2016; Frommhagen et al., 2018). Typical small molecule reductants used by LPMOs include ascorbic acid (AscA) and gallic acid (GA), which are frequently used in laboratory settings when working with model (lignin-poor) substrates (Vaaje-Kolstad et al., 2010; Eijsink et al., 2019). Redox enzymes known to fuel LPMO reactions include cellobiose dehydrogenase (CDH), various flavoenzymes, and pyrroloquinoline-quinone-dependent pyranose dehydrogenase (Phillips et al., 2011; Garajova et al., 2016; Kracher et al., 2016; Várnai et al., 2018). Recent studies have shown that the nature of the reductant can have a significant impact on the rate of the LPMO reaction. Importantly, these studies claim that this variation is due to differences in the ability of different LPMO-reductant combinations to generate H_2O_2, rather than differences in their ability to reduce the LPMO (Hegnar et al., 2019; Rieder et al., 2021b; Stepnov et al., 2021; Stepnov et al., 2022a). One important distinction between the monooxygenase and peroxygenase reaction schemes concerns the consumption of reducing equivalents, as discussed in more detail below and illustrated in **Figure 9**.

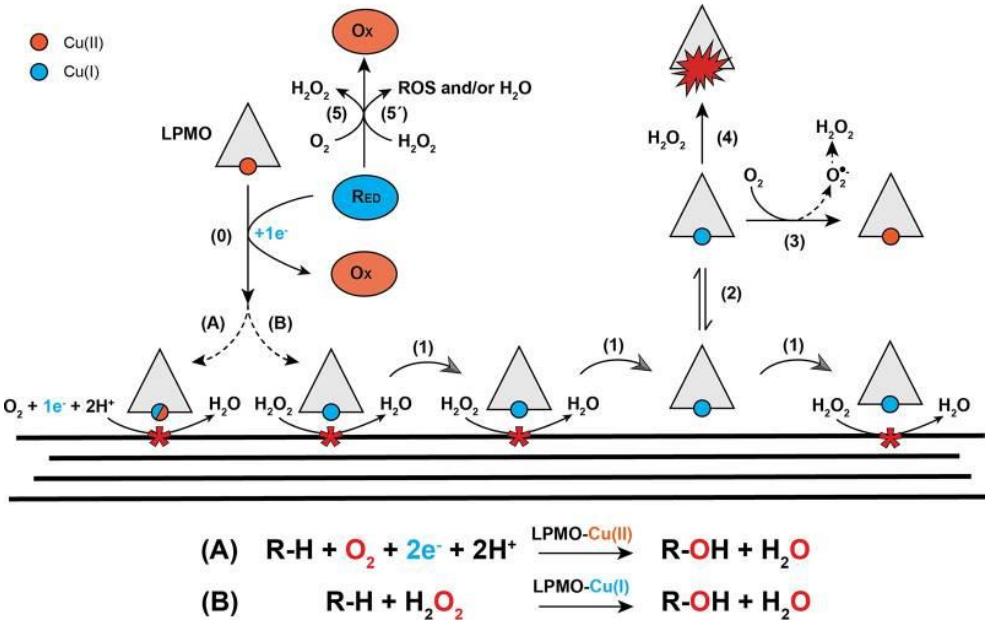

Figure 9. An overview of reactions related to LPMO catalysis. The priming reduction of the LPMO copper co-factor from Cu(II) to Cu(I) by the reducing agent (Red) is shown in step 0. LPMO catalysis then occurs via the monooxygenase (A) or peroxygenase (B) mechanism. In (A), the LPMO uses O_2, an additional electron, and two protons to perform oxidative cleavage of the glycosidic bond. Of note, different mechanisms proposed for the monooxygenase reaction have suggested that the LPMO may be oxidized to the Cu(II) state or remain in the reduced Cu(I) state following catalysis, reflected by the mixed blue and red color of the copper co-factor in reaction (A). In the peroxygenase reaction (B), the reduced LPMO uses H_2O_2 to catalyze the oxidation of the substrate, without requiring supplementation of additional electrons for each catalytic cycle. In the peroxygenase model, each reduced LPMO can thus catalyze multiple turnovers in the presence of H_2O_2 (step 1). Potential non-productive reactions involving the LPMO are illustrated in steps 2-4. Reduced LPMOs not bound to the substrate can reduce O_2, generating H_2O_2 via the formation of a superoxide radical ($O_2^{\bullet-}$), as shown in steps 2 and 3. Furthermore, unbound reduced LPMOs can react directly with H_2O_2, which may lead to the formation of reactive oxygen species (ROS) that can damage or inactivate LPMOs. This is referred to as autocatalytic inactivation and is illustrated in steps 2 and 4. Within the reaction system, H_2O_2 may also be formed via reactions of molecular oxygen with the reductant (step 5). In addition, H_2O_2 can oxidize the reducing agent, which may generate ROS (step 5'). The presence of transition metals in solution may further complicate the illustrated processes, as discussed in more detail in the main text. Reaction schemes for the monooxygenase and peroxygenase reactions are shown below the illustration. The figure was reproduced from (Hegnar et al., 2019).

While various reaction mechanisms proposed for both the monooxygenase and peroxygenase reactions differ in several aspects, following the reduction of the copper co-factor, the principal catalytic step in both paradigms entails the formation of an intermediate LPMO-oxygen species that abstracts a hydrogen atom from the polysaccharide substrate at the scissile glycosidic bond, resulting in a substrate radical species. The details concerning how the hydrogen atom is abstracted are still not fully understood. To complete the catalytic cycle, the substrate radical is hydroxylated by the copper-bound, now protonated oxygen species. The hydroxylated glycosidic bond is unstable, and spontaneous cleavage of this destabilized bond results in the formation of two carbohydrate products, one of which is oxidized (Phillips et al., 2011; Beeson et al., 2015; Walton and Davies, 2016; Bissaro et al., 2017). Proposed schemes for the monooxygenase and peroxygenase reactions are shown in **Figure 9**.

In the monooxygenase reaction, two electrons and two protons are required for each catalytic cycle. Importantly, this implies stoichiometric consumption of the reducing agent for each oxidized product generated. Since only one of the two required electrons can be stored by the copper co-factor, and since the copper co-factor is shielded from the solvent in the enzyme-substrate complex, it is not clear how the second electron arrives at the catalytic center during catalysis. This phenomenon has been termed the second electron conundrum (Bissaro et al., 2018a; Forsberg et al., 2019). A model of CBP21 interacting with crystalline chitin generated by Bissaro and colleagues showed that binding of the LPMO to the substrate results in very limited access to the active site, meaning that enzymatic electron donors or even small-molecule reductants are unable to interact with the LPMO active site in the enzyme-substrate complex (Bissaro et al., 2018a). The inability of enzymatic electron donors to provide reducing equivalents while the LPMO is bound to the substrate has also been demonstrated experimentally (Courtade et al., 2016). Explanations for delivery of the second electron through an electron transfer channel within the protein have been proposed, including by Li and colleagues (Li et al., 2012), but experimental evidence for such mechanisms is yet to be uncovered.

The peroxygenase reaction mechanism was first proposed by Bissaro *et al.* in 2016 (Bissaro et al., 2016; Bissaro et al., 2017). Based on a series of compelling experiments, some of which are detailed below, Bissaro *et al.* proposed that following the initial priming reduction of the LPMO, the electron and protons required for oxidative polysaccharide cleavage are supplied by H_2O_2, which can readily diffuse into the LPMO-substrate complex, as has later been demonstrated (Bissaro et al., 2018a). This proposed mechanism solves the second electron conundrum and leaves the LPMO in a reduced Cu(I) state post-catalysis, enabling multiple catalytic turnovers following a single reduction event.

In their seminal study, Bissaro and co-workers showed that addition of H_2O_2 to an LPMO reaction with Avicel and small amounts of AscA drastically increased the rate of oxidized product formation as compared to the corresponding reaction without exogenously supplied H_2O_2. This experiment also illustrated that when LPMOs are supplemented with H_2O_2, reductant consumption is sub-stoichiometric relative to the amount of oxidized product formed. Additional experiments in this study demonstrated that H_2O_2 can drive LPMO catalysis under anaerobic conditions and that LPMOs preferentially utilize H_2O_2, even when incubated with a large surplus of O_2. From a more applied perspective, experiments in this study also showed that supplementation of the commercial cellulase- and LPMO-containing cocktail Cellic CTec2 with H_2O_2 during reactions with Avicel and AscA resulted in a significant increase in the amount of oxidized product generated and a concomitant increase in saccharification yield as compared to standard reactions without added H_2O_2. Results from this latter experiment also demonstrated near stoichiometric conversion of supplied H_2O_2 to oxidized products, indicating that one molecule of H_2O_2 is consumed per catalytic cycle (Bissaro et al., 2017). Bissaro and colleagues also showed that the amount of H_2O_2 must be strictly controlled to avoid enzyme damage (discussed in section 1.3.4.4.1).

As discussed by Bissaro *et al.*, these findings were expected to have implications for the industrial biorefining sector, where enzymatic saccharification is frequently performed using commercial LPMO-containing cellulase preparations. In fact, recent studies have shown that using H_2O_2 to boost the activity of LPMOs in saccharifications of industrial

substrates is feasible, also at demonstration scale, using relatively low concentrations of exogenously supplied H_2O_2 (Müller et al., 2018; Costa et al., 2020). Of note, another interesting experiment from (Bissaro et al., 2017) showed that glucose oxidase (GOx) can be used for *in situ* generation of H_2O_2 to drive LPMO reactions and that the effect is GOx dose-dependent. Paper II of this thesis describes the ability of GOx to boost the activity of LPMOs in Cellic CTec2 during saccharification of pretreated lignocellulosic substrates. Industrial applications of LPMOs are discussed in more detail in section 1.3.4.5.

Both the catalytic mechanism of LPMOs and the relative importance of the O_2- and H_2O_2-driven reactions remain the subject of debate and current research, as recently reviewed in (Bissaro et al., 2018b; Chylenski et al., 2019; Manavalan et al., 2021). Importantly, multiple kinetic investigations have shown that the peroxygenase reaction is orders of magnitude faster than the monooxygenase reaction, and that when supplied with H_2O_2 and priming amounts of reducing agent, LPMOs catalyze multiple peroxygenase events per priming reduction (Bissaro et al., 2018b; Hangasky et al., 2018; Kuusk et al., 2018; Kont et al., 2020; Hedison et al., 2021; Rieder et al., 2021b). It has been suggested that observed "monooxygenase" reactions, i.e. LPMO reactions with reductant and O_2, are in fact peroxygenase reactions limited by the *in situ* generation of H_2O_2, where the latter is a result of LPMO oxidase activity or direct, abiotic oxidation of the reducing agent (Bissaro et al., 2018b; Stepnov et al., 2021; Stepnov et al., 2022a).

1.3.4.4.1 Off-pathway and non-LPMO driven reactions

A central challenge associated with investigations of LPMO reactions is the abundance of possible "side" reactions that can occur within the reaction system. These reactions, some of which are illustrated in **Figure 9**, can be LPMO-driven, in the form of oxidase or peroxidase reactions, or can be of a more abiotic nature, involving reductants, transition metals, O_2 and/or H_2O_2.

It is well-established that reduced LPMOs can operate as oxidases in the absence of substrate, generating H_2O_2 from molecular oxygen (Kittl et al., 2012). H_2O_2 can also be

generated via abiotic oxidation of the reductant by molecular oxygen, a process that is drastically increased in the presence of free transition metals for several reductants (Stepnov et al., 2021). Recent findings in LPMO research underpin that the extent of abiotic reductant oxidation varies considerably depending on the nature of the reductant (Hegnar et al., 2019; Kuusk et al., 2019; Stepnov et al., 2021). Importantly, in the presence of a relevant carbohydrate substrate, catalytically active LPMOs will productively consume H_2O_2 generated within the system (Bissaro et al., 2018b), explaining why *in situ* formation of H_2O_2 may not be detectable in some reactions (Loose et al., 2016; Hangasky et al., 2018; Filandr et al., 2020).

While the above-mentioned H_2O_2 generation pathways boost LPMO activity, excess concentrations of H_2O_2 may lead to enzyme damage and inactivation (Bissaro et al., 2017; Kuusk et al., 2018; Loose et al., 2018; Müller et al., 2018; Petrović et al., 2018; Kracher et al., 2020). Non-substrate bound reduced LPMOs can react with H_2O_2 in a peroxidase-like reaction, which may lead to autocatalytic inactivation (i.e. oxidative damage of residues in the catalytic center (Bissaro et al., 2017)). Low substrate concentrations or gradual changes in substrate concentrations (which may occur under more applied experimental settings, e.g. industrial saccharification reactions) may exacerbate such off-pathway peroxidase reactions and increase chances of enzyme inactivation (Bissaro et al., 2017; Eijsink et al., 2019).

Autocatalytic inactivation of LPMOs leads to release of copper into solution, which, for several reductants, may promote H_2O_2 generation by catalyzing the reaction of the reductant with O_2. As recently demonstrated experimentally with AscA by Stepnov and colleagues, this can instigate a self-propagating cycle of increased *in situ* H_2O_2 production and LPMO autocatalytic inactivation with concomitant reductant depletion, leading to termination of the LPMO reaction (Stepnov et al., 2022b). Furthermore, reactions between the reductant and H_2O_2 may generate reactive oxygen species (ROS) (Hegnar et al., 2019). Additionally, H_2O_2 generated by any process within the reaction system can engage in Fenton chemistry, reacting with reduced free transition metals leading to the generation of hydroxyl radicals. Fenton chemistry (i.e. abiotic degradation of lignocellulosic biomass) is

employed by certain fungi, as illustrated in **Figure 7**. Importantly, within natural lignocellulose-degrading systems, H_2O_2 will also be generated or consumed by various oxidases and peroxidases. These enzymes are abundant within the array of enzymes produced by natural lignocellulose-degrading microorganisms (Bissaro et al., 2018b), and are discussed in more detail in section 1.3.4.6.

Taken together, these reactions, mediated both by LPMOs and by alternate reaction partners, contribute to the overall intricacy of LPMO catalysis, and illustrate that the study and optimization of LPMO performance requires careful consideration of multiple parameters. The situation becomes even more complex when working with non-model (i.e. "real") lignocellulosic substrates containing redox-active compounds (in particular lignin and lignin-derived compounds, and/or transition metals).

1.3.4.5 LPMOs in biomass processing

The interplay of LPMOs with hydrolases is of considerable interest because optimization of this interplay will be key to harnessing the potential of LPMOs in biomass processing (Eibinger et al., 2014; Eibinger et al., 2017; Karnaouri et al., 2017; Müller et al., 2018; Tokin et al., 2020). In two important studies, Eibinger and colleagues used confocal and atomic force microscopy to show that a cellulolytic LPMO from *N. crassa* (*Nc*LPMO9F) primarily acts on surface-exposed crystalline areas of cellulose. Importantly, this work also showed that LPMO treatment promotes adsorption of the *T. reesei* CBH *Tr*Cel7A to such crystalline regions, resulting in more efficient hydrolysis of cellulose (Eibinger et al., 2014). Subsequent studies using atomic force microscopy resulted in similar conclusions (Eibinger et al., 2017). Based on the observed synergistic effects in saccharification, these studies provide evidence for the hypothesis that at least some LPMOs cleave cellulose in crystalline areas (i.e. areas least accessible to hydrolytic enzymes) and thus produce new chain ends for CBHs. This highlights an important difference between LPMOs and EGs in relation to their mode of synergism with CBHs, since these enzymes respectively cleave crystalline and amorphous parts of the cellulose.

Notably, the oxidation of terminal glucose units after LPMO action will have a multi-faceted impact on CBHs, depending partly on the directionality of the CBH and partly on the ability of individual CBHs to productively bind oxidized chain ends. One of the two new chain ends generated by LPMO activity will be oxidized, and CBHs may vary in terms of how well they interact with such oxidized chain ends (Vermaas et al., 2015).

As previously discussed, it was clear even before the elucidation of their oxidative ability that LPMOs had the potential to improve hydrolysis yields obtained with *T. reesei*-produced cellulase cocktails (Merino and Cherry, 2007). Today, LPMOs are central components of commercial cellulase cocktails such as the Novozymes Cellic CTec series (Cannella et al., 2012; Harris et al., 2014; Müller et al., 2015; Johansen, 2016; Chylenski et al., 2017b). Of note, while the contribution of LPMOs to the efficiency of such cellulase cocktails is clear and important (Cannella and Jørgensen, 2014; Hu et al., 2015; Müller et al., 2015; Müller et al., 2018; Kadić et al., 2019; Costa et al., 2020; Kadić et al., 2021), optimizing this impact is not easy, and requires careful consideration of multiple reaction conditions, as recently reviewed in (Chylenski et al., 2019). Paper II of this thesis provides an example of such optimization.

Early studies indicating that LPMOs boosted the action of cellulases also illustrated that the presence of lignin within biomass promotes LPMO effects (Merino and Cherry, 2007; Harris et al., 2010), although the reason for this effect did not become clear until several years later, when it was discovered that LPMOs require electrons, which lignin can provide. Recent studies indicate that lignin has a dual function in LPMO activation: it is able to both reduce LPMOs and to produce H_2O_2 *in situ* from O_2 (Hu et al., 2014; Westereng et al., 2015; Frommhagen et al., 2016; Muraleedharan et al., 2018; Kont et al., 2019; Perna et al., 2020).

The saccharification of lignin-poor sulfite-pulped spruce requires an externally-added reductant, and it has been shown that lignin-containing spent sulfite liquor can fulfill this role (Chylenski et al., 2017b; Costa et al., 2020). When it comes to the LPMO-reducing and H_2O_2-generating functions of lignin, it is important to note that the type of biomass pretreatment affects lignin reactivity (Rodríguez-Zúñiga et al., 2015). Numerous studies

have implied that the known inhibitory effect of lignin on cellulase activity is due to unproductive binding of enzymes to lignin, and/or due to shielding of the cellulose polysaccharide (Berlin et al., 2006; Rahikainen et al., 2013; Djajadi et al., 2018a; Djajadi et al., 2018b; Yao et al., 2022). Today, it is known that lignin may also be essential for LPMO activity under certain experimental conditions. For example, a recent study by Hansen *et al.* showed that the beneficial effect of 2-naphtol impregnation during steam explosion of spruce on the efficiency of the subsequent saccharification step is due, at least in part, to a change in lignin reactivity that promotes LPMO activity (Hansen et al., 2022). It is thus essential to use real substrates (i.e. pretreated biomass) to test cocktail performance in the development of enzyme cocktails for industrial biomass processing.

As mentioned above, direct supply of H_2O_2 via pumping works very well for saccharification of lignin-poor substrates (Müller et al., 2018; Costa et al., 2020). For lignin-rich substrates, however, the benefits of direct addition of external H_2O_2 are less clear, presumably due to side reactions occurring between supplemented H_2O_2 and lignin (Müller et al., 2018; Kont et al., 2019). Lignin and its derivative compounds are known to participate in a variety of redox reactions, which can both generate and consume H_2O_2 and ROS, especially in the presence of transition metals (Arantes et al., 2012; Bissaro et al., 2018b). *In situ* production of H_2O_2 could help circumvent the problem of lignin reactivity because H_2O_2 may occur close to the LPMO, which will increase its likelihood of being used in productive catalysis. However, when relying on *in situ* production of H_2O_2, it is more difficult to control the amount of H_2O_2 produced. As a consequence, there is a risk of the occurrence of intermittently high concentrations of H_2O_2, which can damage the LPMOs and potentially other enzymes. H_2O_2 accumulation may be controlled by the use of catalases, which convert H_2O_2 to water and O_2. In fact, a study by Scott and colleagues showed that, under certain conditions, enzyme inactivation in reactions with LPMO-containing cellulase preparations could be suppressed by adding catalase (Scott et al., 2016).

1.3.4.6 Other oxidoreductases

In addition to GHs and LPMOs, fungal secretomes are rich in oxidoreductases, redox enzymes populating multiple families in the Auxiliary Activities enzyme class in the CAZy database (Levasseur et al., 2013). A detailed overview of these enzymes and potential interactions between them is provided in a recent review by (Bissaro et al., 2018b). While specific activities of the majority of these enzymes fall outside the scope of this thesis, examples of oxidoreductases of interest include enzymes with oxidase activities, such as glucose-methanol-choline (GMC) oxidoreductases (found in family AA3), and lignin-active laccases and peroxidases (found in AA families 1 and 2, respectively).

CDHs are found in the CAZy family AA3, and are well-known electron providers for LPMOs, capable of reducing the LPMO active site copper co-factor via cytochrome domains (found in family AA8) (Phillips et al., 2011; Tan et al., 2015; Kracher et al., 2016). CDHs can also contribute to LPMO catalysis via generation of H_2O_2, although the oxidase activity of wild-type CDHs is rather low (Kracher et al., 2020). Glucose oxidases (GOxs) are AA3 enzymes with a primary oxidase activity. GOx catalyzes the oxidation of β-D-glucose to gluconic acid while generating H_2O_2 (Kelley and Reddy, 1986). Of note, within the GMC superfamily, dehydrogenases such as CDH can both reduce LPMOs and generate H_2O_2, whereas oxidases can only promote LPMO reactions via generation of H_2O_2 (Garajova et al., 2016; Kracher et al., 2016; Filandr et al., 2020). GOx has recently been shown to be able to drive LPMO activity via *in situ* production of H_2O_2**,** in the presence of a reducing agent (Bissaro et al., 2017). Similar findings have been described by (Filandr et al., 2020). Paper II of this thesis describes experiments demonstrating that the activity of LPMOs in cellulase preparations acting on lignocellulosic substrates is significantly impacted by *in situ* production of H_2O_2 by GOx.

Laccases and peroxidases can indirectly affect LPMO reactions by acting on lignin, and, in the case of peroxidases, by competing for H_2O_2. Enzymes that modify lignin can affect its ability to donate electrons and generate H_2O_2, thus providing possible links to LPMO activity. Indeed, laccase treatment of lignin has been shown to increase LPMO activity

(Brenelli et al., 2018; Perna et al., 2020). The study by Perna and colleagues demonstrated that this effect is due to increased H_2O_2 production via reactions involving laccase-modified lignin. An additional possible link between these enzyme systems is that LPMO-catalyzed *in situ* production of H_2O_2 may drive peroxidase reactions leading to lignin degradation (Li et al., 2019).

Given the variety of redox processes mediated and facilitated by these enzymes, and the fact that many of them are co-secreted with LPMOs and GHs by fungi and involve consumption and production of H_2O_2, it is likely that nature has evolved highly regulated mechanisms of cooperativity between various redox enzyme types involved in biomass conversion (Bissaro et al., 2018b). In order to efficiently and proactively exploit these systems in biomass conversion, however, more research is needed to better understand these complex systems.

1.3.4.7 Oxidative regioselectivity

Regardless of the catalytic mechanism they employ, it is clear that LPMOs catalyze substrate depolymerization by hydroxylation of one of the carbons in the scissile glycosidic bond, resulting in bond destabilization and cleavage (Phillips et al., 2011; Walton and Davies, 2016; Forsberg et al., 2019). The resulting products of oxidative LPMO action are two oligomeric chain ends, a reducing end and a non-reducing end, one of which is oxidized (**Figure 10**). If the oxidation occurs at the C1 position (at the reducing end), the LPMO is considered a C1-oxidizing LPMO. Oxidation of the C1 carbon results in the formation of an unstable 1,5-δ-lactone which is spontaneously converted to a more stable aldonic acid in aqueous solutions. The aldonic acid form of C1-oxidized products dominates at physiological and at high pH (Vaaje-Kolstad et al., 2010; Forsberg et al., 2011; Westereng et al., 2013). If the oxidation occurs at the C4 position (non-reducing end), the LPMO is considered a C4-oxidizer. C4-oxidized products are 4-ketoaldoses, which undergo hydration to form the geminal diol form (Beeson et al., 2012; Isaksen et al., 2014; Westereng et al., 2017). Importantly, C4-oxidized cello-oligomers are unstable at high pH (Westereng et al., 2016). This can complicate their identification and quantification, as certain methods

for carbohydrate analysis, such as high-performance anion exchange chromatography, rely on the use of alkaline pH. Some LPMOs have mixed C1/C4 activity, meaning that they produce mixtures of C1- and C4-oxidized products (Quinlan et al., 2011; Forsberg et al., 2014; Vu et al., 2014a). Of note, only C1-oxidation has been observed for chitin-active LPMOs.

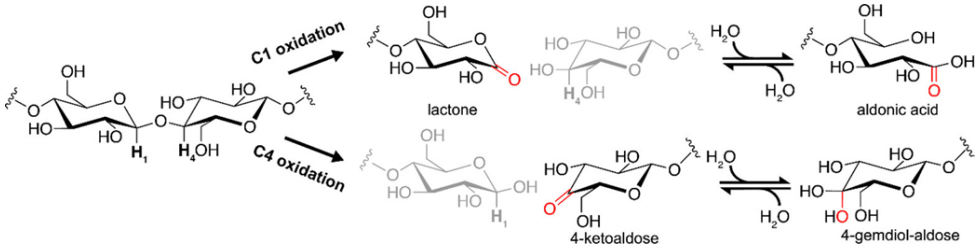

Figure 10. Oxidative regioselectivity of LPMOs. LPMO-catalyzed C1-oxidation of the scissile glycosidic bond results in two oligomeric products, one of which is oxidized at the reducing end. This lactone is in equilibrium with the corresponding aldonic acid. C4-oxidation by the LPMO results in a native product and a 4-ketoaldose (oxidized at the non-reducing end). This species is in equilibrium with its hydrated geminal diol form. The figure was reproduced from (Chylenski et al., 2019).

1.3.4.8 Analysis of LPMO products by mass spectrometry and high-performance anion-exchange chromatography

Unambiguous detection and quantification of LPMO-derived products are essential in furthering the understanding of these enzymes. The analytical distinction between native and oxidized oligosaccharides can, however, be challenging, due to their close structural resemblance (**Figure 10**). Frequently utilized methods for the separation and characterization of LPMO-derived cellulosic products include MALDI-TOF MS (matrix-assisted laser desorption ionization time of flight mass spectrometry) and HPAEC-PAD (high-performance anion-exchange chromatography with pulsed amperometric detection).

In basic terms, the general principle of MALDI-TOF MS involves mixing the analyte with an organic matrix, which crystallizes upon drying, causing co-crystallization of the analyte.

Desorption and ionization of the sample, achieved with a laser beam, produces ions that, when accelerated, will travel towards a detector at different speeds ("time of flight") depending on their mass to charge ratio (*m/z*). This enables their separation and allows for distinction of various species in a mixture based on the *m/z* value (Kaufmann, 1995; Singhal et al., 2015). The charge of the ions can come from a proton, but the adducts usually carry a salt ion, most commonly sodium. Advantages of using MALDI-TOF MS for analysis of carbohydrate species include the rapid sample preparation and analysis time, and, for LPMO-derived oxidized sugars, the easily recognizable substrate cleavage patterns comprised of products with increasing DP and characteristic mass differences (*m/z* + 162 for non-substituted glucans). Signals for oxidized species show *m/z* changes of -2 and +16 relative to the non-oxidized oligomer, corresponding to the dehydrated C1-oxidized lactone and C4-oxidized keto forms, and the hydrated C1-oxidized aldonic acid and C4-oxidized geminal diol forms, respectively.

While the identical masses of the dehydrated and hydrated forms of C1- and C4-oxidized products make it difficult to determine the oxidative regioselectivity of LPMOs based on MALDI-TOF MS alone, practical applications have shown that C1-oxidized products in their aldonic acid form tend to appear as salts of their adducts. The occurrence of signals for such salts is diagnostic for C1-oxidation; there is, however, no "safe" diagnostic signal for C4-oxidation. Under conditions used in MALDI-TOF MS, the lactone-aldonic acid equilibrium strongly favors the aldonic acid form, resulting in relatively weak lactone signals for C1-oxidized products. The equilibrium between the 4-keto and geminal diol forms of C4-oxidized products is more balanced, and drying of the sample within the matrix promotes formation of the dehydrated 4-keto form. Thus, relatively strong *m/z* -2 signals are sometimes considered a sign of C4-oxidation, but verification via chromatography is required. Importantly, while signal intensities resulting from MALDI-TOF MS analysis provide indications as to the abundance of specific compounds in the analyte, MALDI-TOF MS is not a quantitative method, and other analytical tools are therefore required for quantitative studies of LPMO catalysis.

HPAEC-PAD is a routinely used chromatographic method for efficient separation and quantification of carbohydrate species. HPAEC-PAD entails the use of a mobile phase with strongly alkaline pH (e.g. 0.1 M sodium hydroxide, NaOH), which causes deprotonation of analyte sugars. When injected onto an anion exchange column, deprotonated sugars will bind with affinities increasing according to the size of the sugar molecule and number of hydroxyl groups (Lee, 1990). By subsequently applying a gradient of an eluent containing a competing ion (e.g. sodium acetate, NaOAc), carbohydrate species will progressively be displaced from the column according to the number of charges they possess. Their elution is detected in real time by measuring the current generated from the oxidation of the sugar hydroxyl groups at a gold working electrode to which a waveform of potentials is repeatedly applied. The integration of the generated current results in a signal (charge), measured in Coulombs (C), proportional to the carbohydrate concentration. The response of the detector during each waveform integration period is plotted against the run time to generate a chromatogram (detector response in nC on the *y*-axis vs. retention time in minutes on the *x*-axis) (Cataldi et al., 2000; Mechelke et al., 2017).

Regarding analysis of LPMO-generated products, HPAEC-PAD has readily been used to separate native and C1-oxidized products, which are inherently stable at alkaline pH (Forsberg et al., 2011; Phillips et al., 2011; Westereng et al., 2013). Standards for quantification of C1-oxidized cellulose-derived products can be prepared by treating native cello-oligosaccharides with CDH, which converts cello-oligosaccharides to (C1-oxidized) aldonic acids (Forsberg et al., 2018). While C4-oxidized products undergo decomposition at high pH, as demonstrated by (Westereng et al., 2016), HPAEC-PAD can also be used for their detection and quantification because the alkaline conditions generate derivatives with characteristic peaks, as demonstrated by (Müller et al., 2015). A standard can be generated by treating cellopentaose with the strict C4-oxidizing *Nc*LPMO9C, which generates a mixture primarily consisting of equimolar amounts of C4-oxidized cellobiose (Glc4gemGlc) and native cellotriose, where the latter can be quantified using a cellotriose standard. Müller *et al.* demonstrated a linear relationship between the Glc4gemGlc concentration and HPAEC-PAD peak height up to Glc4gemGlc concentrations of 0.1 g/L, allowing for generation of standards that can be used to quantify Glc4gemGlc chromatographically

(Müller et al., 2015). Notably, this method for production of C4-oxidized standards has enabled quantification of LPMO action in saccharification reactions with commercial LPMO-containing cellulase cocktails (Bissaro et al., 2017; Müller et al., 2018; Costa et al., 2020; Hansen et al., 2022) (Paper II of this thesis). Glc4gemGlc is the primary oxidized product emerging in these reactions because the cellulase cocktails primarily contain C4-oxidizing LPMOs, and because Glc4gemGlc is not hydrolyzed by cellulases or β-glucosidases (Müller et al., 2015). Importantly, quantification of C4-oxidized products via this method requires careful attention to sample preparation, ensuring that both the standard and the samples to be analyzed are subjected to the same conditions prior to injection on the HPAEC column (Eijsink et al., 2019).

Years of LPMO research and use of standards have provided a good basis for peak annotation in HPAEC-PAD chromatograms for mixtures of LPMO products. The high ionic strength required for complete elution of longer oxidized species and the use of high pH complicates HPAEC-PAD coupling with MS-based methods that could provide an alternative for peak identification. Today, HPAEC-PAD is considered an essential technique for separation and quantification of oxidized sugars due to its high resolution and sensitivity (Westereng et al., 2013; Mechelke et al., 2017).

A novel HPAEC method for separation of oligosaccharides has recently been developed by Chen and colleagues. This method relies on the use of electrolytically generated eluents consisting of potassium methanesulfonate and potassium hydroxide (KMSA/KOH), replacing traditional NaOAc/NaOH-based HPAEC (Chen et al., 2018). By relying on electrolytic eluent generation via eluent generator cartridges, this method circumvents the need for time-consuming manual eluent preparation, and avoids issues associated with potential accumulation of CO_2 in eluent preparations. In classical HPAEC, CO_2 accumulation presents a challenge because it is converted to carbonate at high pH. Carbonate anions can compete with carbohydrate oxyanions for binding sites on the anion exchange column (Westereng et al., 2017). Paper I of this thesis describes the use of the dual electrolytic eluent generation platform with KMSA/KOH-based eluents established by Chen and

colleagues to develop HPAEC-PAD methods for baseline separation and quantification of LPMO-derived products, including native, C1- and C4-oxidized oligosaccharides.

Continual development of analytical methods for carbohydrate analysis with increased resolution and sensitivity is of high importance, as these methods go hand in hand with the functional characterization of LPMOs and other carbohydrate-active enzymes, and can thus significantly assist in advancing our knowledge of these enzymes. Historical examples of this partnership include the paradigm-shifting discovery of the oxidative ability of LPMOs, where novel chromatographic methods enabled quantification of oxidized chito-oligomers produced by CBP21 (Vaaje-Kolstad et al., 2010), as well as the first demonstration of hemicellulolytic activity of an LPMO, where MALDI-TOF MS and HPAEC-PAD were used to confirm oxidative activity and product identities (Agger et al., 2014).

2 Outline and purpose of the research described in this thesis

LPMOs are redox enzymes that utilize O_2 or H_2O_2 to oxidize their substrates. Since their discovery in 2010, LPMOs have received much attention due to their unique catalytic capabilities and industrial importance. Novel LPMO activities are still being discovered, and it is believed that LPMOs may have alternate roles in bacterial and fungal physiology that have yet to be identified. Despite years of studying LPMOs, much remains to be elucidated, including details of how they interact in concert with other enzymes and co-substrates during polysaccharide depolymerization, and how to best harness their powerful oxidative abilities in industrial biomass conversion processes.

Industrial processing of lignocellulosic biomass has the potential to contribute to the production of fuels and value-added chemicals from a sustainable and renewable source. Enzymatic depolymerization of lignocellulosic polysaccharides is an essential and demanding step in this process, particularly for the dominant crystalline homopolymer cellulose. Commercial cellulolytic enzyme preparations are continuously being developed and modified with the aim of reducing process costs and increasing efficiency. In recent years, LPMOs have been included in such preparations, and while their potential to boost process yields is notable, it is not clear how their activity and contribution to the saccharification process can be optimized.

The aim of the research described in this thesis was therefore to study the role of LPMOs in depolymerization of lignocellulosic biomass through characterization of new LPMOs and elucidation of their substrate specificities (**Paper III and IV**), understanding and optimizing LPMO action during saccharification in synergy with cellulases (**Paper II**), and development of chromatographic methods for separation and quantification of LPMO-derived products (**Paper I**).

Paper I describes the development of methods for quantification of LPMO-derived products using HPAEC-PAD with dual electrolytic eluent generation. Specialized methods were developed to facilitate separation and quantification of native, C1-, and C4-oxidized cello-oligomers, as well as gluconic and glucuronic acid. Emphasis was placed on improvements in precision and sensitivity achieved using automated electrolytic eluent generation of KMSA/KOH-based eluents as compared to traditional methods based on manually prepared NaOAc/NaOH-based eluents.

Paper II describes studies of cellulose saccharification with a thermostable cellulase cocktail from *Thermoascus aurantiacus* and the commercial cellulase preparation Cellic CTec2 using differently pretreated softwood and hardwood substrates. Differences between the two cellulase cocktails were examined with a special focus on the activity of LPMOs and the impact of this activity on the saccharification efficiency. Saccharification reactions with Cellic CTec2 were also performed in the presence of varying amounts of glucose oxidase and two different reductants to study the role of the reductant and the effect of *in situ* H_2O_2 generation on LPMO activity and saccharification efficiency.

Paper III describes the cloning, expression, and characterization of *Sc*LPMO9A, one of 22 predicted AA9 LPMOs encoded in the genome of the fungus *Schizophyllum commune*. Functional characterization and comparison to the well-studied *Nc*LPMO9C from *N. crassa* showed that *Sc*LPMO9A is a C4-oxidizing LPMO active on insoluble amorphous cellulose and soluble cello-oligosaccharides, as well as on several hemicellulosic substrates, and revealed differences between the two enzymes. Studies of the effect of H_2O_2 on the activity of *Sc*LPMO9A on PASC and cellopentaose were performed to assess the peroxygenase activity of this LPMO. Further characterization of *Sc*LPMO9A is underway, including NMR-based studies of the affinity of this enzyme for various oligomeric substrates, and will aid in elucidating the natural role of this AA9 LPMO in degradation of lignocellulosic biomass.

Paper IV describes studies of the oxidative depolymerization of beechwood glucuronoxylan by two AA9 LPMOs from *N. crassa*, *Nc*LPMO9F and *Nc*LPMO9L. This paper contains both MALDI-TOF MS and HPAEC-PAD analysis of product mixtures, revealing a

multitude of xylan-derived LPMO products, which were generated only from cellulose-associated glucuronoxylan, and not from glucuronoxylan alone. Through quantification of cellulose- and xylan-derived oxidized products in reactions with blends of cellulose and glucuronoxylan, it is shown that xylan-active AA9 LPMOs have remarkable differences in their substrate preferences, with some acting preferentially on the cellulose and others on the xylan.

3 Main results and discussion

3.1 Paper I: Chromatographic analysis of oxidized cello-oligomers generated by lytic polysaccharide monooxygenases using dual electrolytic eluent generation

The study of LPMOs is dependent on the ability to reliably analyze and quantify the complex product mixtures generated by their action on various substrates. A novel platform for oligosaccharide analysis using HPAEC-PAD with electrolytically-generated KMSA/KOH-based eluents was recently developed (Chen et al., 2018). In contrast to the traditional manual eluent preparation required for NaOAc/NaOH-based HPAEC, this technology enables the electrolytic generation of KMSA and KOH in two separate eluent-generator cartridges (EGCs) connected in series, meaning that only deionized water must be supplied by the user. In the study described in **Paper I**, using this novel technology implemented with a Dionex ICS-6000 system, we developed a set of methods for separation of native and oxidized cellulose-derived LPMO products. We also compared limits of detection and quantification for LPMO-derived oligosaccharides obtained using KMSA/KOH-based methods to those obtained using conventional NaOAc/NaOH-based HPAEC with a Dionex ICS-5000 system.

The ICS-6000 system was equipped with a 1 x 250 mm Dionex CarboPac PA-200 column, compared to a 3 x 250 mm column of the same type used on the ICS-5000 system. Sample loop volumes were 4 and 5 µL for the ICS-6000 and ICS-5000 systems. respectively. The maximum eluent concentration possible on the ICS-6000 system is 200 mM for KMSA and KOH together, and there is thus a limitation to the maximum amount of elution strength that can be applied. During method optimization, we found that a constant concentration of 100 mM KOH gave the best separation of all compounds examined for all methods developed for oligosaccharide separation. As a consequence, although the elution strength of KMSA is approximately 1.8 times higher than NaOAc (Chen et al., 2018), KMSA concentrations in all oligosaccharide gradients were limited to the range of 0-100 mM,

resulting in somewhat longer gradients compared to previously developed methods for the ICS-5000 system. We developed three primary oligosaccharide gradients for separation and quantification of native, C1-oxidized, and C4-oxidized LPMO products, including a method for analyzing all three product types simultaneously (**Paper I, Table I**). Finding the optimal balance between reducing method run time, increasing separation power, and maintaining reproducibility was the primary focus during method development. To assess the sensitivity of the ICS-6000 operated with electrolytic eluent generation, limits of detection (LOD) and quantification (LOQ) were calculated using the Calibration Approach (Wenzl et al., 2016). To compare precision and detection limits between the ICS-5000 and the ICS-6000 systems in analysis of oxidized products, we analyzed 12 consecutive pseudo-blank samples containing a minimal amount of the relevant compound on both systems, and LOD and LOQ values were calculated based on a three-point standard curve for each compound. LOD and LOQ values calculated for all compounds analyzed in this study using the Calibration Approach and the pseudo-blank approach are shown in **Paper I, Table 2**.

Native cello-oligosaccharides are produced both by hydrolytic cellulases often used in combination with LPMOs in LPMO research, and by LPMOs when cleaving soluble cello-oligomers or cleaving near chain ends of insoluble polymeric substrates. To develop a method for separation of soluble native cello-oligomers, we used a native standard consisting of $Glc_{1\text{-}6}$. The method found to give the best results for separation of native cello-oligosaccharides had a steep initial linear gradient from 0 to 30 mM KMSA (0-6 min), followed by a concave gradient (Dionex curve 7) to 100 mM KMSA (6-10 min), and column washing and re-conditioning phases at 100 mM and 0 mM KMSA (10-15 min and 15.1-24 min, respectively) (**Paper I, Figure 1A**). Using this method, baseline separation of $Glc_{1\text{-}6}$ was achieved within 15 minutes, and high sensitivity of detection was achieved at concentrations as low as 0.0005 g/L for all components. The signal-to-noise ratio for 0.0005 g/L Glc_6, the compound which gave the lowest peak intensity, was calculated to be 162 (**Paper I, Figure 1A inset**), suggesting that even lower concentrations will likely be reliably detected using this setup. Standard curves showed a linear response for all components in the $Glc_{1\text{-}6}$ mixture over the range of 0-0.025 g/L (**Paper I, Figure 1B**), and LOD and LOQ

values calculated using the Calibration Approach ranged from 0.0001–0.0002 g/L and 0.0003–0.0006 g/L, respectively.

Reactions with C1-oxidizing LPMOs generate a mixture of soluble native and oxidized cello-oligomers with DPs ranging from 2-9 (Forsberg et al., 2014). Analysis of such samples using classical HPAEC conditions for oligosaccharide analysis has shown that C1-oxidized cellobiose (GlcGlc1A) frequently co-elutes with the native cellopentaose (Glc_5) (Westereng et al., 2013). We therefore sought to develop a method for simultaneous separation of native and C1-oxidized cello-oligosaccharides that avoids such co-elution. This was achieved using a concave gradient (Dionex gradient 8) from 1 to 100 mM KMSA (0-14 min), followed by washing at 100 mM KMSA (14-17 min) and column re-conditioning to 1 mM KMSA (17.1-26 min) (**Paper I, Figure 2A**). This method achieved baseline separation of all components in the C1-oxidized standard mixture in 20 minutes, while achieving similar separation of native species as the method shown in **Paper I, Figure 1A**. Importantly, no co-elution of longer native compounds with shorter C1-oxidized compounds was observed, meaning that this method can readily be utilized to separate and identify all soluble species that may arise in reactions of C1-oxidizing LPMOs with cellulosic substrates. All components in the C1-oxidized standard showed a linear response over the range of 0-0.01 mM (**Paper I, Figure 2C**), with LODs and LOQs calculated using the Calibration Approach ranging from 0.0003-0.003 mM and 0.001-0.01 mM, respectively. Using the pseudo-blank approach, calculated LOD and LOQ values ranged from 0.00004-0.0002 mM and 0.0001-0.0006 mM, respectively (**Paper I, Table 2**).

Despite their instability at high pH leading to partial on-column decomposition, C4-oxidized product quantification can be achieved by quantification of these decomposition products, which act as proxies for the C4-oxidized species (referred to as “C4-oxidized products” in this study). These species have higher retention times than native and C1-oxidized products, and thus often require longer gradients and higher salt concentrations to achieve elution. To separate native, C1-, and C4-oxidized oligosaccharides that may result from a single reaction containing LPMOs, we developed a 45-minute method that achieved baseline separation of native $Glc_{2\text{-}6}$, $Glc_{1\text{-}5}Glc1A$ (C1-oxidized products), and compounds

reflecting the C4-oxidized dimer and trimer (Glc4gemGlc and Glc4gemGlc$_2$) without co-elution of species of interest (**Paper I, Figure 3A**). The gradient begins with a convex increase in KMSA concentration from 0 mM to 15 mM (Dionex curve 3) (0-8.5 min), followed by a linear increase to 27 mM KMSA (8.5-17 min) and a subsequent concave increase to 100 mM KMSA (Dionex curve 7) (17-27 min), before washing and re-conditioning of the column at 100 and 0 mM KMSA (27.1-36 min and 36.1-45 min, respectively). Glc4gemGlc gave a linear response in the range of 0-0.08 mM, while Glc4gemGlc$_2$ showed linearity in the range of 0-0.005 mM (**Paper I, Figure 3A inset**). LODs and LOQs calculated using the Calibration Approach were 0.001 and 0.0001 mM, and 0.004 and 0.0002 mM, for Glc4gemGlc and Glc4gemGlc$_2$, respectively. Using the pseudo-blank approach, LODs and LOQs were 0.0007 and 0.00004 mM, and 0.002 and 0.0001 mM, for Glc4gemGlc and Glc4gemGlc$_2$, respectively (**Paper I, Table 2**). A mixture of products generated in reactions with a C1-oxidizing (*Sc*LPMO10C) and a C4-oxidizing (*Nc*LPMO9C) LPMO acting on PASC showed that by using this method, all components present in the complex reaction mixture could be separated and potentially quantified (**Paper I, Figure 3B**).

The development of electrolytic eluent generation using dual EGCs and small-diameter columns has enabled the use of lower flow rates, leading to improved signal-to-noise ratios and increased sensitivity, which enables detection of compounds at low concentrations. A detailed comparison of 12 pseudo-blank injections of a sample containing 0.0005 g/L Glc$_{1-5}$Glc1A run on both the ICS-5000 and the ICS-6000 is shown in **Paper I, Figure 4A-E**. While baseline separation of all components in the C1-oxidized standard using the ICS-6000 developed method takes approximately 7 minutes longer than using a corresponding method on the ICS-5000 system, which is a potential disadvantage, the ICS-6000 method gave a very stable detector baseline and considerably increased signal-to-noise ratios for all components. This enables higher accuracy in quantification of products present in low concentrations and increases reproducibility. Similar observations were made for C4-oxidized cello-oligomers. Determination of LODs and LOQs using the pseudo-blank approach resulted in markedly lower values for both C1- and C4-oxidized species when using the ICS-6000 system compared to the ICS-5000 system (**Paper I, Table 2**), confirming

that the ICS-6000 system is more sensitive and results in more accurate quantification of LPMO-generated oxidized products.

LPMOs are present in commercial cellulase cocktails used for the industrial degradation of lignocellulosic substrates. Such modern cellulase blends contain β-glucosidases, which hydrolyze native and C1-oxidized short cello-oligomers into monomeric products. C4-oxidized products will not be degraded by β-glucosidases, but will rarely be longer than two sugar units (Glc4gemGlc) because longer soluble products are readily degraded by the cellulases (Müller et al., 2015). The presence of C1-oxidizing LPMOs in addition to the cellulases and β-glucosidases will result in accumulation of native glucose and gluconic acid (Glc1A). Gluconic acid has poor retention to the anion exchange column, and elutes in the injection peak under standard oligosaccharide HPAEC conditions, as shown in **Paper I, Figure 5A**. To visualize and quantify gluconic acid resulting from the action of C1-oxidizing LPMOs in reactions containing β-glucosidase, we developed an isocratic method using an ICS-6000 setup with a 2 x 150 mm Dionex CarboPac PA-210-Fast-4 µm column. In this setup, a 0.4 µL sample loop volume was used. While the smaller sample loop reduces sensitivity, it also eliminates the need for extensive dilution of samples with high concentrations of analytes. The developed method entailed isocratic elution with 70 mM KOH (0-16 min) before washing at 100 mM KOH (16.1-21 min) and subsequent re-conditioning of the column at 70 mM KOH (21.1-30 min). Using this method, baseline separation of monomeric glucose and gluconic acid, the only cellulose-derived LPMO products remaining after treatment with a β-glucosidase, was accomplished (**Paper I, Figure 5B**). Using the calibration approach, a linear response was observed for gluconic acid in the range of 0-0.05 g/L (**Paper I, Figure 5C**), with an LOD of 0.004 g/L and an LOQ of 0.013 g/L. Products generated by C1-oxidizing LPMOs are usually quantified following treatment of the LPMO product mixture with a cellulase, resulting in predominantly C1-oxidized cellobiose and cellotriose. While this method has shown reproducible results, baseline separation and quantification of these products could potentially be complicated by the presence of hemicellulosic compounds present in the substrate. By degrading C1-oxidized sugars with a β-glucosidase (Cannella et al., 2012) and analyzing the resulting

gluconic acid via the isocratic method described in **Paper I**, quantification of C1-oxidized sugars may be simplified.

In conclusion, the methods described in **Paper I** offer increased sensitivity and precision for analysis and quantification of LPMO-generated native and oxidized cello-oligomers. In addition, as outlined by (Chen et al., 2018), the automatic generation of eluents minimizes baseline fluctuations, essentially eliminates error-prone and time-consuming manual eluent preparation, and minimizes the risk of carbonate accumulation on the column. The study of LPMOs is continuously evolving, and the development of new analytical techniques for identification and quantification of LPMO products is thus central to furthering our understanding of these enzymes. Furthermore, we anticipate that the new technology described in **Paper I** and the methods developed as part of this study will enable development of methods tailored for separation of other carbohydrate products, such as hemicellulose-derived oxidized oligosaccharides, as has been the case for ICS systems relying on NaOAc/NaOH-based eluents (Agger et al., 2014).

3.2 Paper II: Substrate-dependent cellulose saccharification efficiency and LPMO activity of Cellic CTec2 and a thermostable enzyme cocktail from *Thermoascus aurantiacus*, and the impact of H_2O_2-producing glucose oxidase

While the use of lignocellulosic biomass to produce sustainable alternatives to fossil fuels is a highly appealing prospect, the recalcitrance of this material still represents a major challenge in modern biorefining (Balan et al., 2013; Rosales-Calderon and Arantes, 2019). Although major progress in cellulose saccharification has been achieved in the past two decades, in part due to the discovery of LPMOs, optimization of LPMO performance during enzymatic hydrolysis of lignocellulosic biomass remains challenging, especially when using lignin-rich feedstocks (Hu et al., 2014; Rodríguez-Zúñiga et al., 2015; Bissaro et al., 2017; Müller et al., 2018; Calderaro et al., 2020; Costa et al., 2020). *T. aurantiacus* produces a few-component, LPMO-rich blend of cellulolytic enzymes, and due to the thermostable nature of its secretome, has recently gained attention for its potential to be used as a cocktail producer for saccharification of cellulosic substrates at elevated temperatures (McClendon et al., 2012; Schuerg et al., 2017; Fritsche et al., 2020). In the work described in **Paper II**, we have compared this LPMO-rich and relatively simple cellulolytic enzyme cocktail with the commercial cellulase preparation Cellic CTec2 in saccharification of lignin-poor sulfite-pulped spruce (SPS) and lignin-rich steam exploded birch (SEB). In this study, we have used relatively high dry matter concentrations and high temperatures, and have investigated the effects of two commonly used LPMO reducing agents, AscA and GA, when working with the SPS substrate (which, in contrast to SEB, does not contain sufficient reducing power to drive the LPMO reaction). In addition, we tested the effect of adding *in situ* H_2O_2-producing GOx to reactions with Cellic CTec2 acting on SPS or SEB. The goal of this study was to further investigate the role of LPMOs during cellulose depolymerization by cellulase cocktails, and to assess ways in which LPMO activity can be optimized under close-to industrial conditions and with different substrates.

Saccharifications of lignin-poor SPS at 50°C and 60°C with and without 1 mM AscA showed that at 50°C, saccharification yields with Cellic CTec2 were higher than those obtained with the *T. aurantiacus* cocktail (**Paper II, Figure 1A and B**). However, at 60°C, glucan conversion by Cellic CTec2 slowed down early in the saccharification reaction, likely due to thermal inactivation of essential enzymes. In contrast, the *T. aurantiacus* cocktail produced similar saccharification yields at 60°C as Cellic CTec2 did at 50°C, highlighting the thermostability of the *T. aurantiacus* enzymes and the potential of this cocktail for cellulose saccharification at high temperatures. While activation of the LPMOs by addition of AscA to the reaction mixture resulted in notably higher amounts of LPMO products in reactions with the *T. aurantiacus* cocktail at both temperatures (**Paper II, Figure 1C and D**), the boost in saccharification yield was similar for both cocktails. Comparing the amounts of LPMO products generated with the improvement in glucan conversion for both cocktails (**Paper II, Figure 2B**) indicated that although the *T. aurantiacus* cocktail produced more Glc4gemGlc overall, the impact of LPMO activity on glucan conversion was higher for Cellic CTec2 than for the *T. aurantiacus* cocktail. Thus, while LPMO activity clearly contributes to improving overall glucan conversion, very high levels of LPMO activity are not necessarily beneficial. A closer look at the effect of adding AscA on glucan conversion also showed that LPMO activity becomes more important towards the later phase of the saccharification reaction (**Paper II, Figure 2A**), perhaps due to a decrease in the amount of readily accessible substrate for hydrolytic cellulases as the saccharification proceeds. Preliminary studies of saccharification reactions using GA in place of AscA showed low amounts of LPMO products and little-to-no effect of adding GA on glucan conversion. These results highlight the important effect of the reductant on LPMO activity and thus also on glucan conversion.

To investigate potential substrate-dependent differences between the two cocktails, saccharification reactions with lignin-rich SEB were performed (**Paper II, Figure 3A and B**). As discussed above, the ability of lignin-rich feedstocks to provide adequate reducing power for LPMOs is well-documented, and these reactions were therefore performed without addition of an exogenous reductant. Striking differences between the two cocktails were seen in terms of glucan conversion. Cellic CTec2 was far more efficient at 50°C than at

60°C, and also more efficient than the *T. aurantiacus* cocktail at both temperatures. As expected, the *T. aurantiacus* cocktail performed better at 60°C than at 50°C, but in contrast to what was seen with SPS, signs of enzyme inactivation were visible at 60°C, both in terms of reduced glucan conversion and production of the dominant LPMO product, Glc4gemGlc. The observation of initial high levels of Glc4gemGlc, followed by decreasing amounts of this LPMO product observed for both enzyme cocktails at 60°C, is indicative of LPMO inactivation due to excess amounts of H_2O_2. These results indicate that the lignin-derived compounds in SEB create a redox environment that is very different compared to in reactions with SPS, and that the LPMOs in the two cocktails respond differently to different redox conditions. It is conceivable that Cellic CTec2 is better-suited than the *T. aurantiacus* cocktail for hydrolysis of polysaccharides in a lignin-rich feedstock, which likely contains compounds that may inhibit cellulases (Berlin et al., 2006; Ximenes et al., 2011). However, it is clear that saccharification of SEB at 60°C leads to unfavorable reaction conditions for both enzyme preparations, likely due to active redox environments resulting in high levels of H_2O_2, which destabilize the reaction system.

While H_2O_2-feeding during enzymatic saccharification of SPS has been shown to improve saccharification yields, excess levels of H_2O_2 lead to autocatalytic inactivation of LPMOs and may also damage cellulases. It appears that an optimal balance between reducing power and H_2O_2 concentration must be struck in order to optimize LPMO action and maximize saccharification yields. We therefore performed a series of experiments with SPS and SEB using Cellic CTec2 with added GOx for *in situ* H_2O_2 production. For the reactions with SPS, we investigated the use of both AscA and GA in order to probe the impact of the reductant on LPMO activity and saccharification yield in the presence of *in situ*-produced H_2O_2. Addition of GOx to reactions with SPS and AscA resulted in a clear increase in LPMO activity, and, at lower GOx concentrations, improved saccharification yields, and this effect was independent of the concentration of AscA (**Paper II, Figure 4A-C, E-G**). It thus seems that under these conditions, the low amount of lignin in the SPS (3.3% w/w) was adequate for reduction of the LPMOs, and the low GOx concentrations led to production of sufficient but not excess amounts of H_2O_2 for the LPMOs operating in a peroxygenase mode. At higher concentrations of GOx (and thus higher amounts of *in situ*-produced H_2O_2) (**Paper II,**

Figure 4D and H), the reactions showed signs of LPMO inactivation over time and decreased saccharification yields. Results from reactions with high concentrations of GOx and low amounts of reducing power indicated that under these conditions, the reductant became limiting, likely due to increased occurrence of non-productive reactions of reduced unbound LPMOs with H_2O_2, leading to rapid reductant depletion. It is likely that under these conditions, in addition to LPMO inactivation and potential cellulase inactivation, the reaction system becomes unstable due to the release of copper from inactivated LPMOs, which also contributes to reductant depletion (Stepnov et al., 2022b). These results illustrate that while careful consideration and control of reductant and H_2O_2 levels is a prerequisite, GOx can play a useful role in boosting LPMO activity and glucan conversion in saccharification of lignin-poor substrates.

As mentioned above, saccharification reactions with SPS and GA as a reducing agent showed low levels of LPMO activity and decreased saccharification yields as compared to reactions with AscA. To investigate whether these differences were due to reduced levels of H_2O_2 production within the system, we assessed the impact of GA on the saccharification of SPS by Cellic CTec2 in the presence of GOx. Notably, GA appeared to decrease glucan conversion in reactions without GOx (**Paper II, Figure 5A**), which may be due to inhibitory effects of GA on cellulases (Ximenes et al., 2011). As expected based on the initial studies with GA, low levels of Glc4gemGlc were observed in reactions without GOx (**Paper II, Figure 5E**). Addition of GOx resulted in increased LPMO activity (**Paper II, Figure 5F-H**), indicating that the low levels of LPMO activity in reactions with GA without GOx are not due to the inability of GA to sufficiently reduce the LPMOs, but rather due to insufficient reductant-driven H_2O_2 generation. The corresponding glucan conversion data (**Paper II, Figure 5B-D**) indicate that similar to in reactions with AscA, there is a delicate balance that must be achieved between reductant and H_2O_2 concentrations in order to maximize saccharification yields. Importantly, the data in **Paper II** show that differences between reductant performance that become visible in purely reductant-driven reactions may become much smaller, and even insignificant, in reactions with reductant-independent supply of H_2O_2.

To assess the impacts of *in situ* H_2O_2 production by GOx on LPMO activity and saccharification efficiency in the presence of higher amounts of redox-active lignin, we also performed saccharifications of SEB with Cellic CTec2 and GOx (**Paper II, Figure 6**). Addition of GOx to the reaction system decreased glucan conversion, especially at higher GOx levels, and decreasing Glc4gemGlc levels over time indicated inactivation of LPMOs due to excess H_2O_2 concentrations. These results clearly indicate that increasing the H_2O_2 concentration in reaction systems with innate redox capabilities may be detrimental to both cellulase and LPMO activity.

Several interesting conclusions can be drawn from the results of the study described in **Paper II**. First, it is clear that the cellulolytic enzyme cocktail secreted by *T. aurantiacus* has great potential for hydrolysis of pretreated lignin-poor substrates at elevated temperatures. Additionally, *in situ* H_2O_2 production by GOx can improve the LPMO activity and saccharification efficiency of Cellic CTec2 in reactions with lignin-poor substrates. Of note, reactions with GOx were efficient even in the absence of reducing agent, which may provide new avenues for industrial saccharification of SPS using GOx. However, multiple parameters tested in these experiments illustrate that careful control of the reaction conditions is needed to maximize cellulase saccharification while simultaneously maintaining a stable reaction system. Creating optimal, well-controlled conditions is particularly complicated in reactions with redox-active substrates such as SEB. In such reactions, multiple redox reactions will lead to both generation and consumption of H_2O_2, making the outcomes of these reactions less predictable compared to reactions with lignin-poor substrates. Thus, while control of reaction conditions is more straightforward when working with lignin-poor substrates, for lignin-rich feedstocks, process conditions should be optimized with individual substrates in mind. It is also clear that careful consideration of the choice of reducing agent is essential for optimizing glucan conversion and LPMO efficiency when working with substrates with limited reducing power.

3.3 Paper III: Functional characterization of a lytic polysaccharide monooxygenase from *Schizophyllum commune* that degrades non-crystalline substrates and displays strong peroxygenase activity

While LPMOs are generally considered to be essential for depolymerization of insoluble, crystalline polysaccharides such as cellulose and chitin, some LPMOs are active on soluble cello-oligosaccharides and on various hemicelluloses. The functional characterization of LPMOs is essential to furthering our understanding of their catalytic mechanism and substrate specificities, and may provide insight into the biological reasons for their multiplicity in many fungi. **Paper III** describes the cloning, expression, and functional characterization of one of 22 putative AA9 LPMOs from the fungus *Schizophyllum commune*, *Sc*LPMO9A. Previous studies of *S. commune* have shown that *Sc*LPMO9A is secreted during growth of this fungus on a variety of substrates and under different conditions, suggesting that it may play an essential role in substrate depolymerization and nutrient acquisition. In addition, the *S. commune* secretome has shown significant glucan and xylan conversion abilities in saccharification reactions with a range of lignocellulosic substrates (Zhu et al., 2016; Almási et al., 2019).

Phylogenetic analysis of the *Sc*LPMO9A sequence (**Paper III, Figure 1**) indicated that this LPMO clusters with C4-oxdizing LPMOs shown to be active on soluble cello-oligosaccharides, as well as hemicellulosic substrates such as mixed-linkage glucan, glucomannan, and xyloglucan (Frandsen et al., 2016; Simmons et al., 2017). The well-studied *Nc*LPMO9C, active on cellopentaose and cellohexaose, and to a lesser extent cellotetraose, as well as hemicellulosic substrates (Agger et al., 2014; Isaksen et al., 2014), is part of the neighboring cluster. Multiple-sequence alignment (MSA) of the catalytic domains of *Sc*LPMO9A and closely related C4-oxidizing AA9s (**Paper III, Figure 2**) revealed that *Sc*LPMO9A has a tryptophan (Trp202) at a solvent-exposed position in contrast to the other AA9s in the MSA, where a tyrosine is found in this position. This tyrosine has previously been shown to interact with oligomeric substrates during their binding to the LPMO active site (Courtade et al., 2016; Frandsen et al., 2016). A structural model of

*Sc*LPMO9A created using the crystal structure of its closest homolog *Ls*LPMO9A bound to cellohexaose (**Paper III, Figure 3**) revealed a shallow groove type topology of the substrate-binding surface, similar to what has been observed for *Ls*LPMO9A (Frandsen et al., 2016), and differing somewhat from the typical flat binding surfaces commonly observed for LPMOs active on insoluble crystalline substrates.

Following cloning in *Escherichia coli* and subsequent expression and purification, we verified the ability of *Sc*LPMO9A to consume and produce H_2O_2 in a manner expected of AA9 LPMOs using modified versions of previously established assay protocols (Kittl et al., 2012; Breslmayr et al., 2018). The results indicated that *Sc*LPMO9A was correctly folded and contained a redox-active copper-ion in its active site. The redox potential of *Sc*LPMO9A was determined to be 186 +/- 10 mV, a value that is in the range of what has previously been observed for AA9s, and approximately 40 mV lower than the value obtained for *Nc*LPMO9C (Borisova et al., 2015; Petrović et al., 2018).

As expected based on previous studies of *Sc*LPMO9A homologs, mapping of the activity of *Sc*LPMO9A on several cellulosic substrates (**Paper III, Figure 4**) revealed C4-oxidizing activity on cellopentaose and PASC. The main C4-oxidized product from reactions with cellopentaose was Glc4gemGlc, suggesting that *Sc*LPMO9A binds and cleaves cellopentaose similarly to *Nc*LPMO9C (-3 - +2 binding). Interestingly, no activity on Avicel was detected, while such activity has been documented for *Nc*LPMO9C (Isaksen et al., 2014). Likewise, very low activity was observed in reactions with sulfite-pulped spruce (SPS). These results suggest that *Sc*LPMO9A has a preference for soluble and/or amorphous substrates rather than crystalline cellulose.

Further investigation of the activity of *Sc*LPMO9A on soluble cellodextrins (**Paper III, Figure 5**) revealed that *Sc*LPMO9A is also active on both cellohexaose and cellotetraose. The high activity on cellotetraose contrasts with studies of *Nc*LPMO9C, which showed low activity on this short oligomer. Reactions with cellohexaose showed that *Sc*LPMO9A has two productive binding modes, -4 - +2 and -3 - +3, as a mixture of cellobiose, cellotriose, Glc4gemGlc and $Glc4gemGlc_2$ was generated. While similar results were seen in reactions

with *Nc*LPMO9C (although accumulation of cellotetraose was observed, as expected), *Nc*LPMO9C appeared to have a preference for -4 - +2 binding, generating mostly cellotetraose and Glc4gemGlc, and only minor amounts of cellotriose and Glc4gemGlc$_2$. Although concrete quantitative statements cannot be made based solely on peak intensities in the HPAEC-PAD chromatograms and single time point measurements, the chromatograms showed that *Sc*LPMO9A generated more Glc4gemGlc$_2$, perhaps indicating a preference for the -3 - +3 binding mode in cleavage of cellohexaose.

Screening of *Sc*LPMO9A activity on hemicellulosic substrates alone or in combination with PASC revealed activity on mixed-linkage glucan (β-glucan; BG), konjac glucomannan (KGM), and xyloglucan (tamarind xyloglucan, TXG, and xyloglucan oligomers, XGO) (**Paper III, Figures 6-7**). Comparison of HPAEC-PAD product profiles generated by *Sc*LPMO9A with those generated by *Nc*LPMO9C in reactions with KGM and BG showed differences that could be indicative of different preferential substrate-binding modes. In addition, in reactions with KGM and BG alone, product peak intensities were substantially higher for reactions with *Sc*LPMO9A than for reactions with *Nc*LPMO9C, hinting at potential greater affinity of *Sc*LPMO9A for these substrates. In reactions with xyloglucan, product profiles between the two LPMOs looked similar, although *Sc*LPMO9A product peaks were more intense than those of *Nc*LPMO9C, particularly in reactions with the xyloglucan substrates alone. Small differences in the product profiles indicated that these LPMOs may display minor differences in their cleavage patterns when acting on xyloglucan. Further studies of the cleavage pattern obtained with xyloglucan via MALDI-TOF MS (**Paper III, Figures 8-9**) showed that, similarly to *Nc*LPMO9C (Agger et al., 2014; Kojima et al., 2016; Sun et al., 2020), *Sc*LPMO9A is "substitution-sensitive," meaning that the LPMO only, or almost exclusively, cleaves the xyloglucan backbone adjacent to non-substituted glucose moieties. Although (weak) xylan activity has previously been reported for *Ls*LPMO9A (Simmons et al., 2017), with which *Sc*LPMO9A shares 61.1% sequence identity, no activity was detected in reactions of *Sc*LPMO9A with beechwood xylan, birchwood xylan, or arabinoxylan, alone or in combination with PASC.

The ability of LPMOs to boost saccharification of cellulosic substrates, including SPS, is well-documented. However, addition of *Sc*LPMO9A and AscA to an LPMO-poor cellulase cocktail did not boost hydrolysis of SPS (**Paper III, Figure 10**). Although some Glc4gemGlc accumulation was detected, the concentration of LPMO product was lower than what is to be expected for reactions in which an LPMO contributes significantly to cellulose saccharification (e.g. (Müller et al., 2018)). In addition, the amount of C4-oxidized product decreased over the course of the hydrolysis reaction, indicating that Glc4gemGlc production by *Sc*LPMO9A ceased early in the reaction, likely due to a lack of suitable substrate. Given the previously observed limited activity of *Sc*LPMO9A on SPS and its stronger activity on amorphous cellulose and on cello-oligosaccharides, these results may indicate that LPMO products generated in this reaction were a result of *Sc*LPMO9A action on (smaller) amorphous portions of the SPS substrate, which likely does not significantly affect the overall saccharification efficiency for the more crystalline SPS.

To further investigate functional properties of *Sc*LPMO9A, we evaluated its ability to utilize H_2O_2 in reactions with PASC, and compared H_2O_2-driven LPMO activity with the activity under "monooxygenase conditions" (i.e. a reaction without exogenously supplied H_2O_2) (**Paper III, Figure 11**). The approximate rate of Glc4gemGlc production by *Sc*LPMO9A under "monooxygenase conditions" based on the first three minutes of the progress curve without added H_2O_2 was 0.8 min^{-1}. When supplied with H_2O_2, a drastic rate increase was observed. At the first measuring point, product concentrations corresponded to approximately 40% of the added H_2O_2. These product levels indicate close-to stoichiometric conversion of the supplied H_2O_2, as previous studies of CBM-free LPMOs acting on insoluble substrates have shown that approximately 50% of LPMO-generated oxidized species remain in the insoluble substrate under the conditions used (Courtade et al., 2018). Estimation of the reaction rate based on the first three minutes of the progress curve with 250 µM H_2O_2 showed that *Sc*LPMO9A operated at a rate of about 80 min^{-1}, about two orders of magnitude higher than the rate observed for the reaction without supplemented H_2O_2. To the best of our knowledge, this is the highest rate observed for an LPMO acting on an amorphous insoluble substrate (of note, this rate is underestimated, possibly by a lot, since the reaction was finished already by the first measuring point).

A previous in-depth kinetic study of *Nc*LPMO9C showed that this LPMO can catalyze a very efficient peroxygenase reaction when supplied with exogenous H_2O_2 and a soluble substrate, reaching rates of >100 s^{-1} for cellopentaose (Rieder et al., 2021b). Given these data and the observed activity of *Sc*LPMO9A on cellodextrins, we investigated the ability of *Sc*LPMO9A to utilize H_2O_2 in oxidative cleavage of cellopentaose, using a reaction setup where H_2O_2 was only added at the start of the reaction (**Paper III, Figure 12**). Within 30 s, *Sc*LPMO9A catalyzed near stoichiometric conversion of 200 µM H_2O_2, reaching an estimated maximum rate of 11 s^{-1} based on the first 10 s of the progress curves. While increasing the initial H_2O_2 concentration to 400 µM appeared to boost the initial rate of the reaction, progress curves at this higher concentration of H_2O_2 showed signs of LPMO inactivation and/or reductant depletion.

During the course of this work, a study of several fungal AA9s expressed in the yeast *Pichia pastoris*, including *Sc*LPMO9A, was published (Frandsen et al., 2021). Remarkably, the authors did not detect activity of *Sc*LPMO9A on cellotetraose, or on glucomannan or xyloglucan, whereas activity on Avicel was reported. These results are in stark contrast to the results reported in **Paper III** and discussed above. The data shown in **Paper III** demonstrate that *Sc*LPMO9A is a C4-oxidizing LPMO active on a range of hemicellulosic substrates, in addition to amorphous cellulose and soluble cello-oligosaccharides. The very limited activity on crystalline substrates suggests that *Sc*LPMO9A may have evolved to catalyze reactions not typically associated with LPMO function, which as of yet remain enigmatic. The comparison of *Sc*LPMO9A with the well-studied *Nc*LPMO9C, also active on soluble cellodextrins, suggested a different mode of binding to cellodextrins, enabling *Sc*LPMO9A to perform complete cleavage of 1 mM cellotetraose to native cellobiose and Glc4gemGlc, and leading to a preferential -3 - +3 binding mode for cleavage of cellohexaose. Further studies aimed at uncovering the structural basis for these subtle differences in substrate cleavage preferences are underway. Preliminary kinetic investigations of the peroxygenase activity of *Sc*LPMO9A showed that despite being more sensitive to high levels of H_2O_2 than *Nc*LPMO9C, *Sc*LPMO9A catalyzes an efficient peroxygenase reaction in the presence of relatively low amounts of H_2O_2, not only in reactions with soluble cellopentaose but also in the depolymerization of an insoluble amorphous cellulosic substrate.

3.4 Paper IV: Quantifying oxidation of cellulose-associated glucuronoxylan by two lytic polysaccharide monooxygenases from *Neurospora crassa*

Following the initial discovery of hemicellulolytic activity of *Nc*LPMO9C (Agger et al., 2014), many AA9s have been found to show both cellulolytic and hemicellulolytic activity. However, until recently, oxidative cleavage of xylan had only been convincingly demonstrated for two AA9s, *Mt*LPMO9A from *M. thermophilia* (Frommhagen et al., 2015) and *Mc*LPMO9H from *Malbranchea cinnamomea* (Hüttner et al., 2019). **Paper IV** describes the characterization of several xylan-active AA9 LPMOs, including *Nc*LPMO9F, for which C1-oxidizing cellulose activity had already been demonstrated (Kittl et al., 2012), and the previously uncharacterized *Nc*LPMO9L. Quantification of generated oxidized products allowed, for the first time, comparison of the xylan- and cellulose-oxidizing activities of multiple LPMOs acting on a cellulose-xylan mixture. In addition, phylogenetic and structural analysis enabled the identification of distinctive features shared by xylan-active LPMOs.

Based on phylogenetic analysis indicating that *Nc*LPMO9F and *Nc*LPMO9L clustered closely together with *Mt*LPMO9A and *Mc*LPMO9H (**Paper IV, Figure 1**), for which xylanolytic activity had previously been demonstrated, we screened these LPMOs for activity on beechwood glucuronoxylan (BeWX) alone and in combination with PASC. MALDI-TOF MS analysis revealed the formation of oxidized xylo-oligosaccharides in reactions with PASC and BeWX (**Paper IV, Figure 2**). In addition to oxidized cello-oligomers derived from PASC, oxidized non-substituted and 4-O-methylglucuronylated (GlcAOMe-substituted) xylo-oligosaccharides were detected in reactions with both *Nc*LPMO9F and *Nc*LPMO9L. The presence of sodium adducts of the sodium salts of oxidized xylo-oligosaccharides indicated that both LPMOs perform C1-oxidative cleavage of xylan. The mass spectrum for *Nc*LPMO9F showed a clear prevalence of oxidized xylan-derived products, indicating that in addition to its cellulolytic activity, this LPMO has significant xylanolytic activity. While conclusive statements based solely on MALDI-TOF MS analysis are not possible, the observed product profiles could indicate that *Nc*LPMO9F acts preferentially on xylan in a

cellulose-xylan mixture. The MALDI-TOF MS analysis showed a different ratio between oxidized cellulose- and xylan-derived products for *Nc*LPMO9L, with a seemingly larger fraction of the former.

Intrigued by these results, we pursued HPAEC-PAD analysis of the product mixtures generated in reactions with *Nc*LPMO9F, *Nc*LPMO9L, or *Mc*LPMO9H acting on PASC, PASC and BeWX, or BeWX alone, to obtain a more comprehensive overview of the distributions of cellulose- and xylan-derived LPMO products and how these may differ between the LPMOs (**Paper IV, Figure 3**). The results showed that none of the LPMOs are active on BeWX alone, and that the previously uncharacterized *Nc*LPMO9L performs C1-oxidative cleavage of PASC, generating products similar to those observed in corresponding reactions with *Nc*LPMO9F. All three LPMOs generated mixtures of oxidized cello- and xylo-oligosaccharides when incubated with PASC and BeWX, although, based on HPAEC-PAD peak intensities, the apparent ratios of these two types of oxidized products varied considerably between the enzymes. For instance, *Nc*LPMO9F appeared to generate larger amounts of xylan-derived oxidized products than cellulose-derived oxidized products, corresponding to what was observed in MALDI-TOF MS analysis, while the inverse trend was observed for the product mixture generated by *Nc*LPMO9L, which appeared to primarily contain oxidized cello-oligosaccharides. *Mc*LPMO9H generated a more intermediate mixture of cellulose- and xylan-derived products. Comparison of HPAEC-PAD chromatograms of LPMO-generated product mixtures with an in-house generated C1-oxidized xylo-oligosaccharide standard enabled the identification of non-substituted $Xyl_{1-5}Xyl1A$ ($Xyl2\text{-}6_{ox}$) species (**Paper IV, Figure 4**). The MALDI-TOF MS spectra suggest that remaining unidentified peaks are likely oxidized non-substituted higher DP and GlcAOMe-substituted xylo-oligosaccharides.

To investigate whether PASC- and BeWX-derived oxidized species could be quantified via HPAEC-PAD, we explored the ability to achieve separation and identification of oxidized products after treating *Nc*LPMO9F-generated product mixtures with *Tr*Cel7A (a GH7 cellulase from *T. reesei*) and *Cj*Xyn10A (a GH10 endoxylanase from *Cellvibrio japonicus*). Subsequent HPAEC-PAD analysis (**Paper IV, Figure 5B**) revealed the presence of Glc_{1-}

$_2$Glc1A and Xyl$_{1-2}$Xyl1A in product mixtures from reactions with PASC and BeWX, in addition to presumed native and/or oxidized GlcAOMe-substituted species. The oxidized species of interest (Glc$_{1-2}$Glc1A and Xyl$_{1-2}$Xyl1A) did not co-elute and gave peak intensities well above the baseline, indicating that quantification of these products was possible. A control experiment using the non-xylan active *Gt*LPMO9B from *Gloeophyllum trabeum* showed no formation of oxidized xylo-oligosaccharides, but comparison of product profiles with and without BeWX indicated that the presence of xylan hampered cellulose oxidation by *Gt*LPMO9B (**Paper IV, Figure 5C and D**).

Quantification of *Tr*Cel7A/*Cj*Xyn10A-treated product mixtures generated in reactions of *Nc*LPMO9F with PASC or PASC and BeWX (**Paper IV, Figure 6A**) showed that in the presence of PASC alone, generation of oxidized GlcGlc1A and Glc$_2$Glc1A reached a maximum of 165 μM, far below the theoretical maximum of 1 mM that would be obtained by stoichiometric conversion of supplied AscA. In addition, the progress curve was not linear, which is a sign of enzyme inactivation. When acting on a mixture of PASC and BeWX (**Paper IV, Figure 6B**), the concentration of cellulose-derived oxidized products was lower (80 μM), while the concentration of xylan-derived oxidized products reached 266 μM, indicating that *Nc*LPMO9F acts preferentially on xylan. Additionally, the shape of the progress curve showed less signs of LPMO inactivation, as the levels of oxidized xylan products were continuously increasing throughout the reaction. Taken together, these results suggest that xylan inhibits cellulose oxidation by *Nc*LPMO9F in the PASC-BeWX mixture, likely due to coating of the cellulose fibers that makes these less accessible to the LPMO. Furthermore, the results show that BeWX (when complexed with PASC) is a more suitable substrate for *Nc*LPMO9F than PASC, as evidenced by the levels of Xyl$_{1-2}$Xyl1A generated in reactions with PASC and BeWX being higher than the levels of Glc$_{1-2}$Glc1A generated in reactions with PASC.

Identical quantifications of oxidized cello- and xylo-oligosaccharides produced by *Nc*LPMO9L and *Mc*LPMO9H in reactions with PASC or PASC and BeWX showed remarkable differences in substrate preferences between the LPMOs (**Paper IV, Figure 6C and D**). In reactions with PASC alone, the two *N. crassa* LPMOs generated similar amounts of oxidized

cellobiose and cellotriose, while *Mc*LPMO9H produced nearly twice as much oxidized cello-oligomers. In reactions with PASC and BeWX, *Nc*LPMO9F generated nearly three times more xylan-derived than cellulose-derived oxidized products (3:1 ratio), whereas this ratio was about 1:1 for *Mc*LPMO9H and 0.5:1 for *Nc*LPMO9L. Of note, only quantification of non-substituted oxidized xylo-oligosaccharides was performed, which means that the total amount of xylan oxidation is underestimated.

Further phylogenetic and sequence analysis of these LPMOs revealed that the xylan-active *Nc*LPMO9F and *Mt*LPMO9A are found in a distinct clade, separate from the xylan-active *Nc*LPMO9L and *Mc*LPMO9H, which are located in closely related sister clades (**Paper IV, Figure 1**). While the structural features that determine LPMO substrate specificity remain somewhat enigmatic, it is clear that LPMO substrate-binding surfaces can vary significantly due to sequence variations in variable regions that have been classified as four loops (L2, L3, LS, LC; (Wu et al., 2013)) or five segments (Seg1-5; (Laurent et al., 2019; Sun et al., 2020)). To identify structural features of potential importance for xylanolytic LPMO activity, a multiple-sequence alignment (MSA) was performed including xylan-active *Nc*LPMO9F, *Nc*LPMO9L, *Mc*LPMO9H, and *Mt*LPMO9A, a few AA9 LPMOs considered potentially xylan-active based on phylogenetic analysis, and other AA9 LPMOs for which we could not demonstrate xylan activity (**Paper IV, Figure 7**). In addition, the substrate-binding surfaces of the four xylan-active LPMOs were compared (**Paper IV, Figure 8**). The MSA indicated that the LPMOs active on cellulose-associated xylan have shorter L2 and L3 loops (corresponding to shorter Seg1 and Seg2 segments), as well as a conserved tyrosine residue (Tyr2) adjacent to the first histidine of the histidine brace. This tyrosine appears to face inwards towards the protein core, making it unlikely to contribute to substrate binding. However, the presence of this Tyr2 residue is correlated with the presence of another conserved Tyr in a subgroup of the LPMOs that has xylan-active members (Tyr71 in *Nc*LPMO9F). This Tyr residue, which has previously been associated with oxidative regioselectivity (Borisova et al., 2015), is solvent-exposed and has the potential to interact with a bound substrate. The absence of this tyrosine in *Nc*LPMO9L coupled with the seemingly weaker xylanolytic activity of *Nc*LPMO9L as compared to the other xylan-active

LPMOs makes it tempting to speculate that this residue plays an important role in optimal binding to a xylan substrate.

In the context of lignocellulose depolymerization, the role of xylanolytic enzymes is thought to be not only to degrade xylan, but also to facilitate access to cellulose for cellulolytic enzymes. In the study described in **Paper IV**, we have shown that *Nc*LPMO9F and *Nc*LPMO9L are active on cellulose-associated glucuronoxylan. Through quantification of oxidized xylan- and cellulose-derived products, we demonstrated that xylan is the preferred substrate of *Nc*LPMO9F when acting on a mixture of cellulose and xylan. Quantification of product formation revealed functional variation between the various xylan-active LPMOs. It would be very interesting to study whether this functional variation relates to the variation of naturally occurring xylans with different substitution patterns. Likewise, it would be interesting to study the interplay between xylan-active LPMOs and other xylan-active enzymes, such as enzymes that remove substitutions. Phylogenetic analysis enabled the identification of two previously studied cellulose-active LPMOs presumed to have activity on glucuronoxylan, *Tt*LPMO9E from *T. terrestris* and *Pc*LPMO9D from *Phanerochaete chrysosporium*. Following the publication of **Paper IV**, activity on glucuronoxylan has indeed been demonstrated for *Tt*LPMO9E (Tõlgo et al., 2022). Taken together, these results warrant further studies of LPMOs active on both cellulose and xylan. For example, it would be intriguing to delve deeper into whether *Nc*LPMO9F has primarily evolved to degrade xylan, or whether it naturally serves a dual function, first depolymerizing xylan coating the cellulose fibers before acting on the cellulose within. These types of studies may also help elucidate whether hemicellulolytic LPMO activities could contribute to industrial saccharification of lignocellulosic biomass by removing recalcitrant xylan. Finally, it would be of great interest to carry out protein engineering studies to verify whether the structural features identified as potentially important for the xylan activity of AA9 LPMOs indeed confer this activity to the enzymes.

4 Concluding remarks and future perspectives

Decades of research have significantly advanced and expanded our knowledge of the enzymatic degradation of cellulose and related polysaccharides. The discovery of the oxidative action of LPMOs, and, more recently, the elucidation of their peroxygenase ability, have changed the ways in which we study the enzyme systems involved and revealed novel avenues for harnessing the power of enzymes in the depolymerization of lignocellulose. Nevertheless, several outstanding questions concerning the biological function and catalytic properties of LPMOs remain unanswered, including questions related to the reasons for their multiplicity in many fungi, their catalytic mechanism, their interaction with hydrolytic enzymes and co-substrates during biomass degradation, and potential alternative biological roles they may fulfill in nature.

The research presented in this thesis has addressed a range of fundamental and applied aspects of LPMOs. **Paper I** describes the implementation of an ICS-6000 system with a novel KMSA/KOH dual electrolytic eluent generation platform, which enabled the development of chromatographic methods for sensitive detection and quantification of mono- and oligomeric native, C1-, and C4-oxidized cellulose-derived LPMO products. The research described in **Paper II** demonstrates the industrial potential of an LPMO-rich *T. aurantiacus* cellulase cocktail for saccharification of lignin-poor SPS at high temperatures, and illustrates that, for lignin-poor substrates, addition of GOx can be an advantageous method for *in situ* generation of H_2O_2 to drive LPMO activity and boost glucan saccharification yields. **Paper III** describes the functional characterization of *Sc*LPMO9A, as an example of an LPMO whose primary function does not appear to be the degradation of crystalline cellulose. Instead, this LPMO is active on amorphous cellulose, various hemicelluloses, and cello-oligomers. Kinetic studies of *Sc*LPMO9A revealed strong peroxygenase activity both on cellopentaose and PASC, underpinning the peroxygenase nature of LPMOs. The research described in **Paper IV** led to the demonstration of major xylanolytic activities among some members of the AA9 LPMO family, such as *Nc*LPMO9F

and *Nc*LPMO9L, which degrade beechwood glucuronoxylan when the xylan is mixed with cellulose (PASC). Simultaneous quantification of oxidized xylan- and cellulose-derived LPMO products, which had not been previously described, showed different preferences for these two substrates amongst xylan-active LPMOs.

While the results presented in this thesis contribute to furthering our knowledge of several aspects of LPMOs, these findings also generate questions and hypotheses suitable as topics for future studies. For instance, we expect that the established chromatographic methods based on dual electrolytic generation of KMSA/KOH-based eluents for separation and quantification of cellulose-derived LPMO products described in **Paper I** will provide a foundation for method development for detection and separation of more structurally complex hemicellulose-derived products. The analysis of C4-oxidized cello-oligomers remains problematic due to product instability, and it would be interesting and worthwhile to investigate the development of alternate methods for analysis of these compounds, for example methods based on porous graphitized carbon chromatography (Westereng et al., 2016).

The promising results obtained using the *T. aurantiacus* cocktail (**Paper II**) warrant further research, for example on optimizing enzyme production to reach economic viability. Clearly, for certain substrates, this cocktail provides an opportunity for carrying out saccharification reactions at elevated temperatures. The results from **Paper II** emphasize the importance of controlling H_2O_2 levels, and further studies on how to do this in an optimal manner, for different substrates, are of great interest. **Paper II** shows that although *in situ* H_2O_2 generation by GOx is an efficient way to boost LPMO activity, and thus cellulase efficiency in saccharification of lignin-poor substrates, the situation is more complex when using lignin-rich, redox-active substrates. In some cases, the use of catalase as an H_2O_2-scavenger may contribute to achieving an optimal balance between H_2O_2 generation and consumption, as has indeed been documented by Scott and colleagues (who, notably, were not aware of the peroxygenase activity of LPMOs) (Scott et al., 2016). It would be of particular interest to assess whether the use of a thermostable catalase could improve the

saccharification of lignin-rich substrates such as SEB by the *T. aurantiacus* cocktail at high temperatures.

As discussed above, recent studies have demonstrated that copper released by LPMOs upon autocatalytic inactivation can significantly destabilize reaction systems because copper triggers self-propagating H_2O_2 generation (Stepnov et al., 2022b). It could be advantageous, although likely challenging, to consider these findings from an applied perspective in order to learn more about and potentially prevent process conditions that destabilize LPMOs and other enzymes in the reaction system. While it is not clear if copper release from the LPMO is relevant when using industrial substrates (which may contain metal ions), it would certainly be worthwhile to assess the possible impact of adding metal ion scavengers to saccharification reactions. In any case, it is clear that substrate-specific process optimization is crucial for maximization of the LPMO potential and the overall efficiency of lignocellulose saccharification by cellulase cocktails.

The characterization of AA9 LPMOs described in **Paper III** and **Paper IV** add to the growing body of information on the varying substrate specificities of LPMOs, and provide a basis for further research regarding the structural determinants of these substrate specificities and the true biological roles of LPMOs. It is conceivable that LPMOs active on soluble substrates, such as *Sc*LPMO9A, serve a natural purpose not related to lignocellulose conversion which remains to be uncovered. In the case of this LPMO, the apparent lack of activity on crystalline substrates combined with seemingly strong activity on several other substrates warrants further investigation. In fact, NMR-based studies (Courtade et al., 2016) of the interaction between this LPMO and several of its substrates are ongoing, and may lead to the identification of structural features that affect substrate-binding and specificity.

The demonstration by precise quantitative analysis that xylan-active *Nc*LPMO9F and *Nc*LPMO9L, produced by the same organism, generate different cellulose-xylan product ratios when incubated with both polysaccharides suggests that these enzymes have evolved to target distinct sites within the lignocellulose structure. It would therefore be interesting to evaluate if and in what ways xylan activity as such, as well as the varying

xylan preferences, may contribute to improved saccharification of xylan-containing lignocellulosic biomass. Remarkably, the potential of hemicellulolytic LPMO activity for improved biomass processing remains largely unexplored.

In conclusion, the work described in this thesis increases our understanding of LPMO diversity, the application of LPMOs in lignocellulose processing, and the analysis of LPMO-generated mono- and oligosaccharides. LPMOs are fascinating enzymes with a proven, but possibly not fully exploited, potential in biomass processing. The research presented in this thesis will hopefully contribute to a better understanding of LPMOs that will eventually lead to more insight into their biological roles and provide ways to optimize their use in industrial applications.

5 References

AACHMANN, F. L., SØRLIE, M., SKJÅK-BRÆK, G., EIJSINK, V. G. H., & VAAJE-KOLSTAD, G. 2012. NMR structure of a lytic polysaccharide monooxygenase provides insight into copper binding, protein dynamics, and substrate interactions, *Proceedings of the National Academy of Sciences of the United States of America*, 109: 18779-18784.

ADAV, S. S., CHAO, L. T., & SZE, S. K. 2012. Quantitative secretomic analysis of *Trichoderma reesei* strains reveals enzymatic composition for lignocellulosic biomass degradation, *Molecular & Cellular Proteomics*, 11: M111.012419.

ADAV, S. S., RAVINDRAN, A., CHAO, L. T., TAN, L., SINGH, S., & SZE, S. K. 2011. Proteomic analysis of pH and strains dependent protein secretion of *Trichoderma reesei*, *Journal of Proteome Research*, 10: 4579-4596.

AGGER, J. W., ISAKSEN, T., VÁRNAI, A., VIDAL-MELGOSA, S., WILLATS, W. G. T., LUDWIG, R., HORN, S. J., EIJSINK, V. G. H., & WESTERENG, B. 2014. Discovery of LPMO activity on hemicelluloses shows the importance of oxidative processes in plant cell wall degradation, *Proceedings of the National Academy of Sciences of the United States of America*, 111: 6287-6292.

AGOSTONI, M., HANGASKY, J. A., & MARLETTA, M. A. 2017. Physiological and molecular understanding of bacterial polysaccharide monooxygenases, *Microbiology and Molecular Biology Reviews*, 81: e00015-00017.

ALMÁSI, É., SAHU, N., KRIZSÁN, K., BÁLINT, B., KOVÁCS, G. M., KISS, B., CSEKLYE, J., DRULA, E., HENRISSAT, B., NAGY, I., CHOVATIA, M., ADAM, C., LABUTTI, K., LIPZEN, A., RILEY, R., GRIGORIEV, I. V., & NAGY, L. G. 2019. Comparative genomics reveals unique wood-decay strategies and fruiting body development in the *Schizophyllaceae*, *New Phytologist*, 224: 902-915.

ÁLVAREZ, C., REYES-SOSA, F. M., & DÍEZ, B. 2016. Enzymatic hydrolysis of biomass from wood, *Microbial Biotechnology*, 9: 149-156.

ALVES, V. D., FONTES, C. M. G. A., & BULE, P. 2021. Cellulosomes: highly efficient cellulolytic complexes, *Sub-Cellular Biochemistry*, 96: 323-354.

ARANTES, V., JELLISON, J., & GOODELL, B. 2012. Peculiarities of brown-rot fungi and biochemical Fenton reaction with regard to their potential as a model for bioprocessing biomass, *Applied Microbiology and Biotechnology*, 94: 323-338.

ARIAS, P. A., BELLOUIN, N., COPPOLA, E., JONES, R. G., KRINNER, G., MAROTZKE, J., NAIK, V., PALMER, M. D., PLATTNER, G.-K., ROGELJ, J., ROJAS, M., SILLMANN, J., STORELVMO, T., THORNE, P. W., TREWIN, B., ACHUTA RAO, K., ADHIKARY, B., ALLAN, R. P., ARMOUR, K., BALA, G., BARIMALALA, R., BERGER, S., CANADELL, J. G., CASSOU, C., CHERCHI, A., COLLINS, W., COLLINS, W. D., CONNORS, S. L., CORTI, S., CRUZ, F., DENTENER, F. J., DERECZYNSKI, C., DI LUCA, A., DIONGUE NIANG, A., DOBLAS-REYES, F. J., DOSIO, A., DOUVILLE, H., ENGELBRECHT, F., EYRING, V., FISCHER, E., FORSTER, P., FOX-KEMPER, B., FUGLESTVEDT, J. S., FYFE, J. C., GILLETT, N. P., GOLDFARB, F., GORODETSKAYA, I., GUTIERREZ, J. M., HAMDI, R., HAWKINS, E., HEWITT, H. T., HOPE, P., ISLAM, A. S., JONES, C., KAUFMAN, D. S., KOPP, R. E., KOSAKA, Y., KOSSIN, J., KRAKOVSKA, S., LEE, J.-Y., LI, J., MAURITSEN, T., MAYCOCK,

T. K., MEINSHAUSEN, M., MIN, S.-K., MONTEIRO, P. M. S., NGO-DUC, T., OTTO, F., PINTO, I., PIRANI, A., RAGHAVAN, K., RANASINGHE, R., RUANE, A. C., RUIZ, L., SALLÉE, J.-B., SAMSET, B. H., SATHYENDRANATH, S., SENEVIRATNE, S. I., SÖRENSSON, A. A., SZOPA, S., TAKAYABU, I., TRÉGUIER, A.-M., VAN DEN HURK, B., VAUTARD, R., VON SCHUCKMANN, K., ZAEHLE, S., ZHANG, X., & ZICKFELD, K., *Technical Summary*, in *Climate Change 2021: The Physical Science Basis*, V. Masson-Delmotte, et al., Editors. 2021, Intergovernmental Panel on Climate Change, Cambridge University Press: In Press.

ARMESILLA, A. L., THURSTON, C. F., & YAGÜE, E. 1994. CEL1: a novel cellulose binding protein secreted by *Agaricus bisporus* during growth on crystalline cellulose, *FEMS Microbiology Letters*, 116: 293-299.

ASKARIAN, F., UCHIYAMA, S., MASSON, H., SØRENSEN, H. V., GOLTEN, O., BUNÆS, A. C., MEKASHA, S., RØHR Å, K., KOMMEDAL, E., LUDVIKSEN, J. A., ARNTZEN, M., SCHMIDT, B., ZURICH, R. H., VAN SORGE, N. M., EIJSINK, V. G. H., KRENGEL, U., MOLLNES, T. E., LEWIS, N. E., NIZET, V., & VAAJE-KOLSTAD, G. 2021. The lytic polysaccharide monooxygenase CbpD promotes *Pseudomonas aeruginosa* virulence in systemic infection, *Nature Communications*, 12: 1230.

AVCI, U., ZHOU, X., PATTATHIL, S., DA COSTA SOUSA, L., HAHN, M. G., DALE, B., XU, Y., & BALAN, V. 2019. Effects of extractive ammonia pretreatment on the ultrastructure and glycan composition of corn stover, *Frontiers in Energy Research*, 7.

BALAN, V., BALS, B., CHUNDAWAT, S. P., MARSHALL, D., & DALE, B. E. 2009. Lignocellulosic biomass pretreatment using AFEX, *Methods in Molecular Biology*, 581: 61-77.

BALAN, V., CHIARAMONTI, D., & KUMAR, S. 2013. Review of US and EU initiatives toward development, demonstration, and commercialization of lignocellulosic biofuels, *Biofuels, Bioproducts and Biorefining*, 7: 732-759.

BALS, B., ROGERS, C., JIN, M., BALAN, V., & DALE, B. 2010. Evaluation of ammonia fibre expansion (AFEX) pretreatment for enzymatic hydrolysis of switchgrass harvested in different seasons and locations, *Biotechnology for Biofuels*, 3: 1.

BANERJEE, G., CAR, S., SCOTT-CRAIG, J. S., BORRUSCH, M. S., & WALTON, J. D. 2010. Rapid optimization of enzyme mixtures for deconstruction of diverse pretreatment/biomass feedstock combinations, *Biotechnology for Biofuels*, 3: 22.

BARUAH, J., NATH, B. K., SHARMA, R., KUMAR, S., DEKA, R. C., BARUAH, D. C., & KALITA, E. 2018. Recent trends in the pretreatment of lignocellulosic biomass for value-added products, *Frontiers in Energy Research*, 6.

BECKHAM, G. T., MATTHEWS, J. F., PETERS, B., BOMBLE, Y. J., HIMMEL, M. E., & CROWLEY, M. F. 2011. Molecular-level origins of biomass recalcitrance: decrystallization free energies for four common cellulose polymorphs, *Journal of Physical Chemistry B*, 115: 4118-4127.

BECKHAM, G. T., STÅHLBERG, J., KNOTT, B. C., HIMMEL, M. E., CROWLEY, M. F., SANDGREN, M., SØRLIE, M., & PAYNE, C. M. 2014. Towards a molecular-level theory of carbohydrate processivity in glycoside hydrolases, *Current Opinion in Biotechnology*, 27: 96-106.

BEESON, W. T., PHILLIPS, C. M., CATE, J. H., & MARLETTA, M. A. 2012. Oxidative cleavage of cellulose by fungal copper-dependent polysaccharide monooxygenases, *Journal of the American Chemical Society*, 134: 890-892.

BEESON, W. T., VU, V. V., SPAN, E. A., PHILLIPS, C. M., & MARLETTA, M. A. 2015. Cellulose degradation by polysaccharide monooxygenases, *Annual Review of Biochemistry*, 84: 923-946.

BENGTSSON, O., ARNTZEN, M. Ø., MATHIESEN, G., SKAUGEN, M., & EIJSINK, V. G. H. 2016. A novel proteomics sample preparation method for secretome analysis of *Hypocrea jecorina* growing on insoluble substrates, *Journal of Proteomics*, 131: 104-112.

BENNATI-GRANIER, C., GARAJOVA, S., CHAMPION, C., GRISEL, S., HAON, M., ZHOU, S., FANUEL, M., ROPARTZ, D., ROGNIAUX, H., GIMBERT, I., RECORD, E., & BERRIN, J.-G. 2015. Substrate specificity and regioselectivity of fungal AA9 lytic polysaccharide monooxygenases secreted by *Podospora anserina*, *Biotechnology for Biofuels*, 8: 90.

BERLIN, A., BALAKSHIN, M., GILKES, N., KADLA, J., MAXIMENKO, V., KUBO, S., & SADDLER, J. 2006. Inhibition of cellulase, xylanase and beta-glucosidase activities by softwood lignin preparations, *Journal of Biotechnology*, 125: 198-209.

BHATTACHARYA, A. S., BHATTACHARYA, A., & PLETSCHKE, B. I. 2015. Synergism of fungal and bacterial cellulases and hemicellulases: a novel perspective for enhanced bio-ethanol production, *Biotechnology Letters*, 37: 1117-1129.

BIELY, P., VRŠANSKÁ, M., TENKANEN, M., & KLUEPFEL, D. 1997. Endo-β-1,4-xylanase families: differences in catalytic properties, *Journal of Biotechnology*, 57: 151-166.

BISCHOF, R. H., RAMONI, J., & SEIBOTH, B. 2016. Cellulases and beyond: the first 70 years of the enzyme producer *Trichoderma reesei*, *Microbial Cell Factories*, 15: 106.

BISSARO, B., ISAKSEN, I., VAAJE-KOLSTAD, G., EIJSINK, V. G. H., & RØHR, Å. K. 2018a. How a lytic polysaccharide monooxygenase binds crystalline chitin, *Biochemistry*, 57: 1893-1906.

BISSARO, B., RØHR Å, K., MÜLLER, G., CHYLENSKI, P., SKAUGEN, M., FORSBERG, Z., HORN, S. J., VAAJE-KOLSTAD, G., & EIJSINK, V. G. H. 2017. Oxidative cleavage of polysaccharides by monocopper enzymes depends on H_2O_2, *Nature Chemical Biology*, 13: 1123-1128.

BISSARO, B., RØHR, Å. K., SKAUGEN, M., FORSBERG, Z., HORN, S. J., VAAJE-KOLSTAD, G., & EIJSINK, V. G. H. 2016. Fenton-type chemistry by a copper enzyme: molecular mechanism of polysaccharide oxidative cleavage, *bioRxiv*, DOI: https://doi.org/10.1101/097022.

BISSARO, B., STREIT, B., ISAKSEN, I., EIJSINK, V. G. H., BECKHAM, G. T., DUBOIS, J. L., & RØHR, Å. K. 2020. Molecular mechanism of the chitinolytic peroxygenase reaction, *Proceedings of the National Academy of Sciences of the United States of America*, 117: 1504-1513.

BISSARO, B., VÁRNAI, A., RØHR, Å. K., & EIJSINK, V. G. H. 2018b. Oxidoreductases and reactive oxygen species in conversion of lignocellulosic biomass, *Microbiology and Molecular Biology Reviews*, 82: e00029-00018.

BOMBLE, Y. J., LIN, C.-Y., AMORE, A., WEI, H., HOLWERDA, E. K., CIESIELSKI, P. N., DONOHOE, B. S., DECKER, S. R., LYND, L. R., & HIMMEL, M. E. 2017. Lignocellulose deconstruction in the biosphere, *Current Opinion in Chemical Biology*, 41: 61-70.

BORASTON, A. B., BOLAM, D. N., GILBERT, H. J., & DAVIES, G. J. 2004. Carbohydrate-binding modules: fine-tuning polysaccharide recognition, *Biochemical Journal*, 382: 769-781.

BORISOVA, A. S., ISAKSEN, T., DIMAROGONA, M., KOGNOLE, A. A., MATHIESEN, G., VÁRNAI, A., RØHR, Å. K., PAYNE, C. M., SØRLIE, M., SANDGREN, M., & EIJSINK, V. G. H. 2015.

Structural and functional characterization of a lytic polysaccharide monooxygenase with broad substrate specificity, *Journal of Biological Chemistry*, 290: 22955-22969.

BRENELLI, L., SQUINA, F. M., FELBY, C., & CANNELLA, D. 2018. Laccase-derived lignin compounds boost cellulose oxidative enzymes AA9, *Biotechnology for Biofuels*, 11: 10.

BRESLMAYR, E., HANŽEK, M., HANRAHAN, A., LEITNER, C., KITTL, R., ŠANTEK, B., OOSTENBRINK, C., & LUDWIG, R. 2018. A fast and sensitive activity assay for lytic polysaccharide monooxygenase, *Biotechnology for Biofuels*, 11: 79.

BROWN, R. M., JR. 2004. Cellulose structure and biosynthesis: what is in store for the 21st century?, *Journal of Polymer Science Part A: Polymer Chemistry*, 42: 487-495.

BROWNELL, H. H. & SADDLER, J. N. 1987. Steam pretreatment of lignocellulosic material for enhanced enzymatic hydrolysis, *Biotechnology and Bioengineering*, 29: 228-235.

BURTON, R. A. & FINCHER, G. B. 2014. Evolution and development of cell walls in cereal grains, *Frontiers in Plant Science*, 5: 456.

BUSSE-WICHER, M., GOMES, T. C. F., TRYFONA, T., NIKOLOVSKI, N., STOTT, K., GRANTHAM, N. J., BOLAM, D. N., SKAF, M. S., & DUPREE, P. 2014. The pattern of xylan acetylation suggests xylan may interact with cellulose microfibrils as a twofold helical screw in the secondary plant cell wall of *Arabidopsis thaliana*, *The Plant Journal*, 79: 492-506.

BUSSE-WICHER, M., GRANTHAM, N. J., LYCZAKOWSKI, J. J., NIKOLOVSKI, N., & DUPREE, P. 2016a. Xylan decoration patterns and the plant secondary cell wall molecular architecture, *Biochemical Society Transactions*, 44: 74-78.

BUSSE-WICHER, M., LI, A., SILVEIRA, R. L., PEREIRA, C. S., TRYFONA, T., GOMES, T. C. F., SKAF, M. S., & DUPREE, P. 2016b. Evolution of xylan substitution patterns in gymnosperms and angiosperms: implications for xylan interaction with cellulose, *Plant Physiology*, 171: 2418-2431.

CALDERARO, F., KESER, M., AKEROYD, M., BEVERS, L. E., EIJSINK, V. G. H., VÁRNAI, A., & VAN DEN BERG, M. A. 2020. Characterization of an AA9 LPMO from *Thielavia australiensis*, *Taus*LPMO9B, under industrially relevant lignocellulose saccharification conditions, *Biotechnology for Biofuels*, 13: 195.

CANNELLA, D., HSIEH, C.-W. C., FELBY, C., & JØRGENSEN, H. 2012. Production and effect of aldonic acids during enzymatic hydrolysis of lignocellulose at high dry matter content, *Biotechnology for Biofuels*, 5: 26.

CANNELLA, D. & JØRGENSEN, H. 2014. Do new cellulolytic enzyme preparations affect the industrial strategies for high solids lignocellulosic ethanol production?, *Biotechnology and Bioengineering*, 111: 59-68.

CANNELLA, D., MÖLLERS, K. B., FRIGAARD, N. U., JENSEN, P. E., BJERRUM, M. J., JOHANSEN, K. S., & FELBY, C. 2016. Light-driven oxidation of polysaccharides by photosynthetic pigments and a metalloenzyme, *Nature Communications*, 7: 11134.

CANTERO, D., JARA, R., NAVARRETE, A., PELAZ, L., QUEIROZ, J., RODRÍGUEZ-ROJO, S., & COCERO, M. J. 2019. Pretreatment processes of biomass for biorefineries: current status and prospects, *Annual Review of Chemical and Biomolecular Engineering*, 10: 289-310.

CARVALHEIRO, F., DUARTE, L. C., & GÍRIO, F. M. 2008. Hemicellulose biorefineries: a review on biomass pretreatments, *Journal of Scientific & Industrial Research*, 67: 849-864.

CATALDI, T. R., CAMPA, C., & DE BENEDETTO, G. E. 2000. Carbohydrate analysis by high-performance anion-exchange chromatography with pulsed amperometric

detection: the potential is still growing, *Fresenius Journal of Analytical Chemistry*, 368: 739-758.

CHEN, X., SHEKIRO, J., PSCHORN, T., SABOURIN, M., TAO, L., ELANDER, R., PARK, S., JENNINGS, E., NELSON, R., TRASS, O., FLANEGAN, K., WANG, W., HIMMEL, M. E., JOHNSON, D., & TUCKER, M. P. 2014. A highly efficient dilute alkali deacetylation and mechanical (disc) refining process for the conversion of renewable biomass to lower cost sugars, *Biotechnology for Biofuels*, 7: 98.

CHEN, Y., BARRETO, V., WOODRUFF, A., LU, Z., LIU, Y., & POHL, C. 2018. Dual electrolytic eluent generation for oligosaccharides analysis using high-performance anion-exchange chromatography, *Analytical Chemistry*, 90: 10910-10916.

CHU, S. & MAJUMDAR, A. 2012. Opportunities and challenges for a sustainable energy future, *Nature*, 488: 294-303.

CHYLENSKI, P., BISSARO, B., SØRLIE, M., RØHR, Å. K., VÁRNAI, A., HORN, S. J., & EIJSINK, V. G. H. 2019. Lytic polysaccharide monooxygenases in enzymatic processing of lignocellulosic biomass, *ACS Catalysis*, 9: 4970-4991.

CHYLENSKI, P., FORSBERG, Z., STÅHLBERG, J., VÁRNAI, A., LERSCH, M., BENGTSSON, O., SÆBØ, S., HORN, S. J., & EIJSINK, V. G. H. 2017a. Development of minimal enzyme cocktails for hydrolysis of sulfite-pulped lignocellulosic biomass, *Journal of Biotechnology*, 246: 16-23.

CHYLENSKI, P., PETROVIĆ, D. M., MÜLLER, G., DAHLSTRÖM, M., BENGTSSON, O., LERSCH, M., SIIKA-AHO, M., HORN, S. J., & EIJSINK, V. G. H. 2017b. Enzymatic degradation of sulfite-pulped softwoods and the role of LPMOs, *Biotechnology for Biofuels*, 10: 177.

COSGROVE, D. J. 2005. Growth of the plant cell wall, *Nature Reviews Molecular Cell Biology*, 6: 850-861.

COSTA, T. H. F., KADIC, A., CHYLENSKI, P., VÁRNAI, A., BENGTSSON, O., LIDÉN, G., EIJSINK, V. G. H., & HORN, S. J. 2020. Demonstration-scale enzymatic saccharification of sulfite-pulped spruce with addition of hydrogen peroxide for LPMO activation, *Biofuels, Bioproducts and Biorefining*, 14: 734-745.

COURTADE, G., FORSBERG, Z., HEGGSET, E. B., EIJSINK, V. G. H., & AACHMANN, F. L. 2018. The carbohydrate-binding module and linker of a modular lytic polysaccharide monooxygenase promote localized cellulose oxidation, *Journal of Biological Chemistry*, 293: 13006-13015.

COURTADE, G., WIMMER, R., RØHR, Å. K., PREIMS, M., FELICE, A. K. G., DIMAROGONA, M., VAAJE-KOLSTAD, G., SØRLIE, M., SANDGREN, M., LUDWIG, R., EIJSINK, V. G. H., & AACHMANN, F. L. 2016. Interactions of a fungal lytic polysaccharide monooxygenase with β-glucan substrates and cellobiose dehydrogenase, *Proceedings of the National Academy of Sciences of the United States of America*, 113: 5922-5927.

COUTURIER, M., LADEVEZE, S., SULZENBACHER, G., CIANO, L., FANUEL, M., MOREAU, C., VILLARES, A., CATHALA, B., CHASPOUL, F., FRANDSEN, K. E., LABOUREL, A., HERPOEL-GIMBERT, I., GRISEL, S., HAON, M., LENFANT, N., ROGNIAUX, H., ROPARTZ, D., DAVIES, G. J., ROSSO, M. N., WALTON, P. H., HENRISSAT, B., & BERRIN, J.-G. 2018. Lytic xylan oxidases from wood-decay fungi unlock biomass degradation, *Nature Chemical Biology*, 14: 306-310.

CRAGG, S. M., BECKHAM, G. T., BRUCE, N. C., BUGG, T. D. H., DISTEL, D. L., DUPREE, P., ETXABE, A. G., GOODELL, B. S., JELLISON, J., MCGEEHAN, J. E., MCQUEEN-MASON, S. J., SCHNORR, K., WALTON, P. H., WATTS, J. E. M., & ZIMMER, M. 2015. Lignocellulose

degradation mechanisms across the Tree of Life, *Current Opinion in Chemical Biology*, 29: 108-119.

CRAIG, J. P., CORADETTI, S. T., STARR, T. L., & GLASS, N. L. 2015. Direct target network of the *Neurospora crassa* plant cell wall deconstruction regulators CLR-1, CLR-2, and XLR-1, *mBio*, 6: e01452-01415.

CRUYS-BAGGER, N., ELMERDAHL, J., PRAESTGAARD, E., TATSUMI, H., SPODSBERG, N., BORCH, K., & WESTH, P. 2012. Pre-steady-state kinetics for hydrolysis of insoluble cellulose by cellobiohydrolase Cel7A, *Journal of Biological Chemistry*, 287: 18451-18458.

DA COSTA SOUSA, L., JIN, M., CHUNDAWAT, S. P. S., BOKADE, V., TANG, X., AZARPIRA, A., LU, F., AVCI, U., HUMPULA, J., UPPUGUNDLA, N., GUNAWAN, C., PATTATHIL, S., CHEH, A. M., KOTHARI, N., KUMAR, R., RALPH, J., HAHN, M. G., WYMAN, C. E., SINGH, S., SIMMONS, B. A., DALE, B. E., & BALAN, V. 2016. Next-generation ammonia pretreatment enhances cellulosic biofuel production, *Energy & Environmental Science*, 9: 1215-1223.

DAVIES, G. & HENRISSAT, B. 1995. Structures and mechanisms of glycosyl hydrolases, *Structure*, 3: 853-859.

DAY, A. G., GOEDEGEBUUR, F., GUALFETTI, P., MITCHINSON, C., NEEFE, P., SANDGREN, M., SHAW, A., & STÅHLBERG, J. (2004). *Novel variant Hyprocrea jecorina CBH1 cellulases*. WO-2004/016760-A2.

DE VRIES, R. P. 2003. Regulation of *Aspergillus* genes encoding plant cell wall polysaccharide-degrading enzymes; relevance for industrial production, *Applied Microbiology and Biotechnology*, 61: 10-20.

DEMARTINI, J. D., PATTATHIL, S., AVCI, U., SZEKALSKI, K., MAZUMDER, K., HAHN, M. G., & WYMAN, C. E. 2011. Application of monoclonal antibodies to investigate plant cell wall deconstruction for biofuels production, *Energy & Environmental Science*, 4: 4332-4339.

DJAJADI, D. T., JENSEN, M. M., OLIVEIRA, M., JENSEN, A., THYGESEN, L. G., PINELO, M., GLASIUS, M., JØRGENSEN, H., & MEYER, A. S. 2018a. Lignin from hydrothermally pretreated grass biomass retards enzymatic cellulose degradation by acting as a physical barrier rather than by inducing nonproductive adsorption of enzymes, *Biotechnology for Biofuels*, 11: 85.

DJAJADI, D. T., PIHLAJANIEMI, V., RAHIKAINEN, J., KRUUS, K., & MEYER, A. S. 2018b. Cellulases adsorb reversibly on biomass lignin, *Biotechnology and Bioengineering*, 115: 2869-2880.

DRULA, E., GARRON, M.-L., DOGAN, S., LOMBARD, V., HENRISSAT, B., & TERRAPON, N. 2022. The carbohydrate-active enzyme database: functions and literature, *Nucleic Acids Research*, 50: D571-D577.

DUNLAP, J. C., BORKOVICH, K. A., HENN, M. R., TURNER, G. E., SACHS, M. S., GLASS, N. L., MCCLUSKEY, K., PLAMANN, M., GALAGAN, J. E., BIRREN, B. W., WEISS, R. L., TOWNSEND, J. P., LOROS, J. J., NELSON, M. A., LAMBREGHTS, R., COLOT, H. V., PARK, G., COLLOPY, P., RINGELBERG, C., CREW, C., LITVINKOVA, L., DECAPRIO, D., HOOD, H. M., CURILLA, S., SHI, M., CRAWFORD, M., KOERHSEN, M., MONTGOMERY, P., LARSON, L., PEARSON, M., KASUGA, T., TIAN, C., BAŞTÜRKMEN, M., ALTAMIRANO, L., & XU, J. 2007. Enabling a community to dissect an organism: overview of the *Neurospora* functional genomics project, *Advances in Genetics*, 57: 49-96.

DUWE, A., TIPPKÖTTER, N., & ULBER, R. 2019. Lignocellulose-biorefinery: ethanol-focused, *Advances in Biochemical Engineering/Biotechnology*, 166: 177-215.

EIBINGER, M., GANNER, T., BUBNER, P., ROŠKER, S., KRACHER, D., HALTRICH, D., LUDWIG, R., PLANK, H., & NIDETZKY, B. 2014. Cellulose surface degradation by a lytic polysaccharide monooxygenase and its effect on cellulase hydrolytic efficiency, *Journal of Biological Chemistry*, 289: 35929-35938.

EIBINGER, M., SATTELKOW, J., GANNER, T., PLANK, H., & NIDETZKY, B. 2017. Single-molecule study of oxidative enzymatic deconstruction of cellulose, *Nature Communications*, 8: 894.

EIJSINK, V. G. H., PETROVIĆ, D., FORSBERG, Z., MEKASHA, S., RØHR, A. K., VÁRNAI, A., BISSARO, B., & VAAJE-KOLSTAD, G. 2019. On the functional characterization of lytic polysaccharide monooxygenases (LPMOs), *Biotechnology for Biofuels*, 12: 58.

ERIKSSON, K.-E., PETTERSSON, B., & WESTERMARK, U. 1974. Oxidation: an important enzyme reaction in fungal degradation of cellulose, *FEBS Letters*, 49: 282-285.

FANUEL, M., GARAJOVA, S., ROPARTZ, D., MCGREGOR, N., BRUMER, H., ROGNIAUX, H., & BERRIN, J.-G. 2017. The *Podospora anserina* lytic polysaccharide monooxygenase *Pa*LPMO9H catalyzes oxidative cleavage of diverse plant cell wall matrix glycans, *Biotechnology for Biofuels*, 10: 63.

FAO, *The state of food security and nutrition in the world 2021*, in *Transforming food systems for food security, improved nutrition and affordable healthy diets for all*. 2021, FAO, IFAD, UNICEF, WFP, WHO, Rome, Italy. p. 240.

FELBY, C., NIELSEN, B. R., OLESEN, P. O., & SKIBSTED, L. H. 1997. Identification and quantification of radical reaction intermediates by electron spin resonance spectrometry of laccase-catalyzed oxidation of wood fibers from beech (*Fagus sylvatica*), *Applied Microbiology and Biotechnology*, 48: 459-464.

FERNANDES, A. N., THOMAS, L. H., ALTANER, C. M., CALLOW, P., FORSYTH, V. T., APPERLEY, D. C., KENNEDY, C. J., & JARVIS, M. C. 2011. Nanostructure of cellulose microfibrils in spruce wood, *Proceedings of the National Academy of Sciences of the United States of America*, 108: E1195-1203.

FILANDR, F., MAN, P., HALADA, P., CHANG, H., LUDWIG, R., & KRACHER, D. 2020. The H_2O_2-dependent activity of a fungal lytic polysaccharide monooxygenase investigated with a turbidimetric assay, *Biotechnology for Biofuels*, 13: 37.

FILIATRAULT-CHASTEL, C., NAVARRO, D., HAON, M., GRISEL, S., HERPOËL-GIMBERT, I., CHEVRET, D., FANUEL, M., HENRISSAT, B., HEISS-BLANQUET, S., MARGEOT, A., & BERRIN, J.-G. 2019. AA16, a new lytic polysaccharide monooxygenase family identified in fungal secretomes, *Biotechnology for Biofuels*, 12: 55.

FINCHER, G. B. 2009. Revolutionary times in our understanding of cell wall biosynthesis and remodeling in the grasses, *Plant Physiology*, 149: 27-37.

FITZ, E., WANKA, F., & SEIBOTH, B. 2018. The promoter toolbox for recombinant gene expression in *Trichoderma reesei*, *Frontiers in Bioengineering and Biotechnology*, 6: 135.

FORSBERG, Z., BISSARO, B., GULLESEN, J., DALHUS, B., VAAJE-KOLSTAD, G., & EIJSINK, V. G. H. 2018. Structural determinants of bacterial lytic polysaccharide monooxygenase functionality, *Journal of Biological Chemistry*, 293: 1397-1412.

FORSBERG, Z., MACKENZIE, A. K., SØRLIE, M., RØHR, Å. K., HELLAND, R., ARVAI, A. S., VAAJE-KOLSTAD, G., & EIJSINK, V. G. H. 2014. Structural and functional characterization of

a conserved pair of bacterial cellulose-oxidizing lytic polysaccharide monooxygenases, *Proceedings of the National Academy of Sciences of the United States of America*, 111: 8446-8451.

FORSBERG, Z., SØRLIE, M., PETROVIĆ, D., COURTADE, G., AACHMANN, F. L., VAAJE-KOLSTAD, G., BISSARO, B., RØHR Å, K., & EIJSINK, V. G. 2019. Polysaccharide degradation by lytic polysaccharide monooxygenases, *Current Opinion in Structural Biology*, 59: 54-64.

FORSBERG, Z., VAAJE-KOLSTAD, G., WESTERENG, B., BUNÆS, A. C., STENSTRØM, Y., MACKENZIE, A., SØRLIE, M., HORN, S. J., & EIJSINK, V. G. H. 2011. Cleavage of cellulose by a CBM33 protein, *Protein Science*, 20: 1479-1483.

FOX, J. M., LEVINE, S. E., CLARK, D. S., & BLANCH, H. W. 2012. Initial- and processive-cut products reveal cellobiohydrolase rate limitations and the role of companion enzymes, *Biochemistry*, 51: 442-452.

FRANDSEN, K. E. H., HAON, M., GRISEL, S., HENRISSAT, B., LO LEGGIO, L., & BERRIN, J.-G. 2021. Identification of the molecular determinants driving the substrate specificity of fungal lytic polysaccharide monooxygenases (LPMOs), *Journal of Biological Chemistry*, 296: 100086.

FRANDSEN, K. E. H., SIMMONS, T. J., DUPREE, P., POULSEN, J.-C. N., HEMSWORTH, G. R., CIANO, L., JOHNSTON, E. M., TOVBORG, M., JOHANSEN, K. S., VON FREIESLEBEN, P., MARMUSE, L., FORT, S., COTTAZ, S., DRIGUEZ, H., HENRISSAT, B., LENFANT, N., TUNA, F., BALDANSUREN, A., DAVIES, G. J., LO LEGGIO, L., & WALTON, P. H. 2016. The molecular basis of polysaccharide cleavage by lytic polysaccharide monooxygenases, *Nature Chemical Biology*, 12: 298-303.

FRITSCHE, S., HOPSON, C., GORMAN, J., GABRIEL, R., & SINGER, S. W. 2020. Purification and characterization of a native lytic polysaccharide monooxygenase from *Thermoascus aurantiacus*, *Biotechnology Letters*, 42: 1897-1905.

FROMMHAGEN, M., KOETSIER, M. J., WESTPHAL, A. H., VISSER, J., HINZ, S. W. A., VINCKEN, J.-P., VAN BERKEL, W. J. H., KABEL, M. A., & GRUPPEN, H. 2016. Lytic polysaccharide monooxygenases from *Myceliophthora thermophila* C1 differ in substrate preference and reducing agent specificity, *Biotechnology for Biofuels*, 9: 186.

FROMMHAGEN, M., SFORZA, S., WESTPHAL, A. H., VISSER, J., HINZ, S. W., KOETSIER, M. J., VAN BERKEL, W. J., GRUPPEN, H., & KABEL, M. A. 2015. Discovery of the combined oxidative cleavage of plant xylan and cellulose by a new fungal polysaccharide monooxygenase, *Biotechnology for Biofuels*, 8: 101.

FROMMHAGEN, M., WESTPHAL, A. H., VAN BERKEL, W. J. H., & KABEL, M. A. 2018. Distinct substrate specificities and electron-donating systems of fungal lytic polysaccharide monooxygenases, *Frontiers in Microbiology*, 9: 1080.

FRY, S. C., NESSELRODE, B., MILLER, J. G., & MEWBURN, B. R. 2008. Mixed-linkage (1-->3,1-->4)-beta-D-glucan is a major hemicellulose of *Equisetum* (horsetail) cell walls, *New Phytologist*, 179: 104-115.

GALBE, M. & WALLBERG, O. 2019. Pretreatment for biorefineries: a review of common methods for efficient utilisation of lignocellulosic materials, *Biotechnology for Biofuels*, 12: 294.

GARAJOVA, S., MATHIEU, Y., BECCIA, M. R., BENNATI-GRANIER, C., BIASO, F., FANUEL, M., ROPARTZ, D., GUIGLIARELLI, B., RECORD, E., ROGNIAUX, H., HENRISSAT, B., &

BERRIN, J.-G. 2016. Single-domain flavoenzymes trigger lytic polysaccharide monooxygenases for oxidative degradation of cellulose, *Scientific Reports*, 6: 28276.

GHATTYVENKATAKRISHNA, P. K., ALEKOZAI, E. M., BECKHAM, G. T., SCHULZ, R., CROWLEY, M. F., UBERBACHER, E. C., & CHENG, X. 2013. Initial recognition of a cellodextrin chain in the cellulose-binding tunnel may affect cellobiohydrolase directional specificity, *Biophysical Journal*, 104: 904-912.

GOMEZ, L. D., STEELE-KING, C. G., & MCQUEEN-MASON, S. J. 2008. Sustainable liquid biofuels from biomass: the writing's on the walls, *New Phytologist*, 178: 473-485.

GRANTHAM, N. J., WURMAN-RODRICH, J., TERRETT, O. M., LYCZAKOWSKI, J. J., STOTT, K., IUGA, D., SIMMONS, T. J., DURAND-TARDIF, M., BROWN, S. P., DUPREE, R., BUSSE-WICHER, M., & DUPREE, P. 2017. An even pattern of xylan substitution is critical for interaction with cellulose in plant cell walls, *Nature Plants*, 3: 859-865.

GRITZALI, M. & BROWN, R. D. 1979. 'The cellulase system of *Trichoderma*' in *Hydrolysis of Cellulose: Mechanisms of Enzymatic and Acid Catalysis*. American Chemical Society, 237-260.

GRONDIN, J. M., TAMURA, K., DÉJEAN, G., ABBOTT, D. W., & BRUMER, H. 2017. Polysaccharide utilization loci: fueling microbial communities, *Journal of Bacteriology*, 199: e00860-00816.

HABIBI, Y., LUCIA, L. A., & ROJAS, O. J. 2010. Cellulose nanocrystals: chemistry, self-assembly, and applications, *Chemical Reviews*, 110: 3479-3500.

HALLIWELL, G. & GRIFFIN, M. 1973. The nature and mode of action of the cellulolytic component C_1 of *Trichoderma koningii* on native cellulose, *Biochemical Journal*, 135: 587-594.

HANGASKY, J. A., IAVARONE, A. T., & MARLETTA, M. A. 2018. Reactivity of O_2 versus H_2O_2 with polysaccharide monooxygenases, *Proceedings of the National Academy of Sciences of the United States of America*, 115: 4915-4920.

HANSEN, L. D., ØSTENSEN, M., ARSTAD, B., TSCHENTSCHER, R., EIJSINK, V. G. H., HORN, S. J., & VÁRNAI, A. 2022. 2-Naphthol impregnation prior to steam explosion promotes LPMO-assisted enzymatic saccharification of spruce and yields high-purity lignin, *ACS Sustainable Chemistry & Engineering*, 10: 5233-5242.

HARRIS, P. V., WELNER, D., MCFARLAND, K. C., RE, E., NAVARRO POULSEN, J. C., BROWN, K., SALBO, R., DING, H., VLASENKO, E., MERINO, S., XU, F., CHERRY, J., LARSEN, S., & LO LEGGIO, L. 2010. Stimulation of lignocellulosic biomass hydrolysis by proteins of glycoside hydrolase family 61: structure and function of a large, enigmatic family, *Biochemistry*, 49: 3305-3316.

HARRIS, P. V., XU, F., KREEL, N. E., KANG, C., & FUKUYAMA, S. 2014. New enzyme insights drive advances in commercial ethanol production, *Current Opinion in Chemical Biology*, 19: 162-170.

HEDISON, T. M., BRESLMAYR, E., SHANMUGAM, M., KARNPAKDEE, K., HEYES, D. J., GREEN, A. P., LUDWIG, R., SCRUTTON, N. S., & KRACHER, D. 2021. Insights into the H_2O_2-driven catalytic mechanism of fungal lytic polysaccharide monooxygenases, *The FEBS Journal*, 288: 4115-4128.

HEGNAR, O. A., PETROVIC, D. M., BISSARO, B., ALFREDSEN, G., VÁRNAI, A., & EIJSINK, V. G. H. 2019. pH-Dependent relationship between catalytic activity and hydrogen peroxide production shown via characterization of a lytic polysaccharide

monooxygenase from *Gloeophyllum trabeum*, *Applied and Environmental Microbiology*, 85: e02612-e02618.

HEMSWORTH, G. R., DÉJEAN, G., DAVIES, G. J., & BRUMER, H. 2016. Learning from microbial strategies for polysaccharide degradation, *Biochemical Society Transactions*, 44: 94-108.

HENRISSAT, B., DRIGUEZ, H., VIET, C., & SCHÜLEIN, M. 1985. Synergism of cellulases from *Trichoderma reesei* in the degradation of cellulose, *Bio/Technology*, 3: 722-726.

HLALUKANA, N., MAGENGELELE, M., MALGAS, S., & PLETSCHKE, B. I. 2021. Enzymatic conversion of mannan-rich plant waste biomass into prebiotic mannooligosaccharides, *Foods*, 10: 2010.

HO, D. P., NGO, H. H., & GUO, W. 2014. A mini review on renewable sources for biofuel, *Bioresource Technology*, 169: 742-749.

HORN, S. J., VAAJE-KOLSTAD, G., WESTERENG, B., & EIJSINK, V. G. H. 2012. Novel enzymes for the degradation of cellulose, *Biotechnology for Biofuels*, 5: 45.

HOUGHTON, J. T., *IPCC First Assessment Report*. 1990, Intergovernmental Panel on Climate Change, Geneva: WMO. Print.

HU, J., ARANTES, V., PRIBOWO, A., GOURLAY, K., & SADDLER, J. N. 2014. Substrate factors that influence the synergistic interaction of AA9 and cellulases during the enzymatic hydrolysis of biomass, *Energy & Environmental Science*, 7: 2308-2315.

HU, J., ARANTES, V., & SADDLER, J. N. 2011. The enhancement of enzymatic hydrolysis of lignocellulosic substrates by the addition of accessory enzymes such as xylanase: is it an additive or synergistic effect?, *Biotechnology for Biofuels*, 4: 36.

HU, J., CHANDRA, R., ARANTES, V., GOURLAY, K., SUSAN VAN DYK, J., & SADDLER, J. N. 2015. The addition of accessory enzymes enhances the hydrolytic performance of cellulase enzymes at high solid loadings, *Bioresource Technology*, 186: 149-153.

HU, J., TIAN, D., RENNECKAR, S., & SADDLER, J. N. 2018. Enzyme mediated nanofibrillation of cellulose by the synergistic actions of an endoglucanase, lytic polysaccharide monooxygenase (LPMO) and xylanase, *Scientific Reports*, 8: 3195.

HÜTTNER, S., VÁRNAI, A., PETROVIĆ, D. M., BACH, C. X., KIM ANH, D. T., THANH, V. N., EIJSINK, V. G. H., LARSBRINK, J., & OLSSON, L. 2019. Specific xylan activity revealed for AA9 lytic polysaccharide monooxygenases of the thermophilic fungus *Malbranchea cinnamomea* by functional characterization, *Applied and Environmental Microbiology*, 85: e01408-e01419.

IGARASHI, K., UCHIHASHI, T., KOIVULA, A., WADA, M., KIMURA, S., OKAMOTO, T., PENTTILÄ, M., ANDO, T., & SAMEJIMA, M. 2011. Traffic jams reduce hydrolytic efficiency of cellulase on cellulose surface, *Science*, 333: 1279-1282.

ISAKSEN, T., WESTERENG, B., AACHMANN, F. L., AGGER, J. W., KRACHER, D., KITTL, R., LUDWIG, R., HALTRICH, D., EIJSINK, V. G., & HORN, S. J. 2014. A C4-oxidizing lytic polysaccharide monooxygenase cleaving both cellulose and cello-oligosaccharides, *Journal of Biological Chemistry*, 289: 2632-2642.

ISIKGOR, F. H. & BECER, C. R. 2015. Lignocellulosic biomass: a sustainable platform for the production of bio-based chemicals and polymers, *Polymer Chemistry*, 6: 4497-4559.

JAGADEESWARAN, G., GAINEY, L., & MORT, A. J. 2018. An AA9-LPMO containing a CBM1 domain in *Aspergillus nidulans* is active on cellulose and cleaves cello-oligosaccharides, *AMB Express*, 8: 171.

JALAK, J., KURAŠIN, M., TEUGJAS, H., & VÄLJAMÄE, P. 2012. Endo-exo synergism in cellulose hydrolysis revisited, *Journal of Biological Chemistry*, 287: 28802-28815.

JENSEN, M. S., FREDRIKSEN, L., MACKENZIE, A. K., POPE, P. B., LEIROS, I., CHYLENSKI, P., WILLIAMSON, A. K., CHRISTOPEIT, T., ØSTBY, H., VAAJE-KOLSTAD, G., & EIJSINK, V. G. H. 2018. Discovery and characterization of a thermostable two-domain GH6 endoglucanase from a compost metagenome, *PLoS One*, 13: e0197862.

JOHANSEN, KATJA S. 2016. Discovery and industrial applications of lytic polysaccharide mono-oxygenases, *Biochemical Society Transactions*, 44: 143-149.

JÖNSSON, L. J. & MARTÍN, C. 2016. Pretreatment of lignocellulose: formation of inhibitory by-products and strategies for minimizing their effects, *Bioresource Technology*, 199: 103-112.

KADIĆ, A., CHYLENSKI, P., HANSEN, M. A. T., BENGTSSON, O., EIJSINK, V. G. H., & LIDÉN, G. 2019. Oxidation-reduction potential (ORP) as a tool for process monitoring of H_2O_2/LPMO assisted enzymatic hydrolysis of cellulose, *Process Biochemistry*, 86: 89-97.

KADIĆ, A., VÁRNAI, A., EIJSINK, V. G. H., HORN, S. J., & LIDÉN, G. 2021. *In situ* measurements of oxidation–reduction potential and hydrogen peroxide concentration as tools for revealing LPMO inactivation during enzymatic saccharification of cellulose, *Biotechnology for Biofuels*, 14: 46.

KADOWAKI, M. A. S., VÁRNAI, A., JAMESON, J.-K., LEITE, A. E. T., COSTA-FILHO, A. J., KUMAGAI, P. S., PRADE, R. A., POLIKARPOV, I., & EIJSINK, V. G. H. 2018. Functional characterization of a lytic polysaccharide monooxygenase from the thermophilic fungus *Myceliophthora thermophila*, *PLoS One*, 13: e0202148.

KALLIOINEN, A., PURANEN, T., & SIIKA-AHO, M. 2014. Mixtures of thermostable enzymes show high performance in biomass saccharification, *Applied Biochemistry and Biotechnology*, 173: 1038-1056.

KARKEHABADI, S., HANSSON, H., KIM, S., PIENS, K., MITCHINSON, C., & SANDGREN, M. 2008. The first structure of a glycoside hydrolase family 61 member, Cel61B from *Hypocrea jecorina*, at 1.6 Å resolution, *Journal of Molecular Biology*, 383: 144-154.

KARLSSON, J., SALOHEIMO, M., SIIKA-AHO, M., TENKANEN, M., PENTTILÄ, M., & TJERNELD, F. 2001. Homologous expression and characterization of Cel61A (EG IV) of *Trichoderma reesei*, *European Journal of Biochemistry*, 268: 6498-6507.

KARNAOURI, A., MURALEEDHARAN, M. N., DIMAROGONA, M., TOPAKAS, E., ROVA, U., SANDGREN, M., & CHRISTAKOPOULOS, P. 2017. Recombinant expression of thermostable processive *Mt*EG5 endoglucanase and its synergism with *Mt*LPMO from *Myceliophthora thermophila* during the hydrolysis of lignocellulosic substrates, *Biotechnology for Biofuels*, 10: 126.

KARPPI, J., ZHAO, H., CHONG, S. L., KOISTINEN, A. E., TENKANEN, M., & MASTER, E. 2020. Quantitative comparison of pyranose dehydrogenase action on diverse xylooligosaccharides, *Frontiers in Chemistry*, 8: 11.

KAUFMANN, R. 1995. Matrix-assisted laser desorption ionization (MALDI) mass spectrometry: a novel analytical tool in molecular biology and biotechnology, *Journal of Biotechnology*, 41: 155-175.

KELLEY, R. L. & REDDY, C. A. 1986. Purification and characterization of glucose oxidase from ligninolytic cultures of *Phanerochaete chrysosporium*, *Journal of Bacteriology*, 166: 269-274.

KELLOCK, M., MAAHEIMO, H., MARJAMAA, K., RAHIKAINEN, J., ZHANG, H., HOLOPAINEN-MANTILA, U., RALPH, J., TAMMINEN, T., FELBY, C., & KRUUS, K. 2019. Effect of hydrothermal pretreatment severity on lignin inhibition in enzymatic hydrolysis, *Bioresource Technology*, 280: 303-312.

KIM, K. H., EUDES, A., JEONG, K., YOO, C. G., KIM, C. S., & RAGAUSKAS, A. 2019. Integration of renewable deep eutectic solvents with engineered biomass to achieve a closed-loop biorefinery, *Proceedings of the National Academy of Sciences of the United States of America*, 116: 13816-13824.

KIM, S.-J., CHANDRASEKAR, B., REA, A. C., DANHOF, L., ZEMELIS-DURFEE, S., THROWER, N., SHEPARD, Z. S., PAULY, M., BRANDIZZI, F., & KEEGSTRA, K. 2020. The synthesis of xyloglucan, an abundant plant cell wall polysaccharide, requires CSLC function, *Proceedings of the National Academy of Sciences of the United States of America*, 117: 20316-20324.

KITTL, R., KRACHER, D., BURGSTALLER, D., HALTRICH, D., & LUDWIG, R. 2012. Production of four *Neurospora crassa* lytic polysaccharide monooxygenases in Pichia pastoris monitored by a fluorimetric assay, *Biotechnology for Biofuels*, 5: 79.

KLEMM, D., HEUBLEIN, B., FINK, H. P., & BOHN, A. 2005. Cellulose: fascinating biopolymer and sustainable raw material, *Angewandte Chemie International Edition*, 44: 3358-3393.

KNOTT, B. C., CROWLEY, M. F., HIMMEL, M. E., STÅHLBERG, J., & BECKHAM, G. T. 2014a. Carbohydrate–protein interactions that drive processive polysaccharide translocation in enzymes revealed from a computational study of cellobiohydrolase processivity, *Journal of the American Chemical Society*, 136: 8810-8819.

KNOTT, B. C., HADDAD MOMENI, M., CROWLEY, M. F., MACKENZIE, L. F., GÖTZ, A. W., SANDGREN, M., WITHERS, S. G., STÅHLBERG, J., & BECKHAM, G. T. 2014b. The mechanism of cellulose hydrolysis by a two-step, retaining cellobiohydrolase elucidated by structural and transition path sampling studies, *Journal of the American Chemical Society*, 136: 321-329.

KOJIMA, Y., VÁRNAI, A., ISHIDA, T., SUNAGAWA, N., PETROVIC, D. M., IGARASHI, K., JELLISON, J., GOODELL, B., ALFREDSEN, G., WESTERENG, B., EIJSINK, V. G., & YOSHIDA, M. 2016. A lytic polysaccharide monooxygenase with broad xyloglucan specificity from the brown-rot fungus *Gloeophyllum trabeum* and its action on cellulose-xyloglucan complexes, *Applied and Environmental Microbiology*, 82: 6557-6572.

KOLBE, S., FISCHER, S., BECIREVIC, A., HINZ, P., & SCHREMPF, H. 1998. The *Streptomyces reticuli* alpha-chitin-binding protein CHB2 and its gene, *Microbiology*, 144: 1291-1297.

KONT, R., BISSARO, B., EIJSINK, V. G. H., & VÄLJAMÄE, P. 2020. Kinetic insights into the peroxygenase activity of cellulose-active lytic polysaccharide monooxygenases (LPMOs), *Nature Communications*, 11: 5786.

KONT, R., PIHLAJANIEMI, V., BORISOVA, A. S., ARO, N., MARJAMAA, K., LOOGEN, J., BÜCHS, J., EIJSINK, V. G. H., KRUUS, K., & VÄLJAMÄE, P. 2019. The liquid fraction from hydrothermal pretreatment of wheat straw provides lytic polysaccharide monooxygenases with both electrons and H_2O_2 co-substrate, *Biotechnology for Biofuels*, 12: 235.

KOSTYLEV, M. & WILSON, D. 2012. Synergistic interactions in cellulose hydrolysis, *Biofuels*, 3: 61-70.

KRACHER, D., FORSBERG, Z., BISSARO, B., GANGL, S., PREIMS, M., SYGMUND, C., EIJSINK, V. G. H., & LUDWIG, R. 2020. Polysaccharide oxidation by lytic polysaccharide monooxygenase is enhanced by engineered cellobiose dehydrogenase, *The FEBS Journal*, 287: 897-908.

KRACHER, D., SCHEIBLBRANDNER, S., FELICE, A. K. G., BRESLMAYR, E., PREIMS, M., LUDWICKA, K., HALTRICH, D., EIJSINK, V. G. H., & LUDWIG, R. 2016. Extracellular electron transfer systems fuel cellulose oxidative degradation, *Science*, 352: 1098-1101.

KUBICKI, J. D., YANG, H., SAWADA, D., O'NEILL, H., OEHME, D., & COSGROVE, D. 2018. The shape of native plant cellulose microfibrils, *Scientific Reports*, 8: 13983.

KUHN, E. M., CHEN, X., & TUCKER, M. P. 2020. Deacetylation and mechanical refining (DMR) and deacetylation and dilute acid (DDA) pretreatment of corn stover, switchgrass, and a 50:50 corn stover/switchgrass blend, *ACS Sustainable Chemistry & Engineering*, 8: 6734-6743.

KURASIN, M. & VÄLJAMÄE, P. 2011. Processivity of cellobiohydrolases is limited by the substrate, *Journal of Biological Chemistry*, 286: 169-177.

KUUSK, S., BISSARO, B., KUUSK, P., FORSBERG, Z., EIJSINK, V. G. H., SØRLIE, M., & VÄLJAMÄE, P. 2018. Kinetics of H_2O_2-driven degradation of chitin by a bacterial lytic polysaccharide monooxygenase, *Journal of Biological Chemistry*, 293: 523-531.

KUUSK, S., KONT, R., KUUSK, P., HEERING, A., SØRLIE, M., BISSARO, B., EIJSINK, V. G. H., & VÄLJAMÄE, P. 2019. Kinetic insights into the role of the reductant in H_2O_2-driven degradation of chitin by a bacterial lytic polysaccharide monooxygenase, *Journal of Biological Chemistry*, 294: 1516-1528.

LADEVÈZE, S., HAON, M., VILLARES, A., CATHALA, B., GRISEL, S., HERPOËL-GIMBERT, I., HENRISSAT, B., & BERRIN, J.-G. 2017. The yeast *Geotrichum candidum* encodes functional lytic polysaccharide monooxygenases, *Biotechnology for Biofuels*, 10: 215.

LAIRSON, L. L., HENRISSAT, B., DAVIES, G. J., & WITHERS, S. G. 2008. Glycosyltransferases: structures, functions, and mechanisms, *Annual Review of Biochemistry*, 77: 521-555.

LANGSTON, J. A., SHAGHASI, T., ABBATE, E., XU, F., VLASENKO, E., & SWEENEY, M. D. 2011. Oxidoreductive cellulose depolymerization by the enzymes cellobiose dehydrogenase and glycoside hydrolase 61, *Applied and Environmental Microbiology*, 77: 7007-7015.

LAURENT, C. V. F. P., SUN, P., SCHEIBLBRANDNER, S., CSARMAN, F., CANNAZZA, P., FROMMHAGEN, M., VAN BERKEL, W. J. H., OOSTENBRINK, C., KABEL, M. A., & LUDWIG, R. 2019. Influence of lytic polysaccharide monooxygenase active site segments on activity and affinity, *International Journal of Molecular Sciences*, 20: 6219.

LEE, R. A. & LAVOIE, J.-M. 2013. From first- to third-generation biofuels: challenges of producing a commodity from a biomass of increasing complexity, *Animal Frontiers*, 3: 6-11.

LEE, Y. C. 1990. High-performance anion-exchange chromatography for carbohydrate analysis, *Analytical Biochemistry*, 189: 151-162.

LENFANT, N., HAINAUT, M., TERRAPON, N., DRULA, E., LOMBARD, V., & HENRISSAT, B. 2017. A bioinformatics analysis of 3400 lytic polysaccharide oxidases from family AA9, *Carbohydrate Research*, 448: 166-174.

LEVASSEUR, A., DRULA, E., LOMBARD, V., COUTINHO, P. M., & HENRISSAT, B. 2013. Expansion of the enzymatic repertoire of the CAZy database to integrate auxiliary redox enzymes, *Biotechnology for Biofuels*, 6: 41.

LI, F., MA, F., ZHAO, H., ZHANG, S., WANG, L., ZHANG, X., & YU, H. 2019. A lytic polysaccharide monooxygenase from a white-rot fungus drives the degradation of lignin by a versatile peroxidase, *Applied and Environmental Microbiology*, 85: e02803-02818.

LI, X., BEESON, W. T., PHILLIPS, C. M., MARLETTA, M. A., & CATE, J. H. D. 2012. Structural basis for substrate targeting and catalysis by fungal polysaccharide monooxygenases, *Structure*, 20: 1051-1061.

LI, Y., LIU, X., LIU, M., WANG, Y., ZOU, Y., YOU, Y., YANG, L., HU, J., ZHANG, H., ZHENG, X., WANG, P., & ZHANG, Z. 2020. *Magnaporthe oryzae* auxiliary activity protein *Mo*Aa91 functions as chitin-binding protein to induce appressorium formation on artificial inductive surfaces and suppress plant immunity, *mBio*, 11: e03304-03319.

LINHARDT, R. J., GALLIHER, P. M., & COONEY, C. L. 1986. Polysaccharide lyases, *Applied Biochemistry and Biotechnology*, 12: 135-176.

LIU, Y., CRUZ-MORALES, P., ZARGAR, A., BELCHER, M. S., PANG, B., ENGLUND, E., DAN, Q., YIN, K., & KEASLING, J. D. 2021. Biofuels for a sustainable future, *Cell*, 184: 1636-1647.

LO LEGGIO, L., SIMMONS, T. J., POULSEN, J.-C. N., FRANDSEN, K. E. H., HEMSWORTH, G. R., STRINGER, M. A., VON FREIESLEBEN, P., TOVBORG, M., JOHANSEN, K. S., DE MARIA, L., HARRIS, P. V., SOONG, C.-L., DUPREE, P., TRYFONA, T., LENFANT, N., HENRISSAT, B., DAVIES, G. J., & WALTON, P. H. 2015. Structure and boosting activity of a starch-degrading lytic polysaccharide monooxygenase, *Nature Communications*, 6: 5961.

LOOSE, J. S., FORSBERG, Z., FRAAIJE, M. W., EIJSINK, V. G., & VAAJE-KOLSTAD, G. 2014. A rapid quantitative activity assay shows that the *Vibrio cholerae* colonization factor GbpA is an active lytic polysaccharide monooxygenase, *FEBS Letters*, 588: 3435-3440.

LOOSE, J. S. M., ARNTZEN, M., BISSARO, B., LUDWIG, R., EIJSINK, V. G. H., & VAAJE-KOLSTAD, G. 2018. Multipoint precision binding of substrate protects lytic polysaccharide monooxygenases from self-destructive off-pathway processes, *Biochemistry*, 57: 4114-4124.

LOOSE, J. S. M., FORSBERG, Z., KRACHER, D., SCHEIBLBRANDNER, S., LUDWIG, R., EIJSINK, V. G. H., & VAAJE-KOLSTAD, G. 2016. Activation of bacterial lytic polysaccharide monooxygenases with cellobiose dehydrogenase, *Protein Science*, 25: 2175-2186.

LUPAŞCU, R. E., GHICA, M. V., DINU-PÎRVU, C.-E., POPA, L., VELESCU, B. Ş., & ARSENE, A. L. 2022. An overview regarding microbial aspects of production and applications of bacterial cellulose, *Materials*, 15: 676.

LUTERBACHER, J. S., RAND, J. M., ALONSO, D. M., HAN, J., YOUNGQUIST, J. T., MARAVELIAS, C. T., PFLEGER, B. F., & DUMESIC, J. A. 2014. Nonenzymatic sugar production from biomass using biomass-derived γ-valerolactone, *Science*, 343: 277-280.

MALGAS, S., MAFA, M. S., MKABAYI, L., & PLETSCHKE, B. I. 2019. A mini review of xylanolytic enzymes with regards to their synergistic interactions during hetero-xylan degradation, *World Journal of Microbiology & Biotechnology*, 35: 187.

MALGAS, S., VAN DYK, J. S., & PLETSCHKE, B. I. 2015. A review of the enzymatic hydrolysis of mannans and synergistic interactions between β-mannanase, β-mannosidase and α-galactosidase, *World Journal of Microbiology and Biotechnology*, 31: 1167-1175.

MANAVALAN, T., STEPNOV, A. A., HEGNAR, O. A., & EIJSINK, V. G. H. 2021. Sugar oxidoreductases and LPMOs – two sides of the same polysaccharide degradation story?, *Carbohydrate Research*, 505: 108350.

MARTINEZ, D., BERKA, R. M., HENRISSAT, B., SALOHEIMO, M., ARVAS, M., BAKER, S. E., CHAPMAN, J., CHERTKOV, O., COUTINHO, P. M., CULLEN, D., DANCHIN, E. G. J., GRIGORIEV, I. V., HARRIS, P., JACKSON, M., KUBICEK, C. P., HAN, C. S., HO, I., LARRONDO, L. F., DE LEON, A. L., MAGNUSON, J. K., MERINO, S., MISRA, M., NELSON, B., PUTNAM, N., ROBBERTSE, B., SALAMOV, A. A., SCHMOLL, M., TERRY, A., THAYER, N., WESTERHOLM-PARVINEN, A., SCHOCH, C. L., YAO, J., BARABOTE, R., NELSON, M. A., DETTER, C., BRUCE, D., KUSKE, C. R., XIE, G., RICHARDSON, P., ROKHSAR, D. S., LUCAS, S. M., RUBIN, E. M., DUNN-COLEMAN, N., WARD, M., & BRETTIN, T. S. 2008. Genome sequencing and analysis of the biomass-degrading fungus *Trichoderma reesei* (syn. *Hypocrea jecorina*), *Nature Biotechnology*, 26: 553-560.

MCCLENDON, S. D., BATTH, T., PETZOLD, C. J., ADAMS, P. D., SIMMONS, B. A., & SINGER, S. W. 2012. *Thermoascus aurantiacus* is a promising source of enzymes for biomass deconstruction under thermophilic conditions, *Biotechnology for Biofuels*, 5: 54.

MCEVOY, A., CREUTZBERG, J., SINGH, R. K., BJERRUM, M. J., & HEDEGÅRD, E. D. 2021. The role of the active site tyrosine in the mechanism of lytic polysaccharide monooxygenase, *Chemical Science*, 12: 352-362.

MECHELKE, M., HERLET, J., BENZ, J. P., SCHWARZ, W. H., ZVERLOV, V. V., LIEBL, W., & KORNBERGER, P. 2017. HPAEC-PAD for oligosaccharide analysis—novel insights into analyte sensitivity and response stability, *Analytical and Bioanalytical Chemistry*, 409: 7169-7181.

MEIER, K. K., JONES, S. M., KAPER, T., HANSSON, H., KOETSIER, M. J., KARKEHABADI, S., SOLOMON, E. I., SANDGREN, M., & KELEMEN, B. 2018. Oxygen activation by Cu LPMOs in recalcitrant carbohydrate polysaccharide conversion to monomer sugars, *Chemical Reviews*, 118: 2593-2635.

MEINSHAUSEN, M., LEWIS, J., MCGLADE, C., GÜTSCHOW, J., NICHOLLS, Z., BURDON, R., COZZI, L., & HACKMANN, B. 2022. Realization of Paris Agreement pledges may limit warming just below 2°C, *Nature*, 604: 304-309.

MEKASHA, S., FORSBERG, Z., DALHUS, B., BACIK, J.-P., CHOUDHARY, S., SCHMIDT-DANNERT, C., VAAJE-KOLSTAD, G., & EIJSINK, V. G. H. 2016. Structural and functional characterization of a small chitin-active lytic polysaccharide monooxygenase domain of a multi-modular chitinase from *Jonesia denitrificans*, *FEBS Letters*, 590: 34-42.

MELELLI, A., ARNOULD, O., BEAUGRAND, J., & BOURMAUD, A. 2020. The middle lamella of plant fibers used as composite reinforcement: investigation by atomic force microscopy, *Molecules*, 25: 632.

MERINO, S. T. & CHERRY, J. 2007. Progress and challenges in enzyme development for biomass utilization, *Advances in Biochemical Engineering/Biotechnology*, 108: 95-120.

MIKKELSON, A., MAAHEIMO, H., & HAKALA, T. K. 2013. Hydrolysis of konjac glucomannan by *Trichoderma reesei* mannanase and endoglucanases Cel7B and Cel5A for the production of glucomannooligosaccharides, *Carbohydrate Research*, 372: 60-68.

MOJZITA, D., RANTASALO, A., & JÄNTTI, J. 2019. Gene expression engineering in fungi, *Current Opinion in Biotechnology*, 59: 141-149.

MONCLARO, A. V., PETROVIĆ, D. M., ALVES, G. S. C., COSTA, M. M. C., MIDORIKAWA, G. E. O., MILLER, R. N. G., FILHO, E. X. F., EIJSINK, V. G. H., & VÁRNAI, A. 2020. Characterization of two family AA9 LPMOs from *Aspergillus tamarii* with distinct activities on xyloglucan reveals structural differences linked to cleavage specificity, *PLoS One*, 15: e0235642.

MORGENSTERN, I., POWLOWSKI, J., & TSANG, A. 2014. Fungal cellulose degradation by oxidative enzymes: from dysfunctional GH61 family to powerful lytic polysaccharide monooxygenase family, *Briefings in Functional Genomics*, 13: 471-481.

MÜLLER, G., CHYLENSKI, P., BISSARO, B., EIJSINK, V. G. H., & HORN, S. J. 2018. The impact of hydrogen peroxide supply on LPMO activity and overall saccharification efficiency of a commercial cellulase cocktail, *Biotechnology for Biofuels*, 11: 209.

MÜLLER, G., VÁRNAI, A., JOHANSEN, K. S., EIJSINK, V. G. H., & HORN, S. J. 2015. Harnessing the potential of LPMO-containing cellulase cocktails poses new demands on processing conditions, *Biotechnology for Biofuels*, 8: 187.

MURALEEDHARAN, M. N., ZOURARIS, D., KARANTONIS, A., TOPAKAS, E., SANDGREN, M., ROVA, U., CHRISTAKOPOULOS, P., & KARNAOURI, A. 2018. Effect of lignin fractions isolated from different biomass sources on cellulose oxidation by fungal lytic polysaccharide monooxygenases, *Biotechnology for Biofuels*, 11: 296.

MUTAHIR, Z., MEKASHA, S., LOOSE, J. S. M., ABBAS, F., VAAJE-KOLSTAD, G., EIJSINK, V. G. H., & FORSBERG, Z. 2018. Characterization and synergistic action of a tetra-modular lytic polysaccharide monooxygenase from *Bacillus cereus*, *FEBS Letters*, 592: 2562-2571.

NEKIUNAITE, L., PETROVIĆ, D. M., WESTERENG, B., VAAJE-KOLSTAD, G., HACHEM, M. A., VÁRNAI, A., & EIJSINK, V. G. H. 2016. *Fg*LPMO9A from *Fusarium graminearum* cleaves xyloglucan independently of the backbone substitution pattern, *FEBS Letters*, 590: 3346-3356.

NEWMAN, R. H., HILL, S. J., & HARRIS, P. J. 2013. Wide-angle x-ray scattering and solid-state nuclear magnetic resonance data combined to test models for cellulose microfibrils in mung bean cell walls, *Plant Physiology*, 163: 1558-1567.

NGUYEN, Q. A., TUCKER, M. P., KELLER, F. A., & EDDY, F. P. 2000. Two-stage dilute-acid pretreatment of softwoods, *Applied Biochemistry and Biotechnology*, 84: 561-576.

NIDETZKY, B., STEINER, W., HAYN, M., & CLAEYSSENS, M. 1994. Cellulose hydrolysis by the cellulases from *Trichoderma reesei*: a new model for synergistic interaction, *Biochemical Journal*, 298: 705-710.

NITSOS, C., ROVA, U., & CHRISTAKOPOULOS, P. 2018. Organosolv fractionation of softwood biomass for biofuel and biorefinery applications, *Energies*, 11: 50.

ODLING-SMEE, L. 2007. Biofuels bandwagon hits a rut, *Nature*, 446: 483-483.

OLSEN, J. P., BORCH, K., & WESTH, P. 2017. Endo/exo-synergism of cellulases increases with substrate conversion, *Biotechnology and Bioengineering*, 114: 696-700.

ØSTBY, H., HANSEN, L. D., HORN, S. J., EIJSINK, V. G. H., & VÁRNAI, A. 2020. Enzymatic processing of lignocellulosic biomass: principles, recent advances and perspectives, *Journal of Industrial Microbiology and Biotechnology*, 47: 623-657.

PAKARINEN, A., HAVEN, M. O., DJAJADI, D. T., VÁRNAI, A., PURANEN, T., & VIIKARI, L. 2014. Cellulases without carbohydrate-binding modules in high consistency ethanol production process, *Biotechnology for Biofuels*, 7: 27.

PARADISI, A., JOHNSTON, E. M., TOVBORG, M., NICOLL, C. R., CIANO, L., DOWLE, A., MCMASTER, J., HANCOCK, Y., DAVIES, G. J., & WALTON, P. H. 2019. Formation of a copper(II)–tyrosyl complex at the active site of lytic polysaccharide monooxygenases following oxidation by H_2O_2, *Journal of the American Chemical Society*, 141: 18585-18599.

PARTHASARATHI, R., ROMERO, R. A., REDONDO, A., & GNANAKARAN, S. 2011. Theoretical study of the remarkably diverse linkages in lignin, *The Journal of Physical Chemistry Letters*, 2: 2660-2666.

PASPALIARI, D. K., LOOSE, J. S., LARSEN, M. H., & VAAJE-KOLSTAD, G. 2015. *Listeria monocytogenes* has a functional chitinolytic system and an active lytic polysaccharide monooxygenase, *The FEBS Journal*, 282: 921-936.

PATEL, A. K., SINGHANIA, R. R., SIM, S. J., & PANDEY, A. 2019. Thermostable cellulases: current status and perspectives, *Bioresource Technology*, 279: 385-392.

PATTATHIL, S., HAHN, M. G., DALE, B. E., & CHUNDAWAT, S. P. 2015. Insights into plant cell wall structure, architecture, and integrity using glycome profiling of native and AFEXTM-pre-treated biomass, *Journal of Experimental Botany*, 66: 4279-4294.

PAULY, M. & KEEGSTRA, K. 2008. Cell-wall carbohydrates and their modification as a resource for biofuels, *The Plant Journal*, 54: 559-568.

PAULY, M. & KEEGSTRA, K. 2016. Biosynthesis of the plant cell wall matrix polysaccharide xyloglucan, *Annual Review of Plant Biology*, 67: 235-259.

PAYNE, C. M., KNOTT, B. C., MAYES, H. B., HANSSON, H., HIMMEL, M. E., SANDGREN, M., STÅHLBERG, J., & BECKHAM, G. T. 2015. Fungal cellulases, *Chemical Reviews*, 115: 1308-1448.

PERCIVAL ZHANG, Y. H., HIMMEL, M. E., & MIELENZ, J. R. 2006. Outlook for cellulase improvement: screening and selection strategies, *Biotechnology Advances*, 24: 452-481.

PERNA, V., MEYER, A. S., HOLCK, J., ELTIS, L. D., EIJSINK, V. G. H., & WITTRUP AGGER, J. 2020. Laccase-catalyzed oxidation of lignin induces production of H_2O_2, *ACS Sustainable Chemistry & Engineering*, 8: 831-841.

PETERSEN, M. Ø., LARSEN, J., & THOMSEN, M. H. 2009. Optimization of hydrothermal pretreatment of wheat straw for production of bioethanol at low water consumption without addition of chemicals, *Biomass and Bioenergy*, 33: 834-840.

PETERSON, R. & NEVALAINEN, H. 2012. *Trichoderma reesei* RUT-C30--thirty years of strain improvement, *Microbiology*, 158: 58-68.

PETROVIĆ, D. M., BISSARO, B., CHYLENSKI, P., SKAUGEN, M., SØRLIE, M., JENSEN, M. S., AACHMANN, F. L., COURTADE, G., VÁRNAI, A., & EIJSINK, V. G. H. 2018. Methylation of the N-terminal histidine protects a lytic polysaccharide monooxygenase from auto-oxidative inactivation, *Protein Science*, 27: 1636-1650.

PETROVIĆ, D. M., VÁRNAI, A., DIMAROGONA, M., MATHIESEN, G., SANDGREN, M., WESTERENG, B., & EIJSINK, V. G. H. 2019. Comparison of three seemingly similar

lytic polysaccharide monooxygenases from *Neurospora crassa* suggests different roles in plant biomass degradation, *Journal of Biological Chemistry*, 294: 15068-15081.

PHILLIPS, C. M., BEESON, W. T., CATE, J. H., & MARLETTA, M. A. 2011. Cellobiose dehydrogenase and a copper-dependent polysaccharide monooxygenase potentiate cellulose degradation by *Neurospora crassa*, *ACS Chemical Biology*, 6: 1399-1406.

PIELHOP, T., AMGARTEN, J., VON ROHR, P. R., & STUDER, M. H. 2016. Steam explosion pretreatment of softwood: the effect of the explosive decompression on enzymatic digestibility, *Biotechnology for Biofuels*, 9: 152.

POIDEVIN, L., BERRIN, J.-G., BENNATI-GRANIER, C., LEVASSEUR, A., HERPOËL-GIMBERT, I., CHEVRET, D., COUTINHO, P. M., HENRISSAT, B., HEISS-BLANQUET, S., & RECORD, E. 2014. Comparative analyses of *Podospora anserina* secretomes reveal a large array of lignocellulose-active enzymes, *Applied Microbiology and Biotechnology*, 98: 7457-7469.

PONNUSAMY, V. K., NGUYEN, D. D., DHARMARAJA, J., SHOBANA, S., BANU, J. R., SARATALE, R. G., CHANG, S. W., & KUMAR, G. 2019. A review on lignin structure, pretreatments, fermentation reactions and biorefinery potential, *Bioresource Technology*, 271: 462-472.

QING, Q. & WYMAN, C. E. 2011. Supplementation with xylanase and β-xylosidase to reduce xylo-oligomer and xylan inhibition of enzymatic hydrolysis of cellulose and pretreated corn stover, *Biotechnology for Biofuels*, 4: 18.

QUINLAN, R. J., SWEENEY, M. D., LO LEGGIO, L., OTTEN, H., POULSEN, J.-C. N., JOHANSEN, K. S., KROGH, K. B. R. M., JØRGENSEN, C. I., TOVBORG, M., ANTHONSEN, A., TRYFONA, T., WALTER, C. P., DUPREE, P., XU, F., DAVIES, G. J., & WALTON, P. H. 2011. Insights into the oxidative degradation of cellulose by a copper metalloenzyme that exploits biomass components, *Proceedings of the National Academy of Sciences of the United States of America*, 108: 15079-15084.

RAGUZ, S., YAGÜE, E., WOOD, D. A., & THURSTON, C. F. 1992. Isolation and characterization of a cellulose-growth-specific gene from *Agaricus bisporus*, *Gene*, 119: 183-190.

RAHIKAINEN, J. L., MARTIN-SAMPEDRO, R., HEIKKINEN, H., ROVIO, S., MARJAMAA, K., TAMMINEN, T., ROJAS, O. J., & KRUUS, K. 2013. Inhibitory effect of lignin during cellulose bioconversion: the effect of lignin chemistry on non-productive enzyme adsorption, *Bioresource Technology*, 133: 270-278.

RAJI, O., ARNLING BÅÅTH, J., VUONG, T. V., LARSBRINK, J., OLSSON, L., & MASTER, E. R. 2021. The coordinated action of glucuronoyl esterase and α-glucuronidase promotes the disassembly of lignin-carbohydrate complexes, *FEBS Letters*, 595: 351-359.

REESE, E. T., SIU, R. G., & LEVINSON, H. S. 1950. The biological degradation of soluble cellulose derivatives and its relationship to the mechanism of cellulose hydrolysis, *Journal of Bacteriology*, 59: 485-497.

RIEDER, L., PETROVIĆ, D., VÄLJAMÄE, P., EIJSINK, V. G. H., & SØRLIE, M. 2021a. Kinetic characterization of a putatively chitin-active LPMO reveals a preference for soluble substrates and absence of monooxygenase activity, *ACS Catalysis*, 11: 11685-11695.

RIEDER, L., STEPNOV, A. A., SØRLIE, M., & EIJSINK, V. G. H. 2021b. Fast and specific peroxygenase reactions catalyzed by fungal mono-copper enzymes, *Biochemistry*, 60: 3633-3643.

RODRÍGUEZ-ZÚÑIGA, U. F., CANNELLA, D., GIORDANO, R. D. C., GIORDANO, R. D. L. C., JØRGENSEN, H., & FELBY, C. 2015. Lignocellulose pretreatment technologies affect the level of enzymatic cellulose oxidation by LPMO, *Green Chemistry*, 17: 2896-2903.

RØDSRUD, G., LERSCH, M., & SJÖDE, A. 2012. History and future of world's most advanced biorefinery in operation, *Biomass and Bioenergy*, 46: 46-59.

ROSALES-CALDERON, O. & ARANTES, V. 2019. A review on commercial-scale high-value products that can be produced alongside cellulosic ethanol, *Biotechnology for Biofuels*, 12: 240.

ROSGAARD, L., PEDERSEN, S., CHERRY, J. R., HARRIS, P., & MEYER, A. S. 2006. Efficiency of new fungal cellulase systems in boosting enzymatic degradation of barley straw lignocellulose, *Biotechnology Progress*, 22: 493-498.

RYTIOJA, J., HILDÉN, K., YUZON, J., HATAKKA, A., DE VRIES, R. P., & MÄKELÄ, M. R. 2014. Plant-polysaccharide-degrading enzymes from Basidiomycetes, *Microbiology and Molecular Biology Reviews*, 78: 614-649.

SABBADIN, F., HEMSWORTH, G. R., CIANO, L., HENRISSAT, B., DUPREE, P., TRYFONA, T., MARQUES, R. D. S., SWEENEY, S. T., BESSER, K., ELIAS, L., PESANTE, G., LI, Y., DOWLE, A. A., BATES, R., GOMEZ, L. D., SIMISTER, R., DAVIES, G. J., WALTON, P. H., BRUCE, N. C., & MCQUEEN-MASON, S. J. 2018. An ancient family of lytic polysaccharide monooxygenases with roles in arthropod development and biomass digestion, *Nature Communications*, 9: 756.

SABBADIN, F., HENRISSAT, B., BRUCE, N. C., & MCQUEEN-MASON, S. J. 2021a. Lytic polysaccharide monooxygenases as chitin-specific virulence factors in crayfish plague, *Biomolecules*, 11.

SABBADIN, F., URRESTI, S., HENRISSAT, B., AVROVA ANNA, O., WELSH LYDIA, R. J., LINDLEY PETER, J., CSUKAI, M., SQUIRES JULIE, N., WALTON PAUL, H., DAVIES GIDEON, J., BRUCE NEIL, C., WHISSON STEPHEN, C., & MCQUEEN-MASON SIMON, J. 2021b. Secreted pectin monooxygenases drive plant infection by pathogenic oomycetes, *Science*, 373: 774-779.

SAITO, A., MIYASHITA, K., BIUKOVIC, G., & SCHREMPF, H. 2001. Characteristics of a *Streptomyces coelicolor* A3(2) extracellular protein targeting chitin and chitosan, *Applied and Environmental Microbiology*, 67: 1268-1273.

SARKAR, P., BOSNEAGA, E., & AUER, M. 2009. Plant cell walls throughout evolution: towards a molecular understanding of their design principles, *Journal of Experimental Botany*, 60: 3615-3635.

SCHELLER, H. V. & ULVSKOV, P. 2010. Hemicelluloses, *Annual Review of Plant Biology*, 61: 263-289.

SCHMIDT, A. S. & THOMSEN, A. B. 1998. Optimization of wet oxidation pretreatment of wheat straw, *Bioresource Technology*, 64: 139-151.

SCHNELLMANN, J., ZELTINS, A., BLAAK, H., & SCHREMPF, H. 1994. The novel lectin-like protein CHB1 is encoded by a chitin-inducible *Streptomyces olivaceoviridis* gene and binds specifically to crystalline alpha-chitin of fungi and other organisms, *Molecular Microbiology*, 13: 807-819.

SCHUERG, T., GABRIEL, R., BAECKER, N., BAKER, S. E., & SINGER, S. W. 2017. *Thermoascus aurantiacus* is an intriguing host for the industrial production of cellulases, *Current Biotechnology*, 6: 89-97.

SCOTT, B. R., HUANG, H. Z., FRICKMAN, J., HALVORSEN, R., & JOHANSEN, K. S. 2016. Catalase improves saccharification of lignocellulose by reducing lytic polysaccharide monooxygenase-associated enzyme inactivation, *Biotechnology Letters*, 38: 425-434.

SCOTT, B. R., ST-PIERRE, P., LAVIGNE, J., MASRI, N., WHITE, T. C., & TOMASHEK, J. J. (2010). *Novel lignin-resistant cellulase enzymes*. US-2010/0221778-A1.

SETHUPATHY, S., MORALES, G. M., GAO, L., WANG, H., YANG, B., JIANG, J., SUN, J., & ZHU, D. 2022. Lignin valorization: status, challenges and opportunities, *Bioresource Technology*, 347: 126696.

SILVA, J. P., TICONA, A. R. P., HAMANN, P. R. V., QUIRINO, B. F., & NORONHA, E. F. 2021. Deconstruction of lignin: from enzymes to microorganisms, *Molecules*, 26: 2299.

SIMMONS, T. J., FRANDSEN, K. E. H., CIANO, L., TRYFONA, T., LENFANT, N., POULSEN, J. C., WILSON, L. F. L., TANDRUP, T., TOVBORG, M., SCHNORR, K., JOHANSEN, K. S., HENRISSAT, B., WALTON, P. H., LO LEGGIO, L., & DUPREE, P. 2017. Structural and electronic determinants of lytic polysaccharide monooxygenase reactivity on polysaccharide substrates, *Nature Communications*, 8: 1064.

SIMMONS, T. J., MORTIMER, J. C., BERNARDINELLI, O. D., PÖPPLER, A.-C., BROWN, S. P., DEAZEVEDO, E. R., DUPREE, R., & DUPREE, P. 2016. Folding of xylan onto cellulose fibrils in plant cell walls revealed by solid-state NMR, *Nature Communications*, 7: 13902.

SINGHAL, N., KUMAR, M., KANAUJIA, P. K., & VIRDI, J. S. 2015. MALDI-TOF mass spectrometry: an emerging technology for microbial identification and diagnosis, *Frontiers in Microbiology*, 6: 791.

SISTA KAMESHWAR, A. K. & QIN, W. 2018. Understanding the structural and functional properties of carbohydrate esterases with a special focus on hemicellulose deacetylating acetyl xylan esterases, *Mycology*, 9: 273-295.

SOCHA, A. M., PARTHASARATHI, R., SHI, J., PATTATHIL, S., WHYTE, D., BERGERON, M., GEORGE, A., TRAN, K., STAVILA, V., VENKATACHALAM, S., HAHN, M. G., SIMMONS, B. A., & SINGH, S. 2014. Efficient biomass pretreatment using ionic liquids derived from lignin and hemicellulose, *Proceedings of the National Academy of Sciences of the United States of America*, 111: E3587-E3595.

SOMERVILLE, C. 2006. Cellulose synthesis in higher plants, *Annual Review of Cell and Developmental Biology*, 22: 53-78.

SOMERVILLE, C., BAUER, S., BRININSTOOL, G., FACETTE, M., HAMANN, T., MILNE, J., OSBORNE, E., PAREDEZ, A., PERSSON, S., RAAB, T., VORWERK, S., & YOUNGS, H. 2004. Toward a systems approach to understanding plant cell walls, *Science*, 306: 2206-2211.

STEPNOV, A. A., CHRISTENSEN, I. A., FORSBERG, Z., AACHMANN, F. L., COURTADE, G., & EIJSINK, V. G. H. 2022a. The impact of reductants on the catalytic efficiency of a lytic polysaccharide monooxygenase and the special role of dehydroascorbic acid, *FEBS Letters*, 596: 53-70.

STEPNOV, A. A., EIJSINK, V. G. H., & FORSBERG, Z. 2022b. Enhanced *in situ* H_2O_2 production explains synergy between an LPMO with a cellulose-binding domain and a single-domain LPMO, *Scientific Reports*, 12: 6129.

STEPNOV, A. A., FORSBERG, Z., SØRLIE, M., NGUYEN, G. S., WENTZEL, A., RØHR Å, K., & EIJSINK, V. G. H. 2021. Unraveling the roles of the reductant and free copper ions in LPMO kinetics, *Biotechnology for Biofuels*, 14: 28.

STERN, P. C., SOVACOOL, B. K., & DIETZ, T. 2016. Towards a science of climate and energy choices, *Nature Climate Change*, 6: 547-555.

STERNBERG, D., VUAYAKUMAR, P., & REESE, E. T. 1977. β-Glucosidase: microbial production and effect on enzymatic hydrolysis of cellulose, *Canadian Journal of Microbiology*, 23: 139-147.

STØPAMO, F. G., RØHR, Å. K., MEKASHA, S., PETROVIĆ, D. M., VÁRNAI, A., & EIJSINK, V. G. H. 2021. Characterization of a lytic polysaccharide monooxygenase from *Aspergillus fumigatus* shows functional variation among family AA11 fungal LPMOs, *Journal of Biological Chemistry*, 297: 101421.

SUDA, M., OHKUMA, J., YAMAGUCHI, A., HIROSE, Y., KONDO, Y., KATO, T., & SHIBATA, D. (2014). *Thermostable cellobiohydrolase*. WO-2014/155566-A1.

SUN, P., LAURENT, C. V. F. P., SCHEIBLBRANDNER, S., FROMMHAGEN, M., KOUZOUNIS, D., SANDERS, M. G., VAN BERKEL, W. J. H., LUDWIG, R., & KABEL, M. A. 2020. Configuration of active site segments in lytic polysaccharide monooxygenases steers oxidative xyloglucan degradation, *Biotechnology for Biofuels*, 13: 95.

SUN, S., SUN, S., CAO, X., & SUN, R. 2016. The role of pretreatment in improving the enzymatic hydrolysis of lignocellulosic materials, *Bioresource Technology*, 199: 49-58.

SUZUKI, K., SUZUKI, M., TAIYOJI, M., NIKAIDOU, N., & WATANABE, T. 1998. Chitin binding protein (CBP21) in the culture supernatant of *Serratia marcescens* 2170, *Bioscience, Biotechnology, and Biochemistry*, 62: 128-135.

TAMBURRINI, K. C., TERRAPON, N., LOMBARD, V., BISSARO, B., LONGHI, S., & BERRIN, J.-G. 2021. Bioinformatic analysis of lytic polysaccharide monooxygenases reveals the pan-families occurrence of intrinsically disordered C-terminal extensions, *Biomolecules*, 11: 1632.

TAN, T.-C., KRACHER, D., GANDINI, R., SYGMUND, C., KITTL, R., HALTRICH, D., HÄLLBERG, B. M., LUDWIG, R., & DIVNE, C. 2015. Structural basis for cellobiose dehydrogenase action during oxidative cellulose degradation, *Nature Communications*, 6: 7542.

TANDRUP, T., FRANDSEN, K. E. H., JOHANSEN, K. S., BERRIN, J.-G., & LO LEGGIO, L. 2018. Recent insights into lytic polysaccharide monooxygenases (LPMOs), *Biochemical Society Transactions*, 46: 1431-1447.

TAYLOR, N. G. 2008. Cellulose biosynthesis and deposition in higher plants, *New Phytologist*, 178: 239-252.

TEERI, T. T., KOIVULA, A., LINDER, M., WOHLFAHRT, G., DIVNE, C., & JONES, T. A. 1998. *Trichoderma reesei* cellobiohydrolases: why so efficient on crystalline cellulose?, *Biochemical Society Transactions*, 26: 173-178.

TENKANEN, M., TAMMINEN, T., & HORTLING, B. 1999. Investigation of lignin-carbohydrate complexes in kraft pulps by selective enzymatic treatments, *Applied Microbiology and Biotechnology*, 51: 241-248.

TOKIN, R., IPSEN, J. Ø., WESTH, P., & JOHANSEN, K. S. 2020. The synergy between LPMOs and cellulases in enzymatic saccharification of cellulose is both enzyme- and substrate-dependent, *Biotechnology Letters*, 42: 1975-1984.

TÕLGO, M., HEGNAR, O. A., ØSTBY, H., VÁRNAI, A., VILAPLANA, F., EIJSINK, V. G. H., & OLSSON, L. 2022. Comparison of six lytic polysaccharide monooxygenases from *Thermothielavioides terrestris* shows that functional variation underlies the multiplicity of LPMO genes in filamentous fungi, *Applied and Environmental Microbiology*, 88: e0009622.

TRANCIK, J. E. 2014. Renewable energy: back the renewables boom, *Nature*, 507: 300-302.

UNDERWOOD, W. 2012. The plant cell wall: a dynamic barrier against pathogen invasion, *Frontiers in Plant Science*, 3: 85.

VAAJE-KOLSTAD, G., FORSBERG, Z., LOOSE, J. S., BISSARO, B., & EIJSINK, V. G. H. 2017. Structural diversity of lytic polysaccharide monooxygenases, *Current Opinion in Structural Biology*, 44: 67-76.

VAAJE-KOLSTAD, G., HORN, S. J., VAN AALTEN, D. M. F., SYNSTAD, B., & EIJSINK, V. G. H. 2005a. The non-catalytic chitin-binding protein CBP21 from *Serratia marcescens* is essential for chitin degradation, *Journal of Biological Chemistry*, 280: 28492-28497.

VAAJE-KOLSTAD, G., HOUSTON, D. R., RIEMEN, A. H. K., EIJSINK, V. G. H., & VAN AALTEN, D. M. F. 2005b. Crystal structure and binding properties of the *Serratia marcescens* chitin-binding protein CBP21, *Journal of Biological Chemistry*, 280: 11313-11319.

VAAJE-KOLSTAD, G., WESTERENG, B., HORN, S. J., LIU, Z., ZHAI, H., SØRLIE, M., & EIJSINK, V. G. H. 2010. An oxidative enzyme boosting the enzymatic conversion of recalcitrant polysaccharides, *Science*, 330: 219-222.

VÄLJAMÄE, P., SILD, V., NUTT, A., PETTERSSON, G., & JOHANSSON, G. 1999. Acid hydrolysis of bacterial cellulose reveals different modes of synergistic action between cellobiohydrolase I and endoglucanase I, *European Journal of Biochemistry*, 266: 327-334.

VALLS, C., PASTOR, F. I. J., RONCERO, M. B., VIDAL, T., DIAZ, P., MARTÍNEZ, J., & VALENZUELA, S. V. 2019. Assessing the enzymatic effects of cellulases and LPMO in improving mechanical fibrillation of cotton linters, *Biotechnology for Biofuels*, 12: 161.

VANDHANA, T. M., REYRE, J.-L., SUSHMAA, D., BERRIN, J.-G., BISSARO, B., & MADHUPRAKASH, J. 2022. On the expansion of biological functions of lytic polysaccharide monooxygenases, *New Phytologist*, 233: 2380-2396.

VÁRNAI, A., HEGNAR, O. A., HORN, S. J., EIJSINK, V. G. H., & BERRIN, J.-G. 2021. 'Fungal Lytic Polysaccharide Monooxygenases (LPMOs): Biological Importance and Applications' in *Encyclopedia of Mycology*. Elsevier: Oxford, 281-294.

VÁRNAI, A., SIIKA-AHO, M., & VIIKARI, L. 2013. Carbohydrate-binding modules (CBMs) revisited: reduced amount of water counterbalances the need for CBMs, *Biotechnology for Biofuels*, 6: 30.

VÁRNAI, A., UMEZAWA, K., YOSHIDA, M., & EIJSINK, V. G. H. 2018. The pyrroloquinoline-quinone-dependent pyranose dehydrogenase from *Coprinopsis cinerea* drives lytic polysaccharide monooxygenase action, *Applied and Environmental microbiology*, 84: e00156-00118.

VERMAAS, J. V., CROWLEY, M. F., BECKHAM, G. T., & PAYNE, C. M. 2015. Effects of lytic polysaccharide monooxygenase oxidation on cellulose structure and binding of oxidized cellulose oligomers to cellulases, *The Journal of Physical Chemistry B*, 119: 6129-6143.

VERMAAS, J. V., KONT, R., BECKHAM, G. T., CROWLEY, M. F., GUDMUNDSSON, M., SANDGREN, M., STÅHLBERG, J., VÄLJAMÄE, P., & KNOTT, B. C. 2019. The dissociation mechanism of processive cellulases, *Proceedings of the National Academy of Sciences of the United States of America*, 116: 23061-23067.

VILLARES, A., MOREAU, C., BENNATI-GRANIER, C., GARAJOVA, S., FOUCAT, L., FALOURD, X., SAAKE, B., BERRIN, J.-G., & CATHALA, B. 2017. Lytic polysaccharide monooxygenases disrupt the cellulose fibers structure, *Scientific Reports*, 7: 40262.

VISSER, H., JOOSTEN, V., PUNT, P. J., GUSAKOV, A. V., OLSON, P. T., JOOSTEN, R., BARTELS, J., VISSER, J., SINITSYN, A. P., EMALFARB, M. A., VERDOES, J. C., & WERY, J. 2011. Development of a mature fungal technology and production platform for industrial enzymes based on a *Myceliophthora thermophila* isolate, previously known as *Chrysosporium lucknowense* C1, *Industrial Biotechnology*, 7: 214-223.

VLASENKO, E., SCHÜLEIN, M., CHERRY, J., & XU, F. 2010. Substrate specificity of family 5, 6, 7, 9, 12, and 45 endoglucanases, *Bioresource Technology*, 101: 2405-2411.

VOINICIUC, C. 2022. Modern mannan: a hemicellulose's journey, *New Phytologist*, 234: 1175-1184.

VU, V. V., BEESON, W. T., PHILLIPS, C. M., CATE, J. H. D., & MARLETTA, M. A. 2014a. Determinants of regioselective hydroxylation in the fungal polysaccharide monooxygenases, *Journal of the American Chemical Society*, 136: 562-565.

VU, V. V., BEESON, W. T., SPAN, E. A., FARQUHAR, E. R., & MARLETTA, M. A. 2014b. A family of starch-active polysaccharide monooxygenases, *Proceedings of the National Academy of Sciences of the United States of America*, 111: 13822-13827.

WADA, M., IKE, M., & TOKUYASU, K. 2010. Enzymatic hydrolysis of cellulose I is greatly accelerated via its conversion to the cellulose II hydrate form, *Polymer Degradation and Stability*, 95: 543-548.

WALTON, P. H. & DAVIES, G. J. 2016. On the catalytic mechanisms of lytic polysaccharide monooxygenases, *Current Opinion in Chemical Biology*, 31: 195-207.

WANG, G. S., PAN, X. J., ZHU, J. Y., GLEISNER, R., & ROCKWOOD, D. 2009. Sulfite pretreatment to overcome recalcitrance of lignocellulose (SPORL) for robust enzymatic saccharification of hardwoods, *Biotechnology Progress*, 25: 1086-1093.

WENZL, T., HAEDRICH, J., SCHAECHTELE, A., ROBOUCH, P., & STROKA, J., *Guidance document for the estimation of LOD and LOQ for measurements in the field of contaminants in feed and food*. 2016, Joint Research Centre (European Commission), Joint Research Centre Technical Reports.

WESTERENG, B., AGGER, J. W., HORN, S. J., VAAJE-KOLSTAD, G., AACHMANN, F. L., STENSTRØM, Y. H., & EIJSINK, V. G. 2013. Efficient separation of oxidized cello-oligosaccharides generated by cellulose degrading lytic polysaccharide monooxygenases, *Journal of Chromatography A*, 1271: 144-152.

WESTERENG, B., ARNTZEN, M. O., AACHMANN, F. L., VARNAI, A., EIJSINK, V. G., & AGGER, J. W. 2016. Simultaneous analysis of C1 and C4 oxidized oligosaccharides, the products of lytic polysaccharide monooxygenases acting on cellulose, *Journal of Chromatography A*, 1445: 46-54.

WESTERENG, B., ARNTZEN, M. O., AGGER, J. W., VAAJE-KOLSTAD, G., & EIJSINK, V. G. H. 2017. Analyzing activities of lytic polysaccharide monooxygenases by liquid chromatography and mass spectrometry, *Methods in Molecular Biology*, 1588: 71-92.

WESTERENG, B., CANNELLA, D., AGGER, J. W., JØRGENSEN, H., ANDERSEN, M. L., EIJSINK, V. G. H., & FELBY, C. 2015. Enzymatic cellulose oxidation is linked to lignin by long-range electron transfer, *Scientific Reports*, 5: 18561.

WESTERENG, B., ISHIDA, T., VAAJE-KOLSTAD, G., WU, M., EIJSINK, V. G. H., IGARASHI, K., SAMEJIMA, M., STÅHLBERG, J., HORN, S. J., & SANDGREN, M. 2011. The putative endoglucanase PcGH61D from *Phanerochaete chrysosporium* is a metal-dependent oxidative enzyme that cleaves cellulose, *PLoS One*, 6: e27807.

WILLIAMS, N. 2008. Biofuel debate deepens, *Current Biology*, 18: R891-R892.

WILSON, D. B. 2004. Studies of *Thermobifida fusca* plant cell wall degrading enzymes, *The Chemical Record*, 4: 72-82.

WINGER, M., CHRISTEN, M., & VAN GUNSTEREN, W. F. 2009. On the conformational properties of amylose and cellulose oligomers in solution, *International Journal of Carbohydrate Chemistry*, 2009: 8.

WINGREN, A., GALBE, M., & ZACCHI, G. 2003. Techno-economic evaluation of producing ethanol from softwood: comparison of SSF and SHF and identification of bottlenecks, *Biotechnology Progress*, 19: 1109-1117.

WOOD, T. M. 1985. Properties of cellulolytic enzyme systems, *Biochemical Society Transactions*, 13: 407-410.

WOOD, T. M. 1988. 'Preparation of crystalline, amorphous, and dyed cellulase substrates' in *Methods in Enzymology*. Academic Press, 19-25.

WU, J., CHANDRA, R., & SADDLER, J. 2019. Alkali–oxygen treatment prior to the mechanical pulping of hardwood enhances enzymatic hydrolysis and carbohydrate recovery through selective lignin modification, *Sustainable Energy & Fuels*, 3: 227-236.

WU, M., BECKHAM, G. T., LARSSON, A. M., ISHIDA, T., KIM, S., PAYNE, C. M., HIMMEL, M. E., CROWLEY, M. F., HORN, S. J., WESTERENG, B., IGARASHI, K., SAMEJIMA, M., STÅHLBERG, J., EIJSINK, V. G. H., & SANDGREN, M. 2013. Crystal structure and computational characterization of the lytic polysaccharide monooxygenase GH61D from the Basidiomycota fungus *Phanerochaete chrysosporium*, *Journal of Biological Chemistry*, 288: 12828-12839.

XIMENES, E., KIM, Y., MOSIER, N., DIEN, B., & LADISCH, M. 2011. Deactivation of cellulases by phenols, *Enzyme and Microbial Technology*, 48: 54-60.

YADAV, S. K., ARCHANA, SINGH, R., SINGH, P. K., & VASUDEV, P. G. 2019. Insecticidal fern protein Tma12 is possibly a lytic polysaccharide monooxygenase, *Planta*, 249: 1987-1996.

YANG, B. & WYMAN, C. E. 2008. Pretreatment: the key to unlocking low-cost cellulosic ethanol, *Biofuels, Bioproducts and Biorefining*, 2: 26-40.

YANG, B. & WYMAN, C. E. 2009. Dilute acid and autohydrolysis pretreatment, *Methods in Molecular Biology*, 581: 103-114.

YAO, F., XU, S., JIANG, Z., ZHAO, J., & HU, C. 2022. The inhibition of *p*-hydroxyphenyl hydroxyl group in residual lignin on enzymatic hydrolysis of cellulose and its underlying mechanism, *Bioresource Technology*, 346: 126585.

ZENG, Y., HIMMEL, M. E., & DING, S. Y. 2017. Visualizing chemical functionality in plant cell walls, *Biotechnology for Biofuels*, 10: 263.

ZENG, Y., ZHAO, S., YANG, S., & DING, S. Y. 2014. Lignin plays a negative role in the biochemical process for producing lignocellulosic biofuels, *Current Opinion in Biotechnology*, 27: 38-45.

ZHANG, B., GAO, Y., ZHANG, L., & ZHOU, Y. 2021a. The plant cell wall: biosynthesis, construction, and functions, *Journal of Integrative Plant Biology*, 63: 251-272.

ZHANG, H., LOPEZ, P. C., HOLLAND, C., LUNDE, A., AMBYE-JENSEN, M., FELBY, C., & THOMSEN, S. T. 2018. The multi-feedstock biorefinery – assessing the compatibility of alternative feedstocks in a 2G wheat straw biorefinery process, *GCB Bioenergy*, 10: 946-959.

ZHANG, X., CHEN, K., LONG, L., & DING, S. 2021b. Two C1-oxidizing AA9 lytic polysaccharide monooxygenases from *Sordaria brevicollis* differ in thermostability, activity, and synergy with cellulase, *Applied Microbiology and Biotechnology*, 105: 8739-8759.

ZHONG, R., CUI, D., & YE, Z. H. 2019. Secondary cell wall biosynthesis, *New Phytologist*, 221: 1703-1723.

ZHONG, R. & YE, Z. H. 2015. Secondary cell walls: biosynthesis, patterned deposition and transcriptional regulation, *Plant & Cell Physiology*, 56: 195-214.

ZHOU, Z., LEI, F., LI, P., & JIANG, J. 2018. Lignocellulosic biomass to biofuels and biochemicals: a comprehensive review with a focus on ethanol organosolv pretreatment technology, *Biotechnology and Bioengineering*, 115: 2683-2702.

ZHU, N., LIU, J., YANG, J., LIN, Y., YANG, Y., JI, L., LI, M., & YUAN, H. 2016. Comparative analysis of the secretomes of *Schizophyllum commune* and other wood-decay Basidiomycetes during solid-state fermentation reveals its unique lignocellulose-degrading enzyme system, *Biotechnology for Biofuels*, 9: 42.

6 Publications

Chromatographic analysis of oxidized cello-oligomers generated by lytic polysaccharide monooxygenases using dual electrolytic eluent generation

Østby, H., Jameson, J.-K., Costa, T., Eijsink, V. G. H., & Arntzen, M. Ø.

Paper I

Journal of Chromatography A 1662 (2022) 462691

Contents lists available at ScienceDirect

Journal of Chromatography A

journal homepage: www.elsevier.com/locate/chroma

Chromatographic analysis of oxidized cello-oligomers generated by lytic polysaccharide monooxygenases using dual electrolytic eluent generation

Heidi Østby, John-Kristian Jameson, Thales Costa, Vincent G.H. Eijsink, Magnus Ø. Arntzen*

Norwegian University of Life Sciences (NMBU), Faculty of Chemistry, Biotechnology, and Food Science, P.O. Box 5003, Ås N-1432, Norway

ARTICLE INFO

Article history:
Received 29 September 2021
Revised 14 November 2021
Accepted 16 November 2021
Available online 19 November 2021

Keywords:
Dual EGC
LPMO
Lytic polysaccharide monooxygenase
Ion chromatography
HPAEC

ABSTRACT

Research on oligosaccharides, including the complicated product mixtures generated by lytic polysaccharide monooxygenases (LPMOs), is growing at a rapid pace. LPMOs are gaining major interest, and the ability to efficiently and accurately separate and quantify their native and oxidized products chromatographically is essential in furthering our understanding of these oxidative enzymes. Here we present a novel set of methods based on dual electrolytic eluent generation, where the conventional sodium acetate/sodium hydroxide (NaOAc/NaOH) eluents in high-performance anion-exchange chromatography (HPAEC) are replaced by electrolytically-generated potassium methane sulfonate/potassium hydroxide (KMSA/KOH). The new methods separate all compounds of interest within 24–45 min and with high sensitivity; limits of detection and quantification were in the range of 0.0001–0.0032 mM and 0.0002–0.0096 mM, respectively. In addition, an average of 3.5 times improvement in analytical CV was obtained. This chromatographic platform overcomes drawbacks associated with manual preparation of eluents and offers simplified operation and rapid method optimization, with increased precision for less abundant LPMO-derived products.

1. Introduction

As the most abundant organic polymer on Earth, cellulose constitutes a highly interesting and desirable potential feedstock for the production of renewable, sustainable fuels and chemicals. Cellulolytic enzymes that catalyze the hydrolysis of this polysaccharide have thus been an important research target for several decades. Reese et al. postulated as early as in 1950 that cellulose degradation encompasses the action of two main enzyme types – one “decrystallizing” enzyme that converts native, crystalline cellulose to more accessible shorter chains, and another that hydrolyzes the shorter cellulose chains to oligo- and monosaccharides [1]. Cellulose breakdown was long believed to be performed solely through the action of hydrolytic enzymes, until a breakthrough discovery in 2010, which showed oxidative cleavage of polysaccharides by a new class of enzymes, namely lytic polysaccharide monooxygenases (LPMOs) [2–10]. LPMOs are critical cellulolytic enzymes because they create chain breaks in highly crystalline areas of the cellulose polymer, and therefore enable access for canonical cellulases to further degrade the substrate. Indeed, cellulolytic LPMOs have become essential in commercial cellulase cocktails, utilized in modern biorefinery operations to produce sustainable, value-added products from second-generation lignocellulosic feedstocks [11,12].

These copper-dependent LPMOs are unique in that they use an oxidative mechanism to cleave glycosidic bonds. Cleavage of cellulose generates a product with an oxidized carbon at the C1 or the C4 position, or, for some LPMOs, a mixture of these products. The C1-oxidized product is a lactone, which is spontaneously hydrated to an aldonic acid. Oxidation at the C4 position generates a ketoaldose which is in equilibrium with its geminal diol form. The hydrated forms of these oxidized sugars, *i.e.*, the aldonic acid or the gemdiol form, are most prevalent in aqueous solutions at physiologically relevant pH [13]. LPMOs acting alone on cellulose will modify the insoluble substrate to contain C1- and/or C4-oxidized sites and will release soluble oxidized cello-oligomers in the range of approximately DP2 – DP10 (DP; degree of polymerization). If the LPMO is part of a cellulolytic enzyme cocktail containing cellulases and a β-glucosidase, soluble oxidized products will be degraded and appear as gluconic acid (for C1 oxidation) or the gemdiol of 4-keto-cellobiose (for C4 oxidation) [14,15]. Proper identification and quantification of LPMO products is of high importance, since this

* Corresponding author.
E-mail address: magnus.arntzen@nmbu.no (M.Ø. Arntzen).

https://doi.org/10.1016/j.chroma.2021.462691

will help understand how these powerful oxidative enzymes work, allow monitoring of LPMO action during cellulose bioprocessing, and enable better harnessing of the power of these remarkable enzymes.

LPMO products pose major challenges regarding separation and quantification via chromatography or mass spectrometry due to their minor structural differences as compared to native oligosaccharides [13,16]. Hydrophilic interaction liquid chromatography (HILIC) and porous graphitized carbon liquid chromatography (PGC-LC) are often used for the separation and identification of oligosaccharide species. HILIC, with its polar stationary phase coupled with a non-polar eluent, enables retention of hydrophilic components [17], and has been used to separate carbohydrates since 1975 [18]. HILIC has previously been used to efficiently separate both neutral and C1-oxidized oligosaccharides [19], but baseline separation of C4-oxidized products has proven challenging with this method [16]. Additionally, high ionic strength of the eluent has been required to yield satisfactory separation of C1-oxidized oligosaccharides, limiting the use of this method with MS detection [16]. PGC columns allow retention of oligosaccharides due to polar interactions between the sugar and the PGC column material [20], and separation is based on size, type of linkage, and 3D-structure [19]. PGC-LC has previously been used to achieve efficient separation of C1- and C4-oxidized species in LPMO product mixtures but causes near co-elution of C4-oxidized and native oligosaccharides. MS-based detection is therefore crucial in product identification, which is possible, as PGC-LC is fully compatible with online MS detection [16,19,21]. The limitation is that medium- to long-chain oligosaccharides tend to show very strong retention to PGC columns; in fact, oligosaccharides with a DP above five are rarely eluted [19].

Although both HILIC and PGC-LC give acceptable separation of oligosaccharides, when it comes to analyzing the complex product mixtures generated by LPMOs, neither method can compete with the sensitivity and separation achieved with high performance anion-exchange chromatography with pulsed amperometric detection (HPAEC-PAD) [19]. In HPAEC, sugar hydroxyl groups are deprotonated by applying an eluent with a high pH, causing the sugars to behave as weak anions and bind to a polymer-based anion-exchange resin [22]. Then, by applying a gradient of increasing salt concentration, the weakly acidic sugar species will be displaced from the column according to the number of charged groups they carry, which corresponds to the chain length of the oligosaccharides. In conventional HPAEC-analysis of oligosaccharides, the eluent is typically a solution of sodium hydroxide (0.1 M NaOH) and the salt is sodium acetate (1 M NaOAc). The NaOAc salt used during the gradient elution acts as a competing ion with the sugars, binding strongly to the column ion-exchange sites, thus displacing the oligosaccharides as the salt concentration increases, resulting in staggered elution [22]. The PAD detection is based on the electrocatalytic oxidation of sugars at high pH catalyzed by a gold working electrode [22]. HPAEC-PAD is generally considered the most advantageous method for the separation of neutral and charged oligosaccharides in terms of both resolution and sensitivity. HPAEC-PAD analysis of LPMO products comes with the disadvantage of not being compatible with MS, due to the fact that elution of charged groups (*i.e.*, the aldonic acids) requires gradients with high salt concentrations [19]. Still, HPAEC-PAD is an excellent method for LPMO research because the method can separate native, C1-, C4-, and C1/C4-oxidized cello-oligomers, despite the minor structural differences between these compounds [16,19]. At high pH, C1-oxidized products are inherently stable aldonic acids. These are relatively simple to analyze using HPAEC-PAD, and can be separated from native products using short run times [19]. C4-oxidized products, however, are unstable at high pH, and will undergo partial on-column decomposition [16]. These decomposition processes generate products that can be used as a proxy for quantifying C4 oxidation [15,16] as well as native products that have lost the (C4-oxidized) sugar at the non-reducing end [13,16].

One major issue associated with HPAEC separation of oligosaccharides is the penetration of CO_2 into the eluents, which eventually leads to accumulation of carbonate on the column. Here the carbonate ions will occupy the anion-exchange sites of the column, causing reduced retention of the analytes [22]. To minimize this effect, eluents are degassed and protected from exposure to air using a continuous flow of N_2 gas. Since this procedure requires meticulous care on the user side, it is prone to error, resulting in unstable retention times. The recently developed technology for electrolytic eluent generation [23] circumvents this issue by only requiring deionized water to be used in the system. By passing the deionized water through eluent generator cartridges (EGCs) and multiple degassers, eluents with the correct hydroxide and salt concentrations are produced on-demand without significant user input, and with no risk of CO_2-contamination.

Recently, a viable platform for oligosaccharide separation using electrolytically generated eluents has been established based on the use of potassium methanesulfonate and potassium hydroxide (KMSA/KOH) [23]. The electrolytic eluent generation occurs in two different EGCs connected in series, one containing concentrated potassium methanesulfonate (KMSA) and one containing concentrated potassium hydroxide (KOH). Dual electrolytic eluent generation technology has already been shown to offer equal performance in oligosaccharide separation as compared to traditional NaOAc/NaOH-based HPAEC-PAD, and entails cleaner, less laborious, and less error-prone eluent generation [23]. To assess the suitability of this new technology for analyzing oxidized oligosaccharides and to generate new methods for LPMO research, we have assessed and further developed the EGC technology for use in HPAEC analysis of the products of LPMO reactions. We demonstrate that dual electrolytic eluent generation is highly suitable for the separation and quantification of oxidized oligosaccharides and present a set of methods for their improved analysis.

2. Materials and methods

2.1. Chromatography

Method development was carried out using an ion chromatography system, ICS-6000 system from Dionex (Thermo Scientific) set up with PAD with a disposable gold electrode utilizing the Dionex Gold-Carbo-Quad waveform (detection potential +0.1 V maintained for 400 ms, followed by 10 ms at -2.0 V, a rapid increase to +0.6 V, and 60 ms at -0.1 V [24]). For oligosaccharide analysis, we used a 1 × 250 mm Dionex CarboPac PA-200 analytical column (Thermo Scientific) connected to a 1 × 50 mm guard column of the same type. The operational flow was 63 µL/min and the sample loop had a volume of 4 µL. For monosaccharide analysis, we used a 2 × 150 mm Dionex CarboPac PA-210-Fast-4 µm column (Thermo Scientific) connected to a 2 × 30 mm guard column of the same type. In this case, the operational flow was 200 µL/min and the sample loop volume was 0.4 µL. The columns were kept at 30 °C. Eluents were generated electrolytically using only distilled H_2O (type I, 18.2 MΩ•cm) and eluent generator cartridges within the instrument (KMSA/KOH for oligosaccharides and KOH only for monosaccharides). The gradients used are described in the Results section and shown in detail in Table 1. For all gradients developed to separate oligosaccharides, a set concentration of 100 mM KOH was used. The concentration of KMSA was varied according to the individual gradient.

For comparative purposes, selected oligosaccharide samples were also analyzed on a Dionex ICS-5000 system (Thermo Scientific), set up with PAD detection and a 3 × 250 mm PA-200 col-

Table 1
Gradients for the three main chromatographic methods for analysis of LPMO products. This table shows three optimized methods for separating native, C1-, and C4-oxidized cello-oligosaccharides using dual EGC with KMSA/KOH and an ICS-6000 HPAEC system. The concentration of KOH was kept constant at 100 mM for all time points in all methods.

Native			Native and C1-oxidized			Native, C1-, and C4-oxidized		
Time [min]	KMSA [mM]	Dionex Curve	Time [min]	KMSA [mM]	Dionex Curve	Time [min]	KMSA [mM]	Dionex Curve
0	0	5	0	1	5	0	0	5
6	30	5	14	100	8	8.5	15	3
10	100	7	17	100	5	17	27	5
15	100	5	17.1	1	5	27	100	7
15.1	0	5	26	1	5	27.1	100	5
24	0	5				36	100	5
						36.1	0	5
						45	0	5

umn Dionex CarboPac PA-200 analytical column (Thermo Scientific) connected to a 3 × 50 mm guard column of the same type, and using previously optimized protocols for NaOH/NaOAc-based elutions [13]. Fresh eluents (A: 0.1 M NaOH; B: 1 M NaOAc, 0.1 M NaOH) were prepared as previously described [13]. The operational flow was 500 µL/min and the sample loop volume was 5 µL. The optimized and routine gradient used for this setup was as follows: 0–3 min, from 100% A to 94.5 % A, 5.5 % B, linear; 3–9 min, from 94.5 % A, 5.5 % B to 85 % A, 15 % B. linear; 9–20 min, from 85 % A, 15 % B to 100 % B, Dionex curve 4; 20–26 min, 100% A.

Chromeleon version 7.2.9 was used for instrument control and analysis for both the ICS-5000 and the ICS-6000. Peaks were integrated using a valley-to-valley baseline and standard curves were created for each component over 3–6 concentration levels, with replicates. The standard curve was obtained by calculating a polynomial regression line (order 2) through all points, including the origin. Limits of detection (LOD) and quantification (LOQ) were calculated based on the Calibration Approach [25]. The lower 2-3 concentrations and the origin were used for linear regression and the LOD was defined as 3.3 × SE_y / slope, and the LOQ as 10 × SE_y / slope, where SE_y is the standard error of the y-intercept. For the comparison of the performance of the ICS-6000 and ICS-5000 when analyzing C1-oxidized oligosaccharides, we measured 12 consecutive pseudo-blanks (water spiked with a known, minimal amount of standard; 0.0005 g/L) and the LOD was defined as 3.9 × STD / slope of a 3-point standard curve for each compound, and the LOQ as 3.3 × LOD [25]. This latter procedure provided more data points compared to the Calibration Approach and allowed for a more accurate comparison of both precision (CV; coefficient of variation) and detection limits of the two systems.

All samples were analyzed as consecutive runs, often within the same day and in total within three months of instrument usage; hence, only minimal day-to-day variation or user-to-user variation is visible within our data. It is anticipated that higher variation may occur during routine analysis, particularly for systems using manually prepared eluents.

2.2. LPMOs and reactions

Both LPMOs utilized in this study (*Sc*LPMO10C and *Nc*LPMO9C) were produced in-house as previously described [5,26] and copper-saturated [27]. Copper-saturation was performed by incubating purified LPMOs with a 3-fold molar excess of Cu(II)SO_4 at room temperature for 30 min. The copper-saturated LPMO was subsequently applied to a PD Midi-Trap G-25 column (GE Healthcare) to remove excess free copper from the LPMO preparation. Protein concentrations were determined spectrophotometrically using A_{280} and theoretical extinction coefficients.

LPMO-catalyzed reactions were performed to generate real product mixtures for use in method development on the ICS-6000 system. Reactions were performed by incubating phosphoric acid-swollen cellulose (PASC, 0.2% w/v; prepared from Avicel according to [28]), LPMO (1 µM), and 1 mM ascorbic acid or gallic acid in Tris-HCl buffer (50 mM, pH 7.5). *Sc*LPMO10C and *Nc*LPMO9C were used to generate C1- and C4-oxidized products, respectively. All reactions were performed in 2 mL Eppendorf tubes with a total reaction volume of 200 µL. The reactions were incubated in an Eppendorf Thermomixer (Eppendorf, Hamburg, Germany) for 20 h at 45 °C with shaking at 1000 rpm and were stopped by filtration using a 96-well filter plate (0.45 µm; Merck Millipore, Billerica, MA). Control experiments without reductant were performed in parallel.

Products from reactions with *Sc*LPMO10C or *Nc*LPMO9C with PASC and ascorbic acid were combined in order to obtain samples containing a mixture of C1- and C4-oxidized LPMO products. In addition, products generated in reactions with *Sc*LPMO10C, PASC and gallic acid were treated with either *Tf*Cel6A (final concentration 1 µM; produced in-house [29,30]) or with a β-glucosidase (final concentration 0.225 mg/mL; kindly provided by Novozymes, Bagsværd, Denmark) for 20 h at 37 °C, in order to convert longer C1-oxidized cello-oligosaccharides to a mixture of native products, cellobionic acid and cellotrionic acid, or to a mixture of glucose and gluconic acid, respectively.

2.3. Native, C1-, C4-, and C6-oxidized cello-oligosaccharide standards

Native cello-oligosaccharides were purchased from Megazyme and combined in order to produce standards containing cello-oligosaccharides ranging in degree of polymerization from 2–6. To produce C1-oxidized standards, native cello-oligosaccharides were mixed to final concentrations of 0.5 mM and treated with *Mt*CDH (produced in-house, as described previously [31]) to a final concentration of 2 µM in sodium acetate buffer (50 mM, pH 5.0). The reaction was incubated in an Eppendorf Thermomixer (Eppendorf, Hamburg, Germany) at 40 °C for 20 h.

To produce C4-oxidized standards, cellopentaose (0.25% w/v Megazyme) was treated with *Nc*LPMO9C (final concentration 2 µM; [15,26]) and ascorbic acid (final concentration 2 mM) in Tris buffer (10 mM, pH 8.0). The reaction was incubated in an Eppendorf Thermomixer (Eppendorf, Hamburg, Germany) for 24 h at 33 °C with shaking at 800 rpm. Reactions were stopped by boiling for 15 min at 100 °C in a heating block.

Gluconic acid and glucuronic acid standards were purchased from Megazyme.

3. Results and discussion

This study was focused on analyzing the products of LPMO reactions using a recently developed, improved ICS equipped with two EGCs (hereafter referred to as ICS-6000). Samples resulting from LPMO reactions typically contain a mixture of native oligosaccharides, C1-oxidized oligosaccharides and C4-oxidized oligosac-

charides, depending on the type of LPMO, the presence or absence of other enzymes, and the substrate.

For assessing the capabilities of the novel ICS, we compared an ICS-6000 equipped with a 1 × 250 mm PA-200 column (63 µL/min flow rate) for dual EGC gradients (KMSA/KOH) with an ICS-5000 equipped with a 3 × 250 mm PA-200 column (500 µL/min flow rate) for conventional gradients (NaOAc/NaOH). Taking into account the difference in column diameter between the two systems, the chosen flow rates should provide comparable chromatographic conditions, leaving the salt, KMSA vs. NaOAc, as the only major variable parameter. The elution strength of the MSA ion is believed to be about 1.8 times stronger than that of the acetate ion [23], and the concentration range allowed by the ICS-6000 instrument is 200 mM for KSMA and KOH together (so, if 100 mM KOH is needed for adequate pH and peak shape, only 0–100 mM KMSA is possible). Limitations in the maximum amount of salt could lead to somewhat increased retention times for compounds binding strongly to the column material.

All methods were optimized towards finding the optimal trade-off between speed, separation power, and reproducibility. We tested both stable KOH concentrations and linear or stepwise changes in KOH-concentration during the gradient. For all oligosaccharides analyzed in this study, a constant KOH-concentration of 100 mM provided the best results. Furthermore, we tested both linear, concave, and convex KMSA gradients, as well as combinations of these, and we monitored the pH-signal of the PAD detector to determine the optimal post-run equilibration time.

3.1. Separation of native cello-oligosaccharides

LPMOs may generate native cello-oligosaccharides when cleaving near polymer chain ends, whereas such native oligomers are the natural products of hydrolytic enzymes, such as cellulases, that are frequently used in combination with LPMOs. When analyzing a standard mixture of cello-oligosaccharides ($Glc_{1\text{-}6}$), we achieved the best results using a steep linear gradient from 0 to 30 mM KMSA over the course of 6 min, followed by a concave gradient (Dionex curve 7) to 100 mM KMSA over the course of 4 min, followed by 5 min at 100 mM KMSA and a 9 min re-equilibration step at 0 mM KMSA (Table 1). This method yielded baseline separation of $Glc_{1\text{-}6}$ within 15 min, with a total time per run of 24 min (Fig. 1A). Due to the small column diameter and comparably large loop size (4 µL), we obtained high sensitivity of detection, down to 0.0005 g/L for all components. For the peak with the lowest intensity (Glc_6; Fig. 1A, inset), the signal-to-noise ratio was as high as 162, which suggests that even lower concentrations could be reliably detected. All components showed a linear response over the concentration range of 0–0.025 g/L, while saturation effects became visible at higher concentrations (Fig. 1B). LODs and LOQs ranged between 0.0001–0.0002 g/L and 0.0003–0.0006 g/L, respectively (Table 2). Of note, Fig. 1 shows a high level of reproducibility between runs and the absence of shifts in elution times.

3.2. Separation of C1-oxidized cello-oligosaccharides

When analyzing the products of a strictly C1-oxidizing LPMO, a typical sample contains a mixture of C1-oxidized cello-oligosaccharides as well as small amounts of native oligomers. Native cello-oligosaccharides have less retention to the PA-200 column than C1-oxidized cello-oligosaccharides, and the oxidized dimer (GlcGlc1A) typically elutes with approximately the same retention time as native Glc_5 [19]. For C1-oxidized compounds, we achieved the best results using a concave gradient (Dionex gradient 8) from 1 to 100 mM KMSA over the course of 14 min, followed by a 3 min washing step at 100 mM KMSA and a 9 min re-conditioning of the column at 1 mM KMSA. *i.e.*, the starting conditions (see Table 1 for details). This 26 min method yielded baseline separation of C1-oxidized species in the DP2–6 range ($Glc_{1\text{-}5}Glc1A$), while separation of native oligomers was similar to what was achieved with the method described above (Fig. 2). All components showed a linear response over the concentration range of 0–0.01 mM, with LOQs down to the range of 0.001–0.01 mM (using the Calibration Approach; LOQs down to the range of 0.00013–0.00056 mM were observed using pseudo-blanks; see Methods section and below). Saturation effects became visible at higher concentrations, only for the longer DPs (Fig. 2C); these effects are not prominent, and adequate quantification up to 0.02 mM is possible when using a polynomial calibration curve. Importantly, with this method there was no co-elution of longer native products with shorter C1-oxidized cello-oligosaccharides, thus enabling efficient separation and identification of all components that may emerge upon treating cellulose with a C1-oxidizing LPMO. Furthermore, Fig. 2 shows a high level of reproducibility between runs and the absence of shifts in elution times.

Surprisingly, when using this highly sensitive ICS-6000 system, we observed splitting of the peaks for the C1-oxidized products at the highest applied concentration (0.02 mM). Such splitting has not been reported before, and we currently do not have an explanation for why this occurs. During protocol optimization, minimization of peak splitting was introduced as an additional parameter, but it was not possible to abolish this phenomenon completely without losing too much resolution. For compound quantification, both peaks were jointly integrated.

3.3. Separation of mixtures of native, C1- and C4-oxidized cello-oligosaccharides

C4-oxidized LPMO products undergo on-column modification [16], and the resulting derivative products, which have been successfully used to quantify C4-oxidation [15], have higher retention times than native and most C1-oxidized products. Thus, elution of these derivative products, hereafter referred to as “C4-oxidized” products, requires a higher concentration of KMSA. Some LPMO reactions may contain both C1- and C4-oxidized products, which means that longer gradients are required to achieve good separation of all components. With this in mind, we developed a 45 min method capable of adequate separation of native, C1-, and C4-oxidized cello-oligosaccharides that avoids co-elution of products of interest while yielding baseline separation of $Glc_{2\text{-}6}$, $Glc_{1\text{-}5}Glc1A$, and the dimer and trimeric C4-oxidized product (Fig. 3). Of note, Fig. 3A shows that the response factor for the C4-oxidized products is much lower than for the other products. The low signals for C4-oxidized products create issues, since these signals almost “drown” in the signals for C1-oxidized products which, as shown in Fig. 3A, have much higher response factors. The low response factors for the C4-oxidized products may relate to the fact that the detected compounds are the result of on-column modification processes induced by high pH [16]. The optimized gradient starts with a convex increase in KMSA concentration for 8.5 min, from 0 to 15 mM, using Dionex curve 3. Thereafter, the concentration of KMSA is increased linearly to 27 mM over the course of 8.5 min. Finally, the concentration of KMSA is increased to 100 mM in 10 min using the concave Dionex curve 7. The gradient is completed with two 9 min steps, the first at 100 mM KMSA to wash the column, and the second at 0 mM KMSA to re-condition the column (Table 1). The C4-oxidized dimer showed a linear response over the concentration range of 0–0.08 mM, with LOQ down to 0.0035 mM, while the trimer was linear between 0–0.005 mM with some mild saturation effects for higher concentrations. The LOQ for the trimer was 0.0002 mM (using the Calibration Approach; LOQs down to 0.00239 mM (dimer) and 0.00013 mM (trimer) were observed us-

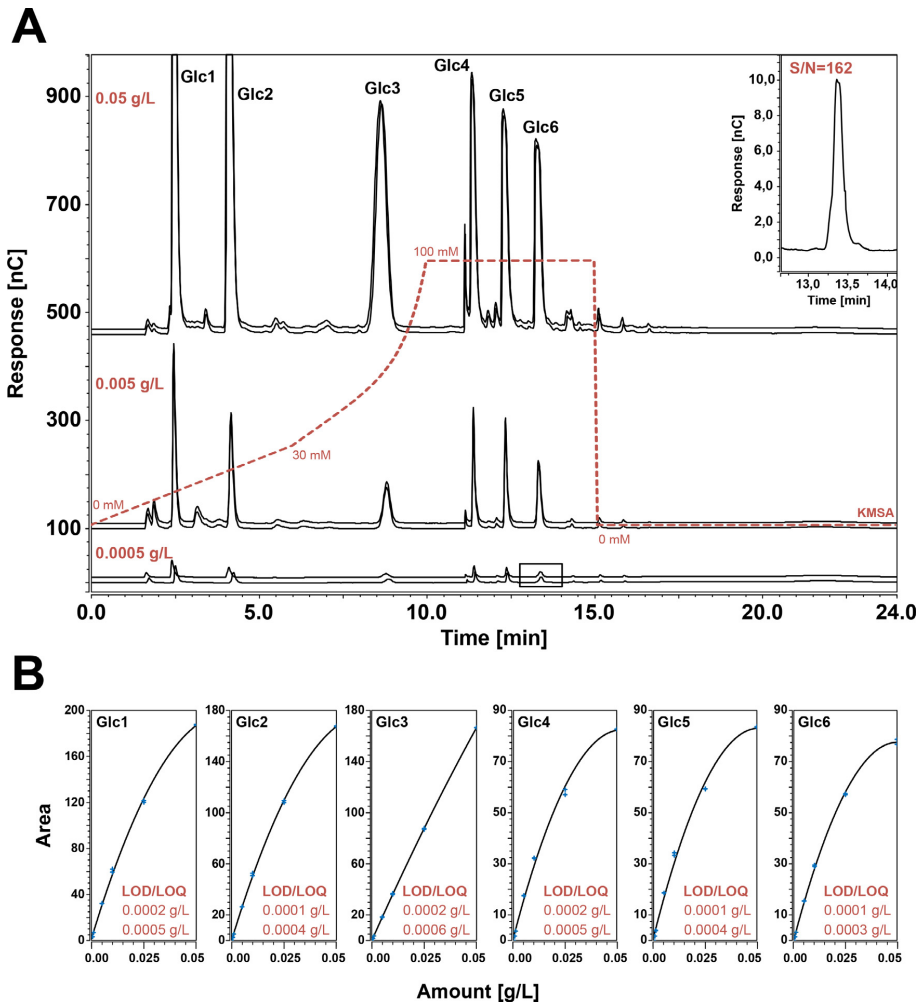

Fig. 1. Separation of native cello-oligosaccharides. Panel (A) shows the gradient (red) used to achieve adequate separation of native cello-oligosaccharides, as well as HPAEC chromatograms of a standard mixture of native cello-oligosaccharides (DP1-6; black labels). The chromatograms show duplicate runs for three different concentrations of standards, overlaid with a small y-offset. The concentration of the standard is shown in red on the left side of the chromatogram. The inset shows a zoom of DP6 at 0.0005 g/L. Panel (B) shows the corresponding standard curves generated via integration of the peaks from the chromatograms in Panel (A); LOD and LOQ values calculated for each compound as indicated in red. (For interpretation of the references to color in this figure legend, the reader is referred to the web version of this article.)

ing pseudo-blanks; see Methods and below). Furthermore, Fig. 3B shows a high level of reproducibility between runs and the absence of shifts in elution times.

Using this method, we then analyzed a mixture of products generated by a strict C1-oxidizing LPMO (*Sc*LPMO10C) and a strict C4-oxidizing LPMO (*Nc*LPMO9C) acting on PASC with ascorbic acid as reductant. Fig. 3B shows that, even for this highly complex mixture of oligomers, all components could be separated and potentially quantified. It is worth noting that HPAEC analysis of product mixtures generated by some LPMOs classified as mixed C1-C4 oxidizing, such as the well-known *Ta*LPMO9A, shows peaks for C4-oxidized products that are higher than peaks for C1-oxidized products [32]. Considering the huge difference in response factors, it would seem that enzymes yielding such a product pattern are almost exclusively C4-oxidizing.

3.4. A comparison of dual EGC (KMSA/KOH) and conventional (NaOAc/NaOH) eluents

An ICS equipped with a PA-200 column and a PAD is an excellent choice of method for analyzing LPMO products ([16,19]; this study). With the recent development of 1 mm PA-200 columns (and even 0.4 mm, not used here) and dual EGC, a lower flow can be used for analyte separation. This typically yields a better signal-to-noise (S/N) ratio and increased sensitivity, particularly when maintaining a relatively large sample loop of 4 µL. Here, we compared our optimized protocol for the ICS-6000, using the 1 mm column and dual EGC (KMSA/KOH), with our routine ICS-5000 protocol with conventional (NaOAc/NaOH) eluents, using 12 repeated injections of C1-oxidized standards of DP2-6. Of note, one major difference between the systems concerns time use:

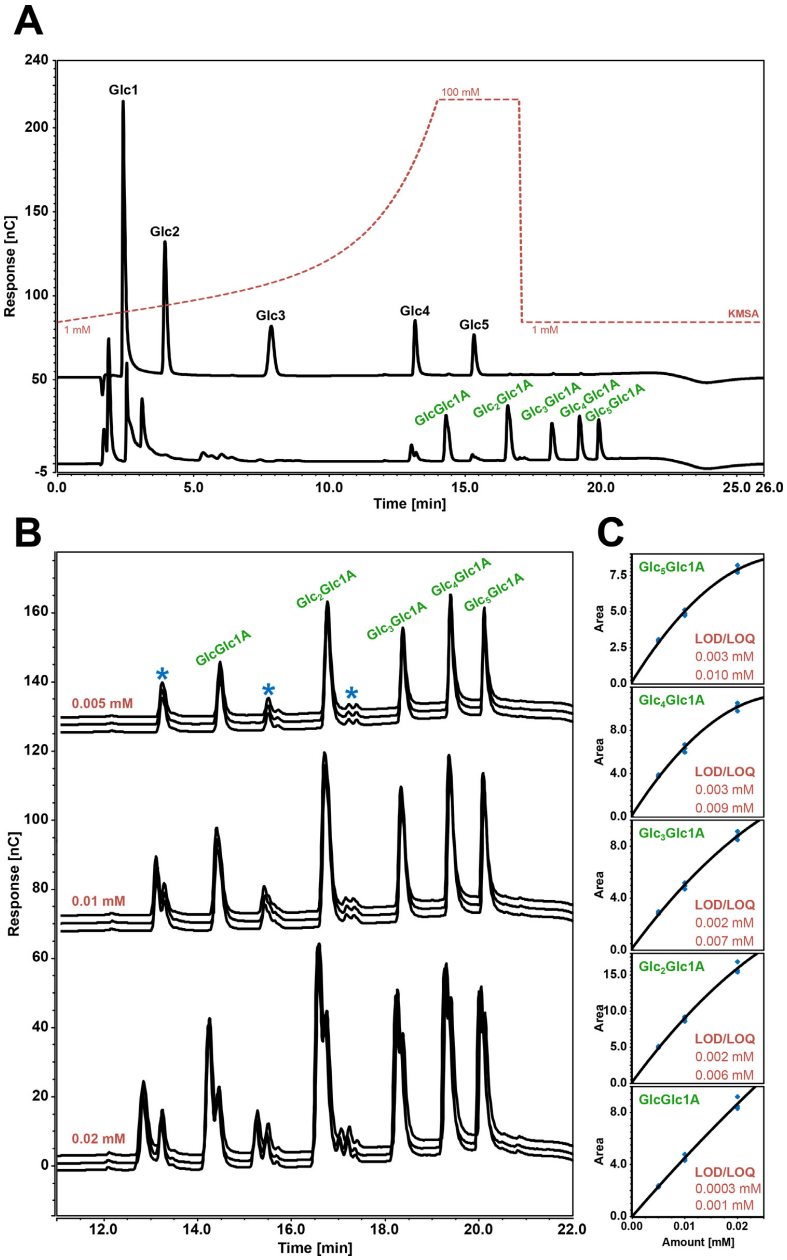

Fig. 2. Separation of native and C1-oxidized oligosaccharides. Panel (A) shows the gradient (red) used to achieve adequate separation of native and C1-oxidized cello-oligosaccharides. Immediately below the gradient, the panel shows chromatograms for a mixture of native cello-oligosaccharide standards (top; DP1-5; 0.005 g/L; black labels) and a mixture of C1-oxidized cello-oligosaccharide standards of chain length (bottom; DP2-6; 0.01 mM; green labels). Panel (B) shows triplicate runs, using the gradient shown in panel A, of three different concentrations of the C1-oxidized cello-oligosaccharide standards (DP2-6), overlaid with a small y-offset. The concentrations of the analytes are shown in red on the left side of the chromatograms. Individual oxidized species are labeled in green in the topmost chromatogram. The peaks marked with a blue star are a mix of native oligosaccharides (see also panel A), and a -30 Da series attributed to the conversion of a hexose to a pentose, which is an artefact that commonly emerges during or after the reaction with CDH. Panel (C) shows standard curves generated via integration of the peaks from the chromatograms in Panel (B). The panel shows the standard curve for each oxidized species. LOD and LOQ values calculated for each standard curve are indicated in red. (For interpretation of the references to color in this figure legend, the reader is referred to the web version of this article.)

Table 2
Determined limits of detection (LOD) and quantification (LOQ). LOD and LOQ were determined either via calibration curves using linear regression, or by multiple injections of pseudo-blank samples; see the Materials and Methods section for details.

	From std. curve		Pseudo-blank injections			
	ICS-6000		ICS-6000		ICS-5000	
	LOD	LOQ	LOD	LOQ	LOD	LOQ
Native method (g/L)						
Glc_1	0.0002	0.0005				
Glc_2	0.0001	0.0004				
Glc_3	0.0002	0.0006				
Glc_4	0.0002	0.0005				
Glc_5	0.0001	0.0004				
Glc_6	0.0001	0.0003				
Native and C1-oxidized method (mM)						
GlcGlc1A	0.0003	0.0011	0.00009	0.00030	0.00036	0.00117
Glc_2Glc1A	0.0019	0.0056	0.00004	0.00013	0.00026	0.00084
Glc_3Glc1A	0.0024	0.0072	0.00017	0.00056	0.00019	0.00064
Glc_4Glc1A	0.0030	0.0090	0.00005	0.00017	0.00022	0.00073
Glc_5Glc1A	0.0032	0.0096	0.00004	0.00014	0.00030	0.00100
Native, C1- and C4-oxidized method (mM)						
Glc4GemGlc	0.0011	0.0035	0.00072	0.00239	0.00291	0.00962
$Glc4GemGlc_2$	0.0001	0.0002	0.00004	0.00013	0.00139	0.00457
D-gluconic acid method (g/L)						
D-gluconic acid	0.0041	0.0125				

the dual EGC is always-on, reducing the time needed for preparing eluents and columns from approximately two hours for the ICS-5000 to approximately ten minutes for the ICS-6000. On the other hand, the maximum KMSA concentration applied to the system is 100 mM, which will, despite the higher elution strength of KMSA, lead to longer gradual gradients with KMSA compared to NaOAc to achieve adequate separation of both native and C1-oxidized oligosaccharides without peak overlaps. With NaOAc (ICS-5000), we achieved good separation within 13 min using a flow of 500 µL/min (Fig. 4B), while 20 min were needed when using KMSA (ICS-6000) and a flow of 63 µL/min (Fig. 4A). The low flow rate of the ICS-6000 produces a very stable detector baseline, while more fluctuations are observed with the ICS-5000 (Fig. 4C). This leads to a considerable difference in signal-to-noise ratio between the systems (Fig. 4D), which affects the accuracy of quantification in the low concentration region and renders the ICS-6000 more sensitive and reproducible. Technically, the reason behind the stable baseline is several technical design improvements of dual EGC systems. I) the concentration is directly generated without the need of a mixing chamber, II) the tubing volume between the pump and detector is much larger relative to the flow rate (the flow passes through two EGC modules and more tubing) causing a dampening-effect on the baseline, and III) the low flow causes less frequent pump pulses compared to a high flow. All these factors contribute to the stable baseline. Additionally, we can observe an increase in signal response on the ICS-6000 compared to ICS-5000 (Fig. 4A and 4B; almost 2 × response on ICS-6000). This is likely due to the relatively large sample loop size on the ICS-6000 (4 µL injected on a 1 mm column) compared to the ICS-5000 (5 µL injected on a 3 mm column), and the effect of the PAD flow cell: (I) a smaller gasket (1 mm on ICS-6000 and 2 mm on ICS-5000), and (II) lower flow, both leading to a higher chance of molecules reaching the electrode surface. Combining the stable baseline with the increase in signal response ultimately leads to markedly higher signal-to-noise ratios obtained with the ICS-6000 as seen in Fig. 4D.

In this experiment, LODs and LOQs were determined by measuring 12 consecutive pseudo-blanks (water spiked with a known, minimal amount of compound) with quantification using a 3-point standard curve (see Methods section). Using 0.0005 g/L C1-oxidized oligosaccharides (approx. 0.0014–0.0005 mM for DP2-6, respectively), we obtained LODs of 0.00004–0.00017 mM for the ICS-6000 and 0.00019–0.00036 mM for the ICS-5000. The LOQs were 0.00013–0.00056 mM and 0.00073–0.00117 mM for the ICS-6000 and the ICS-5000, respectively (Fig. 4E). Of note, experiments with the ICS-6000 showed a markedly lower analytical CV than experiments with the ICS-5000, especially for very low concentrations (Fig. 4E), enabling accurate and reproducible quantification of low-abundant compounds. All 12 replicates showed good reproducibility (relative standard deviation; RSD <0.14%) of retention times for both systems. It is expected that day-to-day variations involving different preparations of manual eluents might affect retention time stability compared to a system with electrolytically generated eluents; however, we have not performed any longitudinal analyses to verify this.

For comparison, we also analyzed 12 reinjections of C4-oxidized oligosaccharides on both systems (data not shown) in order to calculate LOD and LOQ for these compounds with the pseudo-blank approach. This analysis (Table 2) corroborated the results obtained with C1-oxidized oligomers, showing higher sensitivity and more reproducible quantification of low-abundant compounds for the ICS-6000 system. The analytical CVs for the C4-oxidized dimer and trimer were 6.1% and 3.1%, respectively, compared to 19.8% and 25.6% for the ICS-5000. Table 2 summarizes the LOD and LOQ values determined in this study, using the calibration approach or the pseudo-blank approach.

3.5. Detection of the C1-oxidized monosaccharide, D-gluconic acid

D-Gluconic acid is the C1-oxidized monosaccharide that can emerge when a C1-oxidized cello-oligosaccharide, the product of a C1-oxidizing LPMO, is degraded further, *e.g.*, by β-glucosidases. These latter enzymes act from the non-reducing end and have been shown to be able to convert C1-oxidized cello-oligosaccharides to a mixture of glucose and gluconic acid [14]. Under standard conditions for analyzing oligosaccharides, D-gluconic acid will have poor retention and elute too early, namely in the injection peak, along with other monosaccharides in the reaction mixture (Fig. 5A). To create a method for specific detection

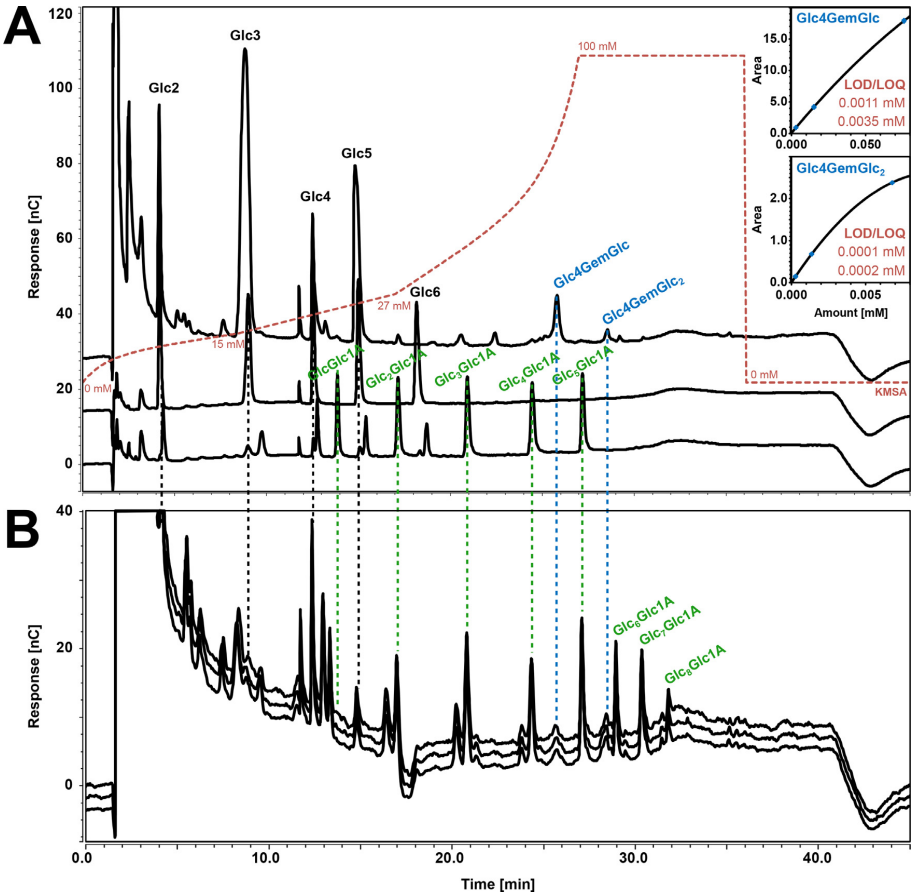

Fig. 3. Separation of native, C1-oxidized and C4-oxidized oligosaccharides. Panel A shows the 45 min gradient (in red) that achieved the best separation of native, C1-oxidized, and C4-oxidized cello-oligosaccharides. The chromatograms show standard samples containing the C4-oxidized dimer and trimer (top; blue labels; 0.08 mM Glc4GemGlc, 0.009 mM $Glc4GemGlc_2$), native oligomers (middle; black labels; 0.01 mM), and C1-oxidized oligomers (bottom; green labels; 0.01 mM). The inserts show standard curves over three levels and calculated LOD and LOQ values for C4-oxidized oligosaccharides. The sample containing C4-oxidized products was generated by incubating Glc_5 with *Nc*LPMO9C, which leads to formation of Glc4GemGlc and Glc_3, and minor amounts of $Glc4GemGlc_2$ and Glc_2. The amount of Glc4GemGlc was determined by quantification of Glc_3 and the amount of $Glc4GemGlc_2$ was determined by quantification of Glc_2. Panel B shows the chromatograms of three replicates of a mixture of products from two LPMO reactions, one C1-oxidizing (*Sc*LPMO10C) and one C4-oxidizing (*Nc*LPMO9C), with PASC and ascorbic acid. Note that *Nc*LPMO9C acts on soluble substrates, which explains why longer C4-oxidized oligomers or native oligomers derived from on-column modification of such oligomers are not observed. (For interpretation of the references to color in this figure legend, the reader is referred to the web version of this article.)

of D-gluconic acid, we used an ICS-6000 setup consisting of a 150 × 2 mm PA-210-Fast-4 µm column connected to a 30 × 2 mm guard column of the same material, operated at 200 µL/min. The column was subjected to isocratic elution with 70 mM KOH for 16 min, followed by a 5 min washing step at 100 mM KOH, and a 9 min re-conditioning at 70 mM KOH. In this setup, we used a 0.4 µL sample loop instead of the 4 µL sample loop used for oligosaccharides, which reduces sensitivity but eliminates the need for (error-prone) dilution of samples with high concentrations. With this setup, we observed a linear response for concentrations between 0.01–0.05 g/L for gluconic acid (Fig. 5C), with LOD of 0.004 g/L and LOQ of 0.013 g/L. While minor saturation effects were visible between 0.05–0.1 g/L, quantification up to 0.1 g/L is still possible using a polynomial calibration curve.

Occasionally, C6 oxidation, leading to the formation of glucuronic acid, has been observed in LPMO reactions [33]. We therefore also assessed separation of glucuronic acid and gluconic acid. We found that for such product mixtures, a 16 min linear gradient of 50–80 mM KOH can be applied, followed by a 5 min washing step at 100 mM KOH, and a 9 min re-conditioning step at 50 mM KOH (Fig. 5B, inset). The only other monomeric product potentially present in an LPMO reaction would be glucose (depending on the substrate used), which elutes at 2.8 min with this method, and does not interfere with the separation of the sugar acids.

Current analysis of the action of C1-active LPMOs (number of cuts) is based on quantification of the C1-oxidized cello-di- and trisaccharides that emerge upon treating the mixture of soluble oxidized cello-oligosaccharides with a cellulase [34] (Fig. 5A). While this procedure has shown reproducible results, analysis of the C1-oxidized dimer and trimer may still be challenging in complex sample mixtures due to co-eluting products, for example various hemicellulose fragments. Alternatively, one could degrade the C1-

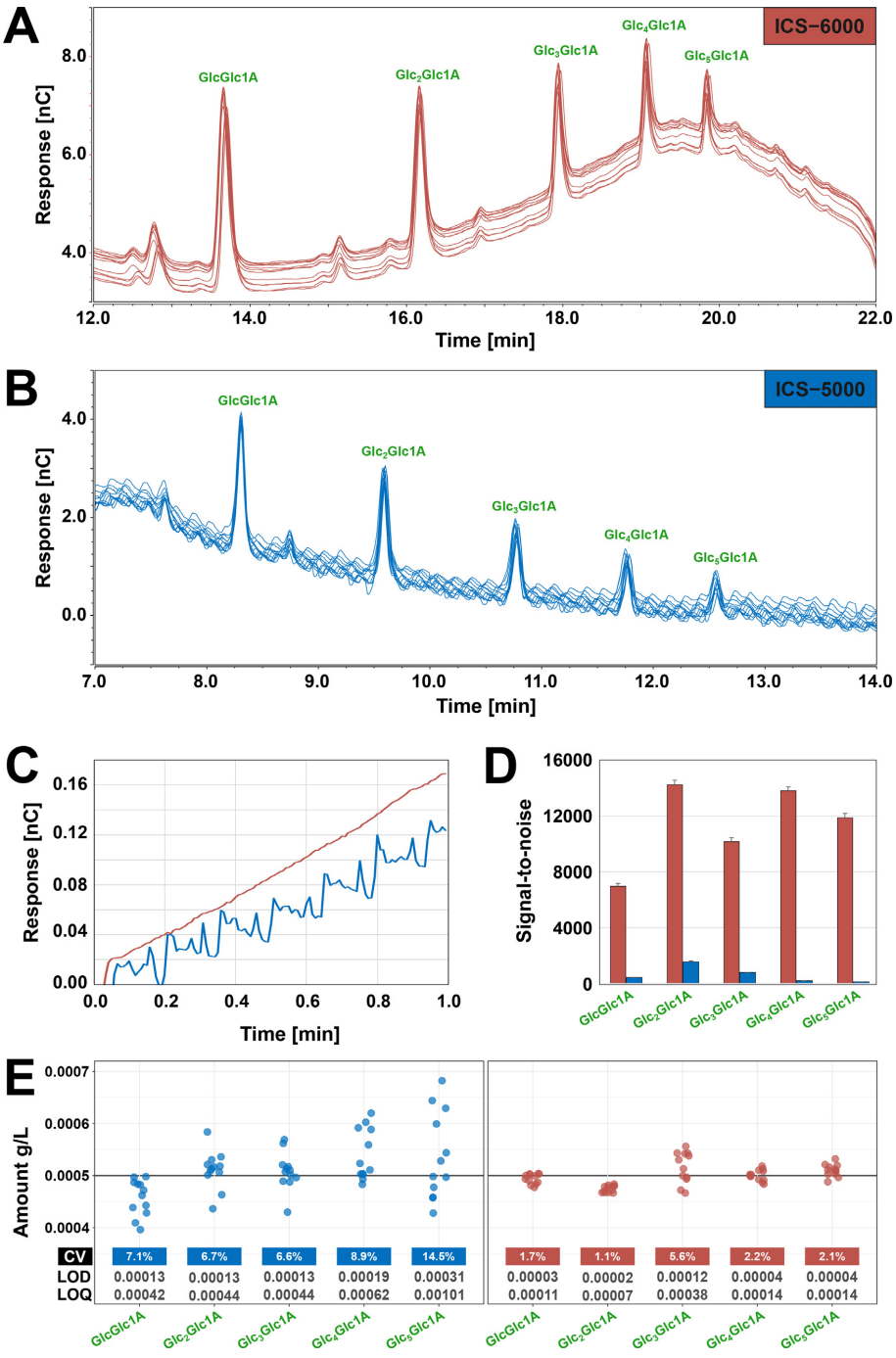

Fig. 4. Comparison of chromatographic performance of the ICS-5000 and ICS-6000 methods. C1-oxidized standards (0.0005 g/L) were analyzed 12 times on an ICS-6000 (A; red) and on an ICS-5000 (B; blue) using optimized methods for both systems. (C) The signal response of the detector measured within the first minute of the gradient, *i.e.*, prior to the injection peak. (D) Signal-to-noise ratio (S/N) for $Glc_{1\text{-}5}Glc1A$ where detector noise is calculated from the curves in C. S/N = 2 × peak height / noise. (E) Quantified amounts of the 12 reinjections for all components on both systems and calculated values for CV, LOD and LOQ (in g/L); for details, see methods. The black line at 0.0005 g/L denotes the theoretical concentration. (For interpretation of the references to color in this figure legend, the reader is referred to the web version of this article.)

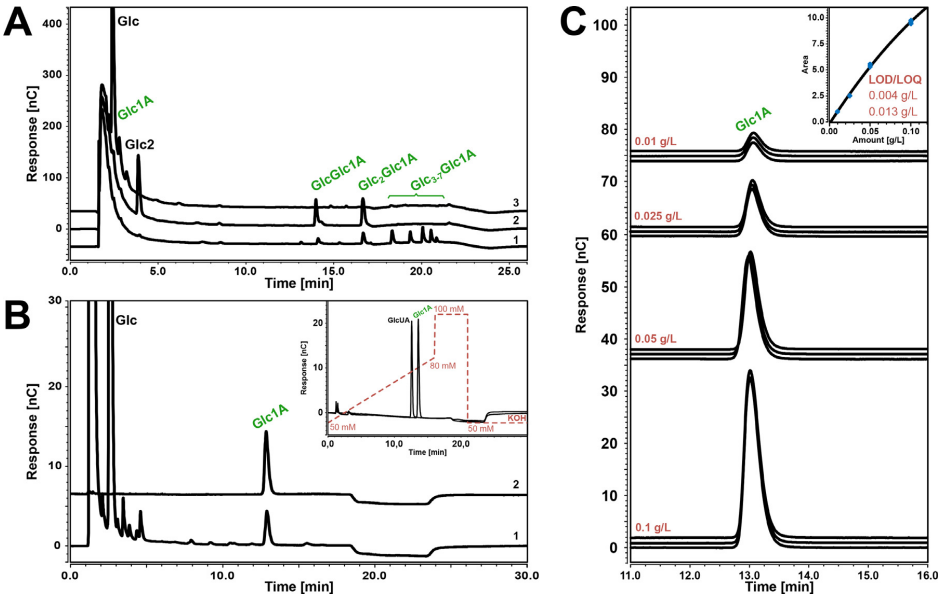

Fig. 5. Detection of d-gluconic acid. Panel (A) shows three samples (1–3) analyzed using the gradient shown in Fig. 2A. 1: Products of a reaction of *Sc*LPMO10C with PASC and gallic acid as reductant. 2: Sample 1 treated with *Tf*Cel6A. 3: Sample 1 treated with β-glucosidase. Control reactions containing only β-glucosidase and buffer (not shown) indicated that small residual peaks in the 18–22 min. region of the chromatogram for sample 3 are compounds in the β-glucosidase preparation, and not residual oxidized products. Panel (B), chromatogram 1, shows sample 3 from panel (A) analyzed with an isocratic gradient at 70 mM KOH. Chromatogram 2 is a 0.025 g/L D-gluconic acid standard. The inset shows an alternative gradient (red) developed to achieve separation of C1- and C6-oxidized glucose, D-gluconic (Glc1A, green label) and glucuronic acid (GlcUA, black label), respectively; the sample contained 0.05 g/L of each compound. Panel (C) shows the D-gluconic acid standard in triplicates at four concentration levels and the obtained standard curve (inset). LOD and LOQ values calculated for the standard curve are indicated in red. (For interpretation of the references to color in this figure legend, the reader is referred to the web version of this article.)

oxidized oligomers with β-glucosidase, converting the oligomers to glucose and D-gluconic acid (Fig. 5A; [14]), and then quantify the latter using the PA-210 column set-up, as shown in Fig. 5B. This method simplifies the analysis of products generated by C1-oxidizing LPMOs, as only one product (D-gluconic acid) is measured instead of di- and trisaccharides. Furthermore, since the product is a monosaccharide, it can be analyzed with a different HPAEC setup (and column) and will not co-elute with other products potentially present in the LPMO reaction.

4. Concluding remarks

Enzymatic assays used for characterizing LPMOs and related enzymes lead to complex product mixtures containing native, C1-, and C4-oxidized oligosaccharides (as well as possibly also C6-oxidized compounds). Depending on the reaction setup, product mixtures may also contain monosaccharides, *e.g.*, glucose and D-gluconic acid. The ability to efficiently and accurately separate and quantify these compounds chromatographically is essential in furthering our understanding of these enzymes. Herein, we have presented new methods for HPAEC, based on dual electrolytic eluent generation where NaOAc/NaOH is replaced by KMSA/KOH. These new methods and the automatic generation of eluents overcome drawbacks associated with manually prepared eluents, primarily time and potential day-to-day variations, and offer simplified operation, increased precision, and higher sensitivity.

As our knowledge of LPMOs expands, so does our understanding of the range of substrates LPMOs can act upon. Novel substrate specificities of LPMOs are continuously being discovered [35–40]. There is thus a need for optimized chromatographic methods able to separate, and help identify, alternative oxidized oligosaccharides, such as, for example, xylan-, xyloglucan-, and glucomannan-derived products. While no such compounds have been analyzed as part of this study, we anticipate that the methods described in this paper can provide a basis for further development of specialized gradients designed to separate other LPMO-generated oxidized products, as has been done for older ICS systems [35]. Regardless, it is clear that the new ICS-6000 system with its low-diameter columns and low flow offers unprecedented separation and sensitivity, combined with easy eluent preparation, gradient optimization, and minimal system drift.

Declaration of Competing Interest

The authors declare that they have no known competing financial interests or personal relationships that could have appeared to influence the work reported in this paper.

CRediT authorship contribution statement

Heidi Østby: Methodology, Validation, Formal analysis, Investigation, Writing – original draft, Visualization. **John-Kristian Jameson:** Methodology, Investigation, Writing – review & editing. **Thales Costa:** Resources, Writing – review & editing. **Vincent G.H. Eijsink:** Methodology, Writing – review & editing, Supervision, Funding acquisition. **Magnus Ø. Arntzen:** Conceptualization, Methodology, Writing – review & editing, Visualization, Supervision, Funding acquisition.

Acknowledgments

The authors would like to thank Bo Emilsson at Nerliens Meszansky, Norway, for valuable help during the initial setup and

planning of these methods. This research was supported by the Research Council of Norway through grants 257622 & 268002 and by the Novo Nordisk Foundation through grant NNF20OC0061313. Infrastructure was supported in part by NorBioLab grants 226247 and 270038 from the Research Council of Norway.

References

[1] E.T. Reese, R.G. Siu, H.S. Levinson, The biological degradation of soluble cellulose derivatives and its relationship to the mechanism of cellulose hydrolysis, J. Bacteriol. 59 (4) (1950) 485–497, doi:10.1128/JB.59.4.485-497.1950.

[2] G. Vaaje-Kolstad, B. Westereng, S.J. Horn, Z. Liu, H. Zhai, M. Sørlie, V.G. Eijsink, An oxidative enzyme boosting the enzymatic conversion of recalcitrant polysaccharides, Science 330 (6001) (2010) 219–222, doi:10.1126/science.1192231.

[3] S.J. Horn, G. Vaaje-Kolstad, B. Westereng, V. Eijsink, Novel enzymes for the degradation of cellulose, Biotechnol. Biofuels 5 (1) (2012) 45, doi:10.1186/1754-6834-5-45.

[4] P. Chylenski, B. Bissaro, M. Sørlie, Å.K. Røhr, A. Várnai, S.J. Horn, V.G.H. Eijsink, Lytic polysaccharide monooxygenases in enzymatic processing of lignocellulosic biomass, ACS Catal. 9 (6) (2019) 4970–4991, doi:10.1021/acscatal.9b00246.

[5] Z. Forsberg, G. Vaaje-Kolstad, B. Westereng, A.C. Bunæs, Y. Stenstrøm, A. MacKenzie, M. Sørlie, S.J. Horn, V.G. Eijsink, Cleavage of cellulose by a CBM33 protein, Protein Sci. 20 (9) (2011) 1479–1483, doi:10.1002/pro.689.

[6] C.M. Phillips, W.T. Beeson, J.H. Cate, M.A. Marletta, Cellobiose dehydrogenase and a copper-dependent polysaccharide monooxygenase potentiate cellulose degradation by neurospora crassa, ACS Chem. Biol. 6 (12) (2011) 1399–1406, doi:10.1021/cb200351y.

[7] R.J. Quinlan, M.D. Sweeney, L. Lo Leggio, H. Otten, J.C.N. Poulsen, K.S. Johansen, K.B.R.M. Krogh, C.I. Jørgensen, M. Tovborg, A. Anthonsen, T. Tryfona, C.P. Walter, P. Dupree, F. Xu, G.J. Davies, P.H. Walton, Insights into the oxidative degradation of cellulose by a copper metalloenzyme that exploits biomass components, Proc. Natl. Acad. Sci. U. S. A. 108 (37) (2011) 15079–15084, doi:10.1073/pnas.1105776108.

[8] M. Dimarogona, E. Topakas, P. Christakopoulos, Recalcitrant polysaccharide degradation by novel oxidative biocatalysts, Appl. Microbiol. Biotechnol. 97 (19) (2013) 8455–8465, doi:10.1007/s00253-013-5197-y.

[9] K.S. Johansen, Lytic polysaccharide monooxygenases: the microbial power tool for lignocellulose degradation, Trends Plant Sci. 21 (11) (2016) 926–936, doi:10.1016/j.tplants.2016.07.012.

[10] M. Frommhagen, A.H. Westphal, W.J.H. van Berkel, M.A. Kabel, Distinct substrate specificities and electron-donating systems of fungal lytic polysaccharide monooxygenases, Front. Microbiol. 9 (2018) 1080, doi:10.3389/fmicb.2018.01080.

[11] H. Østby, L.D. Hansen, S.J. Horn, V.G.H. Eijsink, A. Várnai, Enzymatic processing of lignocellulosic biomass: principles, recent advances and perspectives, J. Ind. Microbiol. Biotechnol. 47 (9) (2020) 623–657, doi:10.1007/s10295-020-02301-8.

[12] Katja S. Johansen, Discovery and industrial applications of lytic polysaccharide mono-oxygenases, Biochem. Soc. Trans. 44 (1) (2016) 143–149, doi:10.1042/BST20150204.

[13] B. Westereng, M.O. Arntzen, J.W. Agger, G. Vaaje-Kolstad, V.G.H. Eijsink, Analyzing activities of lytic polysaccharide monooxygenases by liquid chromatography and mass spectrometry, Methods Mol. Biol. 1588 (2017) 71–92, doi:10.1007/978-1-4939-6899-2_7.

[14] D. Cannella, C.W. Hsieh, C. Felby, H. Jorgensen, Production and effect of aldonic acids during enzymatic hydrolysis of lignocellulose at high dry matter content, Biotechnol. Biofuels 5 (1) (2012) 26, doi:10.1186/1754-6834-5-26.

[15] G. Müller, A. Várnai, K.S. Johansen, V.G. Eijsink, S.J. Horn, Harnessing the potential of LPMO-containing cellulase cocktails poses new demands on processing conditions, Biotechnol. Biofuels 8 (2015) 187, doi:10.1186/s13068-015-0376-y.

[16] B. Westereng, M.O. Arntzen, F.L. Aachmann, A. Varnai, V.G. Eijsink, J.W. Agger, Simultaneous analysis of C1 and C4 oxidized oligosaccharides, the products of lytic polysaccharide monooxygenases acting on cellulose, J. Chromatogr. A 1445 (2016) 46–54, doi:10.1016/j.chroma.2016.03.064.

[17] M. Lammerhofer, HILIC and mixed-mode chromatography: the rising stars in separation science, J. Sep. Sci. 33 (6-7) (2010) 679–680, doi:10.1002/jssc.201090015.

[18] J.C. Linden, C.L. Lawhead, Liquid chromatography of saccharides, J. Chromatogr. A 105 (1) (1975) 125–133, doi:10.1016/S0021-9673(01)81096-7.

[19] B. Westereng, J.W. Agger, S.J. Horn, G. Vaaje-Kolstad, F.L. Aachmann, Y.H. Stenstrøm, V.G. Eijsink, Efficient separation of oxidized cello-oligosaccharides generated by cellulose degrading lytic polysaccharide monooxygenases, J. Chromatogr. A 1271 (1) (2013) 144–152, doi:10.1016/j.chroma.2012.11.048.

[20] C. West, C. Elfakir, M. Lafosse, Porous graphitic carbon: a versatile stationary phase for liquid chromatography, J. Chromatogr. A 1217 (19) (2010) 3201–3216, doi:10.1016/j.chroma.2009.09.052.

[21] Y. Westphal, H.A. Schols, A.G. Voragen, H. Gruppen, Introducing porous graphitized carbon liquid chromatography with evaporative light scattering and mass spectrometry detection into cell wall oligosaccharide analysis, J. Chromatogr. A 1217 (5) (2010) 689–695, doi:10.1016/j.chroma.2009.12.005.

[22] T.R. Cataldi, C. Campa, G.E. De Benedetto, Carbohydrate analysis by high-performance anion-exchange chromatography with pulsed amperometric detection: the potential is still growing, Fresenius J. Anal. Chem. 368 (8) (2000) 739–758, doi:10.1007/s002160000588.

[23] Y. Chen, V. Barreto, A. Woodruff, Z. Lu, Y. Liu, C. Pohl, Dual electrolytic eluent generation for oligosaccharides analysis using high-performance anion-exchange chromatography, Anal. Chem. 90 (18) (2018) 10910–10916, doi:10.1021/acs.analchem.8b02436.

[24] R.D. Rocklin, A.P. Clarke, M. Weitzhandler, Improved long-term reproducibility for pulsed amperometric detection of carbohydrates via a new quadruple-potential waveform, Anal. Chem. 70 (8) (1998) 1496–1501, doi:10.1021/ac970906w.

[25] T. Wenzl, J. Haedrich, A. Schaechtele, P. Robouch, J. Stroka, Guidance document for the estimation of LOD and LOQ for measurements in the field of contaminants in feed and food, Joint research centre (European Commission), Joint Research Centre Technical Reports (2016), doi:10.2787/8931.

[26] T. Isaksen, B. Westereng, F.L. Aachmann, J.W. Agger, D. Kracher, R. Kittl, R. Ludwig, D. Haltrich, V.G. Eijsink, S.J. Horn, A C4-oxidizing lytic polysaccharide monooxygenase cleaving both cellulose and cello-oligosaccharides, J. Biol. Chem. 289 (5) (2014) 2632–2642, doi:10.1074/jbc.M113.530196.

[27] J.S. Loose, Z. Forsberg, M.W. Fraaije, V.G. Eijsink, G. Vaaje-Kolstad, A rapid quantitative activity assay shows that the vibrio cholerae colonization factor GbpA is an active lytic polysaccharide monooxygenase, FEBS Lett. 588 (18) (2014) 3435–3440, doi:10.1016/j.febslet.2014.07.036.

[28] T.M. Wood, Preparation of crystalline, amorphous, and dyed cellulase substrates, Methods Enzymol. (1988) 19–25 Academic Press, doi:10.1016/0076-6879(88)60103-0.

[29] R.E. Calza, D.C. Irwin, D.B. Wilson, Purification and characterization of two .beta.-1,4-endoglucanases from thermomonospora fusca, Biochemistry 24 (26) (1985) 7797–7804, doi:10.1021/bi00347a044.

[30] M. Spezio, D.B. Wilson, P.A. Karplus, Crystal structure of the catalytic domain of a thermophilic endocellulase, Biochemistry 32 (38) (1993) 9906–9916, doi:10.1021/bi00089a006.

[31] M. Zamocky, C. Schumann, C. Sygmund, J. O'Callaghan, A.D. Dobson, R. Ludwig, D. Haltrich, C.K. Peterbauer, Cloning, sequence analysis and heterologous expression in pichia pastoris of a gene encoding a thermostable cellobiose dehydrogenase from myriococcum thermophilum, Protein Expr. Purif. 59 (2) (2008) 258–265, doi:10.1016/j.pep.2008.02.007.

[32] D.M. Petrović, B. Bissaro, P. Chylenski, M. Skaugen, M. Sørlie, M.S. Jensen, F.L. Aachmann, G. Courtade, A. Várnai, V.G.H. Eijsink, Methylation of the N-terminal histidine protects a lytic polysaccharide monooxygenase from auto-oxidative inactivation, Protein Sci. 27 (9) (2018) 1636–1650, doi:10.1002/pro.3451.

[33] C. Chen, J. Chen, Z. Geng, M. Wang, N. Liu, D. Li, Regioselectivity of oxidation by a polysaccharide monooxygenase from chaetomium thermophilum, Biotechnol. Biofuels 11 (1) (2018) 155, doi:10.1186/s13068-018-1156-2.

[34] G. Courtade, Z. Forsberg, E.B. Heggset, V.G.H. Eijsink, F.L. Aachmann, The carbohydrate-binding module and linker of a modular lytic polysaccharide monooxygenase promote localized cellulose oxidation, J. Biol. Chem. 293 (34) (2018) 13006–13015, doi:10.1074/jbc.RA118.004269.

[35] J.W. Agger, T. Isaksen, A. Várnai, S. Vidal-Melgosa, W.G.T. Willats, R. Ludwig, S.J. Horn, V.G.H. Eijsink, B. Westereng, Discovery of LPMO activity on hemicelluloses shows the importance of oxidative processes in plant cell wall degradation, Proc. Natl. Acad. Sci. U. S. A. 111 (17) (2014) 6287–6292, doi:10.1073/pnas.1323629111.

[36] V.V. Vu, W.T. Beeson, E.A. Span, E.R. Farquhar, M.A. Marletta, A family of starch-active polysaccharide monooxygenases, Proc. Natl. Acad. Sci. U. S. A. 111 (38) (2014) 13822–13827, doi:10.1073/pnas.1408090111.

[37] M. Frommhagen, S. Sforza, A.H. Westphal, J. Visser, S.W. Hinz, M.J. Koetsier, W.J. van Berkel, H. Gruppen, M.A. Kabel, Discovery of the combined oxidative cleavage of plant xylan and cellulose by a new fungal polysaccharide monooxygenase, Biotechnol. Biofuels 8 (2015) 101, doi:10.1186/s13068-015-0284-1.

[38] M. Couturier, S. Ladeveze, G. Sulzenbacher, L. Ciano, M. Fanuel, C. Moreau, A. Villares, B. Cathala, F. Chaspoul, K.E. Frandsen, A. Labourel, I. Herpoel-Gimbert, S. Grisel, M. Haon, N. Lenfant, H. Rogniaux, D. Ropartz, G.J. Davies, M.N. Rosso, P.H. Walton, B. Henrissat, J.G. Berrin, Lytic xylan oxidases from wood-decay fungi unlock biomass degradation, Nat. Chem. Biol. 14 (3) (2018) 306–310, doi:10.1038/nchembio.2558.

[39] S. Hüttner, A. Várnai, D.M. Petrović, C.X. Bach, D.T. Kim Anh, V.N. Thanh, V.G.H. Eijsink, J. Larsbrink, L. Olsson, Specific xylan activity revealed for AA9 lytic polysaccharide monooxygenases of the thermophilic fungus malbranchea cinnamomea by functional characterization, Appl. Environ. Microbiol. 85 (23) (2019) e01408–e01419, doi:10.1128/AEM.01408-19.

[40] F. Sabbadin, S. Urresti, B. Henrissat, O. Avrova Anna, R.J. Welsh Lydia, J. Lindley Peter, M. Csukai, N. Squires Julie, H. Walton Paul, J. Davies Gideon, C. Bruce Neil, C. Whisson Stephen, J. McQueen-Mason Simon, Secreted pectin monooxygenases drive plant infection by pathogenic oomycetes, Science 373 (6556) (2021) 774–779, doi:10.1126/science.abj1342.

Substrate-dependent cellulose saccharification efficiency and LPMO activity of Cellic CTec2 and a thermostable enzyme cocktail from *Thermoascus aurantiacus*, and the impact of H_2O_2-producing glucose oxidase

Østby, H., Várnai, A., Gabriel, R., Chylenski, P., Horn, S. J., Singer, S. W., & Eijsink, V. G. H.

Paper II

Substrate-dependent cellulose saccharification efficiency and LPMO activity of Cellic CTec2 and a thermostable enzyme cocktail from *Thermoascus aurantiacus*, and the impact of H_2O_2-producing glucose oxidase

Heidi Østby[1], Anikó Várnai[1], Raphael Gabriel[2,3,4], Piotr Chylenski[1], Svein J. Horn[1], Steven W. Singer[2,3], and Vincent G. H. Eijsink[1,*]

[1]Norwegian University of Life Sciences (NMBU), Faculty of Chemistry, Biotechnology, and Food Science, P.O. Box 5003, N-1432 Ås, Norway

[2]Joint BioEnergy Institute, Emeryville, CA, 94608, USA

[3]Biological Systems and Engineering Division, Lawrence Berkeley National Laboratory, Berkeley, CA 94720

[4]Institut für Genetik, Technische Universität Braunschweig, Spielmannstr. 7, 38106, Braunschweig, Germany

[*]Address correspondence to Vincent G. H. Eijsink, vincent.eijsink@nmbu.no
Norwegian University of Life Sciences (NMBU), Faculty of Chemistry, Biotechnology, and Food Science, P.O. Box 5003, N-1432 Ås, Norway, Telephone: +47 67232463.

Abstract

Harnessing the power of lytic polysaccharide monooxygenases (LPMOs) requires deeper insights into LPMO behavior during saccharification of industrial substrates, while improvements could also be achieved by using higher temperatures. We have compared the performance of a simple, LPMO-rich cellulolytic enzyme cocktail from the thermophilic fungus *Thermoascus aurantiacus* with the performance of the commercial cellulase preparation Cellic CTec2, using relatively high (10 % w/v) dry matter conditions and elevated temperatures. In saccharification of (lignin-poor) sulfite-pulped spruce at 60°C, the *T. aurantiacus* cocktail gave saccharification yields similar to those obtained with Cellic CTec2 at 50°C. Quantification of C4-oxidized LPMO products showed that while a certain amount of LPMO activity clearly contributed to overall saccharification efficiency, very high levels of LPMO activity were not necessarily beneficial. Reactions with steam-exploded birch, rich in redox-active lignin, highlighted a strong impact of the feedstock on cocktail performance. In this case, the reaction with Cellic CTec2 at 50°C was clearly most efficient. At 60°C, enzyme inactivation became apparent for both cocktails, likely due to detrimental redox processes. Addition of H_2O_2-generating glucose oxidase to reactions with Cellic CTec2 at 50°C led to strongly increased LPMO activity and, only for reactions with the lignin-poor substrate, improved saccharification yields. These results underpin the potential of the *T. aurantiacus* cocktail for hydrolysis of lignin-poor substrates, and the usefulness of glucose oxidase for optimizing their saccharification. They also show that the efficiency of LPMO-containing cellulase cocktails is highly dependent on the nature of the reductant and the substrate.

Introduction

Lignocellulosic biomass is a renewable alternative to fossil fuels and its efficient exploitation can contribute to the global move towards a bio-based economy. However, the extreme recalcitrance of lignocellulose to biological degradation and industrial processing, due mainly to its physical characteristics, represents a major bottleneck in the large-scale production of fuels and specialized chemicals from this feedstock [1-4]. Enormous efforts are dedicated within industry to overcoming this recalcitrance, for example through efforts to optimize the enzymatic depolymerization of one of its main constituents, cellulose [3, 4]. To enable efficient cellulose saccharification, lignocellulosic feedstocks must be subjected to physical and/or chemical pretreatments such as sulfite pulping or steam explosion, which serve to remove or rearrange lignin and/or hemicellulose components in the substrate and leave the cellulose fibers more exposed to subsequent enzymatic attack [2, 3].

Many microorganisms secrete cocktails of enzymes that work synergistically to degrade cellulose and other components of lignocellulosic substrates. For example, several fungal strains, including mesophilic *Trichoderma* [5] and *Aspergillus* sp. [6], thermophilic *Myceliophthora thermophila* (also known as *Thermothelomyces thermophilus*) [7], and *Thermoascus aurantiacus* [8] are known to secrete powerful cellulolytic enzymes. These enzyme cocktails include multiple types of cellulases, such as cellobiohydrolases, which act on the reducing and non-reducing ends of cellulose chains to release cellobiose, endoglucanases, which act within the cellulose chains to create novel ends upon which cellobiohydrolases can act, and β-glucosidases, which convert released cellobiose and cello-oligosaccharides into the monomeric product, glucose [9-11]. These cocktails also contain lytic polysaccharide monooxygenases (LPMOs), which contribute to overall cellulose saccharification by oxidatively cleaving cellulose chains [12-16].

More than ten years after their discovery [17] and despite the industrial importance of LPMOs, the mode of action of these enzymes remains somewhat enigmatic. Remaining questions concern the catalytic mechanism, the nature of the oxygen co-substrate (O_2 or H_2O_2), and how to optimize LPMO performance during industrial biomass processing [18-24]. LPMOs are mono-copper enzymes that hydroxylate either the C1 or the C4 carbon, leading to destabilization and spontaneous cleavage of the scissile glycosidic bond [17, 25-27]. To become catalytically active, LPMOs require an electron donor to reduce the copper from Cu(II) to Cu(I), after which the enzyme may catalyze a monooxygenase (R-H + O_2 + 2 e^- + 2 H^+ -> R-OH + H_2O) or a peroxygenase (R-H + H_2O_2 -> R-OH + H_2O) reaction. The peroxygenase reaction is orders of magnitude faster than the monooxygenase reaction [19-21, 23, 28, 29]. It has been claimed that LPMO catalysis under "monooxygenase conditions" in fact reflects a peroxygenase reaction, limited by *in situ* generation of H_2O_2 resulting from LPMO-catalyzed and/or abiotic oxidation of the reductant (RH_2 + O_2 -> R + H_2O_2; [21, 30, 31]). Reducing equivalents are needed in all these scenarios and may, in nature, originate from the biomass itself, such as from lignin-derived compounds, other redox enzymes secreted together with the LPMOs, or smaller redox-active compounds, such as plant-derived phenolics [32-34]. In laboratory settings with lignin-poor model substrates, chemical reductants such as ascorbic acid (AscA) and gallic acid (GA), or enzymatic electron donors, such as cellobiose dehydrogenase (CDH), are commonly used to drive the LPMO reaction [35]. LPMO reactions may be accelerated by supplying H_2O_2, which can be exogenously added [24] or *in situ*-generated using e.g. CDH [36] or glucose oxidase (GOx) [18].

While accumulating knowledge of LPMO catalysis using cellulosic model substrates points to certain directions regarding how to leverage the full potential of LPMO activity, the situation is more complex when using industrial lignocellulosic feedstocks [15, 16, 24, 37]. In a process configuration, using H_2O_2 may be a more viable option than using molecular O_2, as

proper aeration and efficient oxygen transfer are hard to achieve in high dry matter saccharification reactions [38]. The efficiency of the former approach was recently exemplified at demonstration scale for the saccharification of sulfite-pulped spruce [39]. However, for lignin-rich feedstocks such as steam-exploded woody biomass, administration of H_2O_2 has so far not shown particularly good results, likely due to reactions of H_2O_2 with redox active compounds (e.g. lignin-derived phenolics) in the feedstock [24, 40].

Next to optimally harnessing LPMO activity, another challenge in biomass processing concerns temperature limitations of the enzymes. To enhance saccharification efficiency, increase product solubility, and reduce microbial contamination, it could be beneficial to perform saccharification at elevated temperatures. Thermostable enzyme cocktails can be obtained from thermophilic fungi, such as *M. thermophila* and *T. aurantiacus*. The latter fungus has gained increasing attention during the past decade as a potential cellulase cocktail producer due to initial studies indicating that it produces a powerful cellulolytic enzyme cocktail seemingly consisting of a remarkably low number of key enzyme components compared to other, well-studied cellulase production hosts [8, 41, 42]. These few enzymes (a cellobiohydrolase, an endoglucanase, a xylanase, and an LPMO; [8]) may represent a kind of "minimal enzyme cocktail," and studying these may provide fundamental insight into the optimization of enzymatic biomass saccharification. Notably, the primary *T. aurantiacus* LPMO, *Ta*LPMO9A, is one of the best-studied LPMOs for lignocellulosic biomass processing [13, 26, 42-44].

To gain further insight into how enzymatic saccharification of cellulose could be optimized, we have compared the performance of the commercial cellulase cocktail Cellic CTec2 and the LPMO-rich thermostable cellulase cocktail produced by *T. aurantiacus* in saccharification of a lignin-poor (sulfite-pulped spruce, SPS) and a lignin-rich (steam-exploded birch, SEB) feedstock, using industrially relevant high dry matter concentrations and two

different reductants. Furthermore, we have investigated the effect of *in situ* H_2O_2-generation by glucose oxidase from *Aspergillus niger* (*An*GOx) on LPMO activity and cellulose saccharification efficiency for Cellic CTec2 acting on the lignin-poor and lignin-rich substrates.

Methods

Substrates, enzymes, and chemicals

Sulfite-pulped Norway spruce (SPS) and steam-exploded birch (SEB) were used as cellulosic substrates. SPS (Batch number DP3319) was kindly provided by Borregaard AS [45, 46]; SEB was prepared by steam explosion at 210°C, with 10 min residence time, as previously described [47]. To improve mixing in saccharification experiments, the particle size of the sulfite-pulped spruce was reduced by grinding at 4000 rpm for 2 x 5 s using a GM200 Grindomix (Retsch, Haan, Germany). The composition of the SPS (in % w/w dry matter (DM)) was 87.4% glucan, 2.7% xylan, 5.2% mannan, and 3.3% lignin. The composition of the SEB (in % w/w DM) was 45.8% glucan, 3.6% xylan, 0.0% mannan, and 46.1% lignin.

Cellulase cocktails utilized were the commercial cellulase cocktail Cellic CTec2, kindly provided by Novozymes AS (Bagsværd, Denmark), and a cellulase-containing supernatant of a culture of *T. aurantiacus*. The *T. aurantiacus* cocktail was generated by culturing the fungus with glucose, before shifting the culture to a medium containing 2% Sigmacell, 0.75% arabinose, 25 mM $(NH_4)_2SO_4$, 10 mM citrate, and McClendon salts at pH 6.0, as previously described [48]. The shifted culture was incubated for 72 h and then filtered through Miracloth (Merck Millipore, Billerica, MA, USA) after which the filtrate was sterile-filtered through a 0.2 µm filter (Merck Millipore); the second filtrate was subsequently concentrated via ultrafiltration using an Amicon stirred cell concentrator (Merck Millipore) to a protein concentration of 12 g/L. Cellic CTec2 was stored at 4°C, while the *T. aurantiacus* cocktail was

aliquoted and stored at -20°C. Protein concentrations in the cocktails were determined using the Bio-Rad protein assay (Bio-Rad, USA) based on the Bradford method [49], with bovine serum albumin as reference protein. Glucose oxidase (GOx) from *Aspergillus niger* (*An*GOx; type VII) was purchased from Sigma-Aldrich, and stock solutions were prepared in sodium acetate buffer (50 mM, pH 5.0) and stored at 4°C.

Ascorbic acid (AscA, 100 mM) and gallic acid (GA, 100 mM) stock solutions were prepared in Trace SELECT water (Sigma-Aldrich) and DMSO, respectively, and aliquoted and stored at -20°C. Aliquots were thawed in the dark immediately prior to use.

Saccharification experiments

Saccharification of SPS or SEB was performed aerobically in 60 mL screw-cap glass bottles (Wheaton, Millville, USA) using a working volume of 10 mL. Reactions were carried out in sodium acetate buffer (50 mM, pH 5.0) at 50°C or 60°C and shaken orbitally at 200 rpm in a Minitron Shaker incubator (Infors AG, Bottmingen, Switzerland). The enzyme loading for both cellulase cocktails was 4 mg protein/g DM substrate in all experiments, and the substrate content was 10% w/w DM in all reactions. Of note, these enzyme concentrations are considerably lower, and these dry matter concentrations are considerably higher, compared to previous studies with the *T. aurantiacus* cocktail.

Reactions with SPS were initiated by addition of AscA or GA. When using the lignin-rich SEB, reactions were initiated by the addition of the cellulase cocktail. In reactions containing GOx, this enzyme was added immediately following the addition of the reductant, or immediately following the addition of the cellulase cocktail in the case of reactions lacking reductant.

Samples of 100 µL were taken periodically, and the enzymes were inactivated by incubation at 100°C for 15 min. Samples were subsequently stored at -20°C. Prior to analysis

with high-performance liquid chromatography (HPLC), samples were thawed at 4°C and filtered using a 96-well filter plate (0.45 µm; Merck Millipore) operated with a Millipore vacuum manifold system.

Quantification of cellulase- and LPMO-derived products

Glucose and cellobiose generated by the cellulase cocktails were quantified by HPLC using a Dionex Ultimate 3000 system (Dionex, Sunnyvale, CA, USA) set up with a Shodex RI-101 refractive index detector (Shodex, Japan). A Rezex ROA-organic acid H+ (8%) 300×7.8 mm analytical column (Phenomenex, Torrance, CA, USA) was used for analysis. The column was operated at 65°C with 5 mM H_2SO_4 as eluent using an isocratic flow of 0.6 mL/min [15]. Below, cellobiose and glucose are reported as glucan conversion (% of theoretical maximum conversion). Cellobiose typically amounted to 2 – 4 % and 5 – 8 % of the total reported saccharification yields for reactions with Cellic CTec2 and the *T. aurantiacus* cocktail, respectively.

C4-oxidized cellobiose (Glc4gemGlc), the main LPMO product, was quantified by high-performance anion exchange chromatography (HPAEC) on a Dionex ICS-5000 system (Thermo Scientific, Waltham, MA, USA) set up with pulsed amperometric detection (PAD). A 3×250 mm Dionex CarboPac PA-200 analytical column (Thermo Scientific) connected to a 3×50 mm guard column was used. The column was kept at 30°C. Eluents (A: 0.1 M NaOH, B: 0.1 M NaOH containing 1 M NaOAc) were prepared as previously described [50]. The operational flow was 500 µL/min, and a 39 min multistep gradient was used as reported earlier [51]. In detail, the gradient used was: 0-4.5 min, linear from 100% A to 94.5% A and 5.5% B; 4.5-13.5 min, convex upward (Dionex curve 4) from 94.5% A and 5.5% B to 85% A and 15% B; 13.5-30 min, concave upward (Dionex curve 8) from 85% A and 15% B to 100% B; 30-30.1 min, linear from 100% B to 100% A; 30.1-39 min, constant at 100% A (reconditioning).

Chromeleon version 7.2.9 (Thermo Scientific) was used for instrument control and analysis for both the Dionex Ultimate 3000 and ICS-5000 systems.

Standards for quantification of glucose and cellobiose were purchased from Megazyme (Wicklow, Ireland). Glc4gemGlc standards for quantification of the C4-oxidized dimer (the significantly dominating LPMO product in the reaction mixtures) were produced in-house as previously described [52].

Results and Discussion

Effect of temperature and reductant on cellulase cocktail efficiency in saccharification of sulfite-pulped spruce (SPS) and steam-exploded birch (SEB)

The simplicity of the *T. aurantiacus* cocktail, along with the thermophilic nature of the *T. aurantiacus* fungus, makes this cocktail an intriguing candidate for comparison with current commercially available cellulase cocktails used in the industrial processing of lignocellulosic biomass, such as Cellic CTec2. Previous work with the *T. aurantiacus* and Cellic CTec2 cocktails by Schuerg *et al.* has demonstrated significant differences in thermostability of the two cocktails during saccharification of acid-pretreated corn stover at elevated temperatures [48]. Additionally, work by Fritsche *et al.* has shown significant LPMO- and substrate-dependent differences between the performance of the two cocktails comparing Avicel and acid-pretreated corn stover [42]. In the present work, we have studied the performance of these cocktails at higher dry matter concentrations (10% versus 2%) and lower enzyme dosages (4 mg per g of DM versus 20 mg per g of DM), and we have investigated the contribution of LPMOs by quantifying the dominating oxidized product, C4-oxidized cellobiose (Glc4gemGlc).

In order to promote LPMO activity on lignin-poor cellulosic materials, reducing agents must be supplemented to the reactions. Studies of LPMO efficiency in reactions with various reductants have illustrated that the identity of the reductant significantly impacts LPMO activity due to the greatly varying rates of the H_2O_2-generating reaction between the reductant and molecular O_2 [31]. In the reactions with SPS described below, both ascorbic acid (AscA) and gallic acid (GA) were used.

Saccharification of SPS

Saccharification experiments with SPS were performed at 50°C and 60°C, in the presence and absence of 1 mM AscA. **Figure 1** shows a clear increase in both saccharification yields and LPMO activity for reactions with added AscA, demonstrating the presence and importance of LPMO activity in both cellulase cocktails.

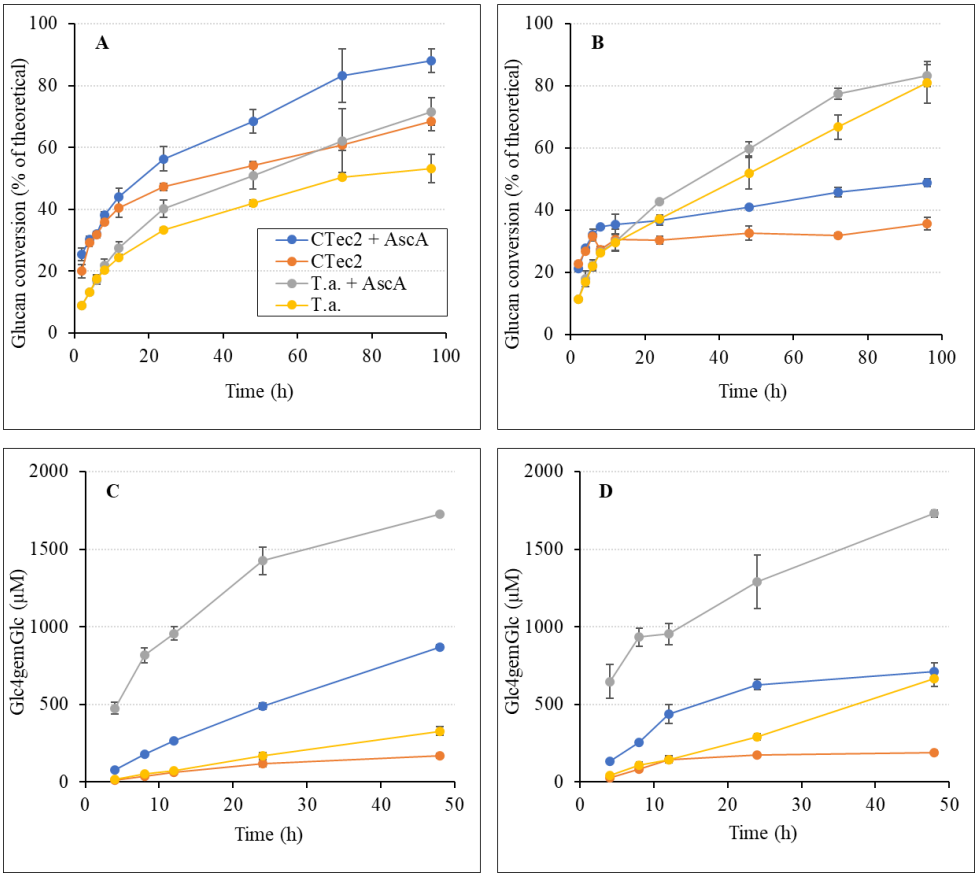

Figure 1. Saccharification of SPS at 50°C and 60°C by Cellic CTec2 ("CTec2") or the *T. aurantiacus* cocktail ("T.a.") at 10% DM in the presence or absence of 1 mM AscA. The left panels (A, C) show experiments carried out at 50°C, while the right panels (B, D) show experiments performed at 60°C. Panels A and B show glucan conversion as a percentage of the theoretical maximum. Panels C and D show production of Glc4gemGlc, the main LPMO product. The legend shown in Panel A is valid for all panels. In all experiments, the enzyme loading was 4 mg/g DM substrate. Note that 1 mM of ascorbic acid can generate more than 1 mM of LPMO product, as recently demonstrated [31]. Error bars indicate standard deviations between triplicates.

At 50°C, Cellic CTec2 outperformed the *T. aurantiacus* cocktail in terms of glucan conversion (**Figure 1A**). On the other hand, at 60°C, the activity of the Cellic CTec2 cocktail slowed down after approx. 8 h (**Figure 1B**), which may be attributed to thermal inactivation of key enzymes at this elevated temperature, and led to lower glucan conversion compared to reactions carried out at 50°C. The *T. aurantiacus* cocktail performed better at 60°C than at 50°C, and while the reactions initially were slower compared to Cellic CTec2, also at 60°C, the saccharification yields after 48 h and up to 96 h at 60°C were very close to those obtained

with Cellic CTec2 at 50°C (**Figure 1A and B**), highlighting the thermostability and potential of the *T. aurantiacus* enzymes.

Figure 1C and D show that there is more LPMO activity in the *T. aurantiacus* cocktail as compared to Cellic CTec2. Despite this difference in apparent LPMO activity, the addition of AscA, i.e., fueling of the LPMO reaction, improved glucan solubilization similarly for both cocktails (**Figure 1A and B; Figure 2A and B**). Interestingly, a closer look at the effect of adding AscA (**Figure 2A**) shows that the impact of the LPMO increased with the extent of saccharification, indicating that LPMOs become more important towards the later phase of the saccharification. The somewhat delayed LPMO effect may be related to a greater need for alleviating substrate limitations that hamper cellulase action once the more easily accessible portions of the substrate have been depolymerized. While LPMO activity is clearly important, **Figure 2B** highlights that the higher levels of LPMO products in reactions with the *T. aurantiacus* cocktail did not translate to higher saccharification yields, compared to Cellic CTec2. Thus, while the *T. aurantiacus* cocktail produced more Glc4gemGlc, Cellic CTec2 appeared to benefit more from LPMO action in terms of improvement of the saccharification yield.

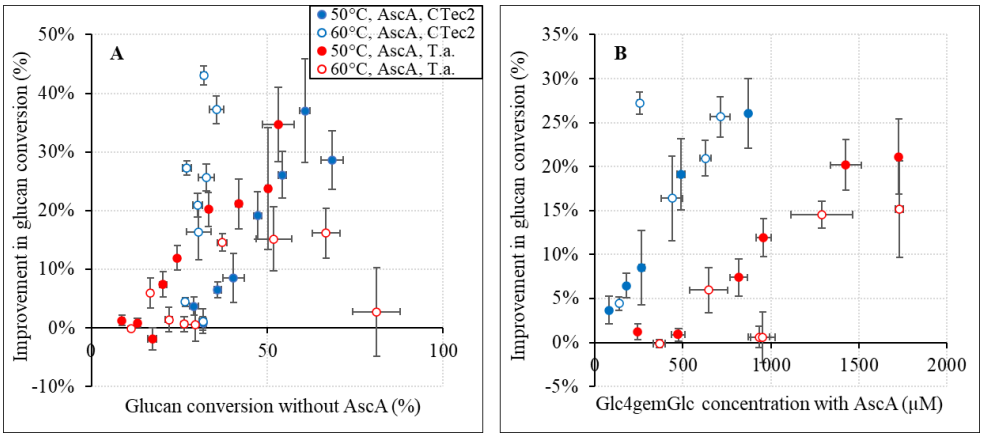

Figure 2. Improvement in glucan conversion as a function of the addition of 1 mM AscA. The figure was generated using the data shown in **Figure 1**. Panel A shows the improvement in glucan conversion as a result of the addition of AscA as a function of the glucan conversion obtained in reactions without reductant. Note that the data points for the reaction with Cellic CTec2 at 60°C deviate because glucan conversion hardly increases after 8 hours (**Figure 1B**). Panel B shows the improvement in glucan conversion as a function of the concentration of detected LPMO products. The legend shown in Panel A is valid for both panels. Error bars indicate standard deviations between triplicates.

Of note, preliminary experiments identical to those shown in **Figure 1** using 1 mM GA as reductant showed much lower LPMO product levels, hardly any effect of the reductant on glucan conversion and, thus, lower overall yields for either enzyme cocktail at both 50°C and 60°C (data not shown). This highlights that the identity of the reductant is critical for LPMO performance and saccharification efficiency. The remarkable effect of GA is discussed further, below.

Saccharification of SEB

Previous comparative studies of the Cellic CTec2 and the *T. aurantiacus* cocktail have led to the suggestion that the (difference in) performance of these cocktails is substrate-dependent [42]. Results obtained at 50°C showed a similar performance of the two cocktails when acting on acid-pretreated corn stover, whereas Cellic CTec2 clearly outperformed the *T. aurantiacus* cocktail in reactions with Avicel (similar to the SPS results shown in **Figure 1A** of the present study).

To assess substrate effects on cocktail performance, experiments similar to the ones depicted in **Figure 1** were carried out using SEB (**Figure 3**). In contrast to SPS, the SEB substrate contains a high proportion of lignin (46.1% vs. 3.3% in SPS). Since lignin-derived compounds can act as reducing agents in LPMO reactions [32, 40, 53, 54], these saccharification experiments were performed without exogenous addition of reductant. Of note, in these reactions, the amount of enzyme added per gram of glucan was about twice as high as in the experiments with SPS.

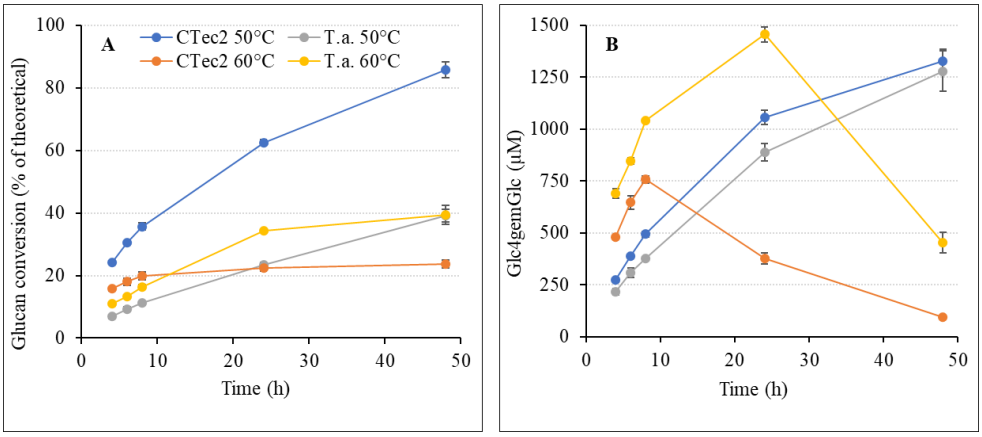

Figure 3. Saccharification of SEB at 10% DM by Cellic CTec2 ("CTec2") and the *T. aurantiacus* cocktail ("T.a.") at 50°C and 60°C. Panel A shows glucan conversion as a percentage of the theoretical maximum, whereas Panel B shows the production of the main LPMO product, Glc4gemGlc. The legend shown in Panel A is valid for both panels. In all experiments, the enzyme loading was 4 mg/g DM substrate. Error bars indicate standard deviations between triplicates.

The glucan saccharification data (**Figure 3A**) for the experiments with SEB showed some remarkable features. First of all, the reaction with Cellic CTec2 at 50°C was by far the most efficient, in contrast to the results obtained with SPS, which showed, e.g., that the *T. aurantiacus* cocktail performed similarly well at 60°C. Furthermore, **Figure 3A** shows that increasing the temperature to 60°C was highly detrimental for the efficiency of Cellic CTec2, much more so than in the reactions with SPS. As another remarkable result, **Figure 3A** shows that, while, as expected, the *T. aurantiacus* cocktail was more efficient on SEB at 60°C than at 50°C, the reaction at 60°C showed clear signs of enzyme inactivation. The progress curve for

the reaction at 60°C shows stagnation in glucan solubilization correlated with cessation of Glc4gemGlc production (**Figure 3B**; see below).

Likewise, the progress curves for the concentration of the main LPMO product, Glc4gemGlc (**Figure 3B**), are remarkably different, compared to the reactions with SPS (**Figure 1C,D**). The lignin-derived compounds in the SEB substrate may create a redox environment that is quite different compared to reactions with AscA and lignin-poor SPS, which may affect reductant levels, *in situ* H_2O_2 production and abiotic H_2O_2 consumption, and, thus, LPMO activity [55]. **Figure 3B** shows that, in contrast to the reactions with SPS (**Figure 1C)**, the *T. aurantiacus* and Cellic CTec2 cocktails produced similar amounts of Glc4gemGlc at 50°C. The reaction with Cellic CTec2 and SEB yielded more LPMO products compared to the reaction with SPS, whereas it is the other way around for the *T. aurantiacus* cocktail. Clearly, the LPMO activity in these two cocktails responds differently to different redox conditions. The relatively lower LPMO activity in the reaction with the *T. aurantiacus* cocktail and SEB at 50°C may explain why, when acting on SEB, this cocktail is more inferior to Cellic CTec2, compared to when acting on SPS. Another explanation may be that Cellic CTec2, optimized for saccharification of corn stover, is better-suited than the *T. aurantiacus* preparation to deal with polysaccharides in a lignin-rich pre-treated material possibly containing lignin-derived cellulase inhibitors [56, 57].

Previous saccharification studies in which Glc4gemGlc was quantified have shown that this product is unstable, especially at higher temperatures [24, 58]. Due to this instability, cessation of LPMO activity will lead to a gradual decrease in detected Glc4gemGlc. Interestingly, the progress curves for LPMO product formation at 60°C show clear signs of LPMO inactivation (**Figure 3B**), starting at about the same time as when the glucan conversion slows down (**Figure 3A**). The progress curves in **Figure 3B** show that LPMO activity at 60°C initially is very high for both cocktails, followed by inactivation starting at about 8 h for Cellic

CTec2 and 24 h for the *T. aurantiacus* cocktail. Such progress curves are typical for LPMO reactions that contain too much H_2O_2. A surplus of H_2O_2 may not only lead to autocatalytic inactivation of the LPMO [18], but may also affect the stability of the other cellulolytic enzymes [59]. The combined data of **Figure 3** thus suggest that enzymatic saccharification of SEB at 60°C leads to unfavorable levels of H_2O_2, lignin radicals, and/or reactive oxygen species (ROS), creating an unstable reaction system.

Using glucose oxidase (GOx) to drive cellulose saccharification

Feeding of H_2O_2 during enzymatic saccharification of SPS with Cellic CTec2 has been shown to improve saccharification rates and yields at demonstration scale (2,000 L) [39]. Other studies on H_2O_2-fed saccharification of Avicel [18, 24] have shown that such reactions entail sub-stoichiometric use of reductant, in contrast with standard reductant-driven reactions (as in **Figure 1**), which entail stoichiometric reductant consumption. Previous studies have also shown that a surplus of H_2O_2, either due to excess levels of H_2O_2 being added or generated *in situ*, or due to lack of substrate availability, will lead to autocatalytic inactivation of the LPMO [18, 30], and may also harm other enzymes in the cellulase cocktail [59]. Finding "the right balance" between the reductant and H_2O_2 concentrations for a particular reaction may be key to optimizing the action of LPMOs and saccharification yields, as also suggested by comparing the results depicted in **Figure 1** and **Figure 3**, discussed above.

With this in mind, we performed saccharification reactions with SPS and SEB using Cellic CTec2 supplemented with varying amounts of AscA or GA, and H_2O_2-producing glucose oxidase (GOx). We only studied Cellic CTec2 because glucose oxidase is not sufficiently stable at 60°C [60], and because Cellic CTec2 showed the best performance at 50°C. The aim was to evaluate the effect of GOx on saccharification efficiency, and to establish whether LPMO activity and cellulose saccharification could be driven using GOx and minor amounts of reductant.

Control experiments

To verify that availability of glucose was not limiting GOx action during saccharification reactions, control saccharification experiments were performed using 236 ng/mL GOx (the highest concentration of GOx used in this study) in reactions with Cellic CTec2 acting on the SPS or SEB substrate, in the absence or presence of 15 mM added glucose. In all cases, saccharification yields were identical between reactions with and without supplemented glucose (data not shown), indicating that the *in situ* saccharification of both substrates by the cellulases and β-glucosidase present in Cellic CTec2 provided adequate amounts of GOx substrate throughout the reactions.

Saccharification of SPS in reactions with GOx

Saccharification reactions with SPS were run using the same conditions as above, at 50^{o}C, but with varying concentrations of AscA and addition of varying amounts of GOx. The results (glucan conversion and LPMO products) are presented in **Figure 4**.

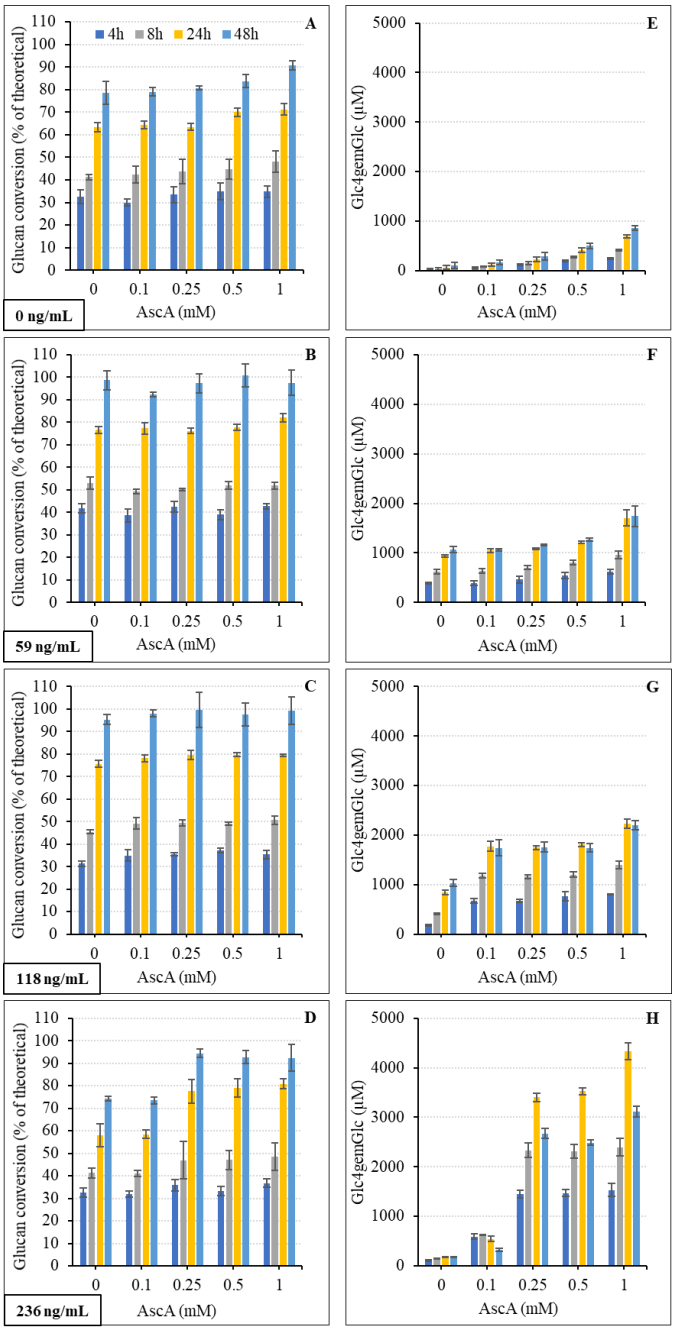

Figure 4. Glucan conversion (Panels A-D) and corresponding accumulation of Glc4gemGlc (Panels E-H) during saccharification of SPS by Cellic CTec2 at 10% DM and 50°C with different AscA (0, 0.1, 0.25, 0.5, 1 mM) and GOx (0, 59, 118, 236 ng/mL) concentrations. The legend shown in Panel A is valid for all panels. The final concentration of GOx is indicated in bold in the bottom left of each set of two corresponding panels. In all experiments, the enzyme loading was 4 mg/g DM substrate. Error bars indicate standard deviations between triplicates. Note that decreasing levels of Glc4gemGlc may occur due to a combination of LPMO inactivation and product instability, as explained when discussing **Figure 3B** in the main text.

The reactions without GOx show that, as expected, increased concentrations of AscA led to increased glucan conversion (**Figure 4A**) and increased LPMO activity (**Figure 4E**). In the reactions with GOx, reductants are still needed to reduce the LPMO, but reductant-driven generation of H_2O_2 likely becomes less important since H_2O_2 is generated by the GOx reaction. Reactions with GOx show a GOx-dose dependent increase in LPMO activity, which, at lower GOx concentrations, is largely independent of added AscA (**Figure 4F and G**)**.** The reactions with 59 ng/mL and 118 ng/mL GOx gave the highest saccharification yields (higher than those obtained in the reaction with 1 mM AscA and no GOx; **Figure 4A-C**) and, like LPMO product levels, these yields were largely independent of the addition of AscA. For example, in the presence of 59 ng/mL GOx, glucan conversion (**Figure 4B**) and LPMO product levels (**Figure 4F**) were nearly identical at all concentrations of AscA tested. Presumably, the 3.3% lignin present in the SPS substrate is enough to act as a reducing agent, activating the LPMOs and allowing them to operate in a peroxygenase mode limited by access to H_2O_2. It seems that in the reactions with 59 ng/mL GOx, the *in situ* production of H_2O_2 corresponded to the levels needed by the LPMOs, and there was enough reducing power in the reaction to maintain a level of active LPMOs sufficient for productive consumption of available H_2O_2.

Comparison of the four panels showing accumulation of Glc4gemGlc (**Figure 4E-H**) indicates that GOx strongly enhanced LPMO activity in a dose-dependent manner, which underpins the dominance of the LPMO peroxygenase reaction fueled by GOx-generated H_2O_2. It is noteworthy, however, that glucan saccharification is not strictly correlated to LPMO activity: while increased LPMO activity certainly helped, as illustrated by comparing the reactions with 59 ng/mL GOx to the reactions without GOx, further increasing the GOx concentration and, consequently, LPMO activity, did not lead to increased glucan conversion. For example, the reactions with 59 ng/mL and 118 ng/mL GOx generally showed similar saccharification yields, while the latter reaction showed considerably higher LPMO activity.

At the highest GOx concentrations, negative impacts become visible. The reactions with 236 ng/mL GOx showed a decrease in LPMO products at 48 h (relative to 24 h), which, as explained above, reflects inactivation of the LPMO, likely due to excess concentrations of H_2O_2. Furthermore, reactions with 118 ng/mL GOx and, more so, 236 ng/mL GOx, showed that the reductant becomes limiting in reactions with no or low amounts of AscA (**Figure 4G and H**). High concentrations of H_2O_2 will increase non-productive peroxidase reactions that oxidize the LPMO and thus increase reductant consumption. Such reactions may occasionally lead to LPMO inactivation [61, 62], and the resulting release of LPMO-bound copper into solution may further contribute to reductant depletion, as discussed recently by Stepnov *et al.* [63]. For the reaction with 236 ng/mL GOx, the reduced LPMO activity at low reductant concentration was accompanied by reduced glucan solubilization (**Figure 4D**), likely due to a combination of reduced LPMO activity and damage to the cellulases, as discussed above for **Figure 3**.

The results depicted in **Figure 4** show that optimized saccharification of SPS with Cellic CTec2 requires a well-balanced reaction with appropriate reductant and H_2O_2-levels, and that GOx could play a role in achieving such balanced reactions.

As discussed above, standard saccharification experiments with Cellic CTec2 and SPS conducted with GA as a reductant showed little LPMO activity and reduced glucan solubilization compared to reactions with AscA. To assess to what extent the lack of impact of GA was due to diminished production of H_2O_2 within the system, we studied saccharification of SPS with varying concentrations of GA and GOx (**Figure 5**).

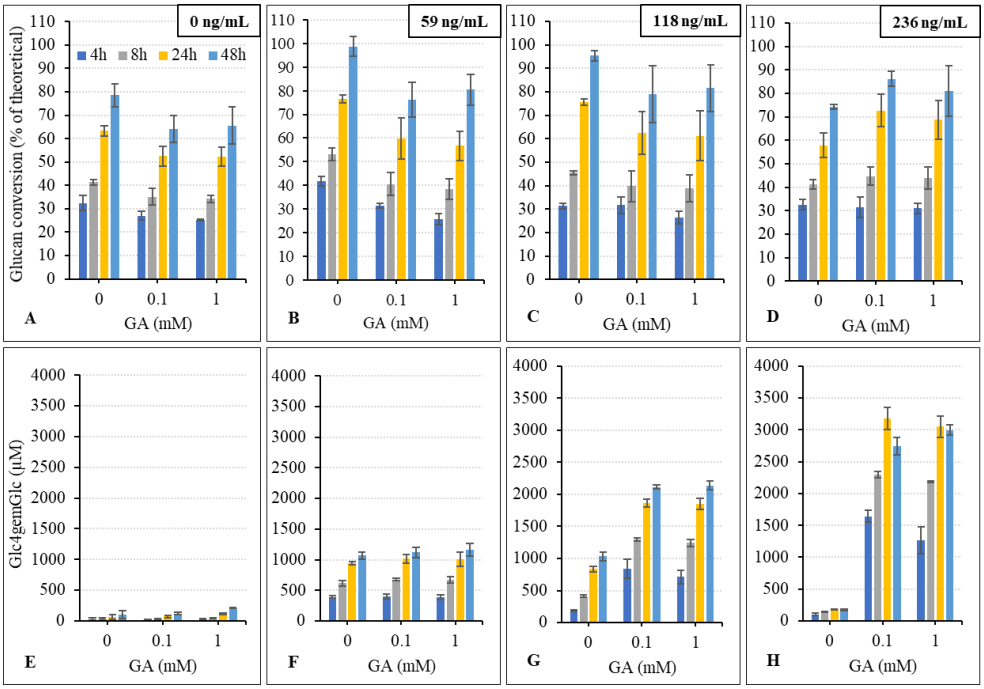

Figure 5. Glucan conversion (Panels A-D) and corresponding accumulation of Glc4gemGlc (Panels E-H) during saccharifications of SPS by Cellic CTec2 at 10% DM and 50°C with different GA (0, 0.1, 1 mM) and GOx (0, 59, 118, 236 ng/mL) concentrations. The legend shown in Panel A, and the *y*-axis labels shown in Panels A and E, are valid for all panels. The final concentration of GOx is indicated in bold in the top right of each set of two corresponding panels. In all experiments, the enzyme loading was 4 mg/g DM substrate. Error bars indicate standard deviations between triplicates.

The reactions without added GOx show that there was very little LPMO activity in the reactions with GA (**Figure 5E**) and that GA seemed to inhibit the cellulolytic reaction (**Figure 5A**). Comparison of **Figure 4A** and **Figure 5A** shows that saccharification yields were, obviously, similar for the reactions without added reductant, and that addition of AscA or GA led to improved and decreased glucan conversion, respectively. The decrease in glucan conversion observed for reactions with GA may be due to inhibitory effects of GA on cellulases, although reports on the impact of GA on cellulase activity show conflicting results [57, 64].

Interestingly, addition of GOx to the reactions led to strongly increased LPMO activity in a GA-dose dependent manner (**Figure 5F-H**), analogous to the reactions with AscA (**Figure**

4F-H). This clearly shows that the lack of LPMO activity in GA-fueled reactions is not due to a lack of LPMO reduction, but rather due to reductant-driven *in situ* generation of H_2O_2 being very low. In this respect, it is worth noting a recent study with a fungal LPMO of the type likely present in Cellic CTec2, which showed that H_2O_2 generation is much faster in the presence of AscA compared to GA [29].

The increased LPMO activity is reflected in increased saccharification yields, in particular in reactions with lower GOx concentrations and no added GA (**Figure 5B and C**). Similar to experiments with AscA and GOx, there is an optimum combination of reductant and GOx for obtaining maximum glucan conversion, but the two reductants show different results and optimal conditions. Like for AscA, LPMO activity is largely independent of the reductant concentration, except at higher GOx concentrations, where signs of reductant depletion (i.e., increased LPMO activity at increased GA concentrations) and enzyme inactivation (reduced LPMO product levels at 48 h compared to 24 h) become visible, likely due to too high levels of H_2O_2. The importance of the reductant at high GOx concentration is also reflected by the fact that reactions with GA gave higher saccharification yields than the reactions without GA only for the reaction with 236 ng/mL GOx, despite the slight inhibiting effect of GA on cellulase activity. It is also noteworthy that at 236 ng/mL GOx, when reductant depletion plays a role, the reaction with 0.1 mM AscA yielded much less Glc4gemGlc than the reaction with 0.1 mM GA (**Figure 4H** and **Figure 5H**). This may reflect increased reactivity of AscA with surplus H_2O_2, or the boosting effect that copper released from damaged LPMOs has on reductant oxidation, which is large for AscA and nearly absent for GA [30].

All in all, the results depicted in **Figure 4** and **Figure 5** show that the saccharification efficiency of lignin-poor SPS depends on multiple factors that must be carefully balanced, and that the choice of reductant has a major effect both in reactions with and without GOx.

Saccharification of SEB with GOx

As discussed above and shown in **Figure 3**, the increased compositional complexity of a lignin-rich substrate has significant impact on LPMO activity, saccharification efficiency, and the relative performance of the two enzyme cocktails tested, with Cellic CTec2 performing much better than the *T. aurantiacus* cocktail. Saccharification reactions with Cellic CTec2 and added GOx showed that, in the case of SEB, GOx activity was detrimental at both tested GOx concentrations (**Figure 6**). Saccharification yields decreased, especially for the reaction with the highest GOx dosage, and LPMO product levels showed GOx-dose dependent signs of enzyme inactivation (i.e., decreasing product levels over time in the reactions with 59 ng/mL and, more so, 236 ng/mL GOx). This further highlights the impact of the redox state of the substrate on cocktail performance. In the case of SEB, it may seem that there easily may be too much H_2O_2 in the system, as also suggested by the 60°C reactions shown in **Figure 3**. Accordingly, generation of extra H_2O_2 by GOx is detrimental rather than beneficial.

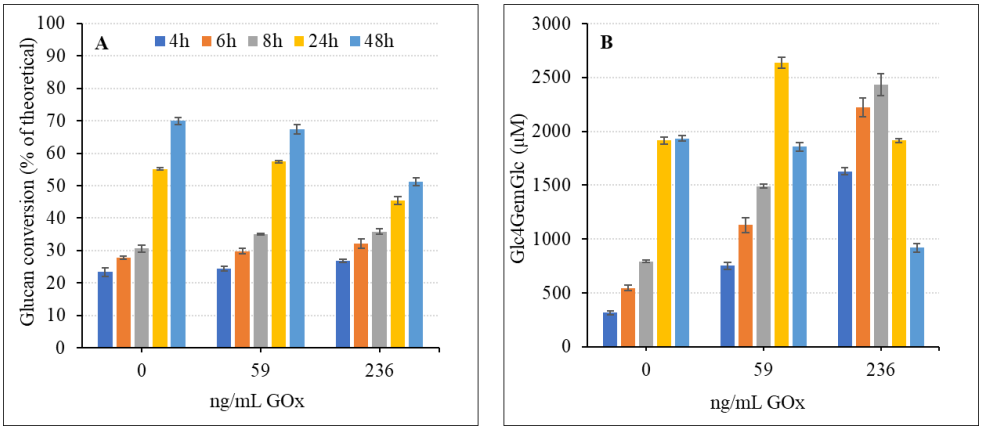

Figure 6. Glucan conversion and Glc4gemGlc levels during saccharification of SEB with Cellic CTec2 at 10% DM and 50°C with different GOx (0, 59, 118, 236 ng/mL) concentrations. Panel A shows the saccharification yield and Panel B shows the levels of Glc4gemGlc. The legend shown in Panel A is valid for both panels. In all experiments, the enzyme loading was 4 mg/g DM substrate. No exogenous electron donor was supplemented to the reactions. Error bars indicate standard deviations between triplicates.

Concluding Remarks

In this study, we have assessed the saccharification efficiency and LPMO activity of the Cellic CTec2 and *T. aurantiacus* cellulolytic enzyme cocktails in reactions with two different cellulosic substrates, using high dry matter conditions. Cellic CTec2 outperformed the *T. aurantiacus* cocktail at 50°C, but at 60°C, the *T. aurantiacus* cocktail was more efficient and performed nearly as well as Cellic CTec2 did at 50°C. The dependence of the LPMO reaction on H_2O_2 was confirmed by showing that H_2O_2-producing GOx improved both LPMO activity and glucan solubilization for Cellic CTec2. Interestingly, in reactions without GOx, AscA is a much better reductant than GA, which is likely due to the higher H_2O_2-producing capacity of the LPMO-AscA combination. Reactions with GOx were efficient even in the absence of added reductant, which opens up alternative processing options and underpins that the rate-limiting contribution of the reductant to LPMO reactions in the absence of GOx relates to H_2O_2 production.

Multiple experiments described above illustrate the well-known fact that excessive amounts of H_2O_2 lead to enzyme inactivation and reduced saccharification yields. To optimize these yields, it is imperative to find an optimal balance between the amounts of reducing power and *in situ*-generated H_2O_2. As shown above, this balance depends both on the reductant and on the substrate used. When working with "clean" substrates such as SPS, control and rationalization are feasible, as also demonstrated in previous studies [24, 65], but this is less feasible for redox-active substrates such as the SEB used here. The redox chemistry of lignin-rich substrates is complex and unpredictable [66], and it is difficult to identify and control redox reactions that may damage critical enzymes and produce or consume LPMO co-substrates. Despite an increasing understanding of LPMO action, it seems clear that saccharification of complex lignin-containing substrates requires substrate-specific optimization of process conditions to maximize saccharification yields and harness the full power of LPMOs. Of note,

the nature of the pretreatment, which will affect lignin reactivity, will co-determine optimal conditions for subsequent enzymatic processing [16, 37, 67].

Scott *et al.* [59] have shown that addition of catalase may have a beneficial effect on enzymatic saccharification of complex lignocellulosic biomass, likely because catalase limits accumulation of high levels of H_2O_2. It would be interesting to assess the use of catalase in some of the reaction setups described above. In particular, a catalase could be used to reduce the very high apparent H_2O_2 production in the reaction with the *T. aurantiacus* cocktail and SEB at 60°C, which not only translates to high initial LPMO activity, but also results in rapid enzyme inactivation. Perhaps a thermostable catalase (or another H_2O_2 scavenger) could enable efficient saccharification of substrates such as SEB at elevated temperatures.

Importantly, while the correlation between LPMO activity and saccharification efficiency of the cellulase cocktails is evident, this correlation is not straightforward. For example, **Figure 1** shows that the reaction with Cellic CTec2 at 50°C in the absence of reductant and the reaction with the *T. aurantiacus* cocktail at 50°C in the presence of reductant give similar saccharification yields despite an approximately 10-fold difference in LPMO activity. This remarkable difference could be due to variation in the synergistic interplay between the different cellulases and LPMOs in the two cocktails, since it is known that different enzyme combinations show different synergistic effects and saccharification efficiencies [68, 69]. On the other hand, experiments with Cellic CTec2 and GOx showed that there seems to be a limit to how much LPMO activity is needed to reach maximum saccharification. The very high LPMO product levels observed in some of these reactions did not translate into increased glucan solubilization.

The compositional simplicity of the *T. aurantiacus* cocktail [8] is intriguing and may indicate that this fungus has evolved to use only a few enzymes that are very well adapted to each other, and that perhaps form nature's minimal effective cellulolytic enzyme cocktail.

However, while the cocktail indeed performs very well in reactions with SPS at 60ºC, it is not particularly good at saccharifying the glucan in SEB, under the conditions assessed here. While further work is needed to potentially increase the performance of the *T. aurantiacus* cocktail on substrates such as SEB, the data obtained with SPS show that this cocktail has great potential for industrial saccharification of lignin-poor substrates at higher temperatures.

In conclusion, the results presented here reveal multiple factors affecting the enzymatic saccharification of pretreated lignocellulosic substrates with LPMO-containing enzyme cocktails under close-to-industrial conditions. While rationalization and control of reaction conditions for lignin-rich substrates remain challenging, reactions with lignin-poor substrates seem more amenable to rational optimization. In this latter case, the use of glucose oxidase for *in situ* generation of H_2O_2 and the use of the *T. aurantiacus* cocktail at elevated temperatures provide interesting options for process optimization.

Associated Content

Author information

Corresponding author:

Vincent G. H. Eijsink

Email: vincent.eijsink@nmbu.no

Phone: +47 67232463

Postal address: Norwegian University of Life Sciences (NMBU), Faculty of Chemistry, Biotechnology, and Food Science, P.O. Box 5003, N-1432 Ås, Norway

Author contributions:

H.Ø. designed experiments, performed research, analyzed data, and wrote the first draft of the manuscript. A.V. designed experiments, analyzed data, edited the manuscript, and carried out supervision. P.C. performed research and edited the manuscript. R.G. performed research, edited the manuscript, and acquired funding. S.W.S., S.J.H. and V.G.H.E. initiated the research, edited the manuscript, carried out supervision, and acquired funding.

Funding:

This work was funded by the Norwegian Research Council (NFR) through projects 268002, 257622 and 270038. The work was also supported by the German Academic Exchange Service (DAAD) through a granted stipend to R.G. (Jahresstipendien für Doktorandinnen und Doktoranden, Studienjahr 2018/19 under the Program Number 57380837). Part of the work was performed at the DOE Joint BioEnergy Institute (http://www.jbei.org) supported by the U.S. Department of Energy, Office of Science, Office of Biological and Environmental Research, through contract DE-AC02-05CH11231 between Lawrence Berkeley National Laboratory and the U.S. Department of Energy.

Conflict of interest disclosure:

The authors declare no competing interests.

References

1. Himmel, M. E., Ding, S. Y., Johnson, D. K., Adney, W. S., Nimlos, M. R., Brady, J. W., & Foust, T. D. 2007. Biomass recalcitrance: engineering plants and enzymes for biofuels production, *Science*, 315: 804-807.
2. Galbe, M., & Wallberg, O. 2019. Pretreatment for biorefineries: a review of common methods for efficient utilisation of lignocellulosic materials, *Biotechnology for Biofuels*, 12: 294.
3. Balan, V., Chiaramonti, D., & Kumar, S. 2013. Review of US and EU initiatives toward development, demonstration, and commercialization of lignocellulosic biofuels, *Biofuels, Bioproducts and Biorefining*, 7: 732-759.
4. Rosales-Calderon, O., & Arantes, V. 2019. A review on commercial-scale high-value products that can be produced alongside cellulosic ethanol, *Biotechnology for Biofuels*, 12: 240.
5. Peterson, R., & Nevalainen, H. 2012. *Trichoderma reesei* RUT-C30--thirty years of strain improvement, *Microbiology*, 158: 58-68.
6. De Vries, R. P. 2003. Regulation of *Aspergillus* genes encoding plant cell wall polysaccharide-degrading enzymes; relevance for industrial production, *Applied Microbiology and Biotechnology*, 61: 10-20.
7. Visser, H., Joosten, V., Punt, P. J., Gusakov, A. V., Olson, P. T., Joosten, R., Bartels, J., Visser, J., Sinitsyn, A. P., Emalfarb, M. A., Verdoes, J. C., & Wery, J. 2011. Development of a mature fungal technology and production platform for industrial enzymes based on a *Myceliophthora thermophila* isolate, previously known as *Chrysosporium lucknowense* C1, *Industrial Biotechnology*, 7: 214-223.
8. Schuerg, T., Gabriel, R., Baecker, N., Baker, S. E., & Singer, S. W. 2017. *Thermoascus aurantiacus* is an intriguing host for the industrial production of cellulases, *Current Biotechnology*, 6: 89-97.
9. Chylenski, P., Forsberg, Z., Ståhlberg, J., Várnai, A., Lersch, M., Bengtsson, O., Sæbø, S., Horn, S. J., & Eijsink, V. G. H. 2017. Development of minimal enzyme cocktails for hydrolysis of sulfite-pulped lignocellulosic biomass, *Journal of Biotechnology*, 246: 16-23.
10. Horn, S. J., Vaaje-Kolstad, G., Westereng, B., & Eijsink, V. G. H. 2012. Novel enzymes for the degradation of cellulose, *Biotechnology for Biofuels*, 5: 45.
11. Jørgensen, H., Kristensen, J. B., & Felby, C. 2007. Enzymatic conversion of lignocellulose into fermentable sugars: challenges and opportunities, *Biofuels, Bioproducts and Biorefining*, 1: 119-134.
12. Harris, P. V., Xu, F., Kreel, N. E., Kang, C., & Fukuyama, S. 2014. New enzyme insights drive advances in commercial ethanol production, *Current Opinion in Chemical Biology*, 19: 162-170.
13. Hu, J., Chandra, R., Arantes, V., Gourlay, K., Susan Van Dyk, J., & Saddler, J. N. 2015. The addition of accessory enzymes enhances the hydrolytic performance of cellulase enzymes at high solid loadings, *Bioresource Technology*, 186: 149-153.
14. Cannella, D., Hsieh, C.-W. C., Felby, C., & Jørgensen, H. 2012. Production and effect of aldonic acids during enzymatic hydrolysis of lignocellulose at high dry matter content, *Biotechnology for Biofuels*, 5: 26.
15. Müller, G., Várnai, A., Johansen, K. S., Eijsink, V. G. H., & Horn, S. J. 2015. Harnessing the potential of LPMO-containing cellulase cocktails poses new demands on processing conditions, *Biotechnology for Biofuels*, 8: 187.
16. Hu, J., Arantes, V., Pribowo, A., Gourlay, K., & Saddler, J. N. 2014. Substrate factors that influence the synergistic interaction of AA9 and cellulases during the enzymatic hydrolysis of biomass, *Energy & Environmental Science*, 7: 2308-2315.
17. Vaaje-Kolstad, G., Westereng, B., Horn, S. J., Liu, Z., Zhai, H., Sørlie, M., & Eijsink, V. G. H. 2010. An oxidative enzyme boosting the enzymatic conversion of recalcitrant polysaccharides, *Science*, 330: 219-222.
18. Bissaro, B., Røhr Å, K., Müller, G., Chylenski, P., Skaugen, M., Forsberg, Z., Horn, S. J., Vaaje-Kolstad, G., & Eijsink, V. G. H. 2017. Oxidative cleavage of polysaccharides by monocopper enzymes depends on H_2O_2, *Nature Chemical Biology*, 13: 1123-1128.

19. Hangasky, J. A., Iavarone, A. T., & Marletta, M. A. 2018. Reactivity of O_2 versus H_2O_2 with polysaccharide monooxygenases, *Proceedings of the National Academy of Sciences of the United States of America*, 115: 4915-4920.
20. Kont, R., Bissaro, B., Eijsink, V. G. H., & Väljamäe, P. 2020. Kinetic insights into the peroxygenase activity of cellulose-active lytic polysaccharide monooxygenases (LPMOs), *Nature Communications*, 11: 5786.
21. Bissaro, B., Várnai, A., Røhr, Å. K., & Eijsink, V. G. H. 2018. Oxidoreductases and reactive oxygen species in conversion of lignocellulosic biomass, *Microbiology and Molecular Biology Reviews*, 82: e00029-18.
22. Wang, B., Wang, Z., Davies, G. J., Walton, P. H., & Rovira, C. 2020. Activation of O_2 and H_2O_2 by lytic polysaccharide monooxygenases, *ACS Catalysis*, 10: 12760-12769.
23. Hedison, T. M., Breslmayr, E., Shanmugam, M., Karnpakdee, K., Heyes, D. J., Green, A. P., Ludwig, R., Scrutton, N. S., & Kracher, D. 2021. Insights into the H_2O_2-driven catalytic mechanism of fungal lytic polysaccharide monooxygenases, *The FEBS Journal*, 288: 4115-4128.
24. Müller, G., Chylenski, P., Bissaro, B., Eijsink, V. G. H., & Horn, S. J. 2018. The impact of hydrogen peroxide supply on LPMO activity and overall saccharification efficiency of a commercial cellulase cocktail, *Biotechnology for Biofuels*, 11: 209.
25. Phillips, C. M., Beeson, W. T., Cate, J. H., & Marletta, M. A. 2011. Cellobiose dehydrogenase and a copper-dependent polysaccharide monooxygenase potentiate cellulose degradation by *Neurospora crassa*, *ACS Chemical Biology*, 6: 1399-1406.
26. Quinlan, R. J., Sweeney, M. D., Lo Leggio, L., Otten, H., Poulsen, J.-C. N., Johansen, K. S., Krogh, K. B. R. M., Jørgensen, C. I., Tovborg, M., Anthonsen, A., Tryfona, T., Walter, C. P., Dupree, P., Xu, F., Davies, G. J., & Walton, P. H. 2011. Insights into the oxidative degradation of cellulose by a copper metalloenzyme that exploits biomass components, *Proceedings of the National Academy of Sciences of the United States of America*, 108: 15079-15084.
27. Beeson, W. T., Phillips, C. M., Cate, J. H., & Marletta, M. A. 2012. Oxidative cleavage of cellulose by fungal copper-dependent polysaccharide monooxygenases, *Journal of the American Chemical Society*, 134: 890-892.
28. Kuusk, S., Bissaro, B., Kuusk, P., Forsberg, Z., Eijsink, V. G. H., Sørlie, M., & Väljamäe, P. 2018. Kinetics of H_2O_2-driven degradation of chitin by a bacterial lytic polysaccharide monooxygenase, *Journal of Biological Chemistry*, 293: 523-531.
29. Rieder, L., Stepnov, A. A., Sørlie, M., & Eijsink, V. G. H. 2021. Fast and specific peroxygenase reactions catalyzed by fungal mono-copper enzymes, *Biochemistry*, 60: 3633-3643.
30. Stepnov, A. A., Forsberg, Z., Sørlie, M., Nguyen, G. S., Wentzel, A., Røhr Å, K., & Eijsink, V. G. H. 2021. Unraveling the roles of the reductant and free copper ions in LPMO kinetics, *Biotechnology for Biofuels*, 14: 28.
31. Stepnov, A. A., Christensen, I. A., Forsberg, Z., Aachmann, F. L., Courtade, G., & Eijsink, V. G. H. 2022. The impact of reductants on the catalytic efficiency of a lytic polysaccharide monooxygenase and the special role of dehydroascorbic acid, *FEBS Letters*, 596: 53-70.
32. Westereng, B., Cannella, D., Agger, J. W., Jørgensen, H., Andersen, M. L., Eijsink, V. G. H., & Felby, C. 2015. Enzymatic cellulose oxidation is linked to lignin by long-range electron transfer, *Scientific Reports*, 5: 18561.
33. Kracher, D., Scheiblbrandner, S., Felice, A. K. G., Breslmayr, E., Preims, M., Ludwicka, K., Haltrich, D., Eijsink, V. G. H., & Ludwig, R. 2016. Extracellular electron transfer systems fuel cellulose oxidative degradation, *Science*, 352: 1098-1101.
34. Frommhagen, M., Westphal, A. H., Van Berkel, W. J. H., & Kabel, M. A. 2018. Distinct substrate specificities and electron-donating systems of fungal lytic polysaccharide monooxygenases, *Frontiers in Microbiology*, 9: 1080.
35. Eijsink, V. G. H., Petrović, D., Forsberg, Z., Mekasha, S., Røhr, A. K., Várnai, A., Bissaro, B., & Vaaje-Kolstad, G. 2019. On the functional characterization of lytic polysaccharide monooxygenases (LPMOs), *Biotechnology for Biofuels*, 12: 58.
36. Kracher, D., Forsberg, Z., Bissaro, B., Gangl, S., Preims, M., Sygmund, C., Eijsink, V. G. H., & Ludwig, R. 2020. Polysaccharide oxidation by lytic polysaccharide monooxygenase is enhanced by engineered cellobiose dehydrogenase, *The FEBS Journal*, 287: 897-908.

37. Rodríguez-Zúñiga, U. F., Cannella, D., Giordano, R. D. C., Giordano, R. D. L. C., Jørgensen, H., & Felby, C. 2015. Lignocellulose pretreatment technologies affect the level of enzymatic cellulose oxidation by LPMO, *Green Chemistry*, 17: 2896-2903.
38. Hou, W., Li, L., & Bao, J. 2017. Oxygen transfer in high solids loading and highly viscous lignocellulose hydrolysates, *ACS Sustainable Chemistry & Engineering*, 5: 11395-11402.
39. Costa, T. H. F., Kadic, A., Chylenski, P., Várnai, A., Bengtsson, O., Lidén, G., Eijsink, V. G. H., & Horn, S. J. 2020. Demonstration-scale enzymatic saccharification of sulfite-pulped spruce with addition of hydrogen peroxide for LPMO activation, *Biofuels, Bioproducts and Biorefining*, 14: 734-745.
40. Calderaro, F., Keser, M., Akeroyd, M., Bevers, L. E., Eijsink, V. G. H., Várnai, A., & Van Den Berg, M. A. 2020. Characterization of an AA9 LPMO from *Thielavia australiensis*, *Taus*LPMO9B, under industrially relevant lignocellulose saccharification conditions, *Biotechnology for Biofuels*, 13: 195.
41. Mcclendon, S. D., Batth, T., Petzold, C. J., Adams, P. D., Simmons, B. A., & Singer, S. W. 2012. *Thermoascus aurantiacus* is a promising source of enzymes for biomass deconstruction under thermophilic conditions, *Biotechnology for Biofuels*, 5: 54.
42. Fritsche, S., Hopson, C., Gorman, J., Gabriel, R., & Singer, S. W. 2020. Purification and characterization of a native lytic polysaccharide monooxygenase from *Thermoascus aurantiacus*, *Biotechnology Letters*, 42: 1897-1905.
43. Harris, P. V., Welner, D., Mcfarland, K. C., Re, E., Navarro Poulsen, J. C., Brown, K., Salbo, R., Ding, H., Vlasenko, E., Merino, S., Xu, F., Cherry, J., Larsen, S., & Lo Leggio, L. 2010. Stimulation of lignocellulosic biomass hydrolysis by proteins of glycoside hydrolase family 61: structure and function of a large, enigmatic family, *Biochemistry*, 49: 3305-3316.
44. Petrović, D. M., Bissaro, B., Chylenski, P., Skaugen, M., Sørlie, M., Jensen, M. S., Aachmann, F. L., Courtade, G., Várnai, A., & Eijsink, V. G. H. 2018. Methylation of the N-terminal histidine protects a lytic polysaccharide monooxygenase from auto-oxidative inactivation, *Protein Science*, 27: 1636-1650.
45. Chylenski, P., Petrović, D. M., Müller, G., Dahlström, M., Bengtsson, O., Lersch, M., Siika-Aho, M., Horn, S. J., & Eijsink, V. G. H. 2017. Enzymatic degradation of sulfite-pulped softwoods and the role of LPMOs, *Biotechnology for Biofuels*, 10: 177.
46. Rødsrud, G., Lersch, M., & Sjöde, A. 2012. History and future of world's most advanced biorefinery in operation, *Biomass and Bioenergy*, 46: 46-59.
47. Kalyani, D. C., Zamanzadeh, M., Müller, G., & Horn, S. J. 2017. Biofuel production from birch wood by combining high solid loading simultaneous saccharification and fermentation and anaerobic digestion, *Applied Energy*, 193: 210-219.
48. Schuerg, T., Prahl, J. P., Gabriel, R., Harth, S., Tachea, F., Chen, C. S., Miller, M., Masson, F., He, Q., Brown, S., Mirshiaghi, M., Liang, L., Tom, L. M., Tanjore, D., Sun, N., Pray, T. R., & Singer, S. W. 2017. Xylose induces cellulase production in *Thermoascus aurantiacus*, *Biotechnology for Biofuels*, 10: 271.
49. Bradford, M. M. 1976. A rapid and sensitive method for the quantitation of microgram quantities of protein utilizing the principle of protein-dye binding, *Analytical Biochemistry*, 72: 248-254.
50. Westereng, B., Arntzen, M. O., Agger, J. W., Vaaje-Kolstad, G., & Eijsink, V. G. H. 2017. Analyzing activities of lytic polysaccharide monooxygenases by liquid chromatography and mass spectrometry, *Methods in Molecular Biology*, 1588: 71-92.
51. Hegnar, O. A., Østby, H., Petrović, D. M., Olsson, L., Várnai, A., & Eijsink, V. G. H. 2021. Quantifying oxidation of cellulose-associated glucuronoxylan by two lytic polysaccharide monooxygenases from *Neurospora crassa*, *Applied and Environmental Microbiology*, 87: e0165221.
52. Østby, H., Jameson, J.-K., Costa, T., Eijsink, V. G. H., & Arntzen, M. Ø. 2022. Chromatographic analysis of oxidized cello-oligomers generated by lytic polysaccharide monooxygenases using dual electrolytic eluent generation, *Journal of Chromatography A*, 1662: 462691.
53. Muraleedharan, M. N., Zouraris, D., Karantonis, A., Topakas, E., Sandgren, M., Rova, U., Christakopoulos, P., & Karnaouri, A. 2018. Effect of lignin fractions isolated from different

biomass sources on cellulose oxidation by fungal lytic polysaccharide monooxygenases, *Biotechnology for Biofuels*, 11: 296.

54. Brenelli, L., Squina, F. M., Felby, C., & Cannella, D. 2018. Laccase-derived lignin compounds boost cellulose oxidative enzymes AA9, *Biotechnology for Biofuels*, 11: 10.
55. Kont, R., Pihlajaniemi, V., Borisova, A. S., Aro, N., Marjamaa, K., Loogen, J., Büchs, J., Eijsink, V. G. H., Kruus, K., & Väljamäe, P. 2019. The liquid fraction from hydrothermal pretreatment of wheat straw provides lytic polysaccharide monooxygenases with both electrons and H_2O_2 co-substrate, *Biotechnology for Biofuels*, 12: 235.
56. Berlin, A., Balakshin, M., Gilkes, N., Kadla, J., Maximenko, V., Kubo, S., & Saddler, J. 2006. Inhibition of cellulase, xylanase and beta-glucosidase activities by softwood lignin preparations, *Journal of Biotechnology*, 125: 198-209.
57. Ximenes, E., Kim, Y., Mosier, N., Dien, B., & Ladisch, M. 2011. Deactivation of cellulases by phenols, *Enzyme and Microbial Technology*, 48: 54-60.
58. Westereng, B., Arntzen, M. O., Aachmann, F. L., Varnai, A., Eijsink, V. G., & Agger, J. W. 2016. Simultaneous analysis of C1 and C4 oxidized oligosaccharides, the products of lytic polysaccharide monooxygenases acting on cellulose, *Journal of Chromatography A*, 1445: 46-54.
59. Scott, B. R., Huang, H. Z., Frickman, J., Halvorsen, R., & Johansen, K. S. 2016. Catalase improves saccharification of lignocellulose by reducing lytic polysaccharide monooxygenase-associated enzyme inactivation, *Biotechnology Letters*, 38: 425-434.
60. Gouda, M. D., Singh, S. A., Rao, A. G., Thakur, M. S., & Karanth, N. G. 2003. Thermal inactivation of glucose oxidase. Mechanism and stabilization using additives, *Journal of Biological Chemistry*, 278: 24324-24333.
61. Kuusk, S., & Väljamäe, P. 2021. Kinetics of H_2O_2-driven catalysis by a lytic polysaccharide monooxygenase from the fungus *Trichoderma reesei*, *Journal of Biological Chemistry*, 297: 101256.
62. Kuusk, S., Kont, R., Kuusk, P., Heering, A., Sørlie, M., Bissaro, B., Eijsink, V. G. H., & Väljamäe, P. 2019. Kinetic insights into the role of the reductant in H_2O_2-driven degradation of chitin by a bacterial lytic polysaccharide monooxygenase, *Journal of Biological Chemistry*, 294: 1516-1528.
63. Stepnov, A. A., Eijsink, V. G. H., & Forsberg, Z. 2022. Enhanced *in situ* H_2O_2 production explains synergy between an LPMO with a cellulose-binding domain and a single-domain LPMO, *Scientific Reports*, 12: 6129.
64. Xin, D., Blossom, B. M., Lu, X., & Felby, C. 2022. Improving cellulases hydrolytic action: an expanded role for electron donors of lytic polysaccharide monooxygenases in cellulose saccharification, *Bioresource Technology*, 346: 126662.
65. Kadić, A., Várnai, A., Eijsink, V. G. H., Horn, S. J., & Lidén, G. 2021. *In situ* measurements of oxidation–reduction potential and hydrogen peroxide concentration as tools for revealing LPMO inactivation during enzymatic saccharification of cellulose, *Biotechnology for Biofuels*, 14: 46.
66. Peciulyte, A., Samuelsson, L., Olsson, L., Mcfarland, K. C., Frickmann, J., Østergård, L., Halvorsen, R., Scott, B. R., & Johansen, K. S. 2018. Redox processes acidify and decarboxylate steam-pretreated lignocellulosic biomass and are modulated by LPMO and catalase, *Biotechnology for Biofuels*, 11: 165.
67. Hansen, L. D., Østensen, M., Arstad, B., Tschentscher, R., Eijsink, V. G. H., Horn, S. J., & Várnai, A. 2022. 2-Naphthol impregnation prior to steam explosion promotes LPMO-assisted enzymatic saccharification of spruce and yields high-purity lignin, *ACS Sustainable Chemistry & Engineering*, 10: 5233-5242.
68. Tokin, R., Ipsen, J. Ø., Westh, P., & Johansen, K. S. 2020. The synergy between LPMOs and cellulases in enzymatic saccharification of cellulose is both enzyme- and substrate-dependent, *Biotechnology Letters*, 42: 1975-1984.
69. Keller, M. B., Badino, S. F., Røjel, N., Sørensen, T. H., Kari, J., Mcbrayer, B., Borch, K., Blossom, B. M., & Westh, P. 2021. A comparative biochemical investigation of the impeding effect of C1-oxidizing LPMOs on cellobiohydrolases, *Journal of Biological Chemistry*, 296: 100504.

820

Functional characterization of a lytic polysaccharide monooxygenase from *Schizophyllum commune* that degrades non-crystalline substrates and displays strong peroxygenase activity

Østby, H., Christensen, I. A., Hennum, K., Várnai, A., Courtade, G., Hegnar, O. A., Aachmann, F. L., & Eijsink, V. G. H.

Paper III

Functional characterization of a lytic polysaccharide monooxygenase from *Schizophyllum commune* that degrades non-crystalline substrates and displays strong peroxygenase activity

Heidi Østby[1], Idd A. Christensen[2], Karen Hennum[1], Anikó Várnai[1], Gaston Courtade[2], Olav A. Hegnar[1], Finn L. Aachmann[2], and Vincent G. H. Eijsink[1,*]

[1]Norwegian University of Life Sciences (NMBU), Faculty of Chemistry, Biotechnology, and Food Science, P.O. Box 5003, N-1432 Ås, Norway

[2]Norwegian University of Science and Technology (NTNU), NOBIPOL, Department of Biotechnology and Food Science, Trondheim, Norway

[*]Address correspondence to Vincent G. H. Eijsink, vincent.eijsink@nmbu.no

Norwegian University of Life Sciences (NMBU), Faculty of Chemistry, Biotechnology, and Food Science, P.O. Box 5003, N-1432 Ås, Norway, **Telephone:** +47 67232463.

Abstract

Lytic polysaccharide monooxygenases (LPMOs) are mono-copper enzymes that use O_2 or H_2O_2 to oxidatively cleave glycosidic bonds. LPMOs are highly prevalent in nature, with some fungal genomes encoding dozens, and the functional variation among these enzymes is a topic of great interest that may eventually shed light on the biological function of this multiplicity. We present the functional characterization of one of the 22 putative AA9-type LPMOs from the fungus *Schizophyllum commune*, *Sc*LPMO9A. The enzyme, expressed in *E. coli*, showed C4-oxidative cleavage of amorphous cellulose and soluble cello-oligosaccharides with a degree of polymerization of four or higher. The enzyme showed activity on xyloglucan, mixed-linkage glucan, and glucomannan, and comparison of product profiles revealed differences with the well-studied C4-oxidizing *Nc*LPMO9C, which is also active on these substrates. While *Nc*LPMO9C is also active on more crystalline forms of cellulose, *Sc*LPMO9A is not. Accordingly, addition of *Sc*LPMO9A to an LPMO-poor cellulase cocktail did not improve saccharification of sulfite-pulped spruce. Studies with addition of H_2O_2 to reaction mixtures with *Sc*LPMO9A and phosphoric acid swollen cellulose, an amorphous substrate, showed that the enzyme carries out a fast and specific peroxygenase reaction that is at least two orders of magnitude faster than the apparent monooxygenase reaction that occurs in the presence of added reductant. Peroxygenase reactions with cellopentaose reached a rate of at least 11 s^{-1}. Together, these results show that *Sc*LPMO9A is an efficient LPMO with a broad substrate range, which, rather than acting on cellulose, has evolved to act on amorphous and soluble glucans.

Introduction

Since their discovery in 2010, lytic polysaccharide monooxygenases (LPMOs) have been the focus of much research with the aim of better understanding their unique properties and harnessing their oxidative power (Vaaje-Kolstad et al., 2010; Hemsworth et al., 2015; Johansen, 2016; Bissaro et al., 2018). While generally considered important for the conversion of recalcitrant insoluble polysaccharides such as cellulose and chitin, LPMOs may be active on a wide range of soluble and insoluble substrates, including various hemicelluloses, cello-oligomers, pectin, and starch (Vandhana et al., 2022). LPMOs are abundant in nature, with some fungal genomes coding for dozens of LPMOs, and the true roles and substrates of many of these enzymes likely remain undiscovered (Lenfant et al., 2017; Frandsen et al., 2021; Tõlgo et al., 2022).

LPMOs are copper-dependent redox enzymes that use an oxidative mechanism (monooxygenase- or peroxygenase-type activity) to catalyze the scission of polysaccharide glycosidic bonds (Vaaje-Kolstad et al., 2010; Phillips et al., 2011; Bissaro et al., 2017; Jones et al., 2020). The active site of LPMOs contains a histidine brace consisting of two conserved histidine residues that coordinate the copper atom (Phillips et al., 2011; Quinlan et al., 2011; Vaaje-Kolstad et al., 2017). LPMO catalysis requires reduction of the copper, which may be achieved by small-molecule reductants such as ascorbic acid, gallic acid, or cysteine, enzymatic electron donors such as cellobiose dehydrogenase, or redox-active compounds in the substrate itself, such as lignin (Vaaje-Kolstad et al., 2010; Phillips et al., 2011; Westereng et al., 2015; Kracher et al., 2016; Frommhagen et al., 2018; Chalak et al., 2019). In the presence of a relevant substrate, reduced LPMOs can utilize either molecular O_2 or H_2O_2 as a co-substrate to catalyze the hydroxylation of a carbon in the scissile glycosidic bond (C1 or C4 in cellulose), leading to spontaneous bond cleavage (Phillips et al., 2011; Beeson et al., 2012; Bissaro et al., 2017). Once reduced, a single

LPMO molecule acting as a peroxygenase can catalyze multiple turnovers (Bissaro et al., 2017; Hedison et al., 2021). Non-substrate-bound reduced LPMOs in solution can react with O_2 to produce H_2O_2 (Kittl et al., 2012; Stepnov et al., 2022), or with H_2O_2, generating reactive oxygen species that may lead to damage and autocatalytic inactivation (Bissaro et al., 2017). While the significance of the monooxygenase vs. peroxygenase reaction is still under debate, it is worth noting that LPMO reactions with H_2O_2 are several orders of magnitude faster than those driven by O_2 (Bissaro et al., 2018; Hangasky et al., 2018; Kuusk et al., 2018; Kont et al., 2020; Hedison et al., 2021; Rieder et al., 2021b).

LPMOs currently populate eight families in the carbohydrate-active enzymes (CAZy) database (http://www.cazy.org/; (Drula et al., 2022)) auxiliary activities (AA) class, which consists of 17 families, and encompasses oxidases, peroxidases, and oxidoreductases in addition to LPMOs (Levasseur et al., 2013). Most characterized fungal LPMOs can be found in the AA9 family, which at the time of writing contained 34 functionally characterized LPMOs with activities on insoluble and soluble cellulosic and hemicellulosic substrates. The N-terminal histidine of AA9 LPMOs, which is part of the copper-binding histidine brace, carries a methylation (Quinlan et al., 2011), which likely helps to protect the enzymes from oxidative damage (Petrović et al., 2018). Of note, non-methylated variants of these LPMOs have been produced in the yeast *Pichia pastoris* and are active. Well-studied examples of AA9 LPMOs include *Nc*LPMO9C from *Neurospora crassa*, *Ls*LPMO9A from *Lentinus similis*, and *Cv*LPMO9A from *Collariella virescens* (Isaksen et al., 2014; Borisova et al., 2015; Frandsen et al., 2016; Simmons et al., 2017; Tandrup et al., 2020; Brander et al., 2021), which stand out due to their proven ability to act on soluble substrates, including cello-oligomers, and hemicelluloses such as glucomannan and xyloglucan.

The ability of LPMOs to boost the action of canonical glycoside hydrolases makes them interesting candidates for use in the valorization of recalcitrant polysaccharides in lignocellulosic biomass (Cannella et al., 2012; Hemsworth et al., 2015; Müller et al., 2018). Indeed, modern cellulase cocktails used in lignocellulosic biorefineries contain LPMOs and their contribution to cellulose saccharification efficiency is evident (Harris et al., 2014; Müller et al., 2015; Johansen, 2016; Costa et al., 2020). So far, LPMO action in bioprocessing has exclusively been focused on oxidative degradation of cellulose, whereas the potential impact of hemicellulolytic LPMO activities, if present in commercial cocktails, has not been addressed. The continued elucidation of novel LPMOs acting on various lignocellulosic polysaccharides may provide novel tools for biomass processing and may help understand the biological reasons for the large LPMO multiplicity observed in some fungal species.

Basidiomycetes wood-decaying filamentous fungi are a rich source of enzymes for the depolymerization of complex plant matter, including LPMOs. The genome of one such Basidiomycete fungus, *Schizophyllum commune*, was first sequenced in 2010, and showed, in addition to genes coding for an extensive array of glycoside hydrolases active on cellulose, xylan, and pectin, the presence of genes encoding 22 putative AA9s (Ohm et al., 2010). A comparative study of four fungi including *S. commune* by Zhu and colleagues indicated that the *S. commune* secretome had significantly higher cellulase and xylanase activities than other white- and brown-rot fungi tested during solid-state fermentation of Jerusalem artichoke stalk. Proteomic analysis of the *S. commune* secretome revealed the presence of a wide range of cellulolytic and hemicellulolytic enzymes, and eight AA9s, including *Sc*LPMO9A. In addition, the crude enzyme cocktail from *S. commune* outperformed a commercial enzyme blend from *Trichoderma longibrachiatum* in saccharifications of multiple lignocellulosic substrates, both in conversion of

glucan and xylan (Zhu et al., 2016). A comparative study of *S. commune* and the closely related *Auriculariopsis ampla* found that *Sc*LPMO9A (and the orthologous gene in *A. ampla*) is among the top three upregulated AA9s in vegetative mycelium growing on poplar wood in both species (Almási et al., 2019).

As an AA9 candidate for in-depth characterization, *Sc*LPMO9A is of particular interest, as it is produced by *S. commune* under different conditions, growing on different substrates, hinting at a crucial role of this enzyme during growth and nutrient acquisition. In this study we have cloned, produced and purified *Sc*LPMO9A, and performed an in-depth functional characterization of this enzyme. The properties of this single domain AA9 LPMO, active on soluble substrates, are compared to the properties of the well-studied *Nc*LPMO9C. We show that *Sc*LPMO9A is active on a range of soluble and amorphous substrates, whereas its activity on crystalline cellulose substrates is limited, suggesting that this enzyme's natural role is not in saccharification of recalcitrant cellulose. Additionally, we show that *Sc*LPMO9A is a rapid consumer of H_2O_2, both in reactions with soluble cellopentaose and in the oxidative depolymerization of insoluble amorphous cellulose.

Methods

Sequence and structure analysis

A multiple sequence alignment (MSA) was created using T-Coffee Expresso (http://tcoffee.crg.cat/apps/tcoffee/index.html; (Armougom et al., 2006)) by aligning the sequence of *Sc*LPMO9A with 46 other characterized AA9s, using only the AA9 domains and removing signal peptides. The MSA was edited in AliView (Larsson, 2014), and the resulting MSA was used for phylogenetic analysis using the ProtTest 3.4 software package, by calculating likelihood scores

using all included substitution matrices, all improvements, and four categories for rate variation, empirical amino acid frequencies, and a fixed BIONJ JTT tree for base likelihood calculations (Darriba et al., 2011). A consensus tree was built with all 120 likelihood scores using the Akaike information criterion (AIC). The resulting consensus tree was edited using the iTol v6 online tool (https://itol.embl.de/; (Letunic and Bork, 2007)). Homology modeling of *Sc*LPMO9A using *Ls*LPMO9A bound to cellohexaose (PDB: 5ACI 61.1% sequence identity) as a template structure was performed using PHYRE (Kelley et al., 2015), and the resulting model was analyzed in PyMOL (The PyMOL Molecular Graphics System, Version 2.0, Schrödinger, LLC).

Protein expression and purification

A gene fragment containing the signal peptide pelB (MKYLLPTAAAGLLLLAAQPAMA) (Zhang et al., 2018) fused with the gene encoding *Sc*LPMO9A (UniProt: D8Q364; residues 20-247) was codon-optimized for expression in *Escherichia coli* and *de novo* synthesized by GenScript (Piscataway, USA). Restriction sites for NdeI and NotI were included upstream and downstream of the coding area, respectively. The pelB-*Sc*LPMO9A fragment was isolated from the Genscript vector by digestion with NdeI and NotI, and ligated into the compatible NdeI and NotI sites of the pJB_SP_*Sm*-vector (Courtade et al., 2017), (replacing the SP_*Sm* gene fragment), generating pJB_pelB_*Sc*. The pJB_pelB_*Sc* plasmid was transformed into competent *E. coli* T7 express cells (New England Biolabs) using a heat shock protocol. Plasmid DNA was isolated from the cells using the Wizard® Plus SV Minipreps DNA purification system (Promega) and the plasmid was verified by full vector sequencing.

To express *Sc*LPMO9A, a pre-culture containing 5 mL LB medium with 100 µg/mL ampicillin and inoculated with pJB_pelB_*Sc* containing *E. coli* was grown at 30°C and 220 rpm

overnight. The pre-culture was used to inoculate 500 mL 2x LB medium with 100 µg/mL ampicillin in a 2 L baffled shake flask, followed by incubation at 30°C and 220 rpm to OD_{600} 0.6-0.8. After incubating the culture on ice for 5 minutes, m-toluic acid (Sigma-Aldrich, St. Louis, MO, USA) was added to a final concentration of 0.1 mM, after which the culture was incubated overnight at 16°C and 220 rpm. The pellet was harvested by centrifugation, and subjected to osmotic shock to prepare a periplasmatic extract (Manoil and Beckwith, 1986), which was filtered using a 0.22 µm sterile filter and stored at 4°C prior to protein purification.

Purification of *Sc*LPMO9A was performed by anion-exchange chromatography using an Äkta Purifier system with a 5 mL HiTrap DEAE FF column (GE Healthcare, Uppsala, Sweden), equilibrated with 50 mM Tris-HCl pH 7.5. After loading the sterile-filtered periplasmic extract onto the column, *Sc*LPMO9A was eluted using a 0-50% gradient of 50 mM Tris-HCl, 1 M NaCl pH 7.5 over 90 column volumes. Protein purity was assessed using SDS-PAGE. Fractions containing *Sc*LPMO9A were pooled and the buffer was exchanged to 50 mM Tris-HCl pH 7.5 before the protein was concentrated using a 10-kDa Vivaspin centrifugal tube (Sartorius, Göttingen, Germany). The protein concentration was determined spectrophotometrically at 280 nm using the theoretical molar extinction coefficient (51005 $M^{-1} \cdot cm^{-1}$), determined using the ExPASy ProtParam tool (Gasteiger et al., 2005).

Expression and purification of *Nc*LPMO9C were performed as described earlier (Kittl et al., 2012), and copper saturation of both LPMOs was performed as previously described (Loose et al., 2014).

Substrates and chemicals

Cellulosic substrates used in this study included Avicel PH-101 (Sigma-Aldrich), PASC (prepared from Avicel as described in (Wood, 1988)), cellotetraose, cellopentaose, and cellohexaose (all purchased from Megazyme, Wicklow, Ireland), and sulfite-pulped spruce (batch number DP3319; composition in % w/w dry matter: 87.4% glucan, 2.7% xylan, 5.2% mannan, and 3.3% lignin), kindly provided by Borregaard AS (Rødsrud et al., 2012; Chylenski et al., 2017). Hemicellulosic substrates used were low viscosity konjac glucomannan (KGM), xyloglucan from tamarind seed (TXG), medium viscosity mixed-linkage glucan from barley (β(1,3;1,4)-glucan; BG), higher DP xyloglucan oligos (XGO), birchwood xylan, beechwood xylan, and low-viscosity arabinoxylan from wheat flour. All hemicellulosic substrates were purchased from Megazyme.

Ascorbic acid (AscA) was used as a reducing agent in all LPMO reactions. Aliquots of a stock solution of 100 mM AscA prepared in Trace SELECT water (Sigma-Aldrich) were prepared and stored at -20°C. Aliquots were thawed in the dark immediately prior to use.

Production and consumption of H_2O_2

An adapted version of the Amplex Red assay (Kittl et al., 2012) was used to quantify H_2O_2 production by *Sc*LPMO9A and *Nc*LPMO9C. Reaction mixtures contained 3 µM LPMO, 100 µM Amplex Red (Thermo Fischer Scientific, Waltham, MA, USA), 0.5 U horseradish peroxidase (Sigma-Aldrich), and 50 µM AscA in 50 mM BisTris-HCl pH 6.5, and reactions were initiated by the addition of AscA. The reactions were incubated at 30°C in a Varioscan LUX plate reader (Thermo Fischer Scientific), and the production of resorufin was measured spectrophotometrically at 563 nm every 22 s over a total time of 6500 s. Control reactions containing 3 µM $CuSO_4$ in place of the LPMO were performed in parallel.

An assay adapted from (Breslmayr et al., 2018) was used to measure H_2O_2 consumption by the LPMOs. Reaction mixtures contained 3 µM LPMO, 1 mM 2,6-dimethoxyphenol (Sigma-Aldrich), and 100 µM H_2O_2 in 50 mM BisTris pH 6.5 and reactions were initiated by addition of the LPMO. Reactions were incubated at 30°C in a Varioscan LUX plate reader (Thermo Fischer Scientific), and the absorbance at 469 nm was measured every 30 s over a total time of 600 s. Control reactions containing 3 µM $CuSO_4$ in place of the LPMO were performed in parallel.

Determination of the redox potential

The cell potential for the redox couple *Sc*LPMO9A-Cu2+/*Sc*LPMO9A-Cu+ was determined as previously described (Aachmann et al., 2012; Forsberg et al., 2014; Borisova et al., 2015). Oxygen-free solutions of 300 µM reduced N,N,N',N'-tetramethyl-1,4-phenylenediamine (TMPred) (Sigma-Aldrich) (30 µL) and 70 µM Cu^{2+}-saturated *Sc*LPMO9A (30 µL) were mixed in UVettes (Eppendorf, Hamburg, Germany) in 20 mM PIPES buffer pH 6.0, and incubated at 300.85 K under anaerobic conditions. Absorbance at 610 nm was measured using a NanoPhotometer C40 (Implen GmbH, München, Germany) until the signal became stable (5 minutes). The extinction coefficient of oxidized TMP (TMPox) (14.0 mM^{-1} cm^{-1}; (Sørlie et al., 2000)) was used to calculate the concentration of TMPox, which is equal to the concentration of *Sc*LPMO9A-Cu+. Finally, the cell potential of the *Sc*LPMO9A-Cu2+/*Sc*LPMO9A-Cu+ couple was determined using the previously determined cell potential of TMPox/TMPred (273 mV; (Liu et al., 1997)).

LPMO reactions with cellulosic and hemicellulosic substates

*Sc*LPMO9A was tested on a range of cellulosic and hemicellulosic substrates to assess its substrate specificity. Reactions with *Nc*LPMO9C were included for comparative purposes. Reactions containing 1 µM *Sc*LPMO9A or *Nc*LPMO9C and individual substrates, or hemicellulosic substrates in combination with PASC, were incubated in 50 mM BisTris-HCl pH 6.5 at 40°C and 1000 rpm in an Eppendorf Thermomixer (Eppendorf, Hamburg, Germany) for 16 h. In reactions with polymeric cellulosic substrates and with hemicellulosic substrates, the substrate concentration was 2 g/L or 4 g/L (with the exception of reactions with sulfite-pulped spruce, which contained 10 g/L substrate). In reactions containing a mixture of PASC and hemicellulosic substrate, the final concentration of both substrates was 2 g/L (total substrate content 4 g/L). In reactions with soluble oligomeric cellulose substrates (cellotetraose, cellopentaose and cellohexaose), the substrate concentration was either 2 g/L or 1 mM. Reactions were initiated by the addition of 1 mM AscA, and stopped by removing insoluble substrates by filtration using a 96-well filter plate (0.45 µm; Merck Millipore, Billerica, MA, USA) operated with a Millipore vacuum manifold system. In the case of soluble substrates, reactions were stopped by boiling for 10 min before filtration. Samples were subsequently stored at -20°C prior to analysis by HPAEC-PAD and/or MALDI-TOF MS. All reactions were performed in triplicate, and control reactions without addition of AscA were performed in parallel.

H_2O_2-driven activity on PASC and cellopentaose

To assess the impact of H_2O_2 on product generation by *Sc*LPMO9A acting on PASC, reactions containing 1 µM LPMO, 2 g/L PASC, 1 mM AscA, and 0, 50, 100, or 250 µM H_2O_2 in 50 mM Tris-HCl pH 7.5 were prepared. The reactions were initiated by addition of AscA, and

incubated at 45°C and 1000 rpm in an Eppendorf Thermomixer (Eppendorf). H_2O_2 was added to the reactions immediately prior to the AscA. Samples were taken at 3, 6, 9, 30, and 60 min and remaining insoluble substrate was removed by filtration using a 96-well filter plate (0.45 µm; Merck Millipore) operated with a Millipore vacuum manifold system. Samples were subsequently stored at -20°C prior to analysis by HPAEC-PAD. All reactions were performed in triplicate, and control reactions without addition of AscA were performed in parallel.

Reactions with cellopentaose to assess the effect of H_2O_2 on *Sc*LPMO9A activity contained 1 µM LPMO, 1 mM cellopentaose, 50 µM AscA, and 200 or 400 µM H_2O_2 in 50 mM sodium acetate buffer pH 5.0. Immediately following the addition of H_2O_2, reactions were initiated by addition of AscA and incubated as described above. Samples were taken at various time points and reactions were quenched by addition of NaOH to a final concentration of 100 mM. Samples were subsequently stored at -20°C prior to analysis of generated native products by HPAEC-PAD. All reactions were performed in triplicate, and control reactions without addition of AscA were performed in parallel.

Synergy with cellulases

Degradation of sulfite-pulped spruce was performed under aerobic conditions in 60 mL screw-cap glass bottles (Wheaton, Millville, USA) using a working volume of 10 mL. The total enzyme loading was 4 mg protein per g dry matter of substrate, and the substrate content was 10% w/w dry matter. The enzymes added were a 9:1 (based on protein content) mix of Celluclast 1.5 L and Novozym 188, both kindly provided by Novozymes AS (Bagsværd, Denmark), and the protein concentrations of these enzyme preparations were determined using the Bio-Rad protein assay (Bio-Rad, USA) based on the Bradford method (Bradford, 1976) using bovine serum albumin as

reference protein. Reactions were initiated by the addition of 1 mM AscA, and incubated at 50°C with orbital shaking at 200 rpm in a Minitron Shaker incubator (Infors AG, Bottmingen, Switzerland). Reactions were performed in duplicate, and control reactions without addition of AscA were performed in parallel. 100 µL samples were taken at 8, 24, 48, and 72 h, and the enzymes were inactivated by boiling for 15 minutes before storage at -20°C. Prior to product quantification, samples were thawed at 4°C and filtered using a 96-well filter plate (0.45 µm; Merck Millipore) operated with a Millipore vacuum manifold system. Quantification of glucose and cellobiose released during hydrolysis was performed by high-performance liquid chromatography using a Dionex Ultimate 3000 system (Dionex, Sunnyvale, CA, USA) with a Shodex RI-101 refractive index detector (Shodex, Japan). A Rezex ROA-organic acid H+ (8%) 300×7.8 mm analytical column (Phenomenex, Torrance, CA, USA) was used, operated at 65°C with 5 mM H_2SO_4 and an isocratic flow of 0.6 mL/min (Müller et al., 2015). Cellobiose levels were below 1 g/L in all samples and are not reported. Glc4gemGlc was quantified by HPAEC-PAD as described below.

Chromatographic analysis of LPMO-derived products by HPAEC-PAD

Products generated in LPMO reactions were analyzed using high-performance anion exchange chromatography with pulsed amperometric detection (HPAEC-PAD) using a Dionex ICS-5000 system (Thermo Fischer Scientific). The ICS-5000 was equipped with a 3×250 mm Dionex CarboPac PA-200 analytical column with a 3×50 mm guard column (Thermo Fischer Scientific), and an operational flow of 500 µL/min was used. Eluents (A: 0.1 M NaOH, B: 0.1 M NaOH containing 1 M NaOAc) were prepared as described previously (Westereng et al., 2017). All samples were diluted two times in distilled water (type I, 18.2 MΩ•cm) prior to analysis using

either a 14-min or a 39-min gradient. The 14-min gradient used was: 0-5 min, convex upward (Dionex curve 4) from 100% A to 90% A and 10% B; 5-8.5 min, concave upward (Dionex curve 8) from 90% A and 10% B to 100% B; 8.5-8.6 min, linear from 100% B to 100% A; 8.6-14 min, constant at 100% A (reconditioning). The 39-min gradient has previously been described (Hegnar et al., 2021). Chromeleon version 7.2.9 (Thermo Fischer Scientific) was used for instrument control and analysis. Cellobiose and cellotriose used to prepare standards for quantification of native products generated from cellopentaose by LPMO action were purchased from Megazyme. C4-oxidized standards for qualitative identification of Glc4gemGlc and Glc4gemGlc$_2$ in product mixtures generated from cellulosic substrates were produced in-house as previously described (Østby et al., 2022).

Product analysis by MALDI-TOF MS

LPMO products from selected samples were analyzed by matrix-assisted laser desorption/ionization time-of-flight mass spectrometry (MALDI-TOF MS) using an Ultraflex instrument (Bruker Daltonics GmbH, Bremen, Germany) with a Nitrogen 337 nm laser, as described previously (Agger et al., 2014). Sample preparation, data collection, and analysis were performed as previously described (Hegnar et al., 2021).

Results and Discussion

Analysis of the structure and sequence of *Sc*LPMO9A

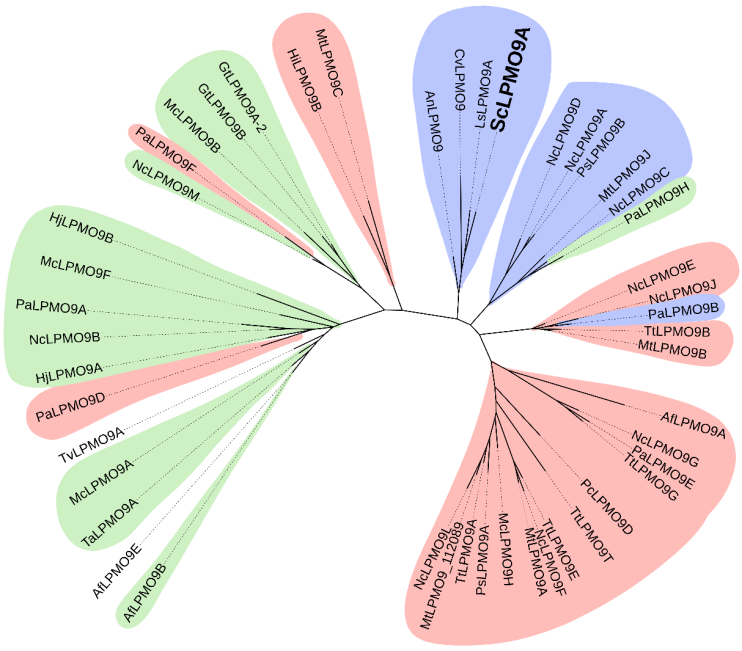

Figure 1. Phylogenetic tree of selected AA9 LPMOs. A multiple-sequence alignment of the catalytic domains of 47 LPMOs, including *Sc*LPMO9A and *Nc*LPMO9C, was performed using T-Coffee Expresso and used to create the phylogenetic tree. The colors in the tree represent LPMO regioselectivity on cellulose (blue: C4-oxidizing; red: C1-oxidizing; green: C1/C4-oxidizing; no color: regioselectivity unknown). All four AA9s grouped in the clade containing *Sc*LPMO9A are active on soluble cello-oligosaccharides.

Phylogenetic analysis of the *Sc*LPMO9A sequence, shown in **Figure 1**, indicated that this enzyme clusters with *Ls*LPMO9A and *Cv*LPMO9, which are C4-oxidizing LPMOs active on soluble cello-oligosaccharides, mixed-linkage glucan, glucomannan, and xyloglucan (Frandsen et

al., 2016; Simmons et al., 2017). Of note, a comparative functional characterization study of *Ls*LPMO9A and *Cv*LPMO9A by Simmons *et al.* indicated that *Ls*LPMO9A has low activity on birchwood xylan, but this specificity was not detected for *Cv*LPMO9A (Simmons et al., 2017). The fourth LPMO clustering with *Sc*LPMO9A (**Figure 1**), *An*LPMO9, is the only one in this cluster with a carbohydrate-binding module (belonging to CAZy family 1, CBM1), and is also known to cleave cellohexaose (Jagadeeswaran et al., 2018). The well-studied CBM1-containing *Nc*LPMO9C from *Neurospora crassa*, shown to be active on cellopentaose, cellohexaose, and to a lesser extent, cellotetraose, in addition to xyloglucan, mixed-linkage glucan, and glucomannan (Agger et al., 2014; Isaksen et al., 2014), appears in the neighboring cluster.

Figure 2. Multiple-sequence alignment of the catalytic domains of the C4-oxidizing AA9s *Sc*LPMO9A, *Ls*LPMO9A, *Cv*LPMO9A, and *Nc*LPMO9C. Sequence identities between *Sc*LPMO9A and the other AA9s are as follows: *Ls*LPMO9A 61.1%, *Cv*LPMO9A 46.6%, *Nc*LPMO9C 45.6%. Fully conserved residues are indicated by an asterisk (*). Active-site histidines are colored blue, and the conserved tyrosine (Tyr163 in *Sc*LPMO9A) involved in copper-coordination (Quinlan et al., 2011) is colored green. Two highly conserved second sphere residues near the copper site (His146 and Gln161) are colored red, whereas a semi-conserved aromatic residue likely involved in substrate-binding (Trp202) is colored purple. Pink arrows and blue rectangles above the amino acid sequences indicate predicted secondary structure elements (sheets and helices, respectively) in the model of *Sc*LPMO9A (using the structure of *Ls*LPMO9A as a template (**Figure 3**). Lines above the sequences represent variable regions in AA9 LPMOs as classified by (Wu et al., 2013) (L2, L3, LS, LC) and (Laurent et al., 2019) (Seg. 1-5).

A comparison of the sequences of *Sc*LPMO9A, *Ls*LPMO9A, *Cv*LPMO9A, and *Nc*LPMO9C (**Figure 2**) shows that residues that make up the histidine brace (His1 and His81), as well as residues in the second coordination sphere of the copper (His146, Gln161, Tyr163), are conserved in *Sc*LPMO9A. Interestingly, *Sc*LPMO9A has a tryptophan (Trp202) at a solvent exposed position where other AA9 LPMOs, including *Ls*LPMO9A, *Nc*LPMO9C, and *Cv*LPMO9A, tend to have a tyrosine. Previous studies have shown that this exposed aromatic residue interacts with bound oligomeric substrates (Courtade et al., 2016; Frandsen et al., 2016) (**Figure 3**). The MSA further shows an alanine residue (Ala78 in *Sc*LPMO9A) shared between *Sc*LPMO9A, *Ls*LPMO9A and *Nc*LPMO9C, known to be common among C4-oxidizing LPMOs, although this correlation is not absolute (e.g., *Cv*LPMO9A has an Asp in this position (Borisova et al., 2015)). The conserved Ser residue (Ser80 in *Sc*LPMO9A) adjacent to the second histidine of the histidine brace is prevalent in C4-oxidizing LPMOs (Beeson et al., 2015). In their study of *Cv*LPMO9A and *Ls*LPMO9A, Simmons *et al.* noted that (weak) xylan-oxidation was only observed for *Ls*LPMO9A. The authors speculated that this may be due to differences in substrate binding residues of the +2 subsite (Asn28, His66, and Asn67 in *Ls*LPMO9A, compared to Thr28, Arg67, and Val68 in *Cv*LPMO9A) (Simmons et al., 2017). *Sc*LPMO9A shares two out of three of these residues with *Ls*LPMO9A (Asn28 and His69), but has an Asp70 in place of the Asn.

A model of *Sc*LPMO9A made using *Ls*LPMO9A bound to cellohexaose as a template, shown in **Figure 3**, depicts a shallow groove type surface topology, similar to what has been reported for *Ls*LPMO9A (Frandsen et al., 2016). This shallow groove topology differs somewhat from the characteristically flat binding surfaces of LPMOs known for their activity on crystalline substrates (Frandsen and Lo Leggio, 2016). Docking of a hexameric substrate by superposition with the structure of *Ls*LPMO9A bound to cellohexaose showed that the hexamer fits well in the

shallow groove of *Sc*LPMO9A, and that binding interactions seen in *Ls*LPMO9A appear to be preserved in *Sc*LPMO9A.

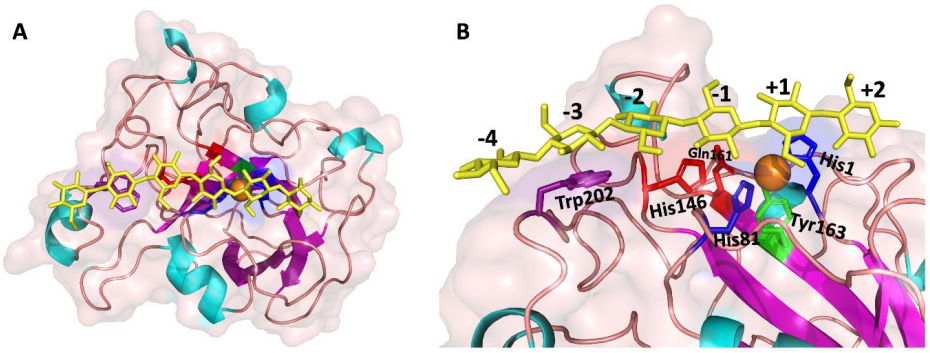

Figure 3. Structural representation of *Sc*LPMO9A seen from the top (A) and a close-up of the substrate binding surface (B). The model was made with PHYRE (Kelley et al., 2015) using the structure of *Ls*LPMO9A (5ACI) as a template. The copper ion coordinated in the active site is shown as an orange sphere. Secondary structure elements are shown in light blue (helices), magenta (strands), and light pink (loop regions). The side chains of the active-site histidines are colored dark blue, and the side chain of the tyrosine in the proximal axial copper coordination site is colored green. The side chains of His146 and Gln161 are colored red, while the side chain of Trp202 is colored purple. A bound cellohexaose unit, with subsite labelling, is shown in yellow. See main text for more details.

Production and consumption of H_2O_2, and redox potential

In order to verify that *E. coli*-expressed *Sc*LPMO9A was correctly folded and copper-saturated, and to ensure it produced and consumed H_2O_2 in a manner expected of AA9 LPMOs, we tested *Sc*LPMO9A in assays adapted from (Kittl et al., 2012) and (Breslmayr et al., 2018). The former assay couples H_2O_2-production by the LPMO (i.e., oxidase activity) to oxidation of Amplex Red by horseradish peroxidase, which can be monitored spectrophotometrically. The latter assay enables spectrophotometric detection of the formation of coerulignone resulting from H_2O_2-dependent oxidation of 2,6-dimethoxyphenol by the LPMO. Purified, copper-saturated *Nc*LPMO9C produced in *P. pastoris* was included for comparative purposes. In both assays, *Sc*LPMO9A performed similarly to *Nc*LPMO9C and in accordance with what has previously been reported for AA9 LPMOs, including for *Nc*LPMO9C (Rieder et al., 2021b; Tõlgo et al., 2022),

indicating that *Sc*LPMO9A was properly folded and contained a coordinated copper in its active site.

The redox potential of *Sc*LPMO9A was determined to be 186 +/- 10 mV, which is a common, albeit rather low value for AA9 LPMOs. For comparison, using the same method, the redox potential of *Nc*LPMO9C was determined to be 224 +/- 3 mV (Borisova et al., 2015).

Mapping activity on cellulosic substrates

To begin mapping of the substrate specificity of *Sc*LPMO9A, three insoluble cellulosic substrates (Avicel, sulfite-pulped spruce, and PASC) were tested. Cellopentaose was also included given the activity of *Sc*LPMO9A homologs on cellodextrins.

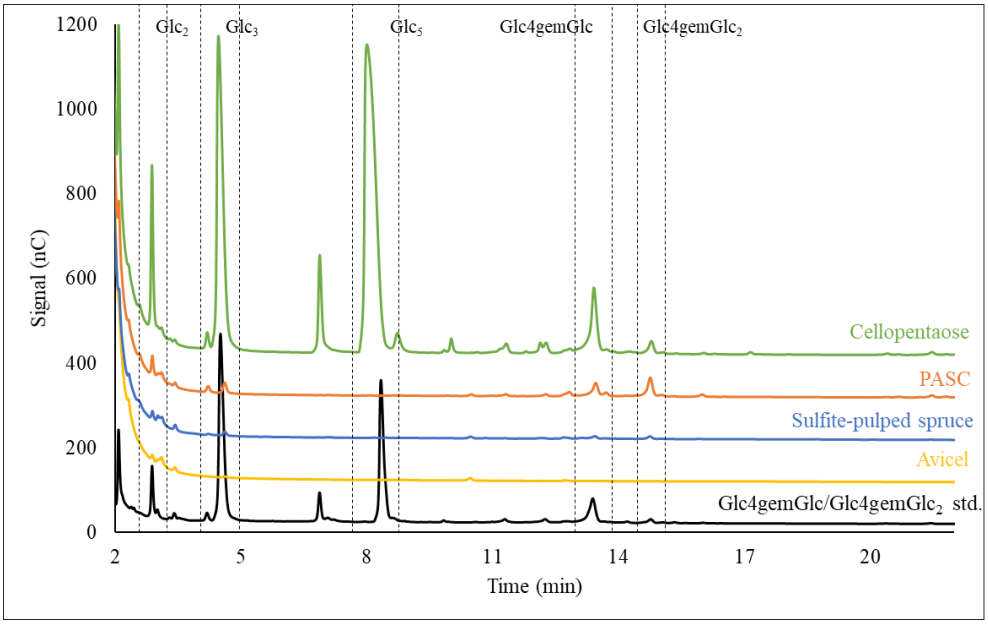

Figure 4. HPAEC-PAD chromatograms of products generated in reactions of *Sc*LPMO9A with cellopentaose (green), PASC (orange), sulfite-pulped spruce (blue), and Avicel (yellow). Sample identities are labeled directly above chromatograms in colors corresponding to the chromatogram. Key products derived from LPMO activity (Glc_2, Glc_3, Glc4gemGlc, $Glc4gemGlc_2$), and Glc_5 are indicated within dashed rectangles. The black chromatogram shows a standard containing Glc4gemGlc and $Glc4gemGlc_2$ (cellopentaose treated with *Nc*LPMO9C; (Müller et al., 2015)). Note that the C4-oxidized products are unstable and that products resulting from tautomerization are visible as minor peaks (Isaksen et al., 2014; Westereng et al., 2016). All reactions were performed with 1 µM LPMO, 2 g/L substrate (or 10 g/L for sulfite-pulped spruce), and 1 mM AscA in 50 mM BisTris-HCl buffer pH 6.5, and were incubated at 40°C and 1000 rpm for 16 h. Control reactions in the absence of AscA did not show any formation of native or C4-oxidized products. All reactions were carried out in triplicate and gave identical product profiles.

HPAEC-PAD analysis of product formation after 16 h of incubation (**Figure 4**) showed that *Sc*LPMO9A is a C4-oxidizing cellulose-active LPMO, as evidenced by the reductant-dependent accumulation of signals representing the C4-oxidized products Glc4gemGlc and $Glc4gemGlc_2$ in reactions with cellopentaose and PASC. No C1-oxidized reaction products were detected for any of the substrates tested. No activity was detected in reactions with the crystalline model substrate Avicel, in contrast to what has been observed for *Nc*LPMO9C, which is active on PASC, Avicel, and cellulose in steam-exploded spruce (Isaksen et al., 2014). The activity of *Sc*LPMO9A on sulfite-pulped spruce, with an expected crystallinity almost as high as Avicel

(Aldaeus et al., 2015), was also low, suggesting that *Sc*LPMO9A has a preference for amorphous cellulose, as present in PASC. The main C4-oxidized product generated from cellopentaose is the C4-oxidized dimer, showing that the substrate preferentially binds from -3 to +2, similar to what has been observed for *Nc*LPMO9C.

To further investigate the activity on soluble cello-oligomers and examine possible differences between *Sc*LPMO9A and *Nc*LPMO9C, reactions with cellotetraose and cellohexaose were analyzed.

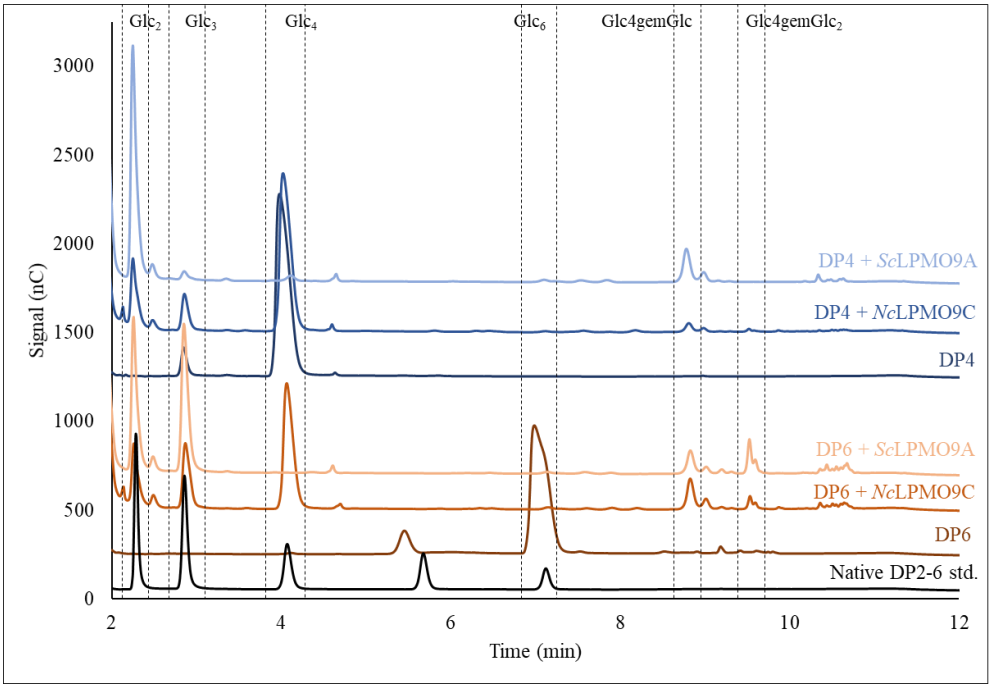

Figure 5. HPAEC-PAD chromatograms for reactions of *Sc*LPMO9A or *Nc*LPMO9C with cellotetraose (DP4) or cellohexaose (DP6). Sample identities are labeled directly above chromatograms in colors corresponding to the relevant chromatogram. Key products derived from LPMO activity (Glc_2, Glc_3, Glc_4, Glc4gemGlc, $Glc4gemGlc_2$), and Glc_6 are indicated within dashed rectangles. Reactions contained 1 mM soluble substrate, 1 µM LPMO, and 1 mM AscA in 50 mM BisTris-HCl pH 6.5, and were incubated at 40°C and 1000 rpm for 16 h. Dark red and dark blue chromatograms show cellohexaose (DP6) and cellotetraose (DP4), respectively, incubated with AscA and without LPMO. A standard consisting of native cello-oligomers from DP2-6 is shown in black. Control reactions in the absence of AscA did not show any formation of native or C4-oxidized products for either LPMO. All reactions were carried out in triplicate and gave identical product profiles.

Figure 5 shows clear differences between *Sc*LPMO9A and *Nc*LPMO9C. As expected based on previous results (Isaksen et al., 2014), *Nc*LPMO9C showed limited activity on cellotetraose (DP4), generating only minor amounts of Glcgem4Glc and native cellobiose after 16 h of incubation. *Sc*LPMO9A, on the other hand, completely degraded cellotetraose into a mixture of cellobiose and Glc4gemGlc. With cellohexaose (DP6), *Nc*LPMO9C generated primarily Glc4gemGlc and cellotetraose, and lesser amounts of cellotriose and $Glc4gemGlc_2$, indicating a preference for -4 - +2 binding. *Sc*LPMO9A, however, appeared to generate more $Glc4gemGlc_2$ than Glc4gemGlc, which is truly a big difference when taking into account that initial -4 - +2 binding will lead to the formation of two Glc4gemGlc (since the resulting native tetramer will be cleaved). While it is not possible to make quantitative statements based on the data in **Figure 5**, it is clear that *Sc*LPMO9A has another preferred binding mode for cellohexaose (-3 - +3) than *Nc*LPMO9C.

Activity on hemicellulosic substrates

The ability of *Sc*LPMO9A to degrade hemicellulosic substrates was assessed and compared with that of *Nc*LPMO9C. Both LPMOs were tested on konjac glucomannan (KGM), mixed-linkage glucan (BG), tamarind xyloglucan (TXG), and xyloglucan oligomers (XGO), alone or in combination with PASC, as various studies have shown that the presence of cellulose may promote LPMO activity on (presumably cellulose-bound) hemicelluloses (Frommhagen et al., 2015; Petrović et al., 2019; Hegnar et al., 2021; Tõlgo et al., 2022). Reactions containing 1 µM LPMO, 1 mM AscA, and 2 g/L hemicellulosic substrate, 2 g/L hemicellulose + 2 g/L PASC, or 4 g/L PASC, were incubated at 40°C and 1000 rpm for 16 h, before products were analyzed by HPAEC-PAD and, in some cases, MALDI-TOF MS. Since these are single time point measurements and

since LPMOs are prone to inactivation, quantitative interpretation of the results presented below requires great care (Eijsink et al., 2019). It should be noted, however, that a suitable substrate protects LPMOs from inactivation, meaning that even if the two LPMOs have different intrinsic susceptibilities to inactivation, major differences in product levels likely reflect a difference in substrate specificity.

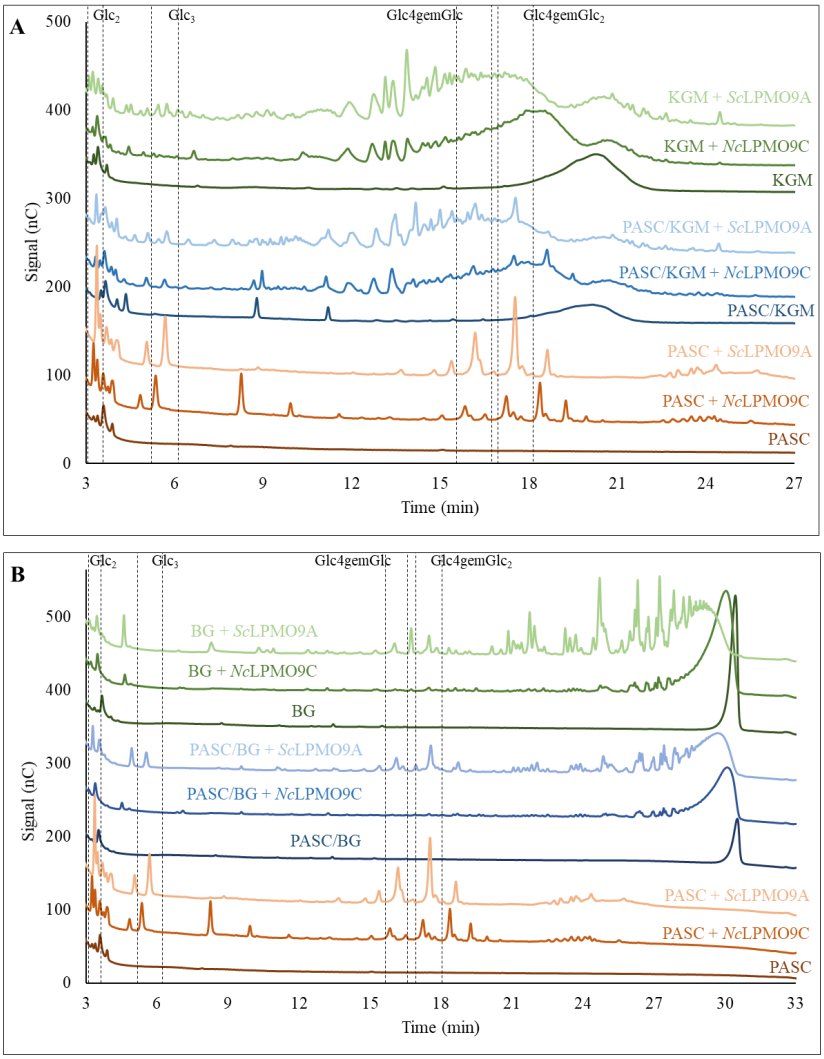

Figure 6. HPAEC-PAD chromatograms for reactions with *Sc*LPMO9A or *Nc*LPMO9C and PASC, konjac glucomannan (KGM), mixed-linkage (β-1,3;1-4) glucan (BG), or mixtures of PASC and KGM or BG. Panel A shows reactions with PASC and KGM, while Panel B shows reactions with PASC and BG. Reaction set-ups are indicated directly above chromatograms in colors corresponding to the relevant chromatogram (all reactions contained 1 mM AscA). Reactions contained 1 µM LPMO, 1 mM AscA, and either 2 g/L KGM or BG, or, in the reactions containing hemicellulosic substrate and PASC, 2 g/L of each substrate (4 g/L total substrate concentration). Reactions with PASC alone contained 4 g/L PASC. Reactions were incubated in 50 mM BisTris-HCl pH 6.5 at 40°C and 1000 rpm for 16 h. Key products derived from LPMO activity on PASC (Glc_2, Glc_3, Glc4gemGlc, $Glc4gemGlc_2$) are indicated within dashed rectangles (note that there is a slight shift between the PASC + *Sc*LPMO9A and the PASC + *Nc*LPMO9C chromatograms). Control reactions in the absence of AscA did not show any product formation for either LPMO. All reactions were carried out in triplicate and gave similar product profiles.

Reactions with KGM showed activity of *Sc*LPMO9A and this activity seemed hardly affected by the presence of PASC (**Figure 6A**). The product profiles of the two enzymes show differences that may indicate differences in substrate-binding preferences and abilities. In particular, *Sc*LPMO9A generates more early-eluting products (5–10 minute region). It is also worth noting the substantially higher peak intensities for products generated by *Sc*LPMO9A acting on KGM alone compared to the analogous reaction with *Nc*LPMO9C. The data thus indicate that the two LPMOs have different affinities for glucomannan and/or that they have different cleavage pattern preferences.

Figure 6B shows that *Sc*LPMO9A is clearly more active on BG than *Nc*LPMO9C, both in reactions with BG alone and in reactions with BG and PASC. The activity difference is most pronounced in the reactions with BG alone, since the reaction of *Sc*LPMO9A with a mixture of PASC and BG yielded less BG-derived products than the reaction with BG alone. The chromatograms for the reactions with *Sc*LPMO9A show a larger variety of products as compared to *Nc*LPMO9C, but this may partly be a false impression due to the general difference in activity. However, one clear and striking difference stands out: when acting on BG alone, in contrast to *Nc*LPMO9C, *Sc*LPMO9A generates a relatively high amount of products eluting in the 15–19-minute region, which likely are C4-oxidized glucan fragments such as Glc4gemGlc and Glc4gemGlc$_2$. This indicates that *Sc*LPMO9A has a greater ability to convert BG to small oligomeric products and is, thus, less inhibited by the β-(1,3) bonds in BG.

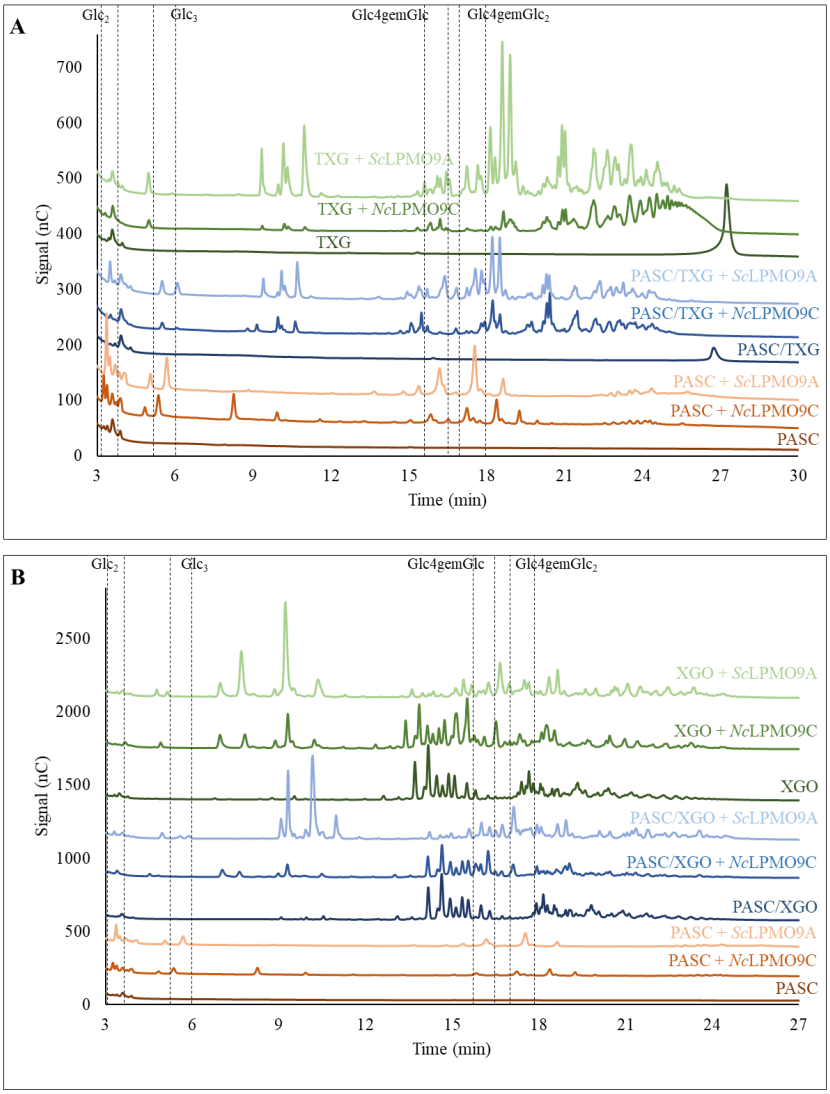

Figure 7. HPAEC-PAD chromatograms for reactions with *Sc*LPMO9A or *Nc*LPMO9C and PASC, tamarind xyloglucan (TXG), xyloglucan oligomers (XGO), or mixtures of PASC and TXG or XGO. Panel A shows reactions with PASC and TXG, while Panel B shows reactions with PASC and XGO. Reaction set-ups are indicated directly above the chromatograms in colors corresponding to the relevant chromatogram (all reactions contained 1 mM AscA). Reactions contained 1 µM LPMO, 1 mM AscA, and either 2 g/L TXG or XGO, or, in the reactions containing hemicellulosic substrate and PASC, 2 g/L of each substrate (4 g/L total substrate concentration). Reactions with PASC alone contained 4 g/L PASC. Reactions were incubated in 50 mM BisTris-HCl pH 6.5 at 40°C and 1000 rpm for 16 h. Key products derived from LPMO activity on PASC (Glc_2, Glc_3, Glc4gemGlc, $Glc4gemGlc_2$) are indicated within dashed rectangles (note that there is a slight shift between the PASC + *Sc*LPMO9A and the PASC + *Nc*LPMO9C chromatograms). Control reactions in the absence of AscA did not show any product formation for either LPMO. All reactions were carried out in triplicate and gave similar product profiles.

HPAEC-PAD chromatograms for reactions with TXG (**Figure 7A**) showed clear activity of *Sc*LPMO9A and *Nc*LPMO9C, both in reactions with PASC/TXG and reactions with TXG alone. *Sc*LPMO9A seemed to generate more products than *Nc*LPMO9C, especially in reactions with only TXG. Overall, the product patterns of the two enzymes look similar and these patterns resemble those generated by previously described LPMOs (including *Nc*LPMO9C) that act on xyloglucan and that are "substitution-sensitive," where the latter means that they only, or primarily, cleave the glucan chain at a non-substituted glucose (Nekiunaite et al., 2016; Monclaro et al., 2020; Sun et al., 2020). Still, **Figure 7A** shows minor differences in the product spectra of the two LPMOs and such differences were also observed when analyzing reactions with a mixture of xyloglucan oligosaccharides, XGO (**Figure 7B**). Thus, the two enzymes do display different cleavage preferences when acting on xyloglucan.

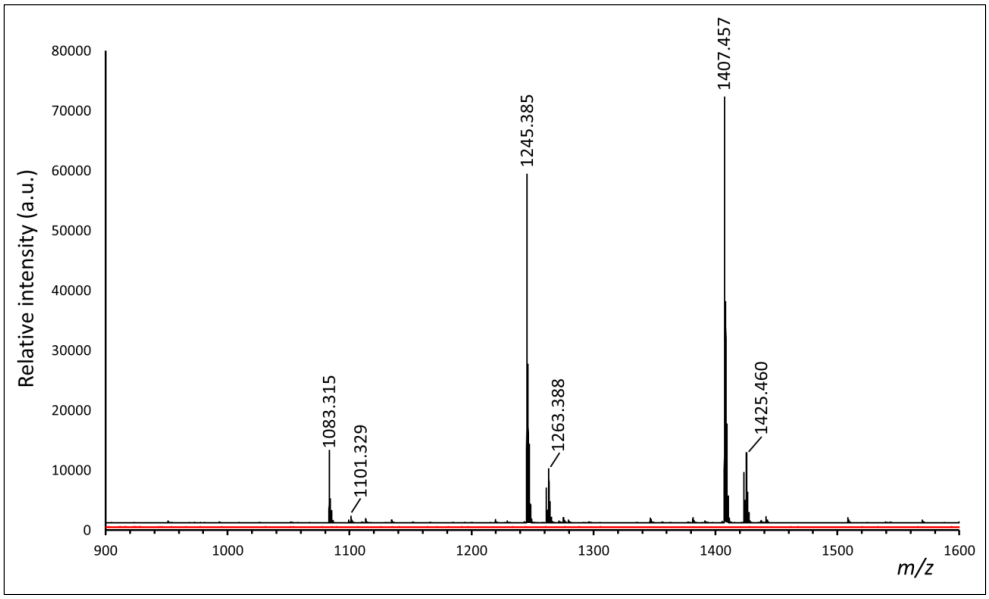

Figure 8. MALDI-TOF MS analysis of products generated in reactions of *Sc*LPMO9A with TXG in the presence of AscA. The spectrum shows the samples analyzed with HPAEC-PAD in **Figure 7A**. The red spectrum shows the corresponding reaction without AscA. The labeled products are the sodium adducts of oxidized species in the non-hydrated keto form (e.g. *m/z* 1083.3) and, to a lesser extent, the corresponding geminal diol form (e.g. *m/z* 1101.3), for GXXX (Hex_4Pen_3), GXXL (Hex_5Pen_3), and GXLL (Hex_6Pen_3), where G is glucose, X is glucose substituted with xylose and L is X substituted with galactose. Note that the positions of the various main chain units (G, X, L) cannot be derived from the MS data. The absence of fragments containing less or more than three pentoses (e.g. 951 for Hex_4Pen_2, or 1539 for Hex_6Pen_4) indicates that the LPMO only cleaves the main chain of TXG at unsubstituted glucoses.

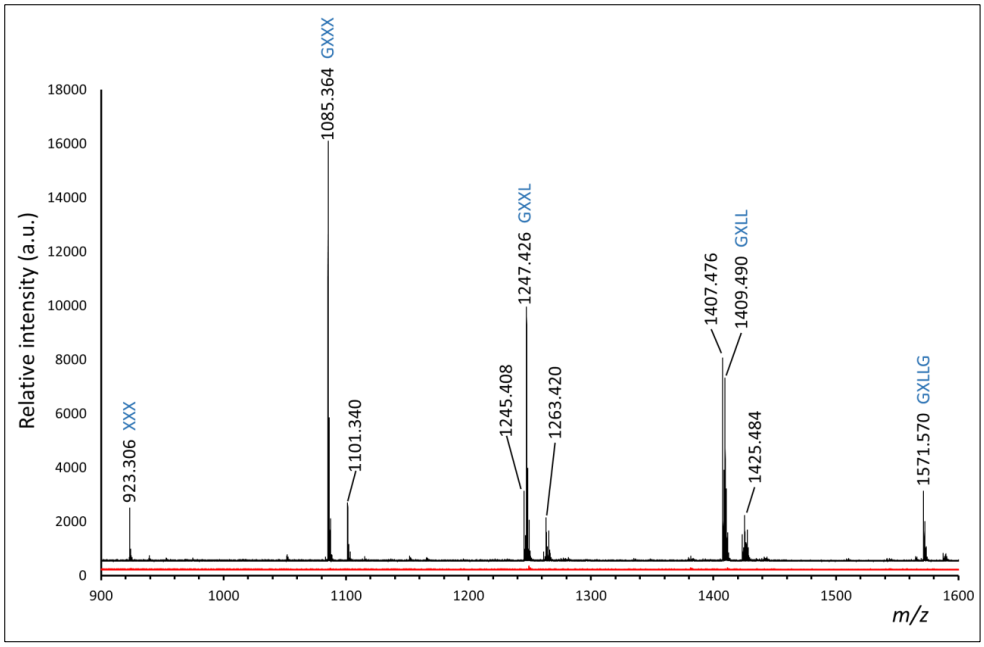

Figure 9. MALDI-TOF analysis of products generated in reactions of *Sc*LPMO9A with XGO in the presence of AscA. The spectrum shows the samples analyzed with HPAEC-PAD in **Figure 7B**. The red spectrum shows the corresponding reaction without AscA. The labeled products are the sodium adducts of native and oxidized species, the formation of which is reductant-dependent. The identities of the native xyloglucan species labeled according to standard xyloglucan nomenclature (G: glucose; X: glucose substituted with a xylose; L: X substituted with a galactose) are indicated in blue next to the *m/z* values. The oxidized keto (-2 *m/z* from the native) and geminal diol (+16 *m/z* from the native) forms of GXXL (Hex_5Pen_3) and GXLL (Hex_6Pen_3) were detected, but only the geminal diol form was detected for oxidized GXXX (Hex_4Pen_3); the signal possibly reflecting this hydrated oxidized product (*m/z* 1101) may also represent a potassium adduct of non-oxidized GXXX.

MALDI-TOF MS analysis of products generated in the reaction with TXG confirmed that *Sc*LPMO9A is substitution-sensitive, since all abundant products contained three pentoses (see **Figure 8** and its legend). The mass spectrum for the various tetrameric products showed xyloglucan-derived oxidized species differing by *m/z* 162 and all containing 3 pentoses (*m/z* 132), corresponding to the oxidized non-hydrated keto species and the hydrated geminal diol species of xyloglucan forms GXXX, GXXL, and GXLL (where G is a β-1,4-linked D-glucose unit, X is a glucosyl substituted with a α-1,6-linked D-xylose, and L corresponds to X but with a further substitution of the xylose with a β-1,2-linked D-galactose, according to standard xyloglucan

nomenclature (Fry et al., 1993)). This TXG product pattern resembles what has previously been observed for *Nc*LPMO9C acting on xyloglucan (Agger et al., 2014; Sun et al., 2020). If *Sc*LPMO9A would be able to cleave next to substituted sugars, other products would also have been observed in the spectrum shown in **Figure 8**, such as at *m/z* 951 (4 hexoses, 2 pentoses) and *m/z* 1539 (6 hexoses, 4 pentoses), as has indeed been observed for TXG-active LPMOs that are less substitution-sensitive (Monclaro et al., 2020; Sun et al., 2020).

MALDI-TOF MS analysis of products generated by *Sc*LPMO9A in the reaction with XGO (**Figure 9**) showed an accumulation of native and oxidized products, including the native XXX (*m/z* 923), GXXX (m/z 1085), GXXL (*m/z* 1247), GXLL (*m/z* 1409), and GXLLG (*m/z* 1571), and oxidized GXXL (*m/z* 1245/1263) and GXLL (*m/z* 1407/1425). This pattern resembles what has previously been shown for *Nc*LPMO9C (Agger et al., 2014; Kojima et al., 2016), and confirms that, like *Nc*LPMO9C, *Sc*LPMO9A cleaves the xyloglucan backbone primarily adjacent to non-substituted glycosyl units.

Screening of *Sc*LPMO9A activity on beechwood xylan, birchwood xylan, and wheat arabinoxylan in combination with PASC, using MALDI-TOF MS for product detection, showed products identical to those observed in reactions with only PASC, while reactions with these substrates alone showed no product formation. Despite differing from *Ls*LPMO9A (for which weak xylan activity has been reported) in only one of the three substrate-binding residues purported to contribute to xylan activity, and despite this difference being minimal (Asn → Asp), *Sc*LPMO9A did not show reductant-dependent oxidative activity towards xylan.

Synergy with cellulases

The contribution of LPMOs to the saccharification of cellulose, including cellulose in sulfite-pulped spruce, is well-documented. LPMO-containing cellulase cocktails work better under conditions that promote LPMO activity (Chylenski et al., 2017; Müller et al., 2018), while addition of LPMOs improves the saccharification power of LPMO-poor cellulase cocktails (Müller et al., 2015; Tuveng et al., 2020). Interestingly, saccharification reactions with sulfite-pulped spruce, under conditions previously used to reveal the clear impact of cellulose-active LPMOs, showed that *Sc*LPMO9A did not boost cellulase hydrolysis by an LPMO-poor cellulase cocktail (**Figure 10A**). The reaction with AscA and the LPMO did show some LPMO product formation (**Figure 10B**), but the glucose production was decreased rather than increased, probably due to the lower cellulase content of this reaction. While higher than in reactions without supplemented LPMO, Glc4gemGlc product levels for the reaction with *Sc*LPMO9A are low compared to what one would expect for a truly cellulose-active LPMO (e.g. (Müller et al., 2018)) and decreased over time, which is due to product instability and indicates that LPMO activity had already stopped at the first measuring point, indicative of limited substrate availability. Considering the results described above, indicating that *Sc*LPMO9A only acts on soluble and amorphous substrates, it is likely that these low levels of LPMO products result from action on amorphous subfractions of the material, the degradation of which does not affect overall saccharification efficiency.

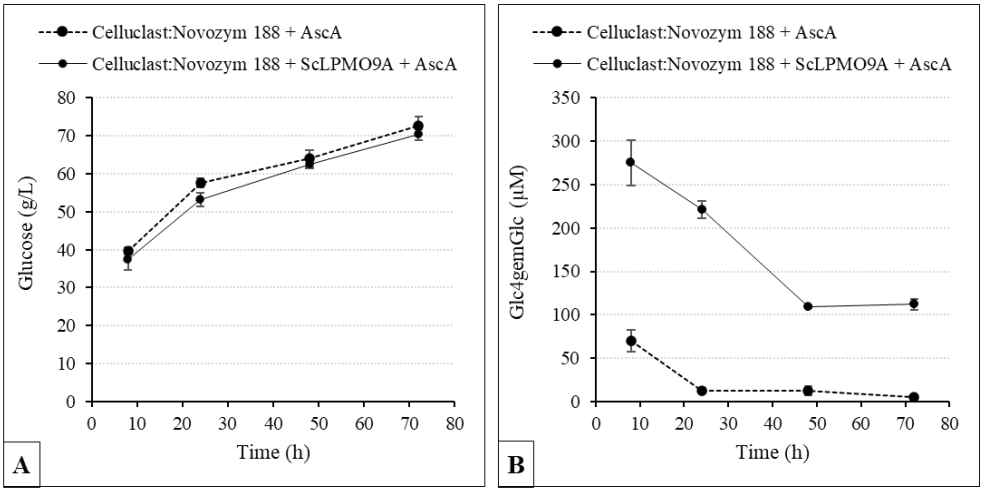

Figure 10. Degradation of sulfite-pulped spruce by an LPMO-poor cellulase blend with or without added ScLPMO9A. Panel A shows glucose yield, and Panel B shows production of Glc4gemGlc. The substrate (10% w/w) was incubated with a Celluclast:Novozym 188 blend in 50 mM sodium acetate buffer pH 5.0. In reactions with LPMO, 10% of this blend was replaced with ScLPMO9A (on a protein basis). Reactions were initiated by adding 1 mM AscA, and incubated at 50°C with orbital shaking at 200 rpm.

Effect of H_2O_2 on oxidized product formation from PASC and cellopentaose

It is now well-established that LPMOs preferentially utilize H_2O_2 as a co-substrate to cleave glycosidic bonds and that the resulting peroxygenase reaction is fast (Bissaro et al., 2017; Kuusk et al., 2018; Rieder et al., 2021b). However, surplus concentrations of H_2O_2 can lead to auto-catalytic oxidation of non-substrate bound LPMOs (Bissaro et al., 2017; Kuusk et al., 2019; Kuusk and Väljamäe, 2021). To assess the ability of *Sc*LPMO9A to productively use H_2O_2, we tested the effect of different initial concentrations of exogenously supplied H_2O_2 on the activity of *Sc*LPMO9A on PASC (**Figure 11**).

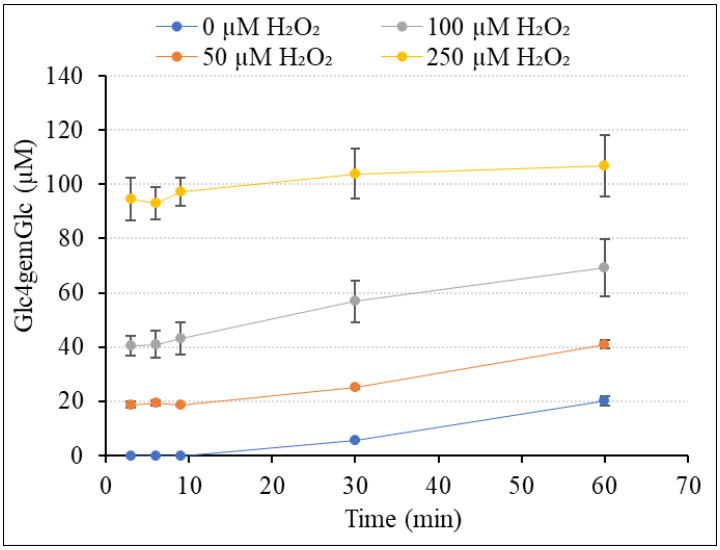

Figure 11. Effect of H_2O_2 on Glc4gemGlc production by *Sc*LPMO9A in reactions with PASC. The figure shows the production of Glc4gemGlc by 1 µM *Sc*LPMO9A in reactions containing 2 g/L PASC, 1 mM AscA, and different initial concentrations of supplemented H_2O_2 (0, 50, 100, or 250 µM). Reactions were performed in 50 mM Tris-HCl pH 7.5 at 45°C and 1000 rpm. Control reactions lacking AscA did not show any formation of Glc4gemGlc. Error bars represent standard deviations between triplicates.

Without addition of H_2O_2, accumulation of Glc4gemGlc happened at a rate in the order of 0.3 min^{-1} (estimated from the progress curve in **Figure 11**). Assuming that Glc4gemGlc represents about 40 % of LPMO cleavages (see below for justification), this means that the LPMO operated at a rate in the order of 0.8 min^{-1}. Such low rates are commonly observed for LPMOs in AscA driven reactions (Bissaro et al., 2018). Addition of H_2O_2 led to a dramatic increase in reaction speed: at the first measuring point, after 3 minutes, Glc4gemGlc levels amounted to approximately 40 % of the added H_2O_2 for all three levels of inclusion. The progress curves starting at 3 minutes show slopes quite similar to the curve for the reaction with AscA only. This clearly shows that all H_2O_2 was consumed after 3 minutes and that the rest of the reaction was AscA-driven. The fact that the levels of Glc4gemGlc after 3 minutes amounted to 40 % of added H_2O_2 shows that some 60 % of LPMO products emerge as other soluble products or are not soluble (i.e., oxidized sites

remaining in the insoluble substrate). As a rule of thumb, one would expect some 50 % of oxidized products to remain in the insoluble substrate in reactions with an LPMO that does not carry a CBM (Courtade et al., 2018). Notably, the progress curve for the reaction with the highest H_2O_2 concentration, 250 µM, shows signs of enzyme inactivation, since the slope of the curve after 3 minutes is lower compared to the other progress curves.

Importantly, the data shows that *Sc*LPMO9A generates Glc4gemGlc very rapidly when supplied with H_2O_2, and uses this co-substrate stoichiometrically to produce Glc4gemGlc. Based on the 3-minute time point for the reaction with 250 µM H_2O_2, the enzyme operated with a rate of at least some 80 min^{-1}, which is two orders of magnitude higher compared to the reaction with AscA only. Thus, *Sc*LPMO9A is a fast consumer of H_2O_2, and preferentially uses this co-substrate stoichiometrically to produce Glc4gemGlc.

Rieder *et al.* have shown that when supplied with H_2O_2 and a soluble substrate, *Nc*LPMO9C is a very efficient peroxygenase, reaching catalytic rates above 100 s^{-1} and with the ability to productively use large amounts of H_2O_2 to stoichiometrically degrade the cello-oligomer substrate (Rieder et al., 2021b). **Figure 12** shows progress curves for one-minute reactions of *Sc*LPMO9A with cellopentaose at two initial H_2O_2 concentrations. When supplemented with 200 µM H_2O_2 (**Figure 12A**), near complete stoichiometric conversion of H_2O_2 was achieved within 30 s. Based on the first 10 s of the experiment, *Sc*LPMO9A reached a rate of at least 11 s^{-1}. When the H_2O_2 concentration was increased to 400 µM (**Figure 12B**), *Sc*LPMO9A generated slightly less than 300 µM product in 1 min. Although initial rates appeared higher than when supplemented with 200 µM H_2O_2 (at least 15 s^{-1}), under these conditions stoichiometric conversion of H_2O_2 was not observed, and the reaction showed signs of LPMO inactivation and/or reductant depletion. Of note, the ratio between Glc_2 and Glc_3 differs between panels A and B, which could be due to

oxidative damage to the enzyme active site at the higher H_2O_2 concentration, which may cause changes in the preferred substrate binding mode (Hangasky et al., 2018).

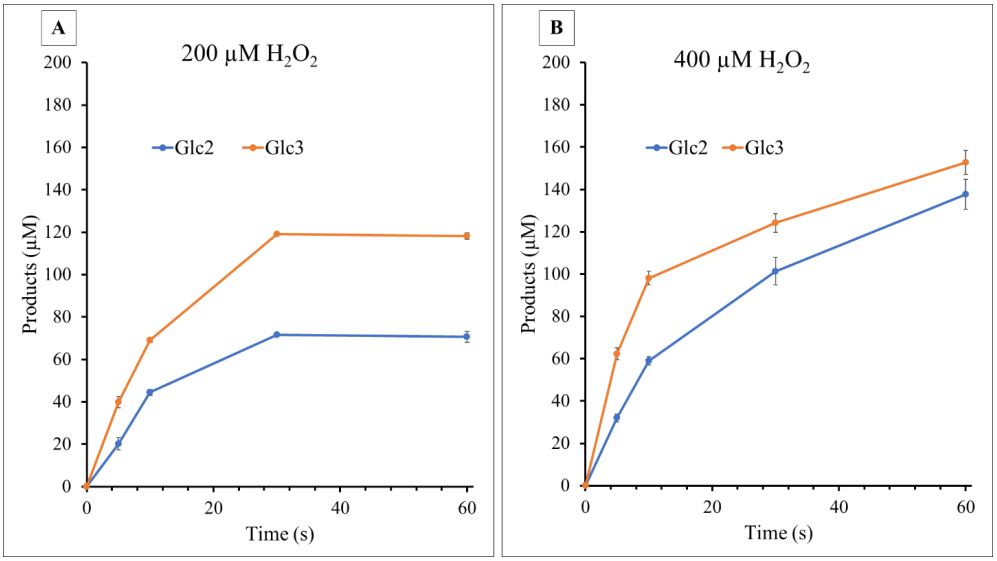

Figure 12. Peroxygenase activity of ScLPMO9A acting on cellopentaose. The figure shows time courses for product formation in reactions containing 1 µM *Sc*LPMO9A, 50 µM AscA, 1 mM cellopentaose, and 200 µM (Panel A) or 400 µM (Panel B) H_2O_2. Reactions were performed in 50 mM sodium acetate buffer pH 5.0 and were incubated at 40°C and 500 rpm. Note that cleavage of cellopentaose leads either to a dimeric or a trimeric product; for example, in panel A, at 30 s, approximately 190 mM of cellopentaose has been converted, resulting in 70 µM of dimer and 120 µM of trimer. Samples were taken at 5, 10, 30, and 60 s. Error bars represent standard deviations between triplicates.

Concluding Remarks

The data presented in the present study show that *Sc*LPMO9A is a C4-oxidizing LPMO with activity on amorphous cellulose, soluble cello-oligosaccharides and various hemicellulose glycans, and limited ability to contribute to the saccharification of crystalline cellulose. The complete degradation of 1 mM cellotetraose under the conditions tested is of particular interest, since this is not commonly observed in LPMOs active on cello-oligomers (Isaksen et al., 2014). Further in-depth analysis of the substrate-binding residues surrounding the active site of

*Sc*LPMO9A, preferably based on crystal structures, is needed to explain the structural basis for the observed activity on cellotetraose.

Comparison of *Sc*LPMO9A and *Nc*LPMO9C in the degradation of glucomannan, mixed-linkage glucan, and xyloglucan, showed that the enzymes have similar properties, such as both being substitution-sensitive in TXG degradation. The product profiles did show subtle differences however, which indicate functional differences that merit further study. The relative peak intensities observed in HPAEC-PAD analysis indicate that *Sc*LPMO9A may have stronger activity on selected hemicellulosic substrates, especially in the absence of cellulose. In contrast to what has been observed for *Ls*LPMO9A (Simmons et al., 2017), its close homolog, *Sc*LPMO9A did not show any activity on the xylan substrates tested in this study.

During the course of this study, a study containing comparative functional data for eight fungal C4-oxidizing LPMOs, including *Sc*LPMO9A, was published (Frandsen et al., 2021). All these LPMOs were expressed in the yeast *Pichia pastoris* and shown to be active on cello-oligomers and/or hemicellulosic glycans, albeit with seemingly different efficiencies. Remarkably, while some of the LPMOs described in this study seemed to show a substrate spectrum similar to the two LPMOs studied above, Frandsen *et al.* concluded that ScLPMO9A is not active on glucomannan and TXG, nor on cellotetraose. Clearly, the conclusions of the present study are quite different.

The discovery that LPMOs may use H_2O_2 rather than O_2 to break down glycosidic bonds has created some controversy, but has also shown that LPMOs are faster enzymes than originally believed. As an example, the recent work by (Frandsen et al., 2021) reports rates for cellohexaose conversion in a "monooxygenase" (i.e. reductant-driven) reaction in the order of 1 min^{-1}, which, notably, is enormously slow, but common in the LPMO field. On the other hand, using

peroxygenase conditions, Rieder *et al.* recently reported rates of >100 s^{-1} for conversion of cellopentaose by *Nc*LPMO9C (Rieder et al., 2021b). Although *Sc*LPMO9A appears to be more sensitive to H_2O_2 than *Nc*LPMO9C under the conditions tested in the present study, *Sc*LPMO9A still uses H_2O_2 very efficiently when acting on cellopentaose, reaching a rate of approx. 11 s^{-1} when supplied with 200 µM H_2O_2. We also show that *Sc*LPMO9A readily uses H_2O_2 to degrade PASC, reaching rates in the order of at least several per second rather than about 1 min^{-1}. To the best of our knowledge, this is the first time that such a high LPMO activity is demonstrated on this much used amorphous cellulosic substrate.

All in all, *Sc*LPMO9A seems specifically tailored to work on amorphous and soluble substrates, as also suggested by its inability to boost degradation of sulfite-pulped spruce by an LPMO-poor cellulase cocktail. As such, *Sc*LPMO9A resembles recently described *Af*AA11B, a chitin-active LPMO which was shown to, in fact, have little activity on insoluble chitin, while being very active on soluble chito-oligosaccharides (Rieder et al., 2021a).

Given that powerful hydrolytic cellulases co-secreted with LPMOs in natural biomass-degrading ecosystems readily depolymerize soluble oligosaccharides, it is unlikely that fungi have evolved LPMOs with the specialized purpose of degrading these oligomers. Thus, it is conceivable that enzymes such as *Sc*LPMO9A play hitherto undiscovered roles in lignocellulose conversion, or perhaps even the conversion of non-lignocellulosic substrates. In this regard, the strong activity of *Sc*LPMO9A on soluble cello-oligomers, and its lack of activity on crystalline cellulose, are intriguing and warrant further investigation.

Associated Content

Author information

Corresponding author:
Vincent G. H. Eijsink
Email: vincent.eijsink@nmbu.no
Phone: +47 67232463
Postal address: Norwegian University of Life Sciences (NMBU), Faculty of Chemistry, Biotechnology, and Food Science, P.O. Box 5003, N-1432 Ås, Norway

Author contributions:
H.Ø. designed experiments, performed research, analyzed data, and wrote the first draft of the manuscript. I.A.C., K.H., and G.C. designed experiments, performed research, and analyzed data. A.V. designed experiments, analyzed data, and carried out supervision. O.A.H. designed experiments, performed research, analyzed data, and edited the manuscript. F.L.A. and V.G.H.E. initiated the research, analyzed data, edited the manuscript, carried out supervision, and acquired funding.

Funding:
This work was funded by the Norwegian Research Council (NFR) through projects 268002, 269408, and 270038.

Conflict of interest disclosure:
The authors declare no competing interests.

References

AACHMANN, F. L., SØRLIE, M., SKJÅK-BRÆK, G., EIJSINK, V. G. H., & VAAJE-KOLSTAD, G. 2012. NMR structure of a lytic polysaccharide monooxygenase provides insight into copper binding, protein dynamics, and substrate interactions, *Proceedings of the National Academy of Sciences of the United States of America*, 109: 18779-18784.

AGGER, J. W., ISAKSEN, T., VÁRNAI, A., VIDAL-MELGOSA, S., WILLATS, W. G. T., LUDWIG, R., HORN, S. J., EIJSINK, V. G. H., & WESTERENG, B. 2014. Discovery of LPMO activity on hemicelluloses shows the importance of oxidative processes in plant cell wall degradation, *Proceedings of the National Academy of Sciences of the United States of America*, 111: 6287-6292.

ALDAEUS, F., LARSSON, K., SRNDOVIC, J. S., KUBAT, M., KARLSTRÖM, K., PECIULYTE, A., OLSSON, L., & LARSSON, P. T. 2015. The supramolecular structure of cellulose-rich wood pulps can be a determinative factor for enzymatic hydrolysability, *Cellulose*, 22: 3991-4002.

ALMÁSI, É., SAHU, N., KRIZSÁN, K., BÁLINT, B., KOVÁCS, G. M., KISS, B., CSEKLYE, J., DRULA, E., HENRISSAT, B., NAGY, I., CHOVATIA, M., ADAM, C., LABUTTI, K., LIPZEN, A., RILEY, R., GRIGORIEV, I. V., & NAGY, L. G. 2019. Comparative genomics reveals unique wood-decay strategies and fruiting body development in the *Schizophyllaceae*, *New Phytologist*, 224: 902-915.

ARMOUGOM, F., MORETTI, S., POIROT, O., AUDIC, S., DUMAS, P., SCHAELI, B., KEDUAS, V., & NOTREDAME, C. 2006. Expresso: automatic incorporation of structural information in multiple sequence alignments using 3D-Coffee, *Nucleic Acids Research*, 34: 604-608.

BEESON, W. T., PHILLIPS, C. M., CATE, J. H., & MARLETTA, M. A. 2012. Oxidative cleavage of cellulose by fungal copper-dependent polysaccharide monooxygenases, *Journal of the American Chemical Society*, 134: 890-892.

BEESON, W. T., VU, V. V., SPAN, E. A., PHILLIPS, C. M., & MARLETTA, M. A. 2015. Cellulose degradation by polysaccharide monooxygenases, *Annual Review of Biochemistry*, 84: 923-946.

BISSARO, B., RØHR Å, K., MÜLLER, G., CHYLENSKI, P., SKAUGEN, M., FORSBERG, Z., HORN, S. J., VAAJE-KOLSTAD, G., & EIJSINK, V. G. H. 2017. Oxidative cleavage of polysaccharides by monocopper enzymes depends on H_2O_2, *Nature Chemical Biology*, 13: 1123-1128.

BISSARO, B., VÁRNAI, A., RØHR, Å. K., & EIJSINK, V. G. H. 2018. Oxidoreductases and reactive oxygen species in conversion of lignocellulosic biomass, *Microbiology and Molecular Biology Reviews*, 82: e00029-00018.

BORISOVA, A. S., ISAKSEN, T., DIMAROGONA, M., KOGNOLE, A. A., MATHIESEN, G., VÁRNAI, A., RØHR, Å. K., PAYNE, C. M., SØRLIE, M., SANDGREN, M., & EIJSINK, V. G. H. 2015. Structural and functional characterization of a lytic polysaccharide monooxygenase with broad substrate specificity, *Journal of Biological Chemistry*, 290: 22955-22969.

BRANDER, S., TOKIN, R., IPSEN, J. Ø., JENSEN, P. E., HERNÁNDEZ-ROLLÁN, C., NØRHOLM, M. H. H., LO LEGGIO, L., DUPREE, P., & JOHANSEN, K. S. 2021. Scission of glucosidic bonds by a *Lentinus similis* lytic polysaccharide monooxygenases is strictly dependent on H_2O_2 while the oxidation of saccharide products depends on O_2, *ACS Catalysis*, 11: 13848-13859.

BRESLMAYR, E., HANŽEK, M., HANRAHAN, A., LEITNER, C., KITTL, R., ŠANTEK, B., OOSTENBRINK, C., & LUDWIG, R. 2018. A fast and sensitive activity assay for lytic polysaccharide monooxygenase, *Biotechnology for Biofuels*, 11: 79.

CANNELLA, D., HSIEH, C.-W. C., FELBY, C., & JØRGENSEN, H. 2012. Production and effect of aldonic acids during enzymatic hydrolysis of lignocellulose at high dry matter content, *Biotechnology for Biofuels*, 5: 26.

CHALAK, A., VILLARES, A., MOREAU, C., HAON, M., GRISEL, S., D'ORLANDO, A., HERPOËL-GIMBERT, I., LABOUREL, A., CATHALA, B., & BERRIN, J.-G. 2019. Influence of the carbohydrate-binding module on the activity of a fungal AA9 lytic polysaccharide monooxygenase on cellulosic substrates, *Biotechnology for Biofuels*, 12: 206.

CHYLENSKI, P., PETROVIĆ, D. M., MÜLLER, G., DAHLSTRÖM, M., BENGTSSON, O., LERSCH, M., SIIKA-AHO, M., HORN, S. J., & EIJSINK, V. G. H. 2017. Enzymatic degradation of sulfite-pulped softwoods and the role of LPMOs, *Biotechnology for Biofuels*, 10: 177.

COSTA, T. H. F., KADIC, A., CHYLENSKI, P., VÁRNAI, A., BENGTSSON, O., LIDÉN, G., EIJSINK, V. G. H., & HORN, S. J. 2020. Demonstration-scale enzymatic saccharification of sulfite-pulped spruce with addition of hydrogen peroxide for LPMO activation, *Biofuels, Bioproducts and Biorefining*, 14: 734-745.

COURTADE, G., FORSBERG, Z., HEGGSET, E. B., EIJSINK, V. G. H., & AACHMANN, F. L. 2018. The carbohydrate-binding module and linker of a modular lytic polysaccharide monooxygenase promote localized cellulose oxidation, *Journal of Biological Chemistry*, 293: 13006-13015.

COURTADE, G., LE, S. B., SÆTROM, G. I., BRAUTASET, T., & AACHMANN, F. L. 2017. A novel expression system for lytic polysaccharide monooxygenases, *Carbohydrate Research*, 448: 212-219.

COURTADE, G., WIMMER, R., RØHR, Å. K., PREIMS, M., FELICE, A. K. G., DIMAROGONA, M., VAAJE-KOLSTAD, G., SØRLIE, M., SANDGREN, M., LUDWIG, R., EIJSINK, V. G. H., & AACHMANN, F. L. 2016. Interactions of a fungal lytic polysaccharide monooxygenase with β-glucan substrates and cellobiose dehydrogenase, *Proceedings of the National Academy of Sciences of the United States of America*, 113: 5922-5927.

DARRIBA, D., TABOADA, G. L., DOALLO, R., & POSADA, D. 2011. ProtTest 3: fast selection of best-fit models of protein evolution, *Bioinformatics*, 27: 1164-1165.

DRULA, E., GARRON, M.-L., DOGAN, S., LOMBARD, V., HENRISSAT, B., & TERRAPON, N. 2022. The carbohydrate-active enzyme database: functions and literature, *Nucleic Acids Research*, 50: D571-D577.

EIJSINK, V. G. H., PETROVIĆ, D., FORSBERG, Z., MEKASHA, S., RØHR, A. K., VÁRNAI, A., BISSARO, B., & VAAJE-KOLSTAD, G. 2019. On the functional characterization of lytic polysaccharide monooxygenases (LPMOs), *Biotechnology for Biofuels*, 12: 58.

FORSBERG, Z., MACKENZIE, A. K., SØRLIE, M., RØHR, Å. K., HELLAND, R., ARVAI, A. S., VAAJE-KOLSTAD, G., & EIJSINK, V. G. H. 2014. Structural and functional characterization of a conserved pair of bacterial cellulose-oxidizing lytic polysaccharide monooxygenases, *Proceedings of the National Academy of Sciences of the United States of America*, 111: 8446-8451.

FRANDSEN, K. E. H., HAON, M., GRISEL, S., HENRISSAT, B., LO LEGGIO, L., & BERRIN, J.-G. 2021. Identification of the molecular determinants driving the substrate specificity of fungal lytic polysaccharide monooxygenases (LPMOs), *Journal of Biological Chemistry*, 296: 100086.

FRANDSEN, K. E. H. & LO LEGGIO, L. 2016. Lytic polysaccharide monooxygenases: a crystallographer's view on a new class of biomass-degrading enzymes, *IUCrJ*, 3: 448-467.

FRANDSEN, K. E. H., SIMMONS, T. J., DUPREE, P., POULSEN, J.-C. N., HEMSWORTH, G. R., CIANO, L., JOHNSTON, E. M., TOVBORG, M., JOHANSEN, K. S., VON FREIESLEBEN, P., MARMUSE, L., FORT, S., COTTAZ, S., DRIGUEZ, H., HENRISSAT, B., LENFANT, N., TUNA, F., BALDANSUREN, A., DAVIES, G. J., LO LEGGIO, L., & WALTON, P. H. 2016. The molecular basis of polysaccharide cleavage by lytic polysaccharide monooxygenases, *Nature Chemical Biology*, 12: 298-303.

FROMMHAGEN, M., SFORZA, S., WESTPHAL, A. H., VISSER, J., HINZ, S. W., KOETSIER, M. J., VAN BERKEL, W. J., GRUPPEN, H., & KABEL, M. A. 2015. Discovery of the combined oxidative cleavage of plant xylan and cellulose by a new fungal polysaccharide monooxygenase, *Biotechnology for Biofuels*, 8: 101.

FROMMHAGEN, M., WESTPHAL, A. H., VAN BERKEL, W. J. H., & KABEL, M. A. 2018. Distinct substrate specificities and electron-donating systems of fungal lytic polysaccharide monooxygenases, *Frontiers in Microbiology*, 9: 1080.

FRY, S. C., YORK, W. S., ALBERSHEIM, P., DARVILL, A., HAYASHI, T., JOSELEAU, J.-P., KATO, Y., LORENCES, E. P., MACLACHLAN, G. A., MCNEIL, M., MORT, A. J., GRANT REID, J. S., SEITZ, H. U., SELVENDRAN, R. R., VORAGEN, A. G. J., & WHITE, A. R. 1993. An unambiguous nomenclature for xyloglucan-derived oligosaccharides, *Physiologia Plantarum*, 89: 1-3.

GASTEIGER, E., HOOGLAND, C., GATTIKER, A., DUVAUD, S. E., WILKINS, M. R., APPEL, R. D., & BAIROCH, A. 2005. 'Protein identification and analysis tools on the ExPASy Server' in *The Proteomics Protocols Handbook*. Humana Press: Totowa, NJ, USA, 571-607.

HANGASKY, J. A., IAVARONE, A. T., & MARLETTA, M. A. 2018. Reactivity of O_2 versus H_2O_2 with polysaccharide monooxygenases, *Proceedings of the National Academy of Sciences of the United States of America*, 115: 4915-4920.

HARRIS, P. V., XU, F., KREEL, N. E., KANG, C., & FUKUYAMA, S. 2014. New enzyme insights drive advances in commercial ethanol production, *Current Opinion in Chemical Biology*, 19: 162-170.

HEDISON, T. M., BRESLMAYR, E., SHANMUGAM, M., KARNPAKDEE, K., HEYES, D. J., GREEN, A. P., LUDWIG, R., SCRUTTON, N. S., & KRACHER, D. 2021. Insights into the H_2O_2-driven catalytic mechanism of fungal lytic polysaccharide monooxygenases, *The FEBS Journal*, 288: 4115-4128.

HEGNAR, O. A., ØSTBY, H., PETROVIĆ, D. M., OLSSON, L., VÁRNAI, A., & EIJSINK, V. G. H. 2021. Quantifying oxidation of cellulose-associated glucuronoxylan by two lytic polysaccharide monooxygenases from *Neurospora crassa*, *Applied and Environmental Microbiology*, 87: e0165221.

HEMSWORTH, G. R., JOHNSTON, E. M., DAVIES, G. J., & WALTON, P. H. 2015. Lytic polysaccharide monooxygenases in biomass conversion, *Trends in Biotechnology*, 33: 747-761.

ISAKSEN, T., WESTERENG, B., AACHMANN, F. L., AGGER, J. W., KRACHER, D., KITTL, R., LUDWIG, R., HALTRICH, D., EIJSINK, V. G., & HORN, S. J. 2014. A C4-oxidizing lytic polysaccharide monooxygenase cleaving both cellulose and cello-oligosaccharides, *Journal of Biological Chemistry*, 289: 2632-2642.

JAGADEESWARAN, G., GAINEY, L., & MORT, A. J. 2018. An AA9-LPMO containing a CBM1 domain in *Aspergillus nidulans* is active on cellulose and cleaves cello-oligosaccharides, *AMB Express*, 8: 171.

JOHANSEN, KATJA S. 2016. Discovery and industrial applications of lytic polysaccharide mono-oxygenases, *Biochemical Society Transactions*, 44: 143-149.

JONES, S. M., TRANSUE, W. J., MEIER, K. K., KELEMEN, B., & SOLOMON, E. I. 2020. Kinetic analysis of amino acid radicals formed in H_2O_2-driven Cu^I LPMO reoxidation implicates dominant homolytic reactivity, *Proceedings of the National Academy of Sciences of the United States of America*, 117: 11916-11922.

KELLEY, L. A., MEZULIS, S., YATES, C. M., WASS, M. N., & STERNBERG, M. J. E. 2015. The Phyre2 web portal for protein modeling, prediction and analysis, *Nature Protocols*, 10: 845-858.

KITTL, R., KRACHER, D., BURGSTALLER, D., HALTRICH, D., & LUDWIG, R. 2012. Production of four *Neurospora crassa* lytic polysaccharide monooxygenases in Pichia pastoris monitored by a fluorimetric assay, *Biotechnology for Biofuels*, 5: 79.

KOJIMA, Y., VÁRNAI, A., ISHIDA, T., SUNAGAWA, N., PETROVIC, D. M., IGARASHI, K., JELLISON, J., GOODELL, B., ALFREDSEN, G., WESTERENG, B., EIJSINK, V. G., & YOSHIDA, M. 2016. A lytic polysaccharide monooxygenase with broad xyloglucan specificity from the brown-rot fungus *Gloeophyllum trabeum* and its action on cellulose-xyloglucan complexes, *Applied and Environmental Microbiology*, 82: 6557-6572.

KONT, R., BISSARO, B., EIJSINK, V. G. H., & VÄLJAMÄE, P. 2020. Kinetic insights into the peroxygenase activity of cellulose-active lytic polysaccharide monooxygenases (LPMOs), *Nature Communications*, 11: 5786.

KRACHER, D., SCHEIBLBRANDNER, S., FELICE, A. K. G., BRESLMAYR, E., PREIMS, M., LUDWICKA, K., HALTRICH, D., EIJSINK, V. G. H., & LUDWIG, R. 2016. Extracellular electron transfer systems fuel cellulose oxidative degradation, *Science*, 352: 1098-1101.

KUUSK, S., BISSARO, B., KUUSK, P., FORSBERG, Z., EIJSINK, V. G. H., SØRLIE, M., & VÄLJAMÄE, P. 2018. Kinetics of H_2O_2-driven degradation of chitin by a bacterial lytic polysaccharide monooxygenase, *Journal of Biological Chemistry*, 293: 523-531.

KUUSK, S., KONT, R., KUUSK, P., HEERING, A., SØRLIE, M., BISSARO, B., EIJSINK, V. G. H., & VÄLJAMÄE, P. 2019. Kinetic insights into the role of the reductant in H_2O_2-driven degradation of chitin by a bacterial lytic polysaccharide monooxygenase, *Journal of Biological Chemistry*, 294: 1516-1528.

KUUSK, S. & VÄLJAMÄE, P. 2021. Kinetics of H_2O_2-driven catalysis by a lytic polysaccharide monooxygenase from the fungus *Trichoderma reesei*, *Journal of Biological Chemistry*, 297: 101256.

LARSSON, A. 2014. AliView: a fast and lightweight alignment viewer and editor for large datasets, *Bioinformatics*, 30: 3276-3278.

LAURENT, C. V. F. P., SUN, P., SCHEIBLBRANDNER, S., CSARMAN, F., CANNAZZA, P., FROMMHAGEN, M., VAN BERKEL, W. J. H., OOSTENBRINK, C., KABEL, M. A., & LUDWIG, R. 2019. Influence of lytic polysaccharide monooxygenase active site segments on activity and affinity, *International Journal of Molecular Sciences*, 20: 6219.

LENFANT, N., HAINAUT, M., TERRAPON, N., DRULA, E., LOMBARD, V., & HENRISSAT, B. 2017. A bioinformatics analysis of 3400 lytic polysaccharide oxidases from family AA9, *Carbohydrate Research*, 448: 166-174.

LETUNIC, I. & BORK, P. 2007. Interactive Tree Of Life (iTOL): an online tool for phylogenetic tree display and annotation, *Bioinformatics*, 23: 127-128.

LEVASSEUR, A., DRULA, E., LOMBARD, V., COUTINHO, P. M., & HENRISSAT, B. 2013. Expansion of the enzymatic repertoire of the CAZy database to integrate auxiliary redox enzymes, *Biotechnology for Biofuels*, 6: 41.

LIU, Y., SEEFELDT, L. C., & PARKER, V. D. 1997. Entropies of redox reactions between proteins and mediators: the temperature dependence of reversible electrode potentials in aqueous buffers, *Analytical Biochemistry*, 250: 196-202.

LOOSE, J. S., FORSBERG, Z., FRAAIJE, M. W., EIJSINK, V. G., & VAAJE-KOLSTAD, G. 2014. A rapid quantitative activity assay shows that the *Vibrio cholerae* colonization factor GbpA is an active lytic polysaccharide monooxygenase, *FEBS Letters*, 588: 3435-3440.

MANOIL, C. & BECKWITH, J. 1986. A genetic approach to analyzing membrane protein topology, *Science*, 233: 1403-1408.

MONCLARO, A. V., PETROVIĆ, D. M., ALVES, G. S. C., COSTA, M. M. C., MIDORIKAWA, G. E. O., MILLER, R. N. G., FILHO, E. X. F., EIJSINK, V. G. H., & VÁRNAI, A. 2020. Characterization of two family AA9 LPMOs from *Aspergillus tamarii* with distinct activities on xyloglucan reveals structural differences linked to cleavage specificity, *PLoS One*, 15: e0235642.

MÜLLER, G., CHYLENSKI, P., BISSARO, B., EIJSINK, V. G. H., & HORN, S. J. 2018. The impact of hydrogen peroxide supply on LPMO activity and overall saccharification efficiency of a commercial cellulase cocktail, *Biotechnology for Biofuels*, 11: 209.

MÜLLER, G., VÁRNAI, A., JOHANSEN, K. S., EIJSINK, V. G. H., & HORN, S. J. 2015. Harnessing the potential of LPMO-containing cellulase cocktails poses new demands on processing conditions, *Biotechnology for Biofuels*, 8: 187.

NEKIUNAITE, L., PETROVIĆ, D. M., WESTERENG, B., VAAJE-KOLSTAD, G., HACHEM, M. A., VÁRNAI, A., & EIJSINK, V. G. H. 2016. *Fg*LPMO9A from *Fusarium graminearum* cleaves xyloglucan independently of the backbone substitution pattern, *FEBS Letters*, 590: 3346-3356.

OHM, R. A., DE JONG, J. F., LUGONES, L. G., AERTS, A., KOTHE, E., STAJICH, J. E., DE VRIES, R. P., RECORD, E., LEVASSEUR, A., BAKER, S. E., BARTHOLOMEW, K. A., COUTINHO, P. M., ERDMANN, S., FOWLER, T. J., GATHMAN, A. C., LOMBARD, V., HENRISSAT, B., KNABE, N., KÜES, U., LILLY, W. W., LINDQUIST, E., LUCAS, S., MAGNUSON, J. K., PIUMI, F., RAUDASKOSKI, M., SALAMOV, A., SCHMUTZ, J., SCHWARZE, F. W. M. R., VANKUYK, P. A., HORTON, J. S., GRIGORIEV, I. V., & WÖSTEN, H. A. B. 2010. Genome sequence of the model mushroom *Schizophyllum commune*, *Nature Biotechnology*, 28: 957-963.

ØSTBY, H., JAMESON, J.-K., COSTA, T., EIJSINK, V. G. H., & ARNTZEN, M. Ø. 2022. Chromatographic analysis of oxidized cello-oligomers generated by lytic polysaccharide monooxygenases using dual electrolytic eluent generation, *Journal of Chromatography A*, 1662: 462691.

PETROVIĆ, D. M., BISSARO, B., CHYLENSKI, P., SKAUGEN, M., SØRLIE, M., JENSEN, M. S., AACHMANN, F. L., COURTADE, G., VÁRNAI, A., & EIJSINK, V. G. H. 2018. Methylation of the N-terminal histidine protects a lytic polysaccharide monooxygenase from auto-oxidative inactivation, *Protein Science*, 27: 1636-1650.

PETROVIĆ, D. M., VÁRNAI, A., DIMAROGONA, M., MATHIESEN, G., SANDGREN, M., WESTERENG, B., & EIJSINK, V. G. H. 2019. Comparison of three seemingly similar lytic polysaccharide monooxygenases from *Neurospora crassa* suggests different roles in plant biomass degradation, *Journal of Biological Chemistry*, 294: 15068-15081.

PHILLIPS, C. M., BEESON, W. T., CATE, J. H., & MARLETTA, M. A. 2011. Cellobiose dehydrogenase and a copper-dependent polysaccharide monooxygenase potentiate cellulose degradation by *Neurospora crassa*, *ACS Chemical Biology*, 6: 1399-1406.

QUINLAN, R. J., SWEENEY, M. D., LO LEGGIO, L., OTTEN, H., POULSEN, J.-C. N., JOHANSEN, K. S., KROGH, K. B. R. M., JØRGENSEN, C. I., TOVBORG, M., ANTHONSEN, A., TRYFONA, T., WALTER, C. P., DUPREE, P., XU, F., DAVIES, G. J., & WALTON, P. H. 2011. Insights into the oxidative degradation of cellulose by a copper metalloenzyme that exploits biomass components, *Proceedings of the National Academy of Sciences of the United States of America*, 108: 15079-15084.

RIEDER, L., PETROVIĆ, D., VÄLJAMÄE, P., EIJSINK, V. G. H., & SØRLIE, M. 2021a. Kinetic characterization of a putatively chitin-active LPMO reveals a preference for soluble substrates and absence of monooxygenase activity, *ACS Catalysis*, 11: 11685-11695.

RIEDER, L., STEPNOV, A. A., SØRLIE, M., & EIJSINK, V. G. H. 2021b. Fast and specific peroxygenase reactions catalyzed by fungal mono-copper enzymes, *Biochemistry*, 60: 3633-3643.

RØDSRUD, G., LERSCH, M., & SJÖDE, A. 2012. History and future of world's most advanced biorefinery in operation, *Biomass and Bioenergy*, 46: 46-59.

SIMMONS, T. J., FRANDSEN, K. E. H., CIANO, L., TRYFONA, T., LENFANT, N., POULSEN, J. C., WILSON, L. F. L., TANDRUP, T., TOVBORG, M., SCHNORR, K., JOHANSEN, K. S., HENRISSAT, B., WALTON, P. H., LO LEGGIO, L., & DUPREE, P. 2017. Structural and electronic determinants of lytic polysaccharide monooxygenase reactivity on polysaccharide substrates, *Nature Communications*, 8: 1064.

SØRLIE, M., SEEFELDT, L. C., & PARKER, V. D. 2000. Use of stopped-flow spectrophotometry to establish midpoint potentials for redox proteins, *Analytical Biochemistry*, 287: 118-125.

STEPNOV, A. A., EIJSINK, V. G. H., & FORSBERG, Z. 2022. Enhanced *in situ* H_2O_2 production explains synergy between an LPMO with a cellulose-binding domain and a single-domain LPMO, *Scientific Reports*, 12: 6129.

SUN, P., LAURENT, C. V. F. P., SCHEIBLBRANDNER, S., FROMMHAGEN, M., KOUZOUNIS, D., SANDERS, M. G., VAN BERKEL, W. J. H., LUDWIG, R., & KABEL, M. A. 2020. Configuration of active site segments in lytic polysaccharide monooxygenases steers oxidative xyloglucan degradation, *Biotechnology for Biofuels*, 13: 95.

TANDRUP, T., TRYFONA, T., FRANDSEN, K. E. H., JOHANSEN, K. S., DUPREE, P., & LO LEGGIO, L. 2020. Oligosaccharide binding and thermostability of two related AA9 lytic polysaccharide monooxygenases, *Biochemistry*, 59: 3347-3358.

TÕLGO, M., HEGNAR, O. A., ØSTBY, H., VÁRNAI, A., VILAPLANA, F., EIJSINK, V. G. H., & OLSSON, L. 2022. Comparison of six lytic polysaccharide monooxygenases from *Thermothielavioides terrestris* shows that functional variation underlies the multiplicity of LPMO genes in filamentous fungi, *Applied and Environmental Microbiology*, 88: e0009622.

TUVENG, T. R., JENSEN, M. S., FREDRIKSEN, L., VAAJE-KOLSTAD, G., EIJSINK, V. G. H., & FORSBERG, Z. 2020. A thermostable bacterial lytic polysaccharide monooxygenase

with high operational stability in a wide temperature range, *Biotechnology for Biofuels*, 13: 194.

VAAJE-KOLSTAD, G., FORSBERG, Z., LOOSE, J. S., BISSARO, B., & EIJSINK, V. G. H. 2017. Structural diversity of lytic polysaccharide monooxygenases, *Current Opinion in Structural Biology*, 44: 67-76.

VAAJE-KOLSTAD, G., WESTERENG, B., HORN, S. J., LIU, Z., ZHAI, H., SØRLIE, M., & EIJSINK, V. G. H. 2010. An oxidative enzyme boosting the enzymatic conversion of recalcitrant polysaccharides, *Science*, 330: 219-222.

VANDHANA, T. M., REYRE, J.-L., SUSHMAA, D., BERRIN, J.-G., BISSARO, B., & MADHUPRAKASH, J. 2022. On the expansion of biological functions of lytic polysaccharide monooxygenases, *New Phytologist*, 233: 2380-2396.

WESTERENG, B., ARNTZEN, M. O., AACHMANN, F. L., VARNAI, A., EIJSINK, V. G., & AGGER, J. W. 2016. Simultaneous analysis of C1 and C4 oxidized oligosaccharides, the products of lytic polysaccharide monooxygenases acting on cellulose, *Journal of Chromatography A*, 1445: 46-54.

WESTERENG, B., ARNTZEN, M. O., AGGER, J. W., VAAJE-KOLSTAD, G., & EIJSINK, V. G. H. 2017. Analyzing activities of lytic polysaccharide monooxygenases by liquid chromatography and mass spectrometry, *Methods in Molecular Biology*, 1588: 71-92.

WESTERENG, B., CANNELLA, D., AGGER, J. W., JØRGENSEN, H., ANDERSEN, M. L., EIJSINK, V. G. H., & FELBY, C. 2015. Enzymatic cellulose oxidation is linked to lignin by long-range electron transfer, *Scientific Reports*, 5: 18561.

WOOD, T. M. 1988. 'Preparation of crystalline, amorphous, and dyed cellulase substrates' in *Methods in Enzymology*. Academic Press, 19-25.

WU, M., BECKHAM, G. T., LARSSON, A. M., ISHIDA, T., KIM, S., PAYNE, C. M., HIMMEL, M. E., CROWLEY, M. F., HORN, S. J., WESTERENG, B., IGARASHI, K., SAMEJIMA, M., STÅHLBERG, J., EIJSINK, V. G. H., & SANDGREN, M. 2013. Crystal structure and computational characterization of the lytic polysaccharide monooxygenase GH61D from the Basidiomycota fungus *Phanerochaete chrysosporium*, *Journal of Biological Chemistry*, 288: 12828-12839.

ZHANG, W., LU, J., ZHANG, S., LIU, L., PANG, X., & LV, J. 2018. Development an effective system to expression recombinant protein in *E. coli* via comparison and optimization of signal peptides: expression of *Pseudomonas fluorescens* BJ-10 thermostable lipase as case study, *Microbial Cell Factories*, 17: 50.

ZHU, N., LIU, J., YANG, J., LIN, Y., YANG, Y., JI, L., LI, M., & YUAN, H. 2016. Comparative analysis of the secretomes of *Schizophyllum commune* and other wood-decay Basidiomycetes during solid-state fermentation reveals its unique lignocellulose-degrading enzyme system, *Biotechnology for Biofuels*, 9: 42.

1040

Quantifying oxidation of cellulose-associated glucuronoxylan by two lytic polysaccharide monooxygenases from *Neurospora crassa*

Hegnar, O. A., Østby, H., Petrović, D. M., Olsson, L., Várnai, A., & Eijsink, V. G. H.

Paper IV

AMERICAN SOCIETY FOR MICROBIOLOGY | Applied and Environmental Microbiology®

ENZYMOLOGY AND PROTEIN ENGINEERING

Quantifying Oxidation of Cellulose-Associated Glucuronoxylan by Two Lytic Polysaccharide Monooxygenases from *Neurospora crassa*

Olav A. Hegnar,[a] Heidi Østby,[a] Dejan M. Petrović,[a] Lisbeth Olsson,[b,c] Anikó Várnai,[a] Vincent G. H. Eijsink[a]

[a]Norwegian University of Life Sciences, Faculty of Chemistry, Biotechnology and Food Science, Ås, Norway
[b]Department of Biology and Biological Engineering, Division of Industrial Biotechnology, Chalmers University of Technology, Gothenburg, Sweden
[c]Wallenberg Wood Science Center, Chalmers University of Technology, Gothenburg, Sweden

ABSTRACT Family AA9 lytic polysaccharide monooxygenases (LPMOs) are abundant in fungi, where they catalyze oxidative depolymerization of recalcitrant plant biomass. These AA9 LPMOs cleave cellulose and some also act on hemicelluloses, primarily other (substituted) β-(1→4)-glucans. Oxidative cleavage of xylan has been shown for only a few AA9 LPMOs, and it remains unclear whether this activity is a minor side reaction or primary function. Here, we show that *Neurospora crassa* LPMO9F (*Nc*LPMO9F) and the phylogenetically related, hitherto uncharacterized *Nc*LPMO9L from *N. crassa* are active on both cellulose and cellulose-associated glucuronoxylan but not on glucuronoxylan alone. A newly developed method for simultaneous quantification of xylan-derived and cellulose-derived oxidized products showed that *Nc*LPMO9F preferentially cleaves xylan when acting on a cellulose–beechwood glucuronoxylan mixture, yielding about three times more xylan-derived than cellulose-derived oxidized products. Interestingly, under similar conditions, *Nc*LPMO9L and the previously characterized *Mc*LPMO9H, from *Malbranchea cinnamomea*, showed different xylan-to-cellulose preferences, giving oxidized product ratios of about 0.5:1 and 1:1, respectively, indicative of functional variation among xylan-active LPMOs. Phylogenetic and structural analysis of xylan-active AA9 LPMOs led to the identification of characteristic structural features, including unique features that do not occur in phylogenetically remote AA9 LPMOs, such as four AA9 LPMOs whose lack of activity toward glucuronoxylan was demonstrated in the present study. Taken together, the results provide a path toward discovery of additional xylan-active LPMOs and show that the huge family of AA9 LPMOs has members that preferentially act on xylan. These findings shed new light on the biological role and industrial potential of these fascinating enzymes.

IMPORTANCE Plant cell wall polysaccharides are highly resilient to depolymerization by hydrolytic enzymes, partly due to cellulose chains being tightly packed in microfibrils that are covered by hemicelluloses. Lytic polysaccharide monooxygenases (LPMOs) seem well suited to attack these resilient copolymeric structures, but the occurrence and importance of hemicellulolytic activity among LPMOs remain unclear. Here, we show that certain AA9 LPMOs preferentially cleave xylan when acting on a cellulose–glucuronoxylan mixture, and that this ability is the result of protein evolution that has resulted in a clade of AA9 LPMOs with specific structural features. Our findings strengthen the notion that the vast arsenal of AA9 LPMOs in certain fungal species provides functional versatility and that AA9 LPMOs may have evolved to promote oxidative depolymerization of a wide variety of recalcitrant, copolymeric plant polysaccharide structures. These findings have implications for understanding the biological roles and industrial potential of LPMOs.

Citation Hegnar OA, Østby H, Petrović DM, Olsson L, Várnai A, Eijsink VGH. 2021. Quantifying oxidation of cellulose-associated glucuronoxylan by two lytic polysaccharide monooxygenases from *Neurospora crassa*. Appl Environ Microbiol 87:e01652-21. https://doi.org/10.1128/AEM.01652-21.

Editor Irina S. Druzhinina, Nanjing Agricultural University

Address correspondence to Vincent G. H. Eijsink, vincent.eijsink@nmbu.no.

Received 22 September 2021
Accepted 2 October 2021
Accepted manuscript posted online 6 October 2021
Published 24 November 2021

KEYWORDS lytic polysaccharide monooxygenases, LPMO, lignocellulose, *Neurospora crassa*, xylan, hemicellulose, glucuronoxylan

In nature, decomposition of plant biomass is primarily performed by fungi. The degradation of plant cell walls requires a large suite of enzymes that work in concert to hydrolyze and oxidize its major polymeric components: cellulose, hemicelluloses, and lignin (1). In fungi, the major secreted enzymes that act on plant cell wall polysaccharides are glycoside hydrolases (GHs), carbohydrate esterases (CEs), and lytic polysaccharide monooxygenases (LPMOs) (2–7). Dikaryotic fungi carry genes encoding LPMOs from five currently recognized LPMO families, namely, AA9, AA11, AA13, AA14, and AA16, that act on various crystalline and amorphous polysaccharides, primarily cellulose and chitin (8). LPMOs are mono-copper enzymes that oxidize chitin or cellulose by hydroxylating either the C-1 or C-4 position of the scissile glycosidic bond, which leads to spontaneous bond cleavage (9–13). LPMOs were originally considered monooxygenases, using O_2 as a cosubstrate (9, 14), but recent work indicates that LPMOs are efficient peroxygenases, using H_2O_2 as a cosubstrate (15–19).

Family AA9 LPMOs are cellulose-active enzymes, some of which can also cleave hemicelluloses containing β-(1→4)-linked glucose units in the polysaccharide backbone, like glucomannan and xyloglucan (20). In addition, oxidative cleavage of xylan has been convincingly demonstrated for two AA9 LPMOs, *Mt*LPMO9A from *Myceliophthora thermophila* (21), originally named *Mt*LPMO9E by Berka et al. (22), and *Mc*LPMO9H from *Malbranchea cinnamomea* (23), both of which are monomodular and (primarily) C-1-oxidizing enzymes, sharing 55.6% sequence identity. These two enzymes produce oxidized xylo-oligomers when incubated with cellulose–glucuronoxylan copolymeric mixtures but are inactive toward soluble xylan alone. The inactivity on soluble xylan is likely due to the 3-fold screw conformation that this polymer has in solution, which is flexible and nonuniform, whereas xylan adopts a 2-fold screw conformation when associated with cellulose, leading to a more rigid and "crystalline" structure (24). It is well known that acetylated, arabinosylated, and/or glucuronylated xylans extracted from various sources, including crops, hardwood, and softwood, interact with cellulose surfaces to various extents (25, 26). It has been shown that glucuronoxylans with even pattern substitution, including acetylglucuronoxylan from *Arabidopsis* (27) and glucuronoarabinoxylan from spruce (28), adapt 2-fold screw conformation upon adsorption to cellulose in plant cell walls.

In a landmark study from 2015, Frommhagen et al. (21) showed production of oxidized xylo-oligomers upon incubation of *Mt*LPMO9A with a mixture of birchwood glucuronoxylan or oat spelt arabinoxylan and regenerated amorphous cellulose. These LPMO products were detected using high-performance anion-exchange chromatography with pulsed amperometric detection (HPAEC-PAD) and matrix-assisted laser desorption-ionization time-of-flight mass spectrometry (MALDI-TOF MS). A similar approach was taken by Hüttner et al. (23) studying *Mc*LPMO9H, where reactions were performed with mixtures of phosphoric acid swollen cellulose (PASC) and birchwood 4-*O*-methylglucuronoxylan. In this case, a wide variety of oxidized xylan products were detected by MALDI-TOF MS, but HPAEC-PAD detection was not described. Additionally, *Ls*LPMO9A from *Lentinus similis* has been suggested by Simmons et al. to act on birchwood glucuronoxylan (29), as it produces soluble native xylo-oligomers in a reductant-dependent manner, although the authors were unable to detect any oxidized xylo-oligomers.

In 2018, a novel xylan-active LPMO family, AA14, was discovered (30), with, until now, only two characterized members, both from the white-rot fungus *Pycnoporus coccineus*. In contrast to the xylan-active AA9 LPMOs, these enzymes are not active on cellulose but are thought to cleave highly refractory xylan that is grafted onto cellulose. Of possible products, only xylotrionic acid (Xyl2Xyl1A) was detected, by mass spectrometry only (30). More recently, it was shown that an AA14 enhances the release of native xylo-oligosaccharides from xylan-rich cellulose fibers by a xylobiohydrolase (31).

The above-mentioned discovery of LPMO activity on cellulose–xylan complexes provides a glimpse of functional diversity among LPMOs that may be needed to degrade different copolymeric structures occurring in plant cell walls, and that may

explain why some biomass-degrading fungi carry up to about 50 LPMO genes. Still, despite the above-mentioned and other findings (e.g., by Petrović et al. [32]), the functional implications of LPMO multiplicity remain poorly understood. Furthermore, not all functionally characterized LPMOs have been characterized to the same extent, which means that certain activities may have remained undetected. For example, considering the abundance of xylan–cellulose copolymeric structures in plant cell walls, one would perhaps expect a greater occurrence, and more in-depth characterization, of xylan-active LPMOs.

The genome of *Neurospora crassa*, an ascomycete bread mold found on decaying leaves in nature, encodes 14 AA9 LPMOs (33) but no AA14 LPMOs, which are primarily found in *Basidiomycetes* (30). At the time of writing, 9 of the 14 AA9 LPMOs in *N. crassa* had been functionally characterized to various extents (32, 34, 35): *Nc*LPMO9A (*gh61-1*, NCU02240), -9B (*gh61-2*, NCU07760), -9C (*gh61-3*, NCU02916), -9D (*gh61-4*, NCU01050), -9E (*gh61-5*, NCU08760), -9F (*gh61-6*, NCU03328), -9G (*gh61-7*, NCU00836), -9J (*gh61-10*, NCU01867), and -9M (*gh61-13*, NCU07898) (32, 34, 35), while the other five AA9 LPMOs, *Nc*LPMO9H (*gh61-8*, NCU03000), -9I (*gh61-9*, NCU05969), -9K (*gh61-11*, NCU07520), -9L (*gh61-12*, NCU02344), and -9N (*gh61-14*, NCU07974), await functional characterization. *N. crassa* currently is the best-characterized fungus in terms of its LPMO repertoire. All characterized *N. crassa* LPMOs are active on cellulose, four are C-1 oxidizing (*Nc*LPMO9E, -9F, -9G, and -9J), three are C-4 oxidizing (*Nc*LPMO9A, -9C, and -9D), two are C-1/C-4 oxidizing (*Nc*LPMO9B and -9M), and six of them carry CBM1 domains (three C-1 oxidizing, *Nc*LPMO9E, -9G, and -9J; two C-4 oxidizing, *Nc*LPMO9A and -9C; one C-1/C-4 oxidizing, *Nc*LPMO9B). Among these, *Nc*LPMO9F, a monomodular LPMO that oxidizes cellulose at the C-1 position, is one of the best-studied AA9 LPMOs. Its activity on cellulose was demonstrated in 2012 (35), and its crystal structure was solved in 2015 (36). In support of the idea that these many LPMOs have different functional roles, it is well established that fungal LPMO genes are differentially expressed both temporally and in response to different substrates, which is also true for *N. crassa* LPMOs (37–39).

So far, research on AA9 LPMOs has mainly been focusing on cellulose oxidation, while activity toward hemicellulosic substrates, particularly xylans, has been described less frequently. Furthermore, hemicellulolytic activities may have been overlooked because of the use of suboptimal reaction conditions, which may lead to rapid enzyme inactivation and low product levels (40). Strikingly, phylogenetic analysis (Fig. 1; see also Fig. S1 in the supplemental material) showed that the two AA9 LPMOs with clear xylanolytic activity, *Mt*LPMO9A and *Mc*LPMO9H, group together with several well-characterized (C-1-oxidizing) AA9s, including *Nc*LPMO9F from *N. crassa* (35, 36), for which activity on xylan has not yet been addressed or demonstrated. Another closely related LPMO is the hitherto uncharacterized *N. crassa* LPMO *Nc*LPMO9L. These four LPMOs belong to a distinct cluster, as is also visible in the analysis of Laurent et al., who classified AA9 LPMOs based on the sequences of five active-site segments (Seg1 to Seg5), placing these LPMOs in a group with relatively short Seg1 and Seg2 segments (41).

Motivated by these phylogenetic observations, we set out to determine if activity on xylan is prevalent among LPMOs that are phylogenetically close to *Mt*LPMO9A and *Mc*LPMO9H, and, if so, if it was possible to identify conserved structural determinants related to xylanolytic activity in AA9 LPMOs. We demonstrate previously overlooked xylanolytic activity of *Nc*LPMO9F, which turned out to preferentially oxidize xylan in 4-*O*-methylglucuronoxylan–cellulose mixtures, and we present a quantitative assessment of xylan oxidation by an LPMO. Additionally, we demonstrate xylanolytic activity for the hitherto uncharacterized *Nc*LPMO9L, which was cloned and expressed as part of this study. Finally, we demonstrate that the preference for cellulose versus xylan in glucuronoxylan–cellulose mixtures varies between xylan-active LPMOs.

RESULTS AND DISCUSSION

***Nc*LPMO9F and *Nc*LPMO9L oxidize xylan in cellulose–glucuronoxylan mixtures.** In our phylogenetic analyses, *Nc*LPMO9F (UniProt identifier [ID] Q1K4Q1) from *N. crassa*

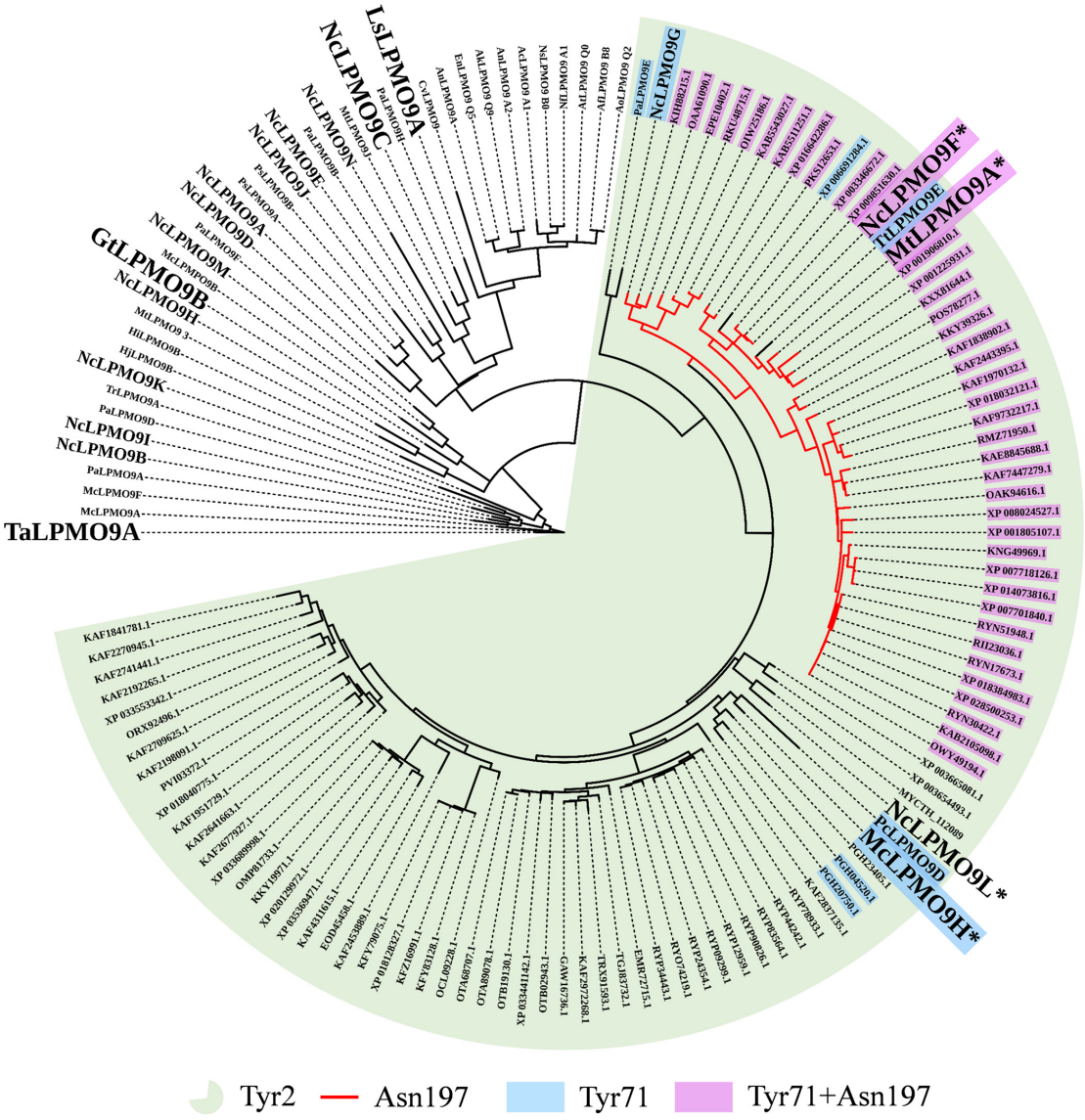

FIG 1 Phylogenetic distance tree of AA9 LPMOs. Multiple-sequence analysis of 34 functionally characterized AA9 LPMOs, all 14 *N. crassa* AA9 LPMOs, *Mc*LPMO9H, and 91 uncharacterized AA9 LPMOs that are most similar to *Nc*LPMO9F and *Mc*LPMO9H was performed using Expresso (T-Coffee), with subsequent phylogenetic analysis performed with ProtTest 3.4. The lettering size for LPMO names is the following: large, LPMOs that were used in this study plus known xylan-active LPMOs *Mc*LPMO9H and *Mt*LPMO9A; medium, all *Nc*LPMO9s (except 9F, 9L, and 9C, which are large) and previously characterized LPMOs that are discussed in the text; small, all other LPMOs. The names of LPMOs with demonstrated xylanolytic activity are marked by an asterisk. The various colors indicate sequence characteristics, as indicated; see the text for further discussion.

clustered closest to the xylan-active *Mt*LPMO9A, whereas the previously uncharacterized *Nc*LPMO9L (UniProt ID Q7S411), also from *N. crassa*, clustered closest to the xylan-active *Mc*LPMO9H (Fig. 1). These four enzymes shared more than 50% identity with each other (see below for a more detailed discussion; also see Fig. S1 in the supplemental material).

To test our hypothesis that the phylogenetic clustering and sequence identities of

these enzymes translate to similar substrate specificities, such as activity on xylan, we first set up reaction mixtures containing either 0.4% (wt/vol) phosphorous acid swollen cellulose (PASC), 0.4% (wt/vol) beechwood glucuronoxylan (BeWX), or 0.4% (wt/vol) PASC and 0.4% (wt/vol) BeWX in combination. MALDI-TOF MS analysis of product mixtures showed the formation of oxidized xylo-oligosaccharides for both *Nc*LPMO9F and *Nc*LPMO9L (Fig. 2), similar to what has been observed for *Mt*LPMO9A (21) and *Mc*LPMO9H (23). Product mixtures obtained from reaction mixtures containing both PASC and BeWX showed masses corresponding to oxidized nonsubstituted and 4-*O*-methylglucuronylated (i.e., GlcAOMe-substituted) xylo-oligosaccharides, in addition to oxidized cello-oligosaccharides. For *Nc*LPMO9F, the products with the most intense signals include the sodium adducts of native Xyl8GlcAOMe (m/z = 1,287), C-1-oxidized Xyl8GlcAOMe (hydrated form; m/z = 1,303), native Xyl9GlcAOMe (m/z = 1,419), C-1-oxidized Xyl9GlcAOMe (hydrated form; m/z = 1,435), and C-1-oxidized Xyl10GlcAOMe (hydrated form; m/z = 1,567). Strikingly, xylan-derived products are strongly dominating the product spectrum, which may be taken to suggest that this well-studied cellulose-active LPMO has a preference for xylan, although these differences may also be due to different behaviors of the various products in the MALDI-TOF MS analysis (chromatographic quantification of products is described below). Curiously, for *Nc*LPMO9L, nonoxidized xylan-derived products were more prominent in the MS spectra than oxidized products, whereas the reductant-free control did not show any indications of a background xylanase activity. Both product profiles show signals corresponding to sodium adducts of the sodium salts of oxidized xylo-oligosaccharides that are diagnostic for C-1 oxidations, such as m/z = 1,267, which is the sodium adduct of the sodium salt of C-1-oxidized Xyl9, and m/z = 1,215, which is the sodium adduct of the double sodium salt of C-1-oxidized Xyl7GlcAOMe.

Activity on cellulose-associated glucuronoxylan by phylogenetically related LPMOs is detectable with HPAEC-PAD. So far, only Frommhagen et al. have been able to detect (weak) signals for LPMO-generated oxidized xylan-derived oligomers (21). Encouraged by the convincing mass spectra of Fig. 2, we explored the use of HPAEC-PAD for detection of xylan-derived products. HPAEC-PAD analysis of product mixtures obtained from reactions with *Nc*LPMO9F, *Nc*LPMO9L, or *Mc*LPMO9H with a mixture of PASC and BeWX showed peaks for both cellulose- and xylan-derived products for all three LPMOs (Fig. 3). None of these LPMOs were active on BeWX alone, and control reactions without reductant did not yield products (Fig. 3). Assays with PASC alone revealed that the novel LPMO, *Nc*LPMO9L, like *Nc*LPMO9F and *Mc*LPMO9H, oxidizes cellulose at the C-1 position to levels comparable with those obtained with *Nc*LPMO9F (Fig. 3).

Xylanolytic activity of *Nc*LPMO9F, *Nc*LPMO9L, and *Mc*LPMO9H is evident from the plethora of non-cellulose-related peaks that emerge in product mixtures derived from reaction mixtures containing PASC–BeWX mixtures and reductant (Fig. 3). The apparent large product diversity is in accordance with the mass spectrometry data shown in Fig. 2. Strikingly, the ratios between the cellulose- and the xylan-derived products varied a lot for the studied LPMOs, indicating different substrate preferences (Fig. 3). For *Nc*LPMO9F, several of the peaks that did not correspond to the usual cellulose-derived LPMO products had much larger areas than the peaks belonging to cellulose-derived products, which suggests that this LPMO prefers xylan over cellulose, as also suggested by the mass spectrometry data shown in Fig. 2. On the other hand, cellulose-derived products were dominating for *Nc*LPMO9L, while *Mc*LPMO9H showed an intermediate product profile.

To annotate some of the unidentified peaks, we generated C-1-oxidized xylo-oligosaccharide standards (degree of polymerization 2 [DP2] to 6) from linear xylo-oligosaccharides by oxidizing the xylosyl unit at the reducing end to xylonic acid (Xyl1A) using a cellobiose dehydrogenase, *Mt*CDH (see Materials and Methods). This approach allowed the identification of oxidized nonsubstituted xylo-oligosaccharides in the reaction mixture (Fig. 4). The many unidentified peaks are likely unsubstituted oxidized xylan products with a higher degree of polymerization and GlcAOMe-substituted

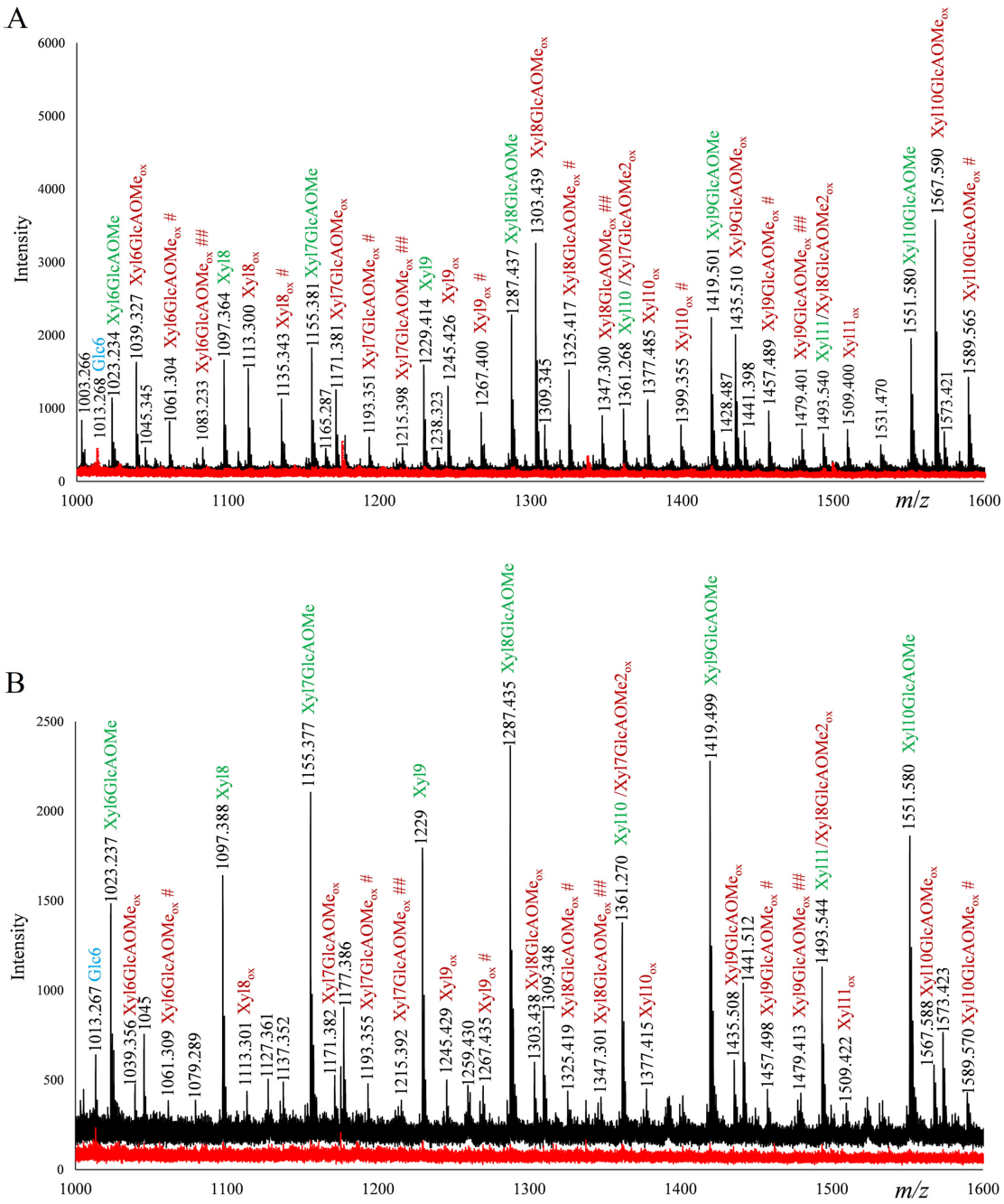

FIG 2 MALDI-TOF MS spectra of products generated by *Nc*LPMO9F and *Nc*LPMO9L in reaction mixtures containing both PASC and BeWX. The reaction mixtures were set up with 1 μM *Nc*LPMO9F (upper) or *Nc*LPMO9L (lower), 0.4% (wt/vol) PASC, and 0.4% (wt/vol) BeWX as the substrate, with (black) or without (red) 1 mM ascorbic acid (AscA) as the reductant, in 50 mM BisTris-HCl buffer, pH 6.0, and incubated at 45°C for 24 h. Reaction mixtures with only PASC generated almost exclusively cellulose-derived products (see Fig. 4 for more details), whereas reactions with only BeWX generated no products (data not shown). All labeled peaks are sodium adducts. Sodium salts (+22 per sodium), which can be formed through binding to GlcAOMe unit(s), and/or the

(Continued on next page)

oligomeric xylan products, a notion that is supported by the MALDI-TOF MS data (Fig. 2), which show several oxidized xylo-oligosaccharide products with DP of >6, both nonsubstituted and GlcAOMe substituted. It is noteworthy that product mixtures from reactions with only PASC, *Nc*LPMO9F, and reductant showed small amounts of oxidized xylo-oligosaccharides, likely resulting from oxidative activity on residual xylan in the PASC preparation (Fig. 4). This has also been observed for *Mc*LPMO9H with MALDI-TOF MS analyses (23).

To ensure that the oxidized xylo-oligomers observed did not result from reactions with reactive oxygen species produced in side reactions involving copper, ascorbic acid (AscA), and/or H_2O_2 (42), we set up control reaction mixtures where either *Nc*LPMO9F or an equimolar amount of $CuSO_4$ was incubated with the substrates in the presence of H_2O_2 and AscA (Fig. S2). Indeed, as expected, in reaction mixtures where the LPMO was replaced with $CuSO_4$, neither reaction mixtures with BeWX alone nor reaction mixtures with BeWX and PASC generated soluble products. Of note, in reaction mixtures where *Nc*LPMO9F was incubated with BeWX and PASC, we observed significant inhibition of LPMO activity in the reaction with 200 μM H_2O_2 (Fig. S2), which is common when LPMO reactions are exposed to higher H_2O_2 concentrations. On the other hand, the reaction with 50 μM H_2O_2 yielded a product profile similar to that shown in Fig. 3.

Additional reactions were performed with the C-4-oxidizing LPMOs *Nc*LPMO9C and *Ls*LPMO9A, both of which have been shown to cleave oligosaccharides and hemicelluloses with a β-(1→4)-linked glucan backbone (20, 29), the C-1/C-4-oxidizing LPMOs *Ta*LPMO9A from *Thermoascus aurantiacus* and *Gt*LPMO9B from *Gloeophyllum trabeum*, both of which are active on xyloglucan (43, 44), and the C-1-oxidizing cellulose-active bacterial AA10 LPMO CelS2 (*Sc*LPMO10C) from *Streptomyces coelicolor* (45). For these LPMOs, we were unable to detect xylan-derived products in reactions with the PASC–BeWX mixture, either by HPAEC-PAD or MALDI-TOF MS (data not shown). Of note, weak xylanolytic activity has previously been suggested for *Ls*LPMO9A based on MS signals only (29).

Quantitative comparison of cellulose and glucuronoxylan oxidation by xylan-active LPMOs. Next, we hydrolyzed the cello- and xylo-oligosaccharides solubilized by *Nc*LPMO9F when acting on a PASC–BeWX mixture with *Tr*Cel7A and *Cj*Xyn10A in an attempt to quantify LPMO activity on cellulose and xylan, using HPAEC-PAD for quantification of the resulting short, oxidized oligomers. As expected, the resulting product mixtures contained cellobionic acid (GlcGlc1A) and cellotrionic acid (Glc2Glc1A), resulting from oxidation of cellulose (Fig. 5A), as well as xylobionic acid (XylXyl1A) and xylotrionic acid (Xyl2Xyl1A), resulting from oxidation of xylan (Fig. 5B). Next to generating oxidized nonsubstituted xylo-oligomers with DP2 to -3, *Cj*Xyn10A-treated sample contained unknown products, which, considering that the BeWX substrate contained GlcAOMe substitutions, could be native or oxidized glucuronylated xylan fragments (Fig. 5B). The product mixtures obtained upon *Cj*Xyn10A treatment of reactions with BeWX showed large peaks, eluting between 11 and 12 min, independent of the presence of reductant during the LPMO reaction (Fig. 5B and D). Additional treatment of these samples with an α-glucuronidase led to a notable peak shift, indicating that these peaks represent native GlcAOMe-substituted xylooligomers that are liberated from BeWX by *Cj*Xyn10A (Fig. S3). Interestingly, a control experiment with *Gt*LPMO9B showed no xylan oxidation, while the presence of xylan decreased product release from cellulose, indicating that the xylan limits access to the PASC substrate (Fig. 5C and D).

Quantification of the emergence of oxidized cello- and xylo-oligosaccharides over time in reactions with *Nc*LPMO9F and PASC (Fig. 6A) or the PASC–BeWX mixture (Fig. 6B)

FIG 2 Legend (Continued)
Xyl1A unit are annotated with # or ##, for one or two Na ions, respectively. Oxidized xylan products are labeled in red, while native products are labeled in green; cellulose-derived products are labeled in blue. Note that most cellulose-derived products are not visible in these spectra because of their lower *m/z* values; these products are well visible in the chromatographic analyses shown in other figures. All reactions were performed in triplicate and resulted in similar product profiles.

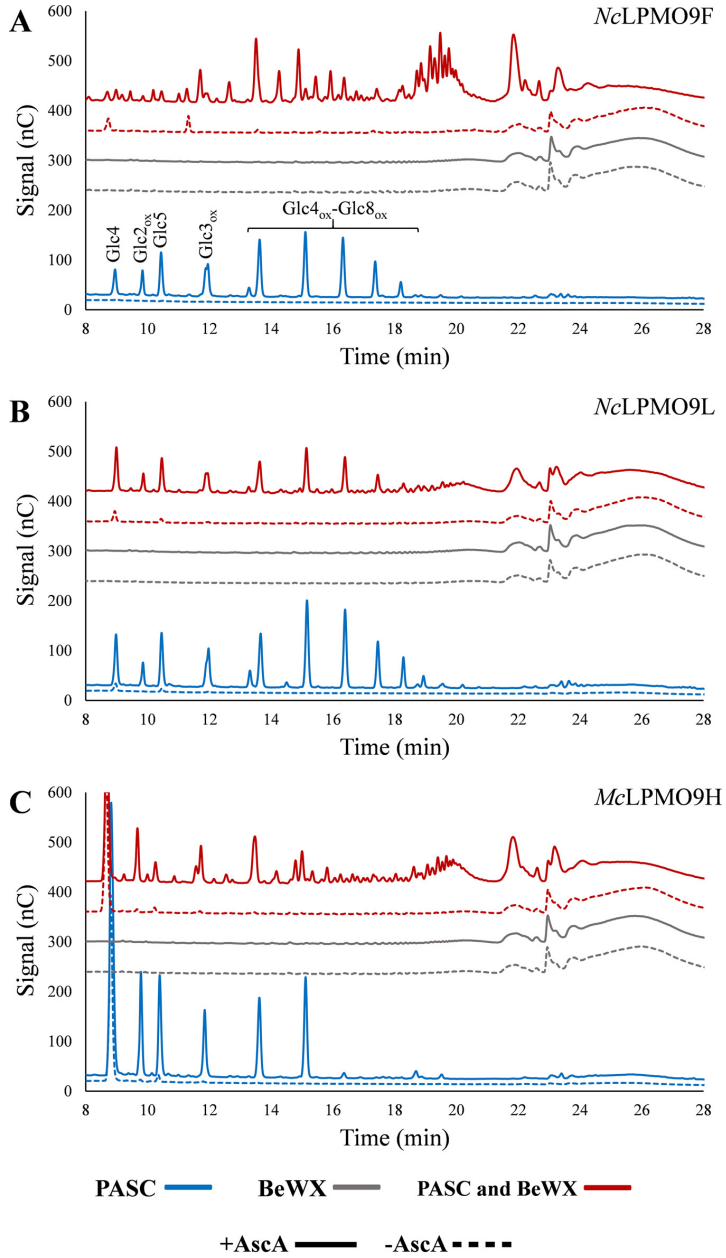

FIG 3 HPAEC-PAD chromatograms of product mixtures from LPMO reactions with PASC, BeWX, or PASC and BeWX. Panels A, B, and C show analyses of reactions with *Nc*LPMO9F, *Nc*LPMO9L, and *Mc*LPMO9H, respectively. All reactions were performed with 1 μM LPMO and either 0.4% PASC, 0.4% BeWX, or 0.4% PASC and 0.4% BeWX, with (solid lines) or without (dashed lines) 1 mM ascorbic acid (AscA), in 50 mM BisTris-HCl buffer, pH 6.0, at 45°C for 24 h. Products in reactions with PASC were native and C-1-oxidized cello-oligomers as indicated in panel A, while reactions with PASC and BeWX showed a mix of native and C-1-oxidized cello- and xylo-oligomers (the xylan-derived products are not annotated). No reductant-dependent products were formed in reactions where BeWX was the only substrate for any of the LPMOs. A more detailed product annotation is provided in Fig. 4. All reactions were performed in triplicate and resulted in identical product profiles.

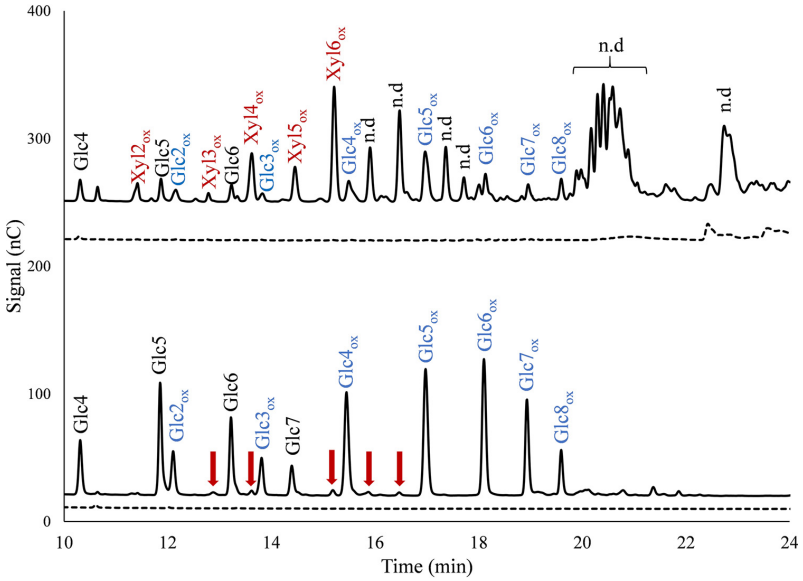

FIG 4 HPAEC-PAD chromatograms of product mixtures generated in reactions of *Nc*LPMO9F with PASC and BeWX (top) or PASC (bottom). Solid chromatograms are for reactions with AscA, while dashed chromatograms are for reactions without AscA. The peaks were annotated using chromatograms of mixtures of native and C-1-oxidized cello- and xylooligosaccharides (DP of 2 to 6). The red arrows indicate oxidized xylo-oligosaccharides resulting from residual xylan in the PASC preparation. Reaction conditions were the same as those for the experiments depicted in Fig. 3. Unannotated putatively xylan-derived products are labeled n.d., for not determined.

revealed that in the presence of AscA, the accumulation of oxidized cello-oligosaccharides stopped after 120 to 180 min, reaching a concentration of 165 μM oxidized products. This product level is far below the theoretical maximum, which is equivalent to the AscA concentration of 1 mM (as also illustrated by the much higher product levels shown in Fig. 6C, discussed below). This low level and the shape of the progress curve indicate that the LPMO lost activity as the reaction progressed. In the reaction mixtures containing both PASC and BeWX, the concentration of oxidized cellulose-derived products was lower, reaching a maximum of 80 μM within 60 min, whereas the concentration of oxidized xylan-derived products (excluding the oxidized glucuronylated xylo-oligosaccharides) was much higher, reaching 266 μM after 240 min. Importantly, in this case, the shape of the progress curve suggests that the reaction proceeded for the full 240-min reaction time.

The progress curves of Fig. 6A and B show some important features. First, the presence of xylan inhibits cellulose conversion by *Nc*LPMO9F, which suggests that BeWX is coating the PASC fibers, making these partially inaccessible to the enzyme. The initial burst in activity on PASC suggests the presence of a more easily accessible cellulose fraction that is not coated by BeWX. Kabel et al. (26) have observed that the degree of substitution of the xylan polymer directly influences the adsorption to cellulose, with unsubstituted xylan having the highest degree of adsorption. Recent data indicate that glucuronoxylan in secondary plant cell walls contains regions with either even or random distribution of glucuronylation (46) and that even distribution favors adsorption to cellulose (27, 28). Hence, it is possible that a variation in distribution of GlcAOMe substitutions along the BeWX polymer yields domains that adsorb to cellulose poorer (domains with more or random substitutions) or better (domains with less or even substitutions), eventually resulting in uneven coating of cellulose in the PASC substrate.

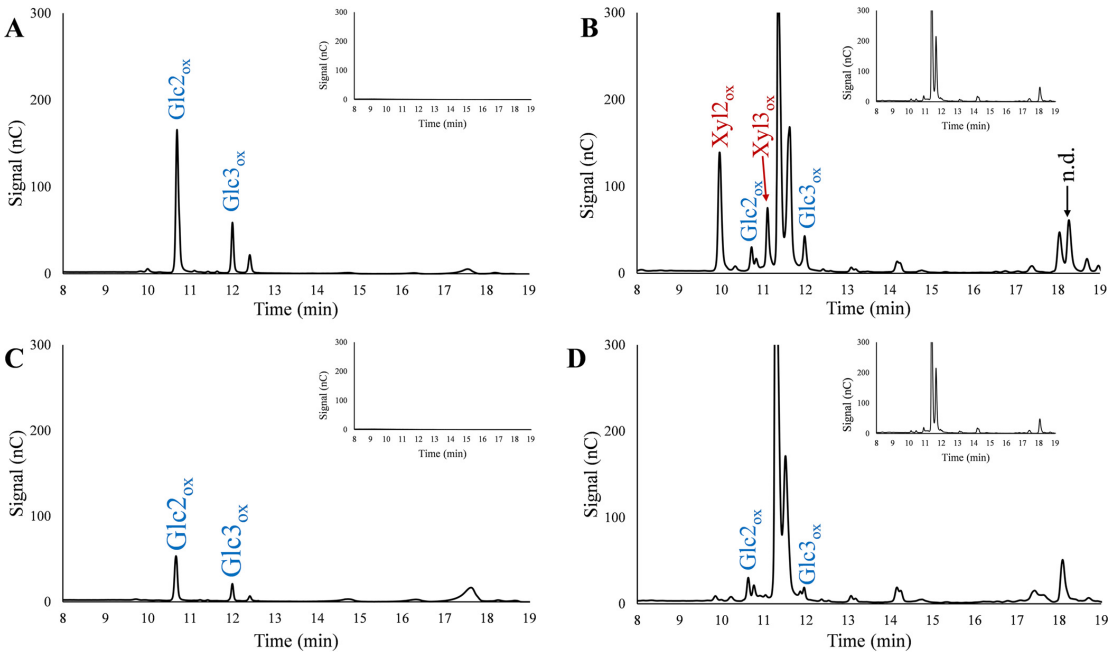

FIG 5 Enzymatic hydrolysis of LPMO products. (A) *Nc*LPMO9F with PASC; (B) *Nc*LPMO9F with PASC and BeWX; (C) *Gt*LPMO9B with PASC; (D) *Gt*LPMO9B with PASC and BeWX. Reductant-free control reactions are shown in the insets. Note the peak marked n.d. (not determined) at 18.4 min, which only appears in reactions with *Nc*LPMO9F and PASC plus BeWX; this could be oxidized glucuronosylated xylan fragments. The two large peaks eluting between 11 and 12 min (independent of the presence of reductant; see the insets in panels B and D) are likely native substituted xylo-oligosaccharides generated from soluble BeWX fragments by *Cj*Xyn10A (see the text and Fig. S3). $Glc2_{ox}$, GlcGlc1A; $Glc3_{ox}$, Glc2Glc1A; $Xyl2_{ox}$, XylXyl1A; $Xyl3_{ox}$, Xyl2Xyl1A.

Importantly, the higher levels of xylan-derived products, relative both to cellulose-derived products in the same reaction (Fig. 6B) and to cellulose-derived products in the PASC only reaction (Fig. 6A), clearly show that BeWX, when mixed with cellulose, is a better substrate for *Nc*LPMO9F than PASC. This is also supported by the apparent differences in LPMO stability, which is known to be compromised when the LPMO is provided with reducing equivalents in the absence of sufficient amounts of a suitable substrate (47). The lower apparent stability of the LPMO in the reaction with PASC only and the higher stability in the reaction with BeWX support the notion that xylan is the better substrate.

After establishing that *Nc*LPMO9F generated quantifiable amounts of oxidized xylo-oligosaccharides, we expanded the quantification to include *Nc*LPMO9L and *Mc*LPMO9H. Reactions were set up as described above, with sample collection after 24 h. In the reaction mixtures with PASC only (Fig. 6C), the oxidized product concentration reached similar levels for *Nc*LPMO9F and *Nc*LPMO9L, with 248 and 272 μM, respectively, whereas *Mc*LPMO9H released more oxidized products, reaching a final concentration of 478 μM. No oxidized cello-oligomers were detected in the absence of reductant or LPMO. In reactions with the PASC–BeWX mixture, all three LPMOs generated oxidized xylo-oligosaccharides (Fig. 6D). In line with conclusions drawn from Fig. 3, *Nc*LPMO9F was by far the most xylan-active of the three LPMOs on BeWX. For this enzyme, the apparent ratio of BeWX and PASC oxidization was 2.7:1. *Mc*LPMO9H showed lower xylanolytic activity, and the apparent ratio of BeWX and PASC oxidization was 0.9:1. *Nc*LPMO9L showed even lower xylanolytic activity, and its apparent ratio of BeWX and PASC oxidation was 0.5:1.

Phylogenetic and structural analysis of xylan-active AA9 LPMOs. To broaden our understanding of what features could be responsible for the observed activity on xylan, we performed phylogenetic and sequence analyses of *Nc*LPMO9F and *Mc*LPMO9H

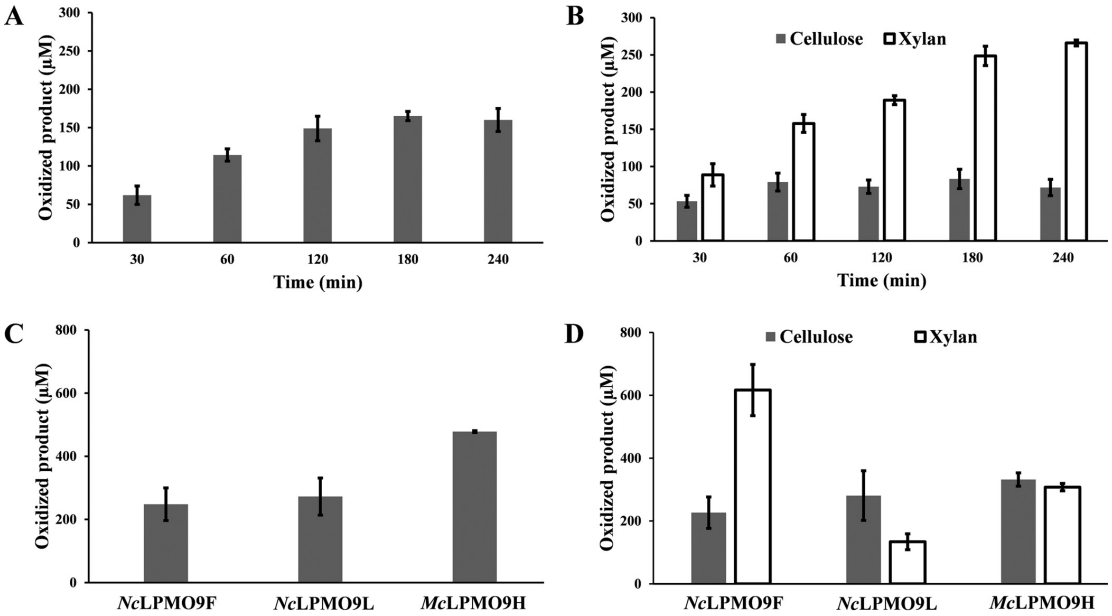

FIG 6 Quantification of oxidized cellulose- and xylan-derived products in reactions with *Nc*LPMO9F. Panels A and B show the formation of oxidized product by *Nc*LPMO9F during a 4-h reaction with PASC or PASC and BeWX, respectively. Panels C and D show oxidized products formed by *Nc*LPMO9F, *Nc*LPMO9L, or *Mc*LPMO9H after 24 h in reactions with PASC or PASC and BeWX, respectively. All reactions were performed with 1 μM LPMO, 1 mM ascorbic acid (AscA), and either 0.4% PASC or 0.4% PASC plus 0.4% BeWX, in 50 mM BisTris-HCl buffer, pH 6.0, at 45°C and 1,000 rpm. Control reactions were performed by replacing AscA with water, and the resulting product mixtures did not show oxidized species (not shown). Before product quantification, product mixtures were hydrolyzed with 1 μM *Tr*Cel7A and 1 μM *Cj*Xyn10A in 75 mM sodium acetate buffer, pH 4.75, for 24 h. Xylobionic acid (XylXyl1A), xylotrionic acid (Xyl2Xyl1A), cellobionic acid (GlcGlc1A), and cellotrionic acid (Glc2Glc1A) concentrations then were measured using HPAEC-PAD and appropriate standards, and the amounts of oxidized DP2 and DP3 products were summed to reach final product levels. Note that for xylan-derived oxidized products, we were only able to quantify linear nonsubstituted products (XylXyl1A and Xyl2Xyl1A). After hydrolysis of LPMO products, we observed a small peak eluting at 18.4 min (Fig. 5) in reactions with PASC and BeWX that likely contains a GlcAOMe-substituted xylan fragment. Thus, the total amount of oxidized xylan-derived product likely is underestimated. Reactions with BeWX only did not yield any oxidized products (not shown). All reactions were performed in triplicate, and standard deviations are indicated.

with 91 uncharacterized homologous proteins selected from a BLAST analysis of the two sequences against the Reference Sequence (RefSeq) database, the remaining 13 *Nc*LPMO9s, and 34 AA9 LPMOs that had been previously characterized to various extents (note that in almost all cases activity on cellulose–xylan mixtures had not been assessed). These analyses (Fig. 1) showed that *Nc*LPMO9F is part of a distinct clade that includes *Mt*LPMO9A, for which (weak) xylanolytic activity was detected (21), and, interestingly, the previously characterized C-1-oxidizing *Tt*LPMO9E from *Thielavia terrestris* (UniProt ID G2RGE5 [48]), for which xylanolytic activity has not yet been assessed. The xylan-active *Mc*LPMO9H and *Nc*LPMO9L occur in closely related sister clades that are separated from the *Nc*LPMO9F clade. Of note, *Mc*LPMO9H is closely related to the previously characterized C-1-oxidizing cellulose-active *Pc*LPMO9D from *Phanerochaete chrysosporium* (49), for which xylanolytic activity has not yet been assessed.

The availability of at least one crystal structure for each of the clades with xylan-active LPMOs and the availability of crystal structures for LPMOs found not to be active on glucuronoxylan provide an opportunity to assess possible structural determinants of xylanolytic activity. Despite some recent progress (50–52), the structural determinants of LPMO substrate specificity remain largely unknown. The substrate-binding surfaces of LPMOs vary considerably (Fig. S4), which is due to large sequence variation in specific regions of the LPMO that have been designated the L2, L3, LS, and LC loops (53) and, more recently, segments Seg1 to -5 (41, 54) (Fig. 7). Interestingly, the LPMOs with activity on cellulose-associated glucuronoxylan have shorter L2 and L3 loops,

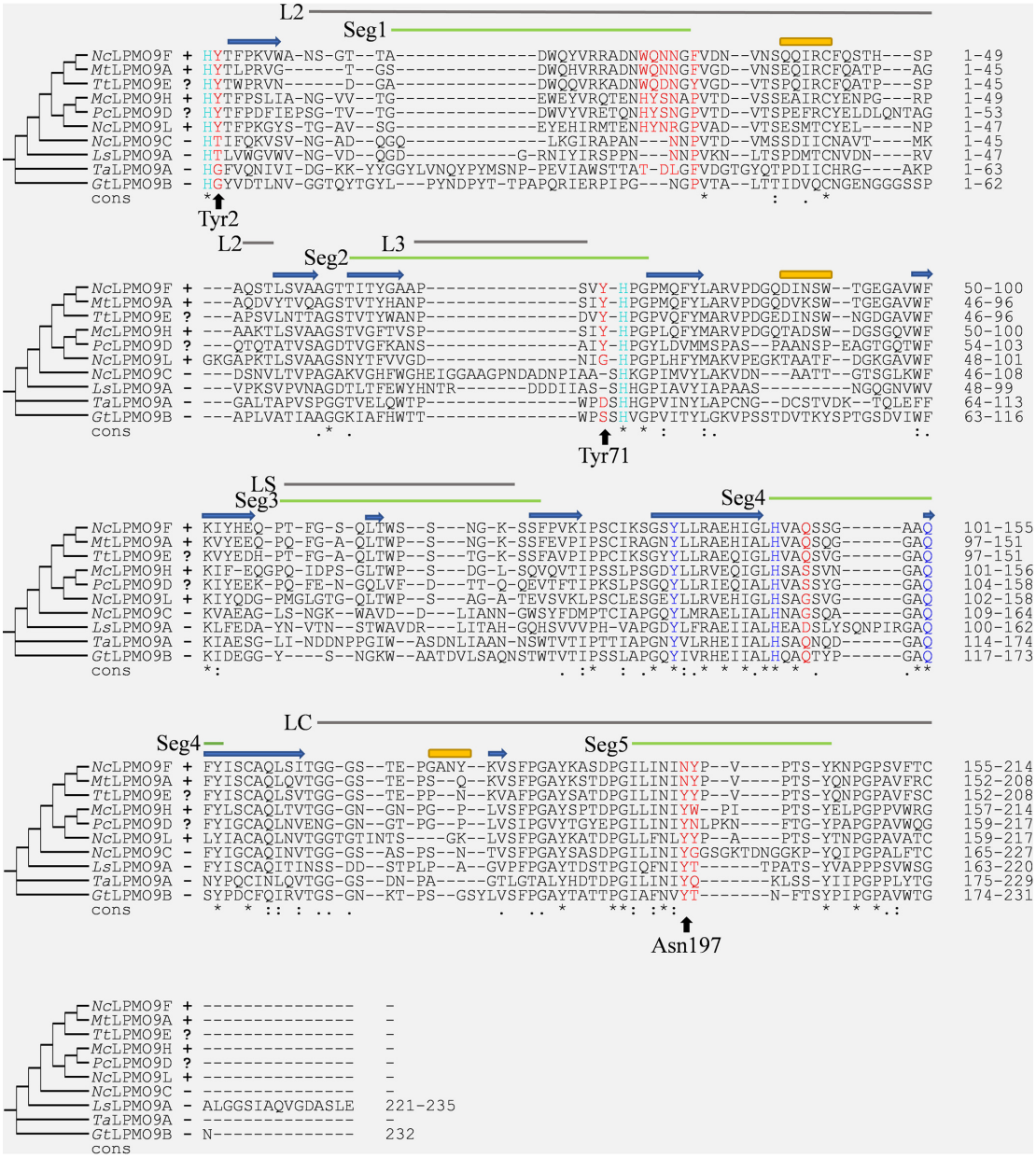

FIG 7 Multiple-sequence alignment of xylan-active and non-xylan-active LPMOs. Expresso alignment of confirmed xylan-active LPMOs (*Nc*LPMO9F, *Nc*LPMO9L, *Mc*LPMO9H, and *Mt*LPMO9A, labeled +), potentially xylan-active LPMOs for which xylanolytic activity has not been assessed (*Tt*LPMO9E and *Pc*LPMO9D, labeled ?), and LPMOs for which no xylanolytic activity could be detected in this study (*Nc*LPMO9C, *Gt*LPMO9B, *Ta*LPMO9A, and *Ls*LPMO9A, labeled –). The amino acid residues forming the His brace are light blue, while other conserved residues near the copper site appear in dark blue. Residues that are potentially relevant for xylanolytic activity, as discussed in the text and shown in Fig. 8, are colored red, whereas the three residues used to color the phylogenetic tree of Fig. 1 are indicated by arrows with labels. The secondary structural elements for *Nc*LPMO9F are shown in blue (strands) and yellow (helices) per the PDB crystal structure (4QI8) (36). Surface-exposed and putatively substrate-binding segments (Seg) are indicated by labeled green lines according to Laurent et al. (41), whereas variable regions (called loops) are indicated by labeled gray lines according to Wu et al. (53) and Borisova et al. (59).

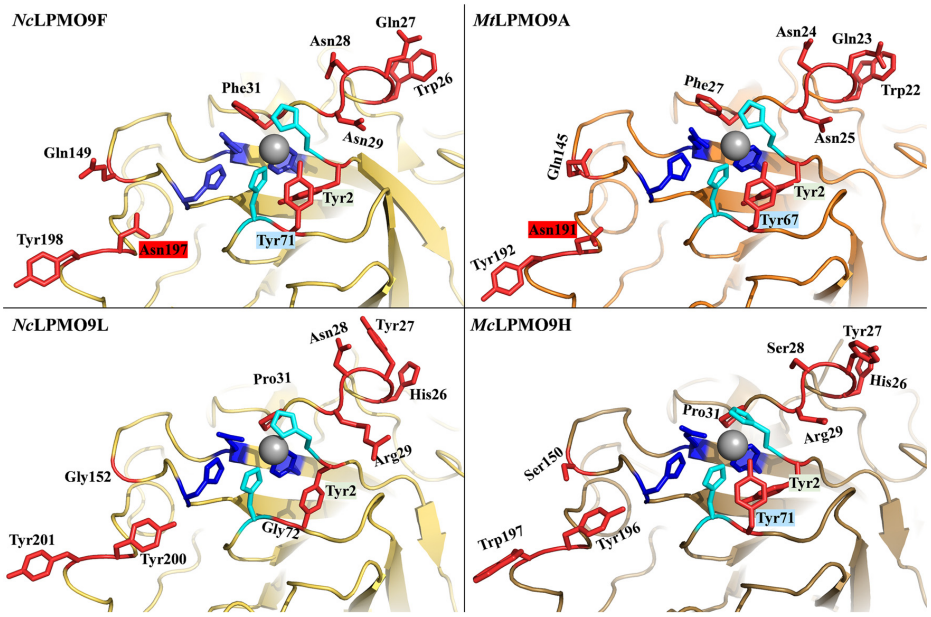

FIG 8 Comparison of the substrate-binding surface of four xylan-active AA9 LPMOs. Surface-exposed residues potentially involved in substrate binding are colored red. The His brace is labeled in light blue, while other conserved residues near the copper site appear in dark blue. Residues that are potentially relevant for xylan binding, as discussed in the text, are colored red. The copper appears as a gray sphere. Labels of residues that were used to color the phylogenetic tree of Fig. 1 are shaded with the corresponding color (Tyr2, Tyr71, and Asn197 in *Nc*LPMO9F). The crystal structure of *Nc*LPMO9F is available from the PDB (entry 4QI8). Models for the remaining LPMOs were built using PHYRE 2.0.

corresponding to shorter Seg1 and Seg2 active-site segments (Fig. 7). From computational and experimental studies of LPMO-substrate complexes, it is clear that both hydrogen bonding and aromatic stacking interactions are important for substrate binding (53, 55–57).

Figures 7 and 8, supported by Fig. S4 to S6, highlight sequence and structural features that seem characteristic for xylan-active LPMOs. Below, we will refer to residue positions according to the position in *Nc*LPMO9F (PDB entry 4QI8). Most notably, all enzymes that cluster with xylan-active LPMOs in Fig. 1 (green cluster) have a conserved tyrosine residue, Tyr2, next to the copper-binding His1 residue (Fig. 7, Fig. S6), which is unique for this subset of AA9 LPMOs. The structures of *Nc*LPMO9F (Fig. 8), *Tt*LPMO9E, and *Pc*LPMO9D show that Tyr2 is not solvent exposed but points inwards and, thus, likely does not contribute directly to substrate binding. Interestingly, in a subset of these LPMOs, the occurrence of this tyrosine is correlated with the occurrence of another, solvent-exposed tyrosine, Tyr71, in *Nc*LPMO9F (see the multiple-sequence alignments [MSAs] in Fig. 7, Fig. S5). In particular, this tyrosine occurs in xylan-active *Mc*LPMO9H and in putatively xylan-active *Pc*LPMO9D and *Tt*LPMO9E but not in xylan-active *Nc*LPMO9L and other AA9 LPMOs, including Tyr2-containing LPMOs (Fig. 1 and 7, Fig. S5). This solvent-exposed Tyr71, which is located within the Seg2 active-site segment, may interact directly with the substrate and may also affect the copper site.

In light of what is known about LPMOs, the occurrence of these two tyrosines (Tyr2 and Tyr71) close to the copper center (Fig. 9) is striking. Both residues are in the second coordination sphere of the copper, and they form a chain of closely connected aromatic residues that also includes the highly conserved tyrosine, Tyr157, in *Nc*LPMO9F whose hydroxyl group occupies the proximal axial copper coordination position.

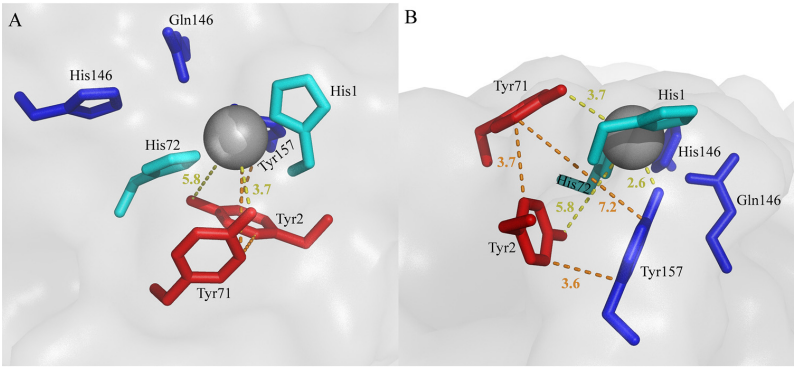

FIG 9 Copper center of *Nc*LPMO9F. The pictures show a top-down view (A) and a side view (B). The closest distances (in Å) between the tyrosine hydroxyls and the copper (yellow lines) and the closest distances between the aromatic rings of the three tyrosines (orange lines) are indicated.

Although further work is needed to elucidate the possible effects of these tyrosines, it is clear that each of them could affect the redox chemistry and redox stability of the copper center (18, 58). The solvent-exposed Tyr71, which has previously been associated with oxidative regioselectivity (59), is of particular interest, since its hydroxyl group occupies a space that is occupied by the C-6 hydroxymethyl group of a glucose in complexes of (C-4-oxidizing) AA9 LPMOs with a cello-oligomer (55, 57). Since there are strong indications from experiments (55, 59) and modeling (60) that cellulose binding to LPMO9s modulates copper site electronics, likely improving oxidant activation, it is tempting to speculate that the hydroxyl group of Tyr71 compensates for the lack of the C-6 hydroxymethyl group in a xylan substrate. While the xylanolytic activity of *Nc*LPMO9L, lacking this tyrosine, shows that Tyr71 is not essential for xylanolytic activity, it is worth noting that of the three xylan-active LPMOs that are compared in Fig. 6D, *Nc*LPMO9L seemed least active on xylan.

Figures 1, 7, and 8 show additional features of the putative substrate-binding surface of xylan-active LPMOs. One particular feature is the presence of an asparagine, Asn197, in *Nc*LPMO9F, in the large majority of members of the *Nc*LPMO9F clade (Fig. S5) at a position where most other AA9 LPMOs, including xylan-active LPMOs outside this clade, have a tyrosine (Fig. 7 and 8, Fig. S4). Computational (53, 61, 62) and experimental studies (61) have shown that this tyrosine interacts with the cellulose substrate through aromatic stacking with the main cellulose chain and hydrogen bonding with adjacent cellulose chains. Figure 8 illustrates that exchanging Tyr with Asn may have a major impact on the substrate-binding surface, and one can speculate that this exchange could explain why *Nc*LPMO9F has the higher activity on xylan (Fig. 6D). Almost all AA9 LPMOs have an exposed aromatic residue in this region, and this is also the case for members of the *Nc*LPMO9F clade (e.g., Tyr198 in *Nc*LPMO9F) (Fig. 8). Interestingly, xylan-active *Nc*LPMO9L and *Mc*LPMO9H have two well-aligned surface-exposed aromatic residues in this region (e.g., Tyr200 and Tyr201 in *Nc*LPMO9L) (Fig. 8), which is an uncommon arrangement among other AA9 LPMOs (Fig. S6). Finally, Fig. 8 illustrates the 26 to 31 region, containing several solvent-exposed residues with hydrogen-bonding potential and showing considerable sequence variation (Fig. S4 and S5), which could affect xylanolytic activity.

Concluding remarks. The abundance of LPMO genes in fungal genomes raises interesting questions on their functional variation. The genomes of dikaryotic fungi with a minimum of one AA9 gene contain, on average, 12 AA9 genes, with some species having more than 50 (8). Such multiplicity likely reflects an evolutionary response to the heterogeneity of lignocellulosic substrates. Xylan is the third most abundant

biopolymer on earth and is found in the cell walls of all grasses, hardwoods, and softwoods, being an important structural component that coats the cellulose microfibrils and facilitates interactions with lignin (63). Enzymes that remove and depolymerize recalcitrant xylan not only provide the organism with sugars for primary metabolism but also give access to the cellulose underneath. While xylanolytic activity has been detected in the AA14 family (30), this LPMO family is not abundant and is missing completely in 36% of basidiomycete genomes, 76% of ascomycete genomes, and in *N. crassa* (33). On the other hand, AA9s are more abundant and equally common in ascomycetes and basidiomycetes (8). Considering the abundance of xylan and its presence in insoluble copolymeric structures with cellulose, it would not be surprising if xylanolytic activity was more widespread in the AA9 family than previously thought.

In this work, we demonstrate that *Nc*LPMO9F, known to be cellulose active, and the previously uncharacterized *Nc*LPMO9L are both able to oxidize glucuronoxylan, an important component of grass and hardwood cell walls (64). Importantly, we provide quantitative data for xylan conversion showing that xylanolytic activity is not a weak side activity but rather the primary activity of at least some xylan-active LPMOs. The various ratios between cellulose- and xylan-derived oxidized products for the three xylan-active LPMOs (Fig. 6D) are remarkable and suggest functional variation that may relate, for example, to xylan variability. Xylans come in many forms, showing compositional and structural variation, and it would be of major interest to assess LPMO activity on a wider range of xylan substrates, such as glucuronoarabinoxylan or arabinoxylan.

The discovery that a previously well-characterized LPMO such as *Nc*LPMO9F acts more efficiently on xylan than on cellulose raises the question of whether other well-characterized cellulose-active LPMOs could have undetected capabilities. Side activities or true bifunctionality may have remained undetected because alternative substrates were not tested, because reaction conditions were wrong (e.g., conditions leading to rapid LPMO inactivation), or because alternative substrates were tested alone rather than in combination with cellulose. The latter is not only important for detecting xylanolytic activity (21, 23) but also may be needed to detect activity on other hemicelluloses, such as xyloglucan (65).

The combination of the functional data obtained in this study and the wealth of sequence and structural data for AA9s allowed us not only to point at a cluster of LPMOs that are likely xylan active (Fig. 1) but also to point at structural features near the copper site and on the substrate-binding surface that may be unique or typical for xylan-active AA9s. It is likely that the ancestral LPMO of the xylan-active cluster is of ancient origin, as LPMOs belonging to this cluster occur in both ascomycete and basidiomycete fungal species. It will be exciting to see whether the importance of structural features identified here will be confirmed by future mutagenesis studies of xylan-active and other LPMOs. In this respect, it must be noted that available data indicate that the substrate specificity of LPMOs is a complex trait that depends on multiple residues on and near the substrate-binding surface (50, 51, 66, 67).

The current findings open up several questions that warrant further research. For example, it remains to be seen if the natural function of *Nc*LPMO9F is to degrade (glucurono) xylan or whether it is a truly bifunctional enzyme that has evolved to sequentially oxidize the xylan coating cellulose fibers in natural substrates, followed by oxidation of cellulose. Of note, bifunctional enzymes are not uncommon in cellulolytic enzyme machineries, as exemplified by the particularly powerful *Tr*Cel7B that acts on both cellulose and xylan (68). Such bifunctional enzymes could give a fitness advantage, as production and secretion of enzymes come at a cost for the organism. Another key question for further studies is whether these xylan-active LPMOs could offer advantages in the industrial processing of lignocellulosic biomass. Depending on the feedstock and the pretreatment method used, recalcitrant xylan may be an obstacle for cellulose saccharification, and it is conceivable that LPMOs such as *Nc*LPMO9F can remove this obstacle.

MATERIALS AND METHODS

Enzymes. *Gt*LPMO9B (UniProt ID S7RK00) from *G. trabeum* was produced and purified as described by Hegnar et al. (43). *Mc*LPMO9H (GenBank ID QDV60872.1) from *M. cinnamomea* was produced and

purified as described by Hüttner et al. (23). *Nc*LPMO9C (NCU02916; UniProt ID Q7SHI8) and *Nc*LPMO9F (NCU03328; UniProt ID Q1K4Q1) from *N. crassa* were produced and purified as outlined by Kittl et al. (35). CelS2 (*Sc*LPMO10C) from *S. coelicolor* was produced and purified as described by Forsberg et al. (69). *Ta*LPMO9A from *T. aurantiacus* (UniProt ID G3XAP7) was produced and purified as reported earlier (70). *Ls*LPMO9A from *L. similis* (GenBank ID ALN96977.1) was produced and purified as described by Rieder et al. (71). Cellobiohydrolase *Tr*Cel7A from *Trichoderma reesei* (UniProt ID P62694) was prepared from a culture filtrate of *T. reesei* QM 9414 (D-74075; VTT Culture Collection, Finland) as described in reference 72, and the endoxylanase *Cj*Xyn10A from *Cellvibrio japonicus* (UniProt ID P14768) was purchased from NZYTech (Lisbon, Portugal). β-Xylosidase from *Bacillus pumilus* and α-glucuronidase from *Geobacillus stearothermophilus* were purchase from Megazyme.

The coding sequence of *Nc*LPMO9L (gene ID NUC02344; UniProt ID Q7S411), including the native signal peptide, was codon optimized and synthesized between an EcoRI site and a Kozak sequence at the 5′ end (GAATTCGAAAGC) and a stop codon and an Acc65I site (TAAGGTACC) at the 3′ end by GenScript (Piscataway, NJ, USA). The gene was excised using restriction digestion and cloned into a linearized pPinkGAP plasmid (73) using ligation. The resulting plasmid was linearized with AflII (New England BioLabs, Ipswich, MA, USA) and transformed into PichiaPink strain 4 (Invitrogen, Life Technologies Corporation AS, Carlsbad, CA, USA) by following the manufacturer's instructions. The transformant with the highest protein production level was selected following a previously described protocol (73).

For production and purification of *Nc*LPMO9L, first, an overnight culture of the strain expressing *Nc*LPMO9L was grown in 12.5 ml BMGY medium in a 250-ml baffled shake flask at 29°C and 250 rpm. The overnight culture was used to inoculate 500 ml BMGY in a 2-liter baffled shake flask, followed by incubation at 29°C with mixing at 200 rpm. The supernatants were harvested after 72 h, and the cells were removed by centrifugation at 4°C and 1,500 $\times$ *g* for 10 min. The culture supernatants were filtered through a 0.2-μm polyethersulfone (PES) membrane and diluted and reconcentrated several times with Milli-Q water and then with 50 mM BisTris-HCl buffer, pH 6.5, using a VivaFlow 200 tangential crossflow concentrator (molecular weight cutoff, MWCO, 10,000; Sartorius Stedim Biotech GmbH, Göttingen, Germany). *Nc*LPMO9L was purified in two steps. First, the concentrated and buffer-exchanged supernatant was loaded onto a 5-ml CM-FF column equilibrated with 50 mM BisTris-HCl buffer, pH 6.5, using 1.5 ml/min flow rate, and eluted with a linear gradient from 0% to 50% 50 mM BisTris-HCl, pH 6.5, 1 M NaCl. The fractions containing *Nc*LPMO9L were pooled and then concentrated and washed with 50 mM BisTris-HCl, pH 6.5, 150 mM NaCl, using VivaSpin centrifugal tubes (MWCO, 10,000; Sartorius Stedim Biotech GmbH). The protein sample was then loaded onto a 120-ml HiLoad 16/600 Superdex column (GE Healthcare Life Sciences, Uppsala, Sweden) equilibrated with 50 mM BisTris-HCl, pH 6.5, 150 mM NaCl, at 1 ml/min flow rate. The fractions containing *Nc*LPMO9L were pooled, concentrated, and washed with 50 mM BisTris-HCl, pH 6.5, using VivaSpin centrifugal tubes (MWCO, 10,000; Sartorius Stedim Biotech Gmbh), followed by sterilization by filtration.

Substrates. Phosphoric acid swollen cellulose (PASC) was prepared from Avicel as described previously (74). Beechwood xylan (BeWX) was purchased from Megazyme (product no. P-XYLNBE; Bray, Ireland). According to the supplier, this xylan contains approximately 13% α-(1→2)-linked substitutions with 4-*O*-methylated glucuronic acid (GlcAOMe).

LPMO reactions. LPMO activity was assessed in 100- or 150-μl reaction mixtures, containing either 0.4% (wt/vol) PASC, 0.4% (wt/vol) BeWX, or 0.4% (wt/vol) PASC plus 0.4% (wt/vol) BeWX as the substrate. The PASC–BeWX mixtures were prepared by mixing the two substrates in 50 mM BisTris-HCl buffer, pH 6.0, after which the mixtures were left at room temperature for 30 min to allow BeWX to adsorb onto the cellulose surface. All reactions were performed with 1 μM LPMO and 1 mM AscA in 50 mM BisTris-HCl buffer, pH 6.0. Samples were incubated in an Eppendorf ThermoMixer C (Eppendorf, Hamburg, Germany) at 45°C and 1,000 rpm for 24 h. Control reactions were performed in the absence of AscA. Reactions were stopped by boiling for 5 min, and the soluble fraction was separated from the insoluble material by filtration using a 96-well filter plate (Millipore; Darmstadt, Germany) operated with a vacuum manifold. Soluble fractions were subsequently analyzed using HPAEC-PAD and MALDI-TOF MS, as described below. All experiments were performed in triplicate.

For time series, reaction mixtures were set up with 600 μl total volume. Reaction mixtures contained 1 μM LPMO, 1 mM AscA, and either 0.4% (wt/vol) PASC, 0.4% BeWX (wt/vol), or 0.4% (wt/vol) PASC plus 0.4% (wt/vol) BeWX in 50 mM BisTris-HCl buffer, pH 6.0. The reaction mixtures were incubated in an Eppendorf ThermoMixer C (Eppendorf, Hamburg, Germany) at 45°C and 1,000 rpm. Samples (100 μl) were taken at 30, 60, 120, 180, and 240 min, and the reaction was stopped by boiling for 5 min, after which the soluble and insoluble fractions were separated by centrifugation at 11,000 $\times$ *g* for 10 min. Control reactions were performed in the absence of AscA. All reactions were performed in triplicate.

For quantification of product formation, the soluble fraction (25 μl) was mixed with 23 μl 150 mM sodium-acetate buffer, pH 4.75, 1 μl *Tr*Cel7A solution (1 μM final concentration), and 1 μl *Cj*Xyn10A solution (1 μM final concentration). The pH was chosen as a compromise between the optimum pHs for *Tr*Cel7A (pH 4.5) and *Cj*Xyn10A (pH 5.0). *Tr*Cel7A converts native and oxidized cello-oligosaccharides to, primarily, native and oxidized dimers, i.e., cellobiose (Glc2), cellobionic acid (GlcGlc1A), or C-4-oxidized cellobiose (Glc4gemGlc), where the occurrence of the latter two depends on the regioselectivity of the LPMO. In addition, minor amounts of glucose and oxidized trimers may be detected. *Cj*Xyn10A converts xylo-oligosaccharides to shorter linear and branched xylo-oligosaccharides, among which native xylobiose (Xyl2) and xylotriose (Xyl3) and their C-1-oxidized forms, xylobionic acid (XylXyl1A) and xylotrionic acid (Xyl2Xyl1A), can be quantified (see below). Soluble products treated in this way were subsequently analyzed using HPAEC-PAD.

Detection and quantification of oxidized products. Oxidized products were analyzed using HPAEC-PAD and MALDI-TOF MS. HPAEC-PAD was performed on a Dionex ICS-5000 system (Dionex, Sunnyvale, CA, USA) equipped with a CarboPac PA200 analytical column (3 by 250 mm) and a CarboPac PA200 guard column (3 by 50 mm). The ICS-5000 instrument was operated with 0.1 M NaOH (eluent A) at a column temperature of 30°C and a flow rate of 0.5 ml/min. A multistep 39-min gradient with increasing amounts of eluent B (0.1 M NaOH plus 1 M NaOAc) was used to elute the products. The gradient was linear from 0 to 5.5% B over 4.5 min; convex upward (gradient type 4) from 5.5% to 15% B over 9 min; concave upward (gradient type 8) from 15% to 100% B over 16.5 min; linear from 100% to 0% B over 0.1 min; stable at 0% B (reconditioning) for 8.9 min.

Chromatograms were analyzed using Chromeleon 7.0 software (Thermo Fischer Scientific, Waltham, MA, USA). Identification of native and oxidized cello- and xylo-oligosaccharides was achieved by using corresponding standards with DP2 to -6. The oxidized cello- and xylo-oligosaccharide standards were prepared by treating 0.05 g/liter Xyl2-Xyl6 or 0.05 g/liter Glc2-Glc6 with 1 μM cellobiose dehydrogenase from *Myriococcum thermophilum* (*Mt*CDH; GenBank ID EF492052.3) (36, 75) in 50 mM Na-acetate buffer, pH 5.0, at 40°C for 20 h. Quantitative estimates of C-1-oxidizing LPMO activity on cellulose and xylan were based on quantification of cellobionic acid (GlcGlc1A) and cellotrionic acid (Glc2Glc1A) for cellulose products and of xylobionic acid (XylXyl1A) and xylotrionic acid (Xyl2Xyl1A) for xylan products (after treating the original products with hydrolases, as described above). These single-compound standards were prepared like the DP2 to -6 mix standards described above. All experiments were performed in triplicate. Analyses of AscA-free and LPMO-free control reactions by HPAEC-PAD showed the presence of small amounts of xylobionic acid, xylotrionic acid, and cellotrionic acid (or other compounds with identical retention times). The areas from these peaks were identical in both types of control reactions and were subtracted when calculating final product concentrations.

Analysis by MALDI-TOF MS was performed with an Ultraflex instrument (Bruker Daltonics GmbH, Bremen, Germany) equipped with a nitrogen 337-nm laser beam, in positive reflector mode, as described previously (20). Sample (1 μl) was mixed with 2 μl matrix solution (10 mg/ml 2,5-dihydroxybenzoic acid in 30% acetonitrile and 0.1% trifluoroacetic acid), applied to a MTP384 ground steel target plate (Bruker Daltonics) and air-dried. Data were collected with flexControl 3.4 (Bruker) and analyzed using mMass v5.5.0 (http://www.mmass.org/).

Sequence and structure analyses. For sequence and phylogenetic analyses of *Nc*LPMO9F and *Mc*LPMO9H, the 50 sequences that were most similar to either protein were obtained using the NCBI BLAST tool (https://blast.ncbi.nlm.nih.gov/Blast.cgi) searched against the UniProt RefSeq database. The sequences were manually checked, and a total of seven incomplete or duplicate sequences were removed. The sequences of *Tt*LPMO9E (UniProt ID G2RGE5) and *Mt*LPMO9A (UniProt ID G2QNT0) were among the 50 most similar to *Nc*LPMO9F, while no characterized LPMOs were among the top 50 most similar to *Mc*LPMO9H. A multiple-sequence alignment (MSA) was generated using the resulting data set of 93 AA9 sequences, all 14 *Nc*LPMO9s, *Mc*LPMO9H, and a selection of 32 characterized AA9 LPMOs, using only the AA9 domain and leaving out signal peptides. The MSA was made with T-Coffee's Expresso tool (http://tcoffee.crg.cat/apps/tcoffee/index.html), which takes into account structural information (76), and was processed using ClustalX 2.1 (77). The resulting MSA (containing 140 sequences) was used for phylogenetic analysis using the ProtTest 3.4 software package (78) by calculating likelihood scores using all included substitution matrices, all improvements (+I, +G, +I +G), and 4 categories for rate variation, empirical amino acid frequencies, and a fixed BIONJ JTT tree for base likelihood calculations. A consensus tree was built with all 120 likelihood scores using the Akaike information criterion (AIC). The resulting consensus tree was edited for publication using iTol v5 (https://itol.embl.de/) (79).

Structure analysis was performed using PyMOL 0.99 (80). The following structures were downloaded from the Protein Data Bank (PDB): 2VTC (*Tr*LPMO9B), 2YET (*Ta*LPMO9A), 3EII (*Tt*LPMO9E), 4B5Q (*Pc*LPMO9D), 4D7U (*Nc*LPMO9C), 4EIR (*Nc*LPMO9D), 4EIS (*Nc*LPMO9M), 4QI8 (*Nc*LPMO9F), 5ACF (*Ls*LPMO9A), 5FOH (*Nc*LPMO9A), 5NLT (*Cv*LPMO9A), 5NNS (*Hi*LPMO9B), 5O2W (*Tr*LPMO9A), 5UFV (*Mt*PMO3, or MYCTH_92668), 6H1Z (*Af*LPMO9B from *Aspergillus fumigatus*), and 6RS6 (*Ls*LPMO9B). Models for *Gt*LPMO9B, *Mc*LPMO9H, *Mt*LPMO9A (MYCTH_85556), and *Nc*LPMO9L were built using the PHYRE2 Protein Fold Recognition Server (81) in the "intensive" modeling mode, using only the AA9 domain and removing the signal peptide. All models and PDB structures were aligned to the crystal structure of *Nc*LPMO9F for structural comparison.

SUPPLEMENTAL MATERIAL

Supplemental material is available online only.

SUPPLEMENTAL FILE 1, PDF file, 3.5 MB.

ACKNOWLEDGMENTS

This work was financed by the Research Council of Norway through grants 262853, 268002 (Enzymes4Fuels), and 257622 (Bio4Fuels) and by the Novo Nordisk Foundation (grant agreement no. NNF-0061165).

We gratefully thank Ivan Ayuso-Fernandez for insightful comments and suggestions on the *in silico* analysis and Lukas Rieder for generously supplying *Ls*LPMO9A.

REFERENCES

1. Cragg SM, Beckham GT, Bruce NC, Bugg TDH, Distel DL, Dupree P, Etxabe AG, Goodell BS, Jellison J, McGeehan JE, McQueen-Mason SJ, Schnorr K, Walton PH, Watts JEM, Zimmer M. 2015. Lignocellulose degradation mechanisms across the Tree of Life. Curr Opin Chem Biol 29:108–119. https://doi.org/10.1016/j.cbpa.2015.10.018.
2. Eastwood DC, Floudas D, Binder M, Majcherczyk A, Schneider P, Aerts A, Asiegbu FO, Baker SE, Barry K, Bendiksby M, Blumentritt M, Coutinho PM, Cullen D, de Vries RP, Gathman A, Goodell B, Henrissat B, Ihrmark K, Kauserud H, Kohler A, LaButti K, Lapidus A, Lavin JL, Lee Y-H, Lindquist E, Lilly W, Lucas S, Morin E, Murat C, Oguiza JA, Park J, Pisabarro AG, Riley R, Rosling A, Salamov A, Schmidt O, Schmutz J, Skrede I, Stenlid J, Wiebenga A, Xie X, Kües U, Hibbett DS, Hoffmeister D, Högberg N, Martin F, Grigoriev IV, Watkinson SC. 2011. The plant cell wall–decomposing machinery underlies the functional diversity of forest fungi. Science 333:762–765. https://doi.org/10.1126/science.1205411.
3. Floudas D, Binder M, Riley R, Barry K, Blanchette RA, Henrissat B, Martínez AT, Otillar R, Spatafora JW, Yadav JS, Aerts A, Benoit I, Boyd A, Carlson A, Copeland A, Coutinho PM, de Vries RP, Ferreira P, Findley K, Foster B, Gaskell J, Glotzer D, Górecki P, Heitman J, Hesse C, Hori C, Igarashi K, Jurgens JA, Kallen N, Kersten P, Kohler A, Kües U, Kumar TKA, Kuo A, LaButti K, Larrondo LF, Lindquist E, Ling A, Lombard V, Lucas S, Lundell T, Martin R, McLaughlin DJ, Morgenstern I, Morin E, Murat C, Nagy LG, Nolan M, Ohm RA, Patyshakuliyeva A, et al. 2012. The Paleozoic origin of enzymatic lignin decomposition reconstructed from 31 fungal genomes. Science 336:1715–1719. https://doi.org/10.1126/science.1221748.
4. Riley R, Salamov AA, Brown DW, Nagy LG, Floudas D, Held BW, Levasseur A, Lombard V, Morin E, Otillar R, Lindquist EA, Sun H, LaButti KM, Schmutz J, Jabbour D, Luo H, Baker SE, Pisabarro AG, Walton JD, Blanchette RA, Henrissat B, Martin F, Cullen D, Hibbett DS, Grigoriev IV. 2014. Extensive sampling of basidiomycete genomes demonstrates inadequacy of the white-rot/brown-rot paradigm for wood decay fungi. Proc Natl Acad Sci U S A 111:9923–9928. https://doi.org/10.1073/pnas.1400592111.
5. Nagy LG, Riley R, Tritt A, Adam C, Daum C, Floudas D, Sun H, Yadav JS, Pangilinan J, Larsson K-H, Matsuura K, Barry K, Labutti K, Kuo R, Ohm RA, Bhattacharya SS, Shirouzu T, Yoshinaga Y, Martin FM, Grigoriev IV, Hibbett DS. 2016. Comparative genomics of early-diverging mushroom-forming fungi provides insights into the origins of lignocellulose decay capabilities. Mol Biol Evol 33:959–970. https://doi.org/10.1093/molbev/msv337.
6. Levasseur A, Drula E, Lombard V, Coutinho PM, Henrissat B. 2013. Expansion of the enzymatic repertoire of the CAZy database to integrate auxiliary redox enzymes. Biotechnol Biofuels 6:41. https://doi.org/10.1186/1754-6834-6-41.
7. Lombard V, Golaconda Ramulu H, Drula E, Coutinho PM, Henrissat B. 2014. The carbohydrate-active enzymes database (CAZy) in 2013. Nucleic Acids Res 42:D490–D495. https://doi.org/10.1093/nar/gkt1178.
8. Várnai A, Hegnar OA, Horn SJ, Eijsink VG, Berrin J-G. 2021. Fungal lytic polysaccharide monooxygenases (LPMOs): biological importance and applications, p 281–294. Encyclopedia of Mycology, vol 2. Elsevier, San Diego, CA. https://doi.org/10.1016/B978-0-12-819990-9.00019-6.
9. Vaaje-Kolstad G, Westereng B, Horn SJ, Liu Z, Zhai H, Sørlie M, Eijsink VG. 2010. An oxidative enzyme boosting the enzymatic conversion of recalcitrant polysaccharides. Science 330:219–222. https://doi.org/10.1126/science.1192231.
10. Quinlan RJ, Sweeney MD, Lo Leggio L, Otten H, Poulsen J-CN, Johansen KS, Krogh KBRM, Jørgensen CI, Tovborg M, Anthonsen A, Tryfona T, Walter CP, Dupree P, Xu F, Davies GJ, Walton PH. 2011. Insights into the oxidative degradation of cellulose by a copper metalloenzyme that exploits biomass components. Proc Natl Acad Sci U S A 108:15079–15084. https://doi.org/10.1073/pnas.1105776108.
11. Phillips CM, Beeson IW, Cate JH, Marletta MA. 2011. Cellobiose dehydrogenase and a copper-dependent polysaccharide monooxygenase potentiate cellulose degradation by Neurospora crassa. ACS Chem Biol 6:1399–1406. https://doi.org/10.1021/cb200351y.
12. Horn SJ, Vaaje-Kolstad G, Westereng B, Eijsink V. 2012. Novel enzymes for the degradation of cellulose. Biotechnol Biofuels 5:45. https://doi.org/10.1186/1754-6834-5-45.
13. Chylenski P, Bissaro B, Sørlie M, Røhr ÅK, Várnai A, Horn SJ, Eijsink VG. 2019. Lytic polysaccharide monooxygenases in enzymatic processing of lignocellulosic biomass. ACS Catal 9:4970–4991. https://doi.org/10.1021/acscatal.9b00246.
14. Courtade G, Ciano L, Paradisi A, Lindley PJ, Forsberg Z, Sørlie M, Wimmer R, Davies GJ, Eijsink VGH, Walton PH, Aachmann FL. 2020. Mechanistic basis of substrate–O_2 coupling within a chitin-active lytic polysaccharide monooxygenase: an integrated NMR/EPR study. Proc Natl Acad Sci U S A 117:19178–19189. https://doi.org/10.1073/pnas.2004277117.
15. Bissaro B, Røhr ÅK, Müller G, Chylenski P, Skaugen M, Forsberg Z, Horn SJ, Vaaje-Kolstad G, Eijsink VG. 2017. Oxidative cleavage of polysaccharides by monocopper enzymes depends on H_2O_2. Nat Chem Biol 13:1123–1128. https://doi.org/10.1038/nchembio.2470.
16. Bissaro B, Streit B, Isaksen I, Eijsink VG, Beckham GT, DuBois JL, Røhr ÅK. 2020. Molecular mechanism of the chitinolytic peroxygenase reaction. Proc Natl Acad Sci U S A 117:1504–1513. https://doi.org/10.1073/pnas.1904889117.
17. Kont R, Bissaro B, Eijsink VG, Väljamäe P. 2020. Kinetic insights into the peroxygenase activity of cellulose-active lytic polysaccharide monooxygenases (LPMOs). Nat Commun 11:5786. https://doi.org/10.1038/s41467-020-19561-8.
18. Jones SM, Transue WJ, Meier KK, Kelemen B, Solomon EI. 2020. Kinetic analysis of amino acid radicals formed in H_2O_2-driven Cu^I LPMO reoxidation implicates dominant homolytic reactivity. Proc Natl Acad Sci U S A 117:11916–11922. https://doi.org/10.1073/pnas.1922499117.
19. Hedison TM, Breslmayr E, Shanmugam M, Karnpakdee K, Heyes DJ, Green AP, Ludwig R, Scrutton NS, Kracher D. 2020. Insights into the H_2O_2-driven catalytic mechanism of fungal lytic polysaccharide monooxygenases. FEBS J 288:4115–4128. https://doi.org/10.1111/febs.15704.
20. Agger JW, Isaksen T, Várnai A, Vidal-Melgosa S, Willats WG, Ludwig R, Horn SJ, Eijsink VG, Westereng B. 2014. Discovery of LPMO activity on hemicelluloses shows the importance of oxidative processes in plant cell wall degradation. Proc Natl Acad Sci U S A 111:6287–6292. https://doi.org/10.1073/pnas.1323629111.
21. Frommhagen M, Sforza S, Westphal AH, Visser J, Hinz SW, Koetsier MJ, van Berkel WJ, Gruppen H, Kabel MA. 2015. Discovery of the combined oxidative cleavage of plant xylan and cellulose by a new fungal polysaccharide monooxygenase. Biotechnol Biofuels 8:101. https://doi.org/10.1186/s13068-015-0284-1.
22. Berka RM, Grigoriev IV, Otillar R, Salamov A, Grimwood J, Reid I, Ishmael N, John T, Darmond C, Moisan M-C, Henrissat B, Coutinho PM, Lombard V, Natvig DO, Lindquist E, Schmutz J, Lucas S, Harris P, Powlowski J, Bellemare A, Taylor D, Butler G, de Vries RP, Allijn IE, van den Brink J, Ushinsky S, Storms R, Powell AJ, Paulsen IT, Elbourne LDH, Baker SE, Magnuson J, Laboissiere S, Clutterbuck AJ, Martinez D, Wogulis M, de Leon AL, Rey MW, Tsang A. 2011. Comparative genomic analysis of the thermophilic biomass-degrading fungi Myceliophthora thermophila and Thielavia terrestris. Nat Biotechnol 29:922–927. https://doi.org/10.1038/nbt.1976.
23. Hüttner S, Várnai A, Petrović DM, Bach CX, Anh DTK, Thanh VN, Eijsink VG, Larsbrink J, Olsson L. 2019. Specific xylan activity revealed for AA9 lytic polysaccharide monooxygenases of the thermophilic fungus Malbranchea cinnamomea by functional characterization. Appl Environ Microbiol 85:e01408-19. https://doi.org/10.1128/AEM.01408-19.
24. Busse-Wicher M, Li A, Silveira RL, Pereira CS, Tryfona T, Gomes TC, Skaf MS, Dupree P. 2016. Evolution of xylan substitution patterns in gymnosperms and angiosperms: implications for xylan interaction with cellulose. Plant Physiol 171:2418–2431. https://doi.org/10.1104/pp.16.00539.
25. Iwata T, Indrarti L, Azuma J-I. 1998. Affinity of hemicellulose for cellulose produced by Acetobacter xylinum. Cellulose 5:215–228. https://doi.org/10.1023/A:1009237401548.
26. Kabel MA, van den Borne H, Vincken J-P, Voragen AG, Schols HA. 2007. Structural differences of xylans affect their interaction with cellulose. Carbohydr Polym 69:94–105. https://doi.org/10.1016/j.carbpol.2006.09.006.
27. Grantham NJ, Wurman-Rodrich J, Terrett OM, Lyczakowski JJ, Stott K, Iuga D, Simmons TJ, Durand-Tardif M, Brown SP, Dupree R, Busse-Wicher M, Dupree P. 2017. An even pattern of xylan substitution is critical for interaction with cellulose in plant cell walls. Nat Plants 3:859–865. https://doi.org/10.1038/s41477-017-0030-8.
28. Terrett OM, Lyczakowski JJ, Yu L, Iuga D, Franks WT, Brown SP, Dupree R, Dupree P. 2019. Molecular architecture of softwood revealed by solid-state NMR. Nat Commun 10:4978. https://doi.org/10.1038/s41467-019-12979-9.
29. Simmons TJ, Frandsen KEH, Ciano L, Tryfona T, Lenfant N, Poulsen JC, Wilson LFL, Tandrup T, Tovborg M, Schnorr K, Johansen KS, Henrissat B, Walton PH, Lo Leggio L, Dupree P. 2017. Structural and electronic determinants of lytic polysaccharide monooxygenase reactivity on polysaccharide

substrates. Nat Commun 8:1064. https://doi.org/10.1038/s41467-017-01247-3.
30. Couturier M, Ladevèze S, Sulzenbacher G, Ciano L, Fanuel M, Moreau C, Villares A, Cathala B, Chaspoul F, Frandsen KE, Labourel A, Herpoël-Gimbert I, Grisel S, Haon M, Lenfant N, Rogniaux H, Ropartz D, Davies GJ, Rosso M-N, Walton PH, Henrissat B, Berrin J-G. 2018. Lytic xylan oxidases from wood-decay fungi unlock biomass degradation. Nat Chem Biol 14:306–310. https://doi.org/10.1038/nchembio.2558.
31. Zerva A, Pentari C, Grisel S, Berrin J-G, Topakas E. 2020. A new synergistic relationship between xylan-active LPMO and xylobiohydrolase to tackle recalcitrant xylan. Biotechnol Biofuels 13:142. https://doi.org/10.1186/s13068-020-01777-x.
32. Petrović DM, Várnai A, Dimarogona M, Mathiesen G, Sandgren M, Westereng B, Eijsink VG. 2019. Comparison of three seemingly similar lytic polysaccharide monooxygenases from Neurospora crassa suggests different roles in plant biomass degradation. J Biol Chem 294:15068–15081. https://doi.org/10.1074/jbc.RA119.008196.
33. Galagan JE, Calvo SE, Borkovich KA, Selker EU, Read ND, Jaffe D, FitzHugh W, Ma L-J, Smirnov S, Purcell S, Rehman B, Elkins T, Engels R, Wang S, Nielsen CB, Butler J, Endrizzi M, Qui D, Ianakiev P, Bell-Pedersen D, Nelson MA, Werner-Washburne M, Selitrennikoff CP, Kinsey JA, Braun EL, Zelter A, Schulte U, Kothe GO, Jedd G, Mewes W, Staben C, Marcotte E, Greenberg D, Roy A, Foley K, Naylor J, Stange-Thomann N, Barrett R, Gnerre S, Kamal M, Kamvysselis M, Mauceli E, Bielke C, Rudd S, Frishman D, Krystofova S, Rasmussen C, Metzenberg RL, Perkins DD, Kroken S, et al. 2003. The genome sequence of the filamentous fungus Neurospora crassa. Nature 422:859–868. https://doi.org/10.1038/nature01554.
34. Vu VV, Beeson WT, Phillips CM, Cate JH, Marletta MA. 2014. Determinants of regioselective hydroxylation in the fungal polysaccharide monooxygenases. J Am Chem Soc 136:562–565. https://doi.org/10.1021/ja409384b.
35. Kittl R, Kracher D, Burgstaller D, Haltrich D, Ludwig R. 2012. Production of four *Neurospora crassa* lytic polysaccharide monooxygenases in *Pichia pastoris* monitored by a fluorimetric assay. Biotechnol Biofuels 5:79. https://doi.org/10.1186/1754-6834-5-79.
36. Tan T-C, Kracher D, Gandini R, Sygmund C, Kittl R, Haltrich D, Hällberg BM, Ludwig R, Divne C. 2015. Structural basis for cellobiose dehydrogenase action during oxidative cellulose degradation. Nat Commun 6:7542. https://doi.org/10.1038/ncomms8542.
37. Tian C, Beeson WT, Iavarone AT, Sun J, Marletta MA, Cate JH, Glass NL. 2009. Systems analysis of plant cell wall degradation by the model filamentous fungus Neurospora crassa. Proc Natl Acad Sci U S A 106:22157–22162. https://doi.org/10.1073/pnas.0906810106.
38. Arntzen MØ, Bengtsson O, Várnai A, Delogu F, Mathiesen G, Eijsink VG. 2020. Quantitative comparison of the biomass-degrading enzyme repertoires of five filamentous fungi. Sci Rep 10:20267. https://doi.org/10.1038/s41598-020-75217-z.
39. Znameroski EA, Coradetti ST, Roche CM, Tsai JC, Iavarone AT, Cate JH, Glass NL. 2012. Induction of lignocellulose-degrading enzymes in Neurospora crassa by cellodextrins. Proc Natl Acad Sci U S A 109:6012–6017. https://doi.org/10.1073/pnas.1118440109.
40. Eijsink VG, Petrovic D, Forsberg Z, Mekasha S, Røhr ÅK, Várnai A, Bissaro B, Vaaje-Kolstad G. 2019. On the functional characterization of lytic polysaccharide monooxygenases (LPMOs). Biotechnol Biofuels 12:58. https://doi.org/10.1186/s13068-019-1392-0.
41. Laurent CV, Sun P, Scheiblbrandner S, Csarman F, Cannazza P, Frommhagen M, van Berkel WJ, Oostenbrink C, Kabel MA, Ludwig R. 2019. Influence of lytic polysaccharide monooxygenase active site segments on activity and affinity. Int J Mol Sci 20:6219. https://doi.org/10.3390/ijms20246219.
42. Fry SC. 1998. Oxidative scission of plant cell wall polysaccharides by ascorbate-induced hydroxyl radicals. Biochem J 332:507–515. https://doi.org/10.1042/bj3320507.
43. Hegnar OA, Petrovic DM, Bissaro B, Alfredsen G, Várnai A, Eijsink VG. 2019. pH-dependent relationship between catalytic activity and hydrogen peroxide production shown via characterization of a lytic polysaccharide monooxygenase from *Gloeophyllum trabeum*. Appl Environ Microbiol 85:e02612-18. https://doi.org/10.1128/AEM.02612-18.
44. Petrovic DM, Bissaro B, Chylenski P, Skaugen M, Sørlie M, Jensen MS, Aachmann FL, Courtade G, Várnai A, Eijsink VG. 2018. Methylation of the N-terminal histidine protects a lytic polysaccharide monooxygenase from auto-oxidative inactivation. Protein Sci 27:1636–1650. https://doi.org/10.1002/pro.3451.
45. Forsberg Z, Vaaje-Kolstad G, Westereng B, Bunæs AC, Stenstrøm Y, MacKenzie A, Sørlie M, Horn SJ, Eijsink VG. 2011. Cleavage of cellulose by a CBM33 protein. Protein Sci 20:1479–1483. https://doi.org/10.1002/pro.689.
46. Bromley JR, Busse-Wicher M, Tryfona T, Mortimer JC, Zhang Z, Brown DM, Dupree P. 2013. GUX 1 and GUX 2 glucuronyltransferases decorate distinct domains of glucuronoxylan with different substitution patterns. Plant J 74:423–434. https://doi.org/10.1111/tpj.12135.
47. Courtade G, Forsberg Z, Heggset EB, Eijsink VG, Aachmann FL. 2018. The carbohydrate-binding module and linker of a modular lytic polysaccharide monooxygenase promote localized cellulose oxidation. J Biol Chem 293:13006–13015. https://doi.org/10.1074/jbc.RA118.004269.
48. Harris PV, Welner D, McFarland KC, Re E, Navarro Poulsen J-C, Brown K, Salbo R, Ding H, Vlasenko E, Merino S, Xu F, Cherry J, Larsen S, Lo Leggio L. 2010. Stimulation of lignocellulosic biomass hydrolysis by proteins of glycoside hydrolase family 61: structure and function of a large, enigmatic family. Biochemistry 49:3305–3316. https://doi.org/10.1021/bi100009p.
49. Westereng B, Ishida T, Vaaje-Kolstad G, Wu M, Eijsink VG, Igarashi K, Samejima M, Ståhlberg J, Horn SJ, Sandgren M. 2011. The putative endoglucanase PcGH61D from Phanerochaete chrysosporium is a metal-dependent oxidative enzyme that cleaves cellulose. PLoS One 6:e27807. https://doi.org/10.1371/journal.pone.0027807.
50. Frandsen KE, Haon M, Grisel S, Henrissat B, Leggio LL, Berrin J-G. 2021. Identification of the molecular determinants driving the substrate specificity of fungal lytic polysaccharide monooxygenases (LPMOs). J Biol Chem 296:100086. https://doi.org/10.1074/jbc.RA120.015545.
51. Jensen MS, Klinkenberg G, Bissaro B, Chylenski P, Vaaje-Kolstad G, Kvitvang HF, Nærdal GK, Sletta H, Forsberg Z, Eijsink VG. 2019. Engineering chitinolytic activity into a cellulose-active lytic polysaccharide monooxygenase provides insights into substrate specificity. J Biol Chem 294:19349–19364. https://doi.org/10.1074/jbc.RA119.010056.
52. Monclaro AV, Petrović DM, Alves GS, Costa MM, Midorikawa GE, Miller RN, Filho EX, Eijsink VG, Várnai A. 2020. Characterization of two family AA9 LPMOs from *Aspergillus tamarii* with distinct activities on xyloglucan reveals structural differences linked to cleavage specificity. PLoS One 15:e0235642. https://doi.org/10.1371/journal.pone.0235642.
53. Wu M, Beckham GT, Larsson AM, Ishida T, Kim S, Payne CM, Himmel ME, Crowley MF, Horn SJ, Westereng B, Igarashi K, Samejima M, Ståhlberg J, Eijsink VGH, Sandgren M. 2013. Crystal structure and computational characterization of the lytic polysaccharide monooxygenase GH61D from the Basidiomycota fungus Phanerochaete chrysosporium. J Biol Chem 288:12828–12839. https://doi.org/10.1074/jbc.M113.459396.
54. Sun P, Laurent CV, Scheiblbrandner S, Frommhagen M, Kouzounis D, Sanders MG, van Berkel WJ, Ludwig R, Kabel MA. 2020. Configuration of active site segments in lytic polysaccharide monooxygenases steers oxidative xyloglucan degradation. Biotechnol Biofuels 13:95. https://doi.org/10.1186/s13068-020-01731-x.
55. Frandsen KEH, Simmons TJ, Dupree P, Poulsen J-CN, Hemsworth GR, Ciano L, Johnston EM, Tovborg M, Johansen KS, von Freiesleben P, Marmuse L, Fort S, Cottaz S, Driguez H, Henrissat B, Lenfant N, Tuna F, Baldansuren A, Davies GJ, Lo Leggio L, Walton PH. 2016. The molecular basis of polysaccharide cleavage by lytic polysaccharide monooxygenases. Nat Chem Biol 12:298–303. https://doi.org/10.1038/nchembio.2029.
56. Courtade G, Wimmer R, Røhr ÅK, Preims M, Felice AKG, Dimarogona M, Vaaje-Kolstad G, Sørlie M, Sandgren M, Ludwig R, Eijsink VGH, Aachmann FL. 2016. Interactions of a fungal lytic polysaccharide monooxygenase with β-glucan substrates and cellobiose dehydrogenase. Proc Natl Acad Sci U S A 113:5922–5927. https://doi.org/10.1073/pnas.1602566113.
57. Tandrup T, Tryfona T, Frandsen KEH, Johansen KS, Dupree P, Lo Leggio L. 2020. Oligosaccharide binding and thermostability of two related AA9 lytic polysaccharide monooxygenases. Biochemistry 59:3347–3358. https://doi.org/10.1021/acs.biochem.0c00312.
58. Paradisi A, Johnston EM, Tovborg M, Nicoll CR, Ciano L, Dowle A, McMaster J, Hancock Y, Davies GJ, Walton PH. 2019. Formation of a copper(II)–tyrosyl complex at the active site of lytic polysaccharide monooxygenases following oxidation by H_2O_2. J Am Chem Soc 141:18585–18599. https://doi.org/10.1021/jacs.9b09833.
59. Borisova AS, Isaksen T, Dimarogona M, Kognole AA, Mathiesen G, Várnai A, Røhr ÅK, Payne CM, Sørlie M, Sandgren M, Eijsink VGH. 2015. Structural and functional characterization of a lytic polysaccharide monooxygenase with broad substrate specificity. J Biol Chem 290:22955–22969. https://doi.org/10.1074/jbc.M115.660183.
60. Wang B, Johnston EM, Li P, Shaik S, Davies GJ, Walton PH, Rovira C. 2018. QM/MM studies into the H_2O_2-dependent activity of lytic polysaccharide monooxygenases: evidence for the formation of a caged hydroxyl radical

intermediate. ACS Catal 8:1346–1351. https://doi.org/10.1021/acscatal.7b03888.
61. Zhou H, Zhang Y, Li T, Tan H, Li G, Yin H. 2020. Distinct interaction of lytic polysaccharide monooxygenase with cellulose revealed by computational and biochemical studies. J Phys Chem Lett 11:3987–3992. https://doi.org/10.1021/acs.jpclett.0c00918.
62. Liu B, Kognole AA, Wu M, Westereng B, Crowley MF, Kim S, Dimarogona M, Payne CM, Sandgren M. 2018. Structural and molecular dynamics studies of a C1-oxidizing lytic polysaccharide monooxygenase from Heterobasidion irregulare reveal amino acids important for substrate recognition. FEBS J 285:2225–2242. https://doi.org/10.1111/febs.14472.
63. Mellerowicz EJ, Gorshkova TA. 2012. Tensional stress generation in gelatinous fibres: a review and possible mechanism based on cell-wall structure and composition. J Exp Bot 63:551–565. https://doi.org/10.1093/jxb/err339.
64. Faik A. 2010. Xylan biosynthesis: news from the grass. Plant Physiol 153:396–402. https://doi.org/10.1104/pp.110.154237.
65. Nekiunaite L, Petrović DM, Westereng B, Vaaje-Kolstad G, Hachem MA, Várnai A, Eijsink VG. 2016. *Fg*LPMO9A from *Fusarium graminearum* cleaves xyloglucan independently of the backbone substitution pattern. FEBS Lett 590:3346–3356. https://doi.org/10.1002/1873-3468.12385.
66. Loose JS, Arntzen MØ, Bissaro B, Ludwig R, Eijsink VG, Vaaje-Kolstad G. 2018. Multipoint precision binding of substrate protects lytic polysaccharide monooxygenases from self-destructive off-pathway processes. Biochemistry 57:4114–4124. https://doi.org/10.1021/acs.biochem.8b00484.
67. Danneels B, Tanghe M, Desmet T. 2019. Structural features on the substrate-binding surface of fungal lytic polysaccharide monooxygenases determine their oxidative regioselectivity. Biotechnol J 14:1800211. https://doi.org/10.1002/biot.201800211.
68. Bailey MJ, Siika-Aho M, Valkeajärvi A, Penttilä ME. 1993. Hydrolytic properties of two cellulases of Trichoderma reesei expressed in yeast. Biotechnol Appl Biochem 17:65–76.
69. Forsberg Z, Røhr ÅK, Mekasha S, Andersson KK, Eijsink VG, Vaaje-Kolstad G, Sørlie M. 2014. Comparative study of two chitin-active and two cellulose-active AA10-type lytic polysaccharide monooxygenases. Biochemistry 53:1647–1656. https://doi.org/10.1021/bi5000433.
70. Chylenski P, Petrović DM, Müller G, Dahlström M, Bengtsson O, Lersch M, Siika-Aho M, Horn SJ, Eijsink VG. 2017. Enzymatic degradation of sulfite-pulped softwoods and the role of LPMOs. Biotechnol Biofuels 10:177. https://doi.org/10.1186/s13068-017-0862-5.
71. Rieder L, Ebner K, Glieder A, Sørlie M. 2021. Novel molecular biological tools for the efficient expression of fungal lytic polysaccharide monooxygenases in Pichia pastoris. Biotechnol Biofuels 14:122. https://doi.org/10.1186/s13068-021-01971-5.
72. Ståhlberg J, Divne C, Koivula A, Piens K, Claeyssens M, Teeri TT, Jones TA. 1996. Activity studies and crystal structures of catalytically deficient mutants of cellobiohydrolase I from *Trichoderma reesei*. J Mol Biol 264:337–349. https://doi.org/10.1006/jmbi.1996.0644.
73. Várnai A, Tang C, Bengtsson O, Atterton A, Mathiesen G, Eijsink VG. 2014. Expression of endoglucanases in Pichia pastoris under control of the GAP promoter. Microb Cell Fact 13:57. https://doi.org/10.1186/1475-2859-13-57.
74. Wood TM. 1988. Preparation of crystalline, amorphous, and dyed cellulase substrates. Methods Enzymol 160:19–25. https://doi.org/10.1016/0076-6879(88)60103-0.
75. Zámocký M, Schümann C, Sygmund C, O'Callaghan J, Dobson ADW, Ludwig R, Haltrich D, Peterbauer CK. 2008. Cloning, sequence analysis and heterologous expression in *Pichia pastoris* of a gene encoding a thermostable cellobiose dehydrogenase from *Myriococcum thermophilum*. Protein Expr Purif 59:258–265. https://doi.org/10.1016/j.pep.2008.02.007.
76. Armougom F, Moretti S, Poirot O, Audic S, Dumas P, Schaeli B, Keduas V, Notredame C. 2006. Expresso: automatic incorporation of structural information in multiple sequence alignments using 3D-Coffee. Nucleic Acids Res 34:W604–W608. https://doi.org/10.1093/nar/gkl092.
77. Larkin MA, Blackshields G, Brown NP, Chenna R, McGettigan PA, McWilliam H, Valentin F, Wallace IM, Wilm A, Lopez R, Thompson JD, Gibson TJ, Higgins DG. 2007. Clustal W and Clustal X version 2.0. Bioinformatics 23:2947–2948. https://doi.org/10.1093/bioinformatics/btm404.
78. Darriba D, Taboada GL, Doallo R, Posada D. 2011. ProtTest 3: fast selection of best-fit models of protein evolution. Bioinformatics 27:1164–1165. https://doi.org/10.1093/bioinformatics/btr088.
79. Letunic I, Bork P. 2019. Interactive Tree Of Life (iTOL) v4: recent updates and new developments. Nucleic Acids Res 47:W256–W259. https://doi.org/10.1093/nar/gkz239.
80. DeLano WL. 2002. Pymol: an open-source molecular graphics tool. CCP4 Newsl Protein Crystallogr 40:82–92.
81. Kelley LA, Mezulis S, Yates CM, Wass MN, Sternberg MJ. 2015. The Phyre2 web portal for protein modeling, prediction and analysis. Nat Protoc 10:845–858. https://doi.org/10.1038/nprot.2015.053.

Quantifying oxidation of cellulose-associated glucuronoxylan by two lytic polysaccharide monooxygenases from *Neurospora crassa*

Olav A. Hegnar[1], Heidi Østby[1], Dejan M. Petrović[1], Lisbeth Olsson[2,3], Anikó Várnai[1], Vincent G.H. Eijsink[1,#]

[1]Norwegian University of Life Sciences, Faculty of Chemistry, Biotechnology and Food Science, Ås, Norway

[2]Department of Biology and Biological Engineering, Division of Industrial Biotechnology, Chalmers University of Technology, Gothenburg, Sweden

[3]Wallenberg Wood Science Center, Chalmers University of Technology, Gothenburg, Sweden

Contents:

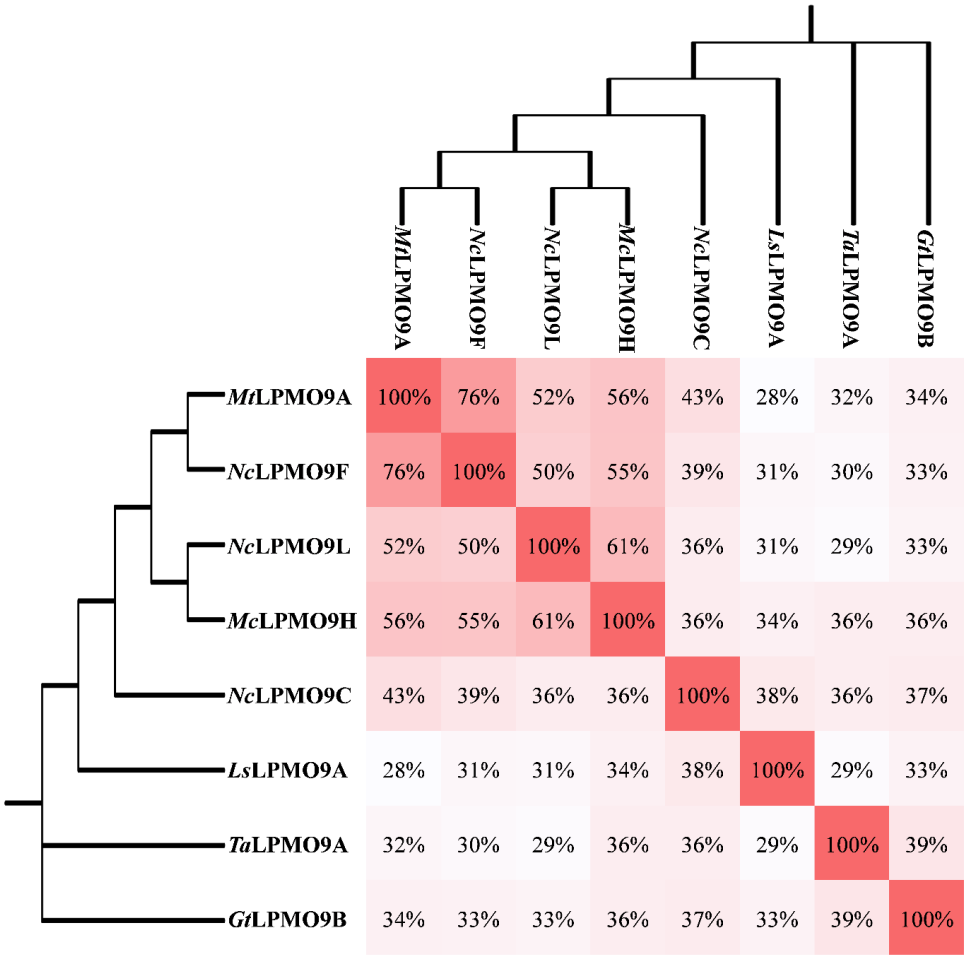

Figure S1. Phylogenetic relationship and sequence identities of selected AA9 LPMOs. The matrix table shows the sequence identities of *Nc*LPMO9F and *Nc*LPMO9L, previously known xylan-active LPMOs *Mt*LPMO9A and *Mc*LPMO9H, and additional well-characterized LPMOs that were used in the present study. The sequence identities apply to the AA9 catalytic domain only, without signal peptides, linkers and CBMs. The phylogenetic consensus tree was built using ProtTest 3.4 using an Expresso (T-Coffee) MSA of the catalytic domains only.

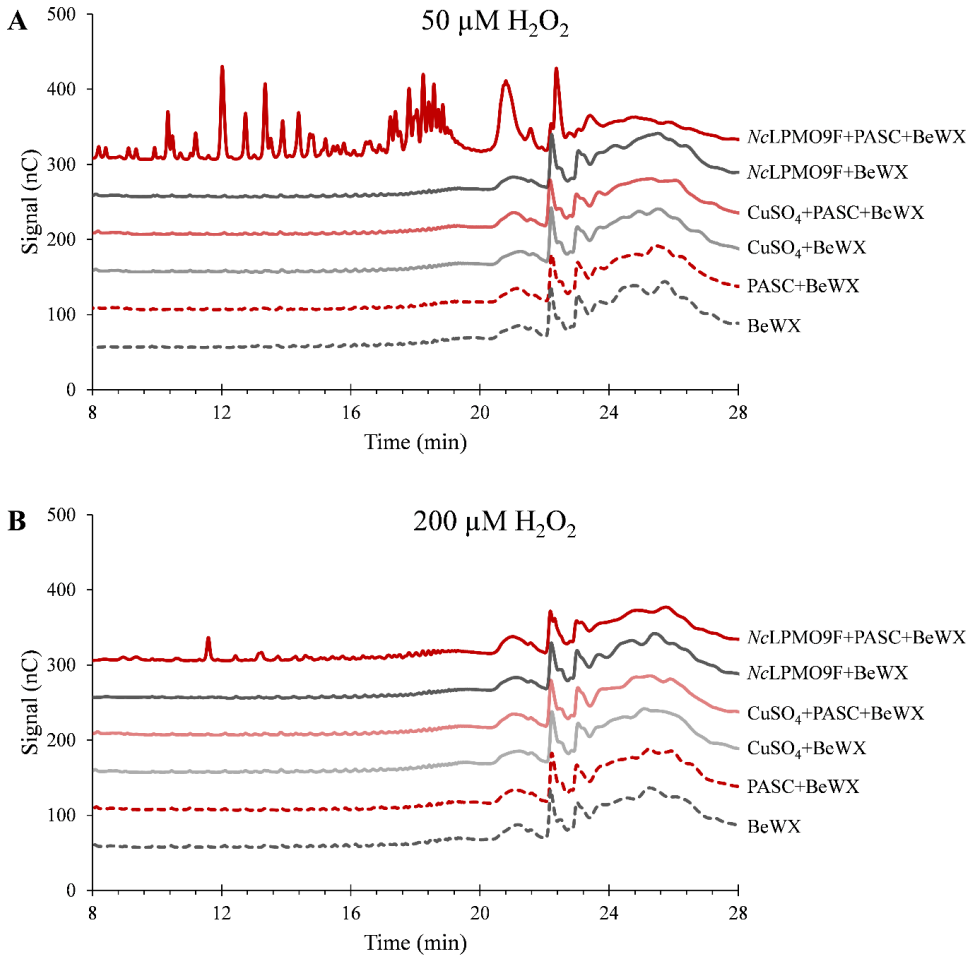

Figure S2. HPAEC-PAD chromatograms of product mixtures from reactions with BeWX or PASC and BeWX, in the presence of H_2O_2. All reactions were performed in 50 mM BisTris-HCl pH 6.0 and were initiated with the addition of 1 mM AscA. Reactions contained either 1 µM *Nc*LPMO9F (solid lines) or 1 µM $CuSO_4$ (transparent lines), or none of these two (dashed lines), and either 0.4% BeWX (w/v) (grey) or 0.4% PASC and 0.4% BeWX (w/v) (red), and either 50 (**A**) or 200 (**B**) µM H_2O_2. . All reactions were incubated at 45°C for 24 hours. All reactions were performed in duplicate and in the duplicate reactions showed similar product profiles in all cases.

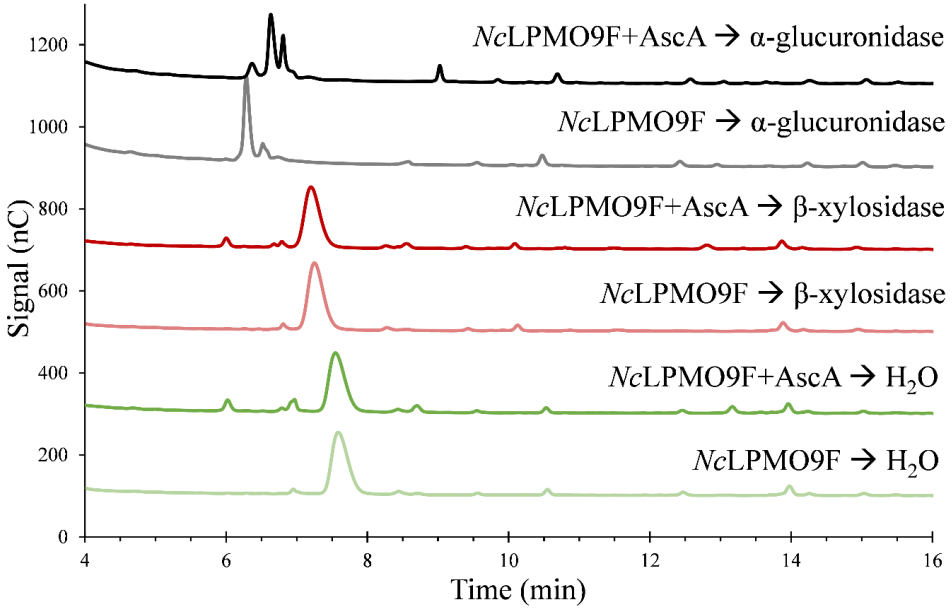

Figure S3. HPAEC-PAD chromatograms of LPMO products treated with different enzymes. A mixture of BeWX (0.4% w/v) and PASC (0.4% w/v) was treated with 1 µM µM *Nc*LPMO9F in the absence or presence of 1 mM AscA, as indicated, in 50 mM BisTris-HCl buffer pH 6.5 at 45°C, overnight. The resulting products where then hydrolyzed with 1 µM *Tr*Cel7A and 1 µM *Cj*Xyn10A for 24 hours in 75 mM sodium acetate buffer pH 4.75 at 37°C**.** Finally, the resulting hydrolysis products were treated with either α-glucuronidase, β-xylosidase or H_2O for 24 hours, as indicated in the chromatograms to the right or the arrows. α-glucuronidase reactions were performed at 70°C in 75 mM Tris buffer pH 7.0, and β-xylosidase reactions were performed at 35°C in 75 mM Tris buffer pH 7.5. Treatment with α-glucuronidase resulted in a clear shift in the large peak at 7.5 minutes in the non- α-glucuronidase treated product mixture, indicating that this peak is composed of GlcAOMe-substituted xylooligomers**.** The effect of xylosidase treatment was less clear, although a minor peak shift may have occurred. All reactions were performed in triplicate and resulted in similar product profiles. The

difference between the elution patterns shown here and those shown in Fig. 5 of the main manuscript are due to differences in the experimental conditions.

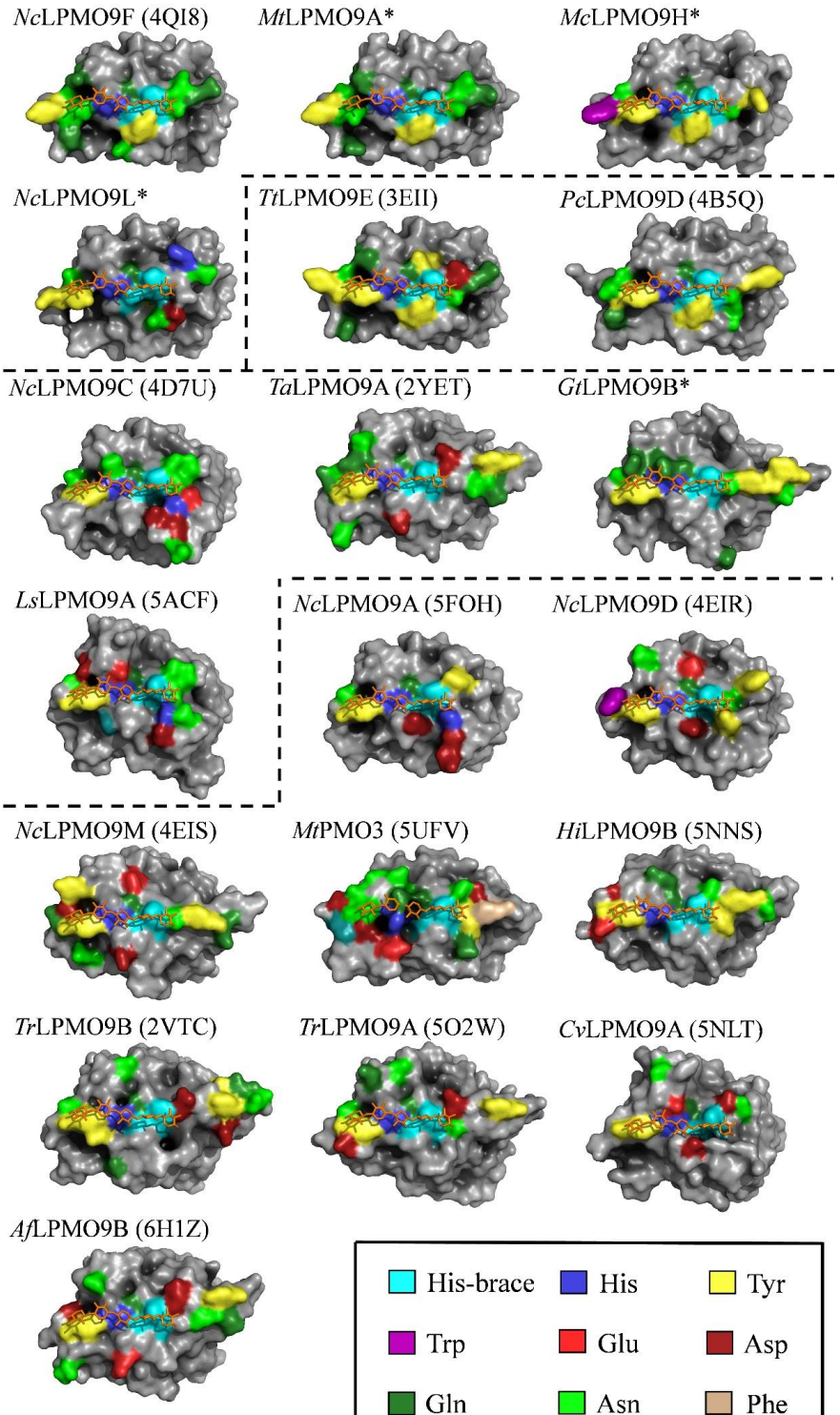
NcLPMO9F (4QI8)
MtLPMO9A*
McLPMO9H*
NcLPMO9L*
TtLPMO9E (3EII)
PcLPMO9D (4B5Q)
NcLPMO9C (4D7U)
TaLPMO9A (2YET)
GtLPMO9B*
LsLPMO9A (5ACF)
NcLPMO9A (5FOH)
NcLPMO9D (4EIR)
NcLPMO9M (4EIS)
MtPMO3 (5UFV)
HiLPMO9B (5NNS)
TrLPMO9B (2VTC)
TrLPMO9A (5O2W)
CvLPMO9A (5NLT)
AfLPMO9B (6H1Z)
His-brace
His
Tyr
Trp
Glu
Asp
Gln
Asn
Phe

Figure S4. Substrate-binding surface of AA9 LPMOs. The figure shows 15 crystal structures labelled with enzyme name and PDB code and PHYRE2 models of *Mt*LPMO9A, *Mc*LPMO9H, *Nc*LPMO9L and *Gt*LPMO9B (marked with *). Residues that are commonly involved in protein-carbohydrate interactions and are located on the substrate-binding surface are coloured, according to the legend in the figure. Note that Tyr2 as discussed in the main text is not solvent-exposed and thus not visible in this view. The dashed lines indicate the following grouping of the structures and models, from top to bottom: LPMOs with proven xylanolytic activity (*Nc*LPMO9F, *Mt*LPMO9A, *Mc*LPMO9H and *Nc*LPMO9L), LPMOs phylogenetically close to LPMOs with proven xylanolytic activity (*Tt*LPMO9E and *Pc*LPMO9D), LPMOs tested in the present study with no detected xylanolytic activity (*Nc*LPMO9C, *Ta*LPMO9A, *Gt*LPMO9B and *Ls*LPMO9A), and nine other AA9 LPMOs. Xylopentaose (Xyl5) is shown in orange and has been superimposed from the crystal structure of *Ls*LPMO9A complexed with Xyl_5 (5NLO) [1].

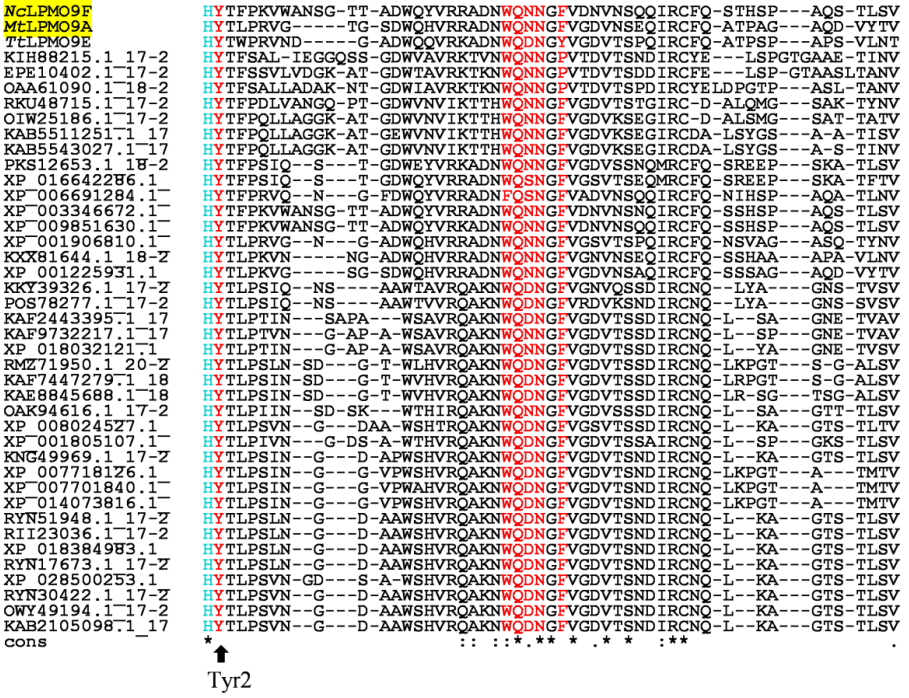
NcLPMO9F
MtLPMO9A
TtLPMO9E
KIH88215.1_17-2
EPE10402.1_17-2
OAA61090.1_18-2
RKU48715.1_17-2
OIW25186.1_17-2
KAB5511251.1_17
KAB5543027.1_17
PKS12653.1_18-2
XP_016642286.1
XP_006691284.1
XP_003346672.1
XP_009851630.1
XP_001906810.1
KXX81644.1_18-2
XP_001225931.1
KKY39326.1_17-2
POS78277.1_17-2
KAF2443395.1_17
KAF9732217.1_17
XP_018032121.1
RMZ71950.1_20-2
KAF7447279.1_18
KAE8845688.1_18
OAK94616.1_17-2
XP_008024527.1
XP_001805107.1
KNG49969.1_17-2
XP_007718126.1
XP_007701840.1
XP_014073816.1
RYN51948.1_17-2
RII23036.1_17-2
XP_018384983.1
RYN17673.1_17-2
XP_028500253.1
RYN30422.1_17-2
OWY49194.1_17-2
KAB2105098.1_17
cons
Tyr2

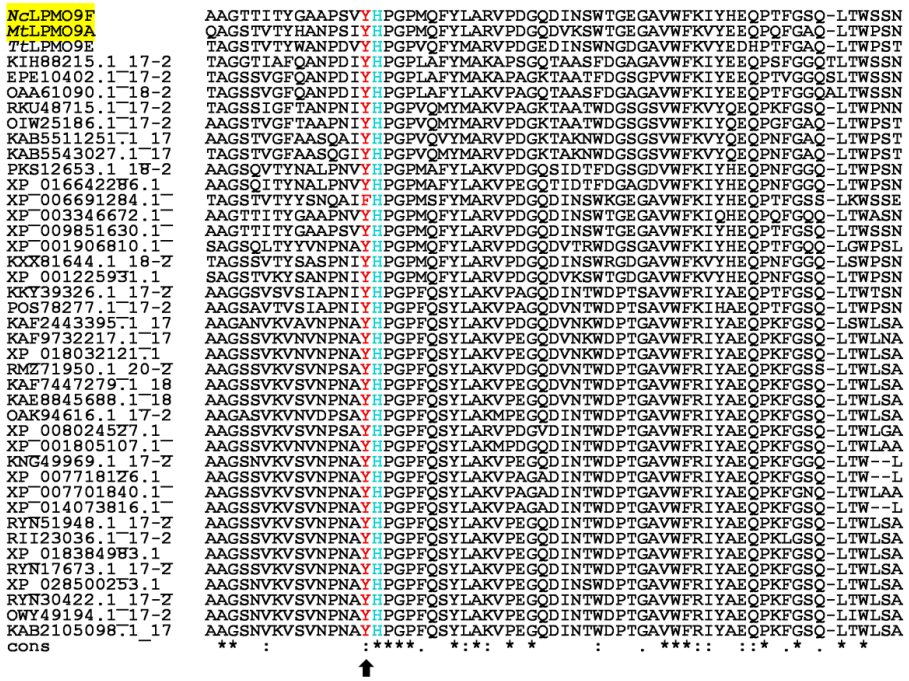
NcLPMO9F
MtLPMO9A
TtLPMO9E
KIH88215.1_17-2
EPE10402.1_17-2
OAA61090.1_18-2
RKU48715.1_17-2
OIW25186.1_17-2
KAB5511251.1_17
KAB5543027.1_17
PKS12653.1_18-2
XP_016642286.1
XP_006691284.1
XP_003346672.1
XP_009851630.1
XP_001906810.1
KXX81644.1_18-2
XP_001225931.1
KKY39326.1_17-2
POS78277.1_17-2
KAF2443395.1_17
KAF9732217.1_17
XP_018032121.1
RMZ71950.1_20-2
KAF7447279.1_18
KAE8845688.1_18
OAK94616.1_17-2
XP_008024527.1
XP_001805107.1
KNG49969.1_17-2
XP_007718126.1
XP_007701840.1
XP_014073816.1
RYN51948.1_17-2
RII23036.1_17-2
XP_018384983.1
RYN17673.1_17-2
XP_028500253.1
RYN30422.1_17-2
OWY49194.1_17-2
KAB2105098.1_17
cons
Tyr71

```
NcLPMO9F            G-------------------------KS--SFPVKIPSCIKSGSYLLRAEHIGLHVAQSSGAA
MtLPMO9A            G-------------------------KS--SFEVPIPSCIRAGNYLLRAEHIALHVAQSQGGA
TtLPMO9E            G-------------------------KS--SFAVPIPPCIKSGYYLLRAEQIGLHVAQSVGGA
KIH88215.1_17-2     G-----------------------LKT---PSVTIPKCLPDGDYLLRIEHIGLHVAQSAGGA
EPE10402.1_17-2     G-----------------------LKT---PSVTLPKCLPNGDYLFRIEHIGLHVAQSTGGA
OAA61090.1_18-2     G-----------------------LKT---PSVTIPKCLPDGDYLVRIEHIGLHVAQSAGGA
RKU48715.1_17-2     G-------------------------AS--RVTVTVPKCLQNGEYLFRIEHIALHVAQSSGGA
OIW25186.1_17-2     N-------------------------KA--TQSVTIPRCLKSGDYLLRIEHIALHSASSSGGA
KAB5511251.1_17     N-------------------------KATQSFTV--PRCLKSGEYLVRIEHIALHSAGSSGGA
KAB5543027.1_17     N-------------------------KA--TQSVTVPRCLKSGEYLVRIEHIALHSAGSSGGA
PKS12653.1_18-2     GMSDFTIIQFAIPATIKEYTNNGGTGKS--NFAVTIPSCIPAGDYLLRAEHIGLHAASSPGGA
XP_016642286.1      G-------------------------KS--NFPVTIPACIAPGDYLLRAEHIGLHAAQSPGGA
XP_006691284.1_     G-------------------------KS--AFPVTIPRCIRPGYYLLRAEHIALHSASTPGGA
XP_003346672.1_     G-------------------------KS--SFPVKIPSCIKSGNYLLRAEHIGLHVAQSSGAA
XP_009851630.1_     G-------------------------KS--SFPVKIPSCIKSGSYLLRAEHIGLHVAQSSGAA
XP_001906810.1_     N-------------------------KG--SFPVTIPRCIRSGYYLLRAEHIALHSASSPGGA
KXX81644.1_18-Z     ------------------------------VPIPRCIRSGYYLLRAEHIGLHVAQSSGGA
XP_001225931.1      G-------------------------KS--SFDVSIPSCIKAGKYLLRAEHIGLHVAQSSGGA
KKY39326.1_17-Z     G-------------------------KS--TMSVTIPKCIPAGDYLMRNEHIGLHVAQSEGAA
POS78277.1_17-2     G-------------------------KS--TMSVTIPKCIPAGNYLMRNEHIALHVAQSQGAA
KAF2443395.1_17     ------------------------A--NYDIKIPACIAPGKYLMRNEHIALHVAQSSGGA
KAF9732217.1_17     ------------------------A--NYDVKIPPCIPAGRYLMRNEHIGLHVAQSPGGA
XP_018032121.1      ------------------------A--NYDIKIPSCIPAGKYLMRNEHIGLHVAQSSGGA
RMZ71950.1_20-Z     ------------------------S--TYNIAIPSCLPAGKYLMRNEHIALHTAGTKGGA
KAF7447279.1_18     ------------------------A--NYNINIPSCIAPGKYLMRNEHIAIHTAGTRGGA
KAE8845688.1_18     ------------------------A--SYNINIPSCIAPGKYLMRNEHIALHTAGSRGGA
OAK94616.1_17-2     ------------------------S--NYDIKIPSCIAPGKYLMRNEHIGLHTAQSAGGA
XP_008024527.1      ------------------------S--TYDIKLPSCIPAGKYLMRNEHIAIHTASSVGGA
XP_001805107.1_     ------------------------A--NYDIKIPSCIAPGKYLMRNEHIAIHNAGTKGGA
KNG49969.1_17-Z     A-----------------------AS--NYDIKIPQCIAPGKYLMRNEHIAIHTASSRGGA
XP_007718126.1      A-----------------------AA--NYDIKIPQCIPAGKYLMRNEHIAIHTAGQRGGA
XP_007701840.1_     G------------------------TYDIKIPQCIAPGKYLMRNEHIAIHTAGQRGGA
XP_014073816.1_     A-----------------------AS--SYDIKIPQCIAPGKYLMRNEHIAIHTAGSRGGA
RYN51948.1_17-Z     ------------------------A--TYDVKIPQCIAPGKYLMRNEHIAIHTAQSKGGA
RII23036.1_17-2     ------------------------A--TYDIKIPQCIAPGKYLMRNEHIAIHTAQSKGGA
XP_018384983.1      ------------------------A--TYDIKIPQCIAPGKYLMRNEHIAIHTAQSKGGA
RYN17673.1_17-Z     ------------------------A--TYDIKIPQCIAPGKYLMRNEHIAIHTAQSKGGA
XP_028500253.1      ------------------------A--NYDIKIPQCIAPGKYLMRNEHIAIHTAQSKGGA
RYN30422.1_17-Z     ------------------------A--NYDIKIPQCIAPGKYLMRNEHIAIHTAQSKGGA
OWY49194.1_17-2     ------------------------A--NYDIKIPQCIAPGKYLMRNEHIAIHTAQSKGGA
KAB2105098.1_17     ------------------------A--NYDIKIPQCIAPGKYLMRNEHIAIHTAQSKGGA
cons                                           :  * *:  * **.* *:*.:* *   *.*
```

```
NcLPMO9F            QFYISCAQLSITGGGSTEPGANYKVSFPGAYKASDPGILININYPVPTSYKNPGPSVFTC
MtLPMO9A            QFYISCAQLQVTGGGSTEPS-Q-KVSFPGAYKSTDPGILININYPVPTSYQNPGPAVFRC
TtLPMO9E            QFYISCAQLSVTGGGSTEPP-N-KVAFPGAYSATDPGILININYYPVPTSYQNPGPAVFSC
KIH88215.1_17-2     QFYISCGQISVSGGGSGSPK-D-LVAFPGAYKATDPGILININYPVPTSYTNPGPAVFTC
EPE10402.1_17-2     QFYISCGQVTVTGGGSKSPT-D-LVAFPGAYKATDPGILININYPVPTSYTNPGPKVFTC
OAA61090.1_18-2     QFYISCGQMTLSGGGSTTPT-D-LVAFPGAYKATDPGILININYPVPTSYTNPGPSVFTC
RKU48715.1_17-2     QFYISCGQISLSGGGNTA-GSP-TVAFPGAYSASDPGILININYPVPTSYTNPGPKVFTC
OIW25186.1_17-2     QFYISCGQISVTGGGSTE-GAP-TVAFPGAYSASDPGILININYPIPTSYVNPGPKVFTC
KAB5511251.1_17     QFYISCGQISVSGGGSTEGGPT--VAFPGAYSASDPGILININYPVPTSYVNPGPKVFSC
KAB5543027.1_17     QFYISCGQISVSGGGSTEGGPT--VAFPGAYSASDPGILININYPVPTSYQNPGPKVFSC
PKS12653.1_18-2     QFYISCAQLTITGGGSTDPP-N-KVAFPGAYKASDPGIQININYPVPTSYQNPGPAVFSC
XP_016642286.1      QFYISCAQLTITGGGSTDPP-N-KVAFPGAYKASDPGIQININYPVPTSYQNPGPAVFKC
XP_006691284.1_     QFYISCAQLAVTGGGSTDPP-N-KVSFPGAYKANDPGIQININYYPVPTSYKNPGPSVFSC
XP_003346672.1_     QFYISCAQLSITGGGNTEPS-N-KVSFPGAYKASDPGILININYPVPTSYKNPGPSVFIC
XP_009851630.1_     QFYISCAQLSITGSGSTEPGANYKVSFPGAYKASDPGILININYPVPTSYKNPGPSVFTC
XP_001906810.1_     QFYISCAQIGVTGGGNTEPS-N-KVSFPGAYSASDPGIQININWPIPTSYRNPGPPVFQC
KXX81644.1_18-Z     QFYISCAQIGVTGGGNTDPP-N-KVSFPGAYRASDPGIMININWPIPTSYQNPGPPVFSC
XP_001225931.1      QFYISCAQIEVTGGGSTEPS-N-KVSFPGAYKASDPGILININWPIPTSYQNPGPPVFKC
KKY39326.1_17-Z     QFYLSCGQLSVTGGGSTQPQ-N-LAAFPGAYSSKDPGILININYPVPTSYVNPGPATFTC
POS78277.1_17-2     QFYLSCAQLSVTGGGSTQPQ-N-LVAFPGAYSATDPGILININYPVPTSYKNPGPATFTC
KAF2443395.1_17     QFYLSCAQIEVTGGGSKAPT-N-LVAFPGAYKASDPGILINVNYPVPTSYVNPGPATFTC
KAF9732217.1_17     QFYLSCAQIDVVGGGSQTPT-D-LAAFPGAYRASDPGILININYPVPTSYVNPGPATFVC
XP_018032121.1      QFYLSCAQIEVTGGGSKTPT-N-LAAFPGAYKASDPGILININYPVPTSYVNPGPATFTC
RMZ71950.1_20-Z     QFYLSCGQLEVTGGGSKSPS-N-LVAFPGAYSATDPGILININYPIPTSYKNPGPATFTC
KAF7447279.1_18     QFYLSCAQIEVTGGGSKTPT-N-LVAFPGAYSATDPGILININYPIPTSYKNPGPPTFTC
KAE8845688.1_18     QFYLSCAQIEVTGGGSKAPT-N-LVAFPGAYSATDPGILININYPIPTSYKNPGPATFTC
OAK94616.1_17-2     QFYLSCAQLDITGGGSKAPT-N-LVAFPGAYKSSDPGILININYPIPTSYTNPGPPTFTC
XP_008024527.1      QFYLSCAQLQITGGGSTNPR-D-LVAFPGAYKATDPGILININYPIPTSYVNPGPPTFTC
XP_001805107.1_     QFYLSCAQLEVTGGGSTAPK-N-LVAFPGAYSATDPGILININYPIPTSYKNPGPDTFTC
KNG49969.1_17-Z     QFYLSCAQIEVTGGGSTAPR-N-LVAFPGAYSATDPGIMININYPIPTSYVNPGPPTFTC
XP_007718126.1      QFYLSCAQIEVTGGGSTSPR-N-LVAFPGAYSATDPGILININYPIPTSYVNPGPPTFTC
XP_007701840.1_     QFYLSCAQIEVTGGGSTSPR-N-LVAFPGAYSATDPGILININYPIPTSYVNPGPPTFTC
XP_014073816.1_     QFYLSCAQIEVTGGGSTSPR-N-LVAFPGAYSATDPGILININWPIPTSYVNPGPPTFTC
RYN51948.1_17-Z     QFYLSCGQLEVTGGGSKAPS-N-LVAFPGAYKATDPGILININYPIPTSYTNPGPPTFTC
RII23036.1_17-2     QFYLSCGQLEVTGGGSKAPS-N-LVAFPGAYKATDPGILININYPIPTSYTNPGPPTFTC
XP_018384983.1      QFYLSCGQLEVTGGGSKAPS-N-LVAFPGAYKATDPGILININYPIPTSYTNPGPPTFTC
RYN17673.1_17-Z     QFYLSCGQLEVTGGGSKAPS-N-LVAFPGAYKATDPGILININYPIPTSYTNPGPPTFTC
XP_028500253.1      QFYLSCAQLEVTGGGSKAPS-N-LVAFPGAYKATDPGILININYPIPTSYTNPGPPTFTC
RYN30422.1_17-Z     QFYLSCAQLEVTGGGSKAPS-N-LVAFPGAYKATDPGILININYPIPTSYTNPGPPTFTC
OWY49194.1_17-2     QFYLSCAQLEVTGGGSKAPS-N-LVAFPGAYKATDPGILININYPIPTSYTNPGPPTFTC
KAB2105098.1_17     QFYLSCAQLEVTGGGSKAPS-N-LVAFPGAYKATDPGILININYPIPTSYTNPGPPTFTC
cons                ***:**.*: : *.*.        .:***** :.**** **: :*:**** **** .* *
                                                                 ⬆
                                                               Asn197
```

Figure S5. Expresso (T-Coffee) multiple sequence alignments of 41 LPMOs in the *Nc*LPMO9F clade. Enzymes with demonstrated xylan activity are highlighted in yellow. Sequence features of xylan active LPMOs that are discussed in the main text are highlighted with red. Three characteristic sequence features of the clade are also highlighted by arrows and labels: Tyr2, Tyr71 and Asn197 (residue numbering according to *Nc*LPMO9F). Conserved residues in the first and second coordination sphere of the copper appear in light and dark blue, as in Fig. S4.

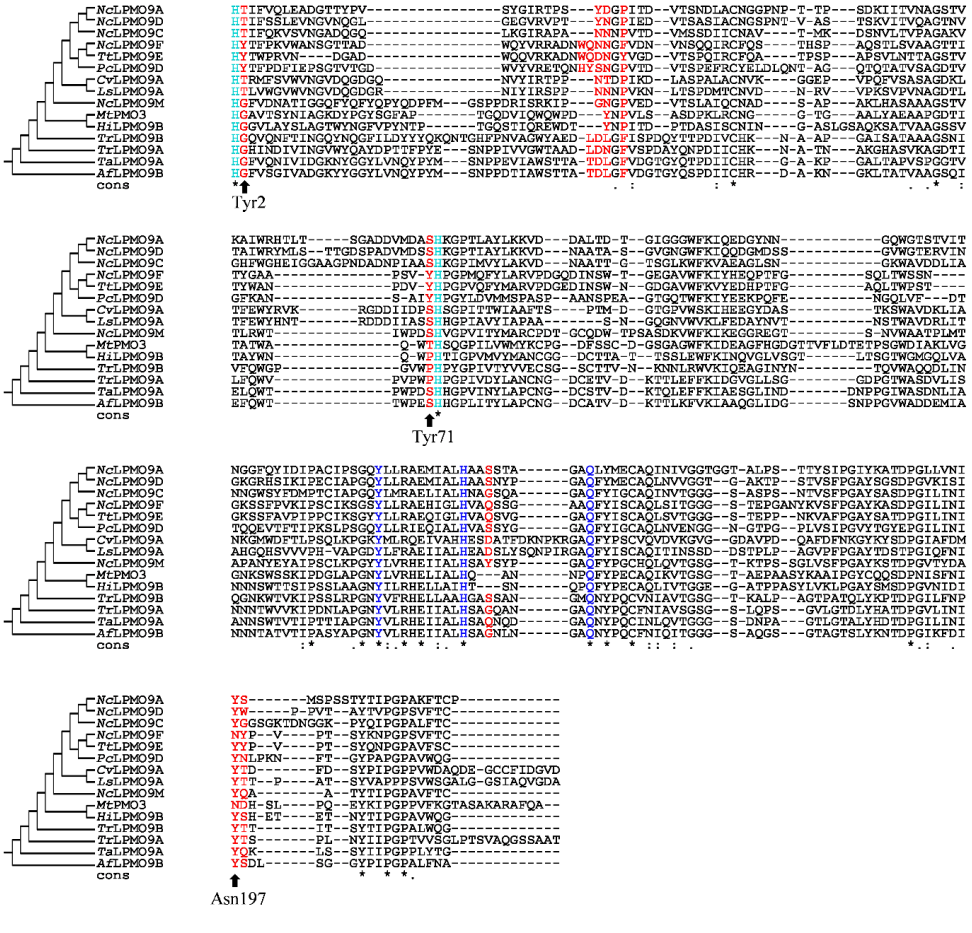

Figure S6. Structure-based multiple sequence alignment of 15 AA9 LPMOs with known crystal structures. Sequence features of xylan-active LPMOs that are discussed in the main text are highlighted with red. The copper-binding histidines appear in light blue, whereas a conserved tyrosine in the proximal axial copper coordination position and a conserved glutamine and histidine in the second coordination sphere appear in dark blue. The PDB codes for the structures are given in Fig. S4 and in the Materials and methods section.

1. Simmons, T.J., et al., *Structural and electronic determinants of lytic polysaccharide monooxygenase reactivity on polysaccharide substrates.* Nature Communications, 2017. **8**(1): p. 1064.

ISBN: 978-82-575-1903-2
ISSN: 1894-6402

Norwegian University
of Life Sciences

Postboks 5003
NO-1432 Ås, Norway
+47 67 23 00 00
www.nmbu.no

114009 / ANDVORDGRAFISK.NO